Development and Use of a Groundwater Model for the Spring Valley Area

Presentation to the Office of the Nevada State Engineer

Prepared by

SOUTHERN NEVADA
WATER AUTHORITY

June 2006

Timothy J. Durbin, a consultant to the Southern Nevada Water Authority (SNWA) prepared this report entitled *"Development and Use of a Groundwater Model for the Spring Valley Area"*, June, 2006. This report is one of several reports prepared in support of SNWA groundwater applications 54003 through 54021 in Spring Valley (Hydrographic Area 184).

Timothy J. Durbin, Consulting Hydrologist
Timothy J. Durbin, Inc.

6/22/06
Date

1.0 INTRODUCTION

1.1 Work Scope

This report describes the development of a groundwater model for the Spring Valley, Nevada, area. The groundwater model covers Spring Valley and the adjacent areas as shown on Figure 1-1 and Figure 1-2. The additional areas include Steptoe, Cave, Dry Lake, Pleasant, Lake, Hamlin, Snake, and Tippet Valleys. However, only part of Dry Lake Valley is included.

The model is based on the estimates of groundwater recharge and discharge developed by Eakin (1962), Rush and Eakin (1963), Rush and Kazmi (1965), Hood and Rush (1965), and Eakin, Hughes, and Moore (1967).

The model development is based on the period 1956 to 2005. The groundwater system within the modeled area was in a steady-state condition in the late 1950s and early 1960s, which is the condition documented by Eakin (1962), Rush and Eakin (1963), Rush and Kazmi (1965), Hood and Rush (1965), and Eakin, Hughes, and Moore (1967). Between the mid-1960s and the mid-1980s some groundwater development occurred. However, the subsequent changes within the groundwater system have been small, and the groundwater system essentially remains in a steady-state condition. The groundwater model is developed based on the hydrologic information describing the steady-state condition in the late 1950s and early 1960s.

1.2 Modeling Approach

The groundwater model was developed using the computer program *FEMFLOW3D*, Version 2.0, which is a program for simulating three-dimensional groundwater systems using the finite-element method. *FEMFLOW3D,* Version 2.0, is an updated version of the U.S. Geological Survey (USGS) computer program *FEMFLOW3D*, Version 1.0 (Durbin and Bond, 1998). Version 1.0 is a simulator based on the finite-element method for numerically solving the governing equation of three-dimensional groundwater flow.

FEMFLOW3D, Version 2.0, includes a module for vertically expanding or contracting the model grid to follow a fluctuating groundwater table, which is a feature not included in Version 1.0. Additionally, Version 2.0 includes a module for simulating a fault as a two-dimensional transmissive feature. Except for the added modules, the mathematical basis and structure of *FEMFLOW3D*, Version 2.0, is essentially the same as described for *FEMFLOW3D*, Version 1.0, by Durbin and Bond (1998) and Durbin and Berenbrock (1985). The documentation of Version 2.0 is in Appendix A. Applications of *FEMFLOW3D*, or its derivatives, are described by Kapple et al. (1984), Yates (1988),

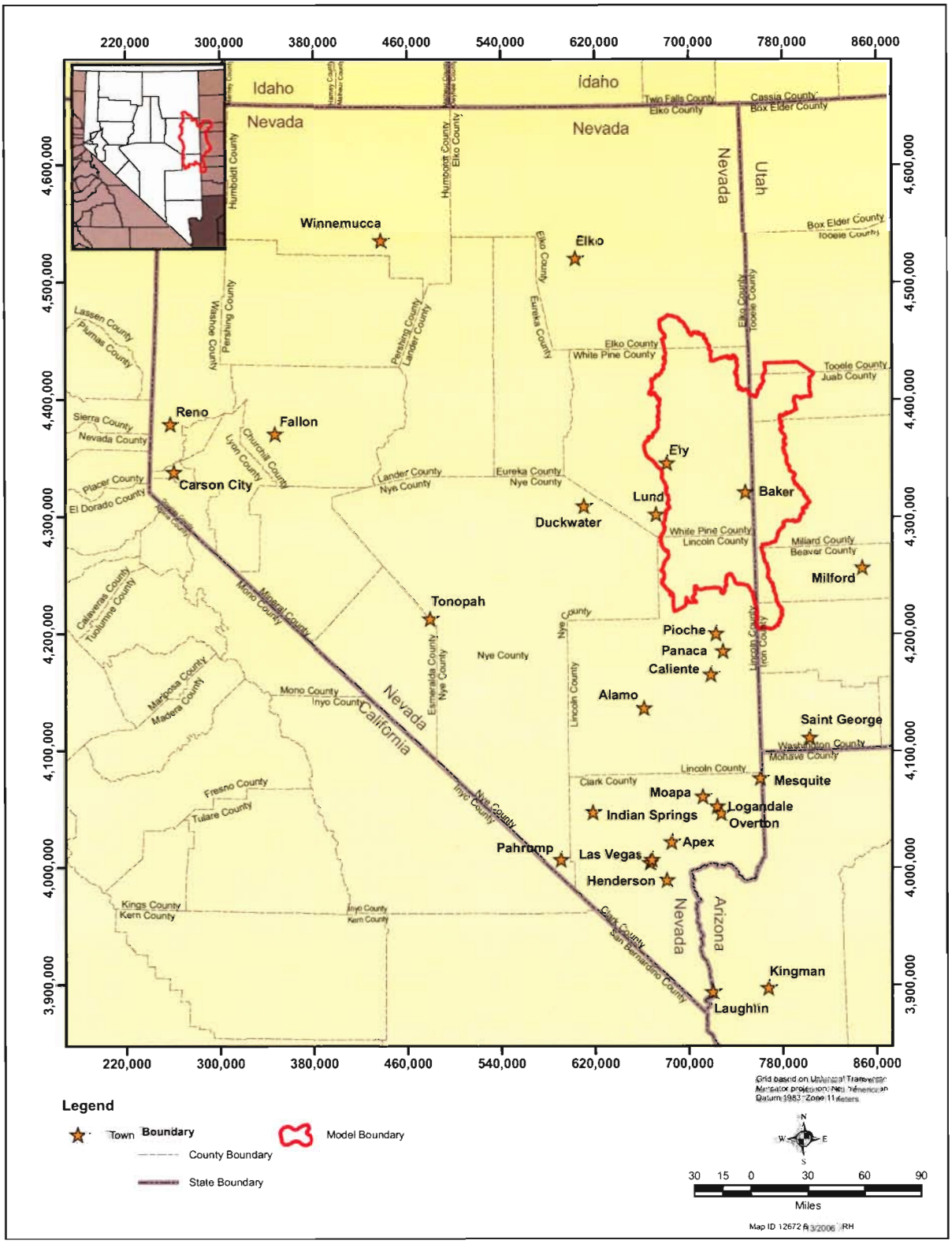

Figure 1-1
Location of the Spring Valley Groundwater Model

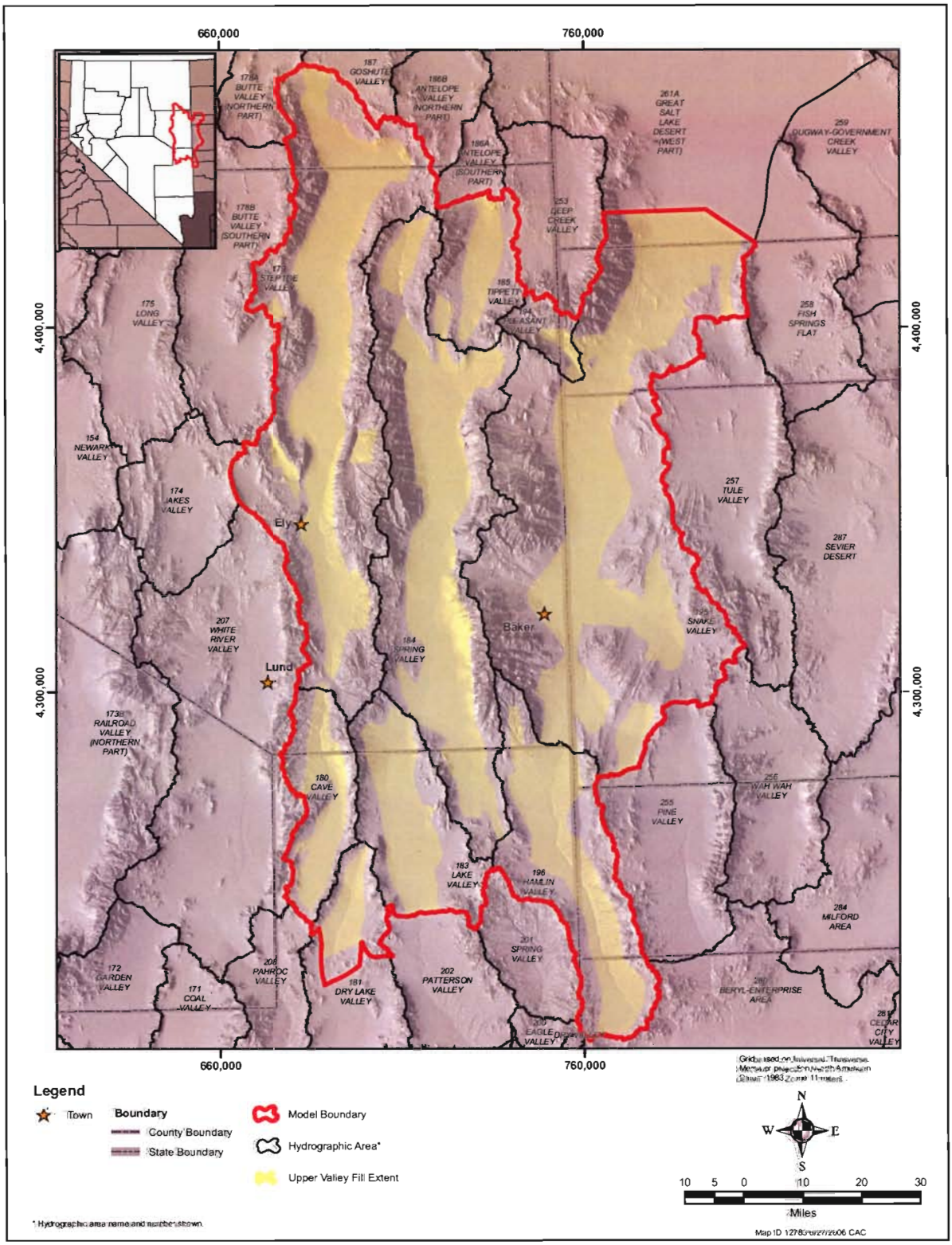

Figure 1-2
Geographic Area Covered by the Groundwater Model

Yates and Van Konyenburg (1998), LaBolle and Fogg (2001), Corbet et al. (1998), and LaBolle et al. (2003).

FEMFLOW3D, Version 2.0, has features that make it particularly suited for use in the modeling of the Spring Valley area. The first important feature is the ability of *FEMFLOW3D* to simulate complex hydrogeologic settings. *FEMFLOW3D* can accommodate a complex of structural compartments that are offset vertically or laterally (Figure 1-3). Because of offsets, hydrogeologic units can be vertically or laterally discontinuous across the modeled area. While the hydrogeologic units might be more or less laterally continuous within a compartment, abrupt elevation changes can occur at the faults representing the compartment boundaries. Furthermore, *FEMFLOW3D* can simulate the compartment-boundary faults as conduits for or barriers to groundwater flow.

For this case, the groundwater flow is essentially bimodal. One component of groundwater flow occurs within the rupture of the faults within the modeled area, where the groundwater flow is two-dimensional. The other component of regional groundwater flow occurs within the structural compartments occupying the regions between major faults. Within these compartments, groundwater flow occurs in the matrix, fractures, and faults within the individual hydrogeologic units. *FEMFLOW3D* can represent this bimodal groundwater flow by simulating two-dimensional groundwater flow within the compartment-bounding faults and three-dimensional flow within the compartments themselves.

The second important feature that makes *FEMFLOW3D* particularly suited for use in the modeling of the Spring Valley area is the robustness of *FEMFLOW3D* with respect to its ability to converge for large-scale complex simulations. *FEMFLOW3D* includes equation solvers and a time-step iteration scheme that are efficient when modeling complex, large-scale hydrologic settings.

1.3 Significant Previous Works

The previous water-resource investigations within the Spring Valley area include work by the USGS, Las Vegas Valley Water District (LVVWD), and SNWA. This and other work were considered in the development of the groundwater model.

The USGS has done specific studies within the Spring Valley area and regional studies that include the Spring Valley area. Eakin (1962), Rush and Eakin (1963), Rush and Kazmi (1965), Hood and Rush (1965), and Eakin, Hughes, and Moore (1967) characterized the hydrogeologic setting within the modeled area and quantified the groundwater recharge and discharge. Harrill and Prudic (1998), Plume (1996), Thomas et al. (1996), and Burbey and Prudic (1991) conducted water-resource studies of the Great Basin. This work included the development of a steady-state groundwater model, which was later converted into a transient-state model (Schaefer and Harrill, 1995). Dettinger (1992), Dettinger et al. (1995), and Burbey (1997) assessed the potential for groundwater development from the regional aquifers extending beneath the Spring Valley area. Nichols (1993, 1994, and 2000) estimated phreatophyte discharge within Steptoe, Spring, and Tippett Valleys and other areas. Bunch and Harrill (1984), Dettinger (1989), Eakin et al. (1951), Eakin (1965), Harrill et al. (1988), Maxey and Eakin (1949), and Moore (1968) conducted miscellaneous studies of regional importance. In

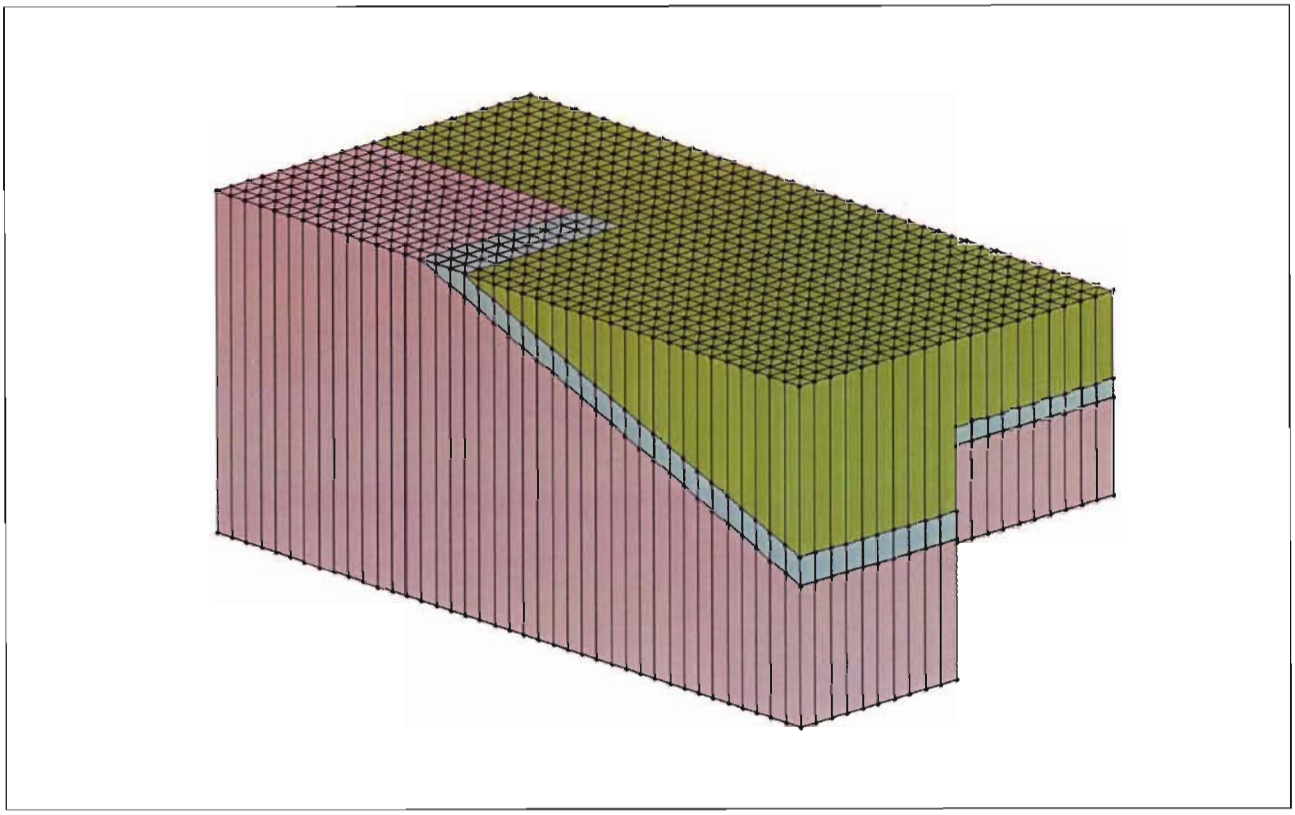

Figure 1-3
Two Structural Compartments Offset by a Fault

addition, the USGS has maintained a large hydrologic-data program within the Spring Valley area and nearby.

The LVVWD and the SNWA have done specific studies within the Spring Valley area. Brothers et al. (1993a), Brothers et al. (1993b), and Brothers et al. (1994) conducted groundwater appraisals within the Spring Valley area, including the development of groundwater models. Katzer and Donovan (2003) evaluated the groundwater recharge and discharge within Spring Valley. Broadbent et al. (1995) conducted a regional study of streamflow recharge. In addition, the LVVWD had maintained, and now the SNWA maintains, a large hydrologic-data program within the Spring Valley area and nearby areas.

1.4 Data Relied Upon

The development of the model is based in part on compilations of basic data and other information. While numerous information sources were relied upon, as represented by the list of cited references in Section 9.0., the more important sources are as follows:

1. Hydrogeologic framework: The development of the model mesh is based on the hydrogeologic model developed by SNWA (2006c).

2. Hydraulic parameters: The evaluation of hydraulic parameters for the model is based in part on aquifer-test data compiled by SNWA staff as described by SNWA (2006b, Volume 1). The evaluation is also based on specific-capacity data and driller's logs compiled for the model area, as described in Section 4.0. The utilized work products include a table listing the aquifer-test locations, well constructions, and hydraulic conductivity. The work products additionally include tables listing the well locations, well constructions, specific-capacity data, and driller's log entries.

3. Precipitation recharge: The specification of precipitation recharge within mountain-block areas is based on the recharge estimates by Eakin (1962), Rush and Eakin (1963), Rush and Kazmi (1965), Hood and Rush (1965), and Eakin, Hughes, and Moore (1967). However, SNWA staff developed a geographic distribution of those recharge estimates for input to the model as described by SNWA (2006b, Volume 2). The utilized work product is an ArcMap raster file.

4. Boundary underflows: The specification of groundwater flows across the model boundary is based on the underflow estimates of Eakin (1962), Rush and Eakin (1963), Rush and Kazmi (1965), Hood and Rush (1965), and Eakin, Hughes, and Moore (1967). However, SNWA staff refined the geographic distribution of the estimated underflows as described by SNWA (2006b, Volume 7). The utilized work product is a table listing the boundary underflows and a map showing their locations.

5. Historical water use: The specification in the model of water use by Ely and McGill is based on estimates developed by SNWA staff as described by SNWA (2006b, Volume 5). The specification of agricultural groundwater use is based on a compilation of certificated groundwater rights as described by SNWA (2006b, Volume 5). The utilized work products include a table listing the consumptive water use by Ely and McGill for the period 1960 to 2005. The work products also include a table listing the diversion points for certificated groundwater rights and the associated irrigated acreages.

6. Phreatophyte discharges: The consumptive use of groundwater by phreatophytes is specified based on the discharge estimates of Eakin (1962), Rush and Eakin (1963), Rush and Kazmi (1965), Hood and Rush (1965), and Eakin, Hughes, and Moore (1967). It is based also on the delineations of phreatophyte areas by SNWA staff as described by SNWA (2006b, Volume 3), including the delineations of meadow, non-meadow, and wet playa areas.

7. Mountain-front streamflow: The specification of mountain-front streamflow within Spring and Snake Valleys is based on streamflow data collected and analyzed by SNWA staff as described by SNWA (2006a). The utilized work product is a table listing the mean annual streamflow for each streamflow location.

8. Spring discharges: The specification of spring discharges and the source depth for springs is based on data collected, compiled, and analyzed by SNWA staff as described by SNWA (2006b, Volume 4). The utilized work product is a table listing the locations, estimated pre-1960 discharges, and the source depths for the monitored springs within the model area.

9. Groundwater levels. The model calibrations is based in part on estimates of pre-1960 groundwater levels and the uncertainty in those estimates developed by SNWA staff as described by SNWA (2006b, Volume 6). The utilized work product is a table listing well locations, screened intervals, estimated groundwater levels, uncertainty due to well location, and uncertainty due to the number and variability of measurements.

This Page Intentionally Left Blank

2.0 DEVELOPMENT OF THE GROUNDWATER MODEL

The development of the Spring Valley groundwater model includes six principal steps. First is the translation of the hydrogeologic framework developed by SNWA (2006c) into a model mesh. Second is the characterization of the hydraulic properties of the groundwater system. Third is the specification of precipitation recharge, community and agricultural water use, and groundwater underflows across the model boundaries. Fourth is the characterization of groundwater discharges to phreatophytes. Fifth is the characterization of groundwater recharge from mountain-front streamflow. Sixth is the calibration of the model.

2.1 Hydrologic Setting

The groundwater model represents the groundwater system that underlies the Spring Valley model area. This system occurs within unconsolidated deposits and consolidated rocks (Figure 2-1). The unconsolidated deposits occupy the valley-floor areas. The consolidated rocks underlie the unconsolidated deposits and crop out within the mountain-block areas. The principal recharge to the groundwater system occurs from precipitation on the consolidated-rock mountain-block areas, and the principal discharge occurs from groundwater consumption by phreatophytes within the valley-floor areas. However, additional discharge occurs as subsurface groundwater flows from the model area to adjacent areas, which occurs mostly through consolidated rocks.

Table 2-1 and Table 2-2 list the water-budget components for the hydrologic system and the groundwater system contained within the hydrologic system. The listed components represent a summary of the groundwater appraisals by Eakin (1962), Rush and Eakin (1963), Rush and Kazmi (1965), Hood and Rush (1965), and Eakin, Hughes, and Moore (1967). These groundwater appraisals represent a steady-state condition for the groundwater system prior to significant groundwater development. For the overall hydrologic system, the average total inflow is 335,800 afy, which is balanced by an average outflow of equal magnitude. For the groundwater system, the average recharge is 311,400 afy, which is balanced by an average discharge of equal amount.

The water-budget components listed in Table 2-1 and Table 2-2 represent an inventory of the inflows and outflows across the control volume for the respective systems. The water budgets for the hydrologic and groundwater systems differ by the definitions of the respective water-budget control volumes. For both control volumes, the bottom surface is the base of the groundwater system, and the lateral boundary is a vertical surface that follows the geographic boundary of the model area. For the groundwater budget, the top surface of the control volume is the groundwater table. For the hydrologic system, the top boundary is a surface above but parallel to the land surface. Consequently, the control volumes differ only by the definition of the top surface.

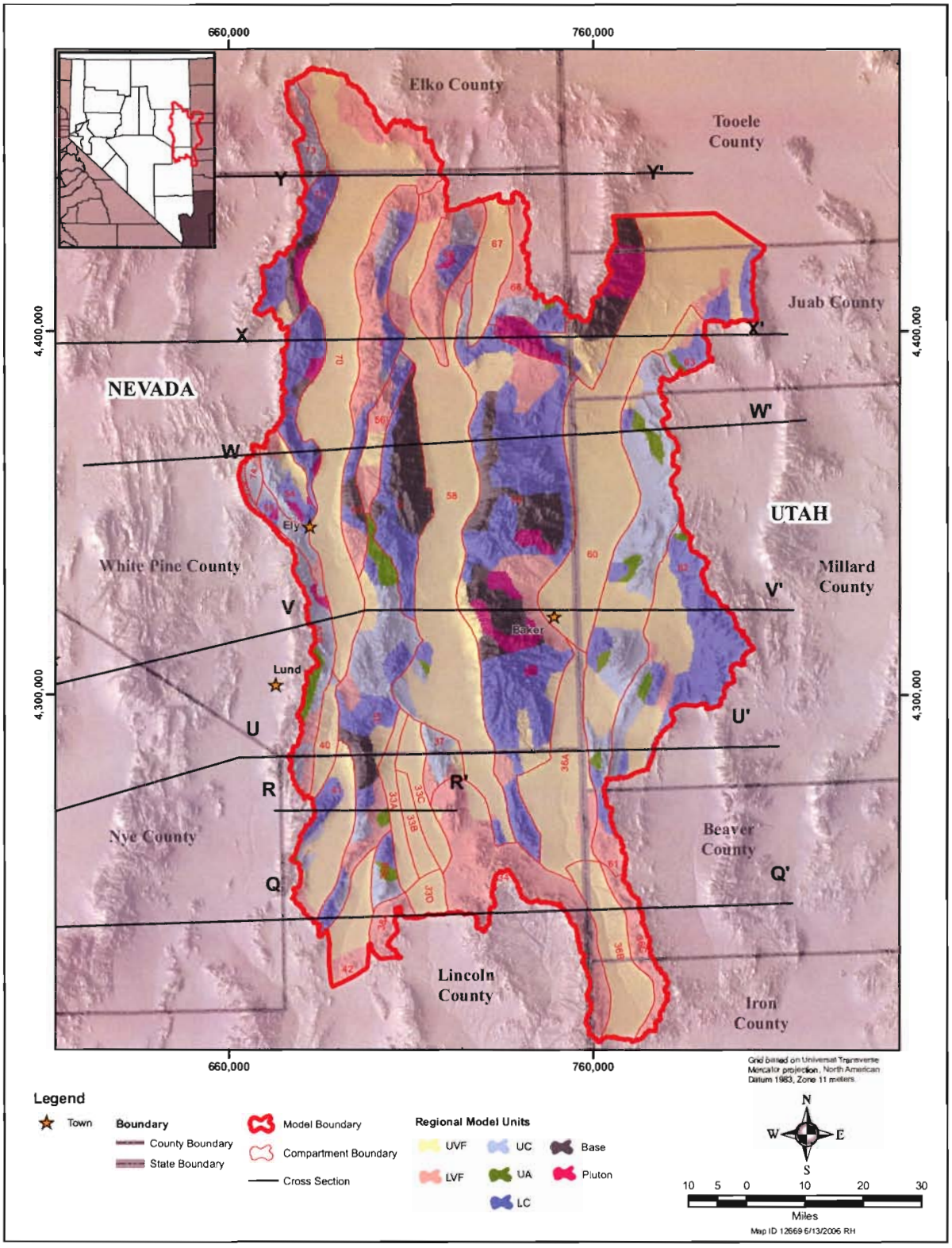

Figure 2-1
Outcrops of Hydrogeologic Units

Table 2-1
Steady-State Water Budget (afy) for Hydrologic System Spring Valley Area

Budget Component	Rate
Inflows	
Mountain-block recharge	
Steptoe Valley	85,000
Tippett Valley	6,900
Spring Valley	65,000
Snake Valley	71,000
Pleasant Valley	5,000
Cave Valley	14,000
Lake Valley	13,000
Dry Lake Valley (northern part)	1,700
Spring Valley mountain-front streamflow	47,500
Snake Valley mountain-front streamflow	2,700
Total	**335,800**
Outflows	
Phreatophyte ET	
Spring Valley	71,000
Steptoe Valley	76,000
Cave Valley	200
Lake Valley	10,000
Snake Valley	88,000
Boundary underflows	
Steptoe Valley	7,000
Lake Valley	3,000
Cave Valley	14,000
Snake Valley	20,000
Dry Lake Valley	1,700
Playa evaporation	
Spring Valley Yeland Lake	21,300
Spring Valley South Playa	7,800
Snake Valley	14,400
Agricultural and community consumptive use	
Steptoe Valley	0
Spring Valley	0
Snake Valley	300
Lake Valley	0
Ely	700
McGil	400
Tolal	**335,800**

For the water budget for the hydrologic system, the inflow quantities represent the net effect of precipitation and evapotranspiration within the mountain-block areas. The difference between precipitation and evapotranspiration is the water yield from the mountain-block areas, which essentially represents the total water yield within the model area. That yield is manifested in the forms of precipitation recharge within the mountain-block areas and streamflow at the mountain fronts. The precipitation recharge in turn is the net effect of direct precipitation recharge within interfluvial areas and stream-groundwater exchanges along the stream reaches within the mountain-block areas. In Table 2-1, the net effect of mountain-block precipitation and

Table 2-2
Steady-State Water Budget (afy) for Groundwater System Spring Valley Area

Budget Component	Rate
Inflows	
Mountain-block recharge	
Steptoe Valley	85,000
Tippett Valley	6,900
Spring Valley	65,000
Snake Valley	71,000
Pleasant Valley	5,000
Hamlin Valley	24,000
Cave Valley	14,000
Lake Valley	13,000
Dry Lake Valley (northern part)	1,700
Spring Valley valley-floor streamflow recharge	18,400
Snake Valley valley-floor streamflow recharge	7,400
Total	311,400
Outflows	
Phreatophyte ET	
Spring Valley	71,000
Steptoe Valley	76,000
Cave Valley	200
Lake Valley	10,000
Snake Valley	88,000
Boundary underflows	
Steptoe Valley	7,000
Lake Valley	3,000
Cave Valley	14,000
Snake Valley	20,000
Dry Lake Valley	1,700
Spring discharges	
Warm Spring	12,400
Big Spring	6,700
Agricultural and community consumptive use	
Steptoe Valley	0
Spring Valley	0
Snake Valley	300
Lake Valley	0
Ely	700
McGil	400
Tolal	**311,400**

evapotranspiration is represented by the table listings for precipitation recharge and mountain-front streamflow.

3.0 REPRESENTATION OF HYDROGEOLOGY IN GROUNDWATER MODEL

3.1 Hydrogeologic Units

SNWA (2006c) developed a geologic and hydrogeologic framework of the Spring Valley area. The hydrogeologic framework includes 12 hydrogeologic units (SNWA, 2006c, Table 4-1). These 12 aggregated the hydrogeologic units into eight regional model units (RMUs). Seven of these units, as listed in Table 3-1, occur within the model area. The seven RMUs are represented separately in the finite-element mesh for the model, based on distinctions among their hydraulic characteristics.

3.1.1 Description of RMUs

The RMUs include unconsolidated deposits and consolidated rocks. The unconsolidated deposits are represented by the upper valley fill RMU. The consolidated rocks include the lower valley fill, upper carbonate rock, lower carbonate rock, basement rock, and plutonic rock RMUs. The generalized outcrops of the RMUs are shown on Figure 2-1.

The upper valley fill RMU consists of playa deposits of Quaternary age, basin sediments of Quaternary and Tertiary age, and some volcanic rocks of Quaternary and Tertiary age. At a regional scale, the upper valley fill is poorly to moderately permeable. The playa deposits consist of silt and clay deposits. The basin sediments consist of alluvial and inter-fingered pluvial deposits. Older alluvial-fan deposits flank the mountain ranges, and younger deposits cover the valley floors and lower slopes of the alluvial fans. The main period of fan building probably took place during late Tertiary and Pleistocene times, following a major uplift of the mountain blocks. The volcanic rocks are comprised of tuffs and lava flows of mostly andesitic compositions. The volcanic rocks mostly underlie the basin sediments, but in places are interbedded with those sediments. Within the Spring Valley area, the upper valley fill RMU is as much as 11,000 ft in thickness. The geographic extent of the upper valley fill is shown on Figure 3-1.

The lower valley fill RMU consists of volcanic rocks of Oligocene and Eocene age and sediments of Eocene, Paleocene, and Late Cretaceous ages. At a regional scale, the lower valley fill is poorly to moderately permeable. The volcanic rocks are comprised of tuffs and lava flows of mostly andesitic compositions. The early Tertiary and Late Cretaceous sediments consist of conglomerate, sandstone, and siltstone. The unit has a very limited geographic extent and thickness. However, within the Spring Valley area, the volcanic rocks are as much as 20,000 ft in thickness. The maximum depth to the base of the lower valley fill is about 24,000 ft. The geographic extent of the lower valley fill is shown on Figure 3-2.

Table 3-1
Translation of Hydrogeologic Units into Regional Model Units

Regional Model Unit		Hydrogeologic Unit	Description
Identifier	Name		
UVF	Upper Valley Fill	QTb	Quaternary and Tertiary basalt - Quaternary and late Tertiary mafic volcanic rocks that are too thin to show on cross sections. These rocks are significant as a separate unit only where they are divided from the older volcanic rocks (Tv) by alluvium.
		QTs	Quaternary and Tertiary sediments - Includes sediments younger than the volcanic section, but may include older sediments where volcanic rocks are minor or nonexistent. Also includes playa deposits.
LVF	Lower Valley Fill	Tv	Tertiary volcanic rocks - Miocene to Eocene volcanic rocks.
		Tos	Older Tertiary sediments - Primarily created for the cross sections; includes the older Tertiary alluvial section below the volcanic section.
PLUT	Plutonic Rock	TJi	Tertiary to Jurassic intrusive rocks - includes all plutons.
UC	Upper Carbonates	PIPc	Permian and Pennsylvanian carbonate rocks - Includes Ely Limestone, Bird Spring Formation, the Park City Group and other units. Includes Triassic carbonate rocks in the Butte Mountains, where these rocks are of limited extent. Also includes Permian red.
UA	Upper Aquitard	Ms	Mississippian siliciclastic rocks - Includes Chainman Shale, Scotty Wash Quartzite, Diamond Peak Formation, Eleana Formation, and others. The Chainman Shale and Scotty Wash Quartzite are not differentiated in Lincoln County, except in the Egan and Schell.
LC	Lower Carbonate Rocks	MOc	Mississippian to Ordovician carbonate rocks - Joana Limestone (Monte Cristo Formation) to Pogonip Group, also includes Chainman Shale in most of Lincoln and Clark County. The Pilot Shale and Eureka Quartzite are also included.
		Ꞓc	Cambrian carbonate rocks - Includes the Bonanza King, Highland Peak, Lincoln Peak, and Pole Canyon Formations, and several units in western Utah.
BASE	Basement Rocks	ꞒpꞒs	Cambrian and Precambrian siliciclastic rocks - Includes the Wood Canyon Formation and the Prospect Mountain and Stirling Quartzites, and the Chisholm Shale, Lyndon Limestone, and Pioche Shale.
		pꞒm	Precambrian metamorphic rocks - Precambrian X, Y, and Z high-grade metamorphic rocks, generally Late Proterozoic. It also includes the Johnnie Formation in the southern map area, and the weakly metamorphosed McCoy Creek and Trout Creek Groups in Schell.

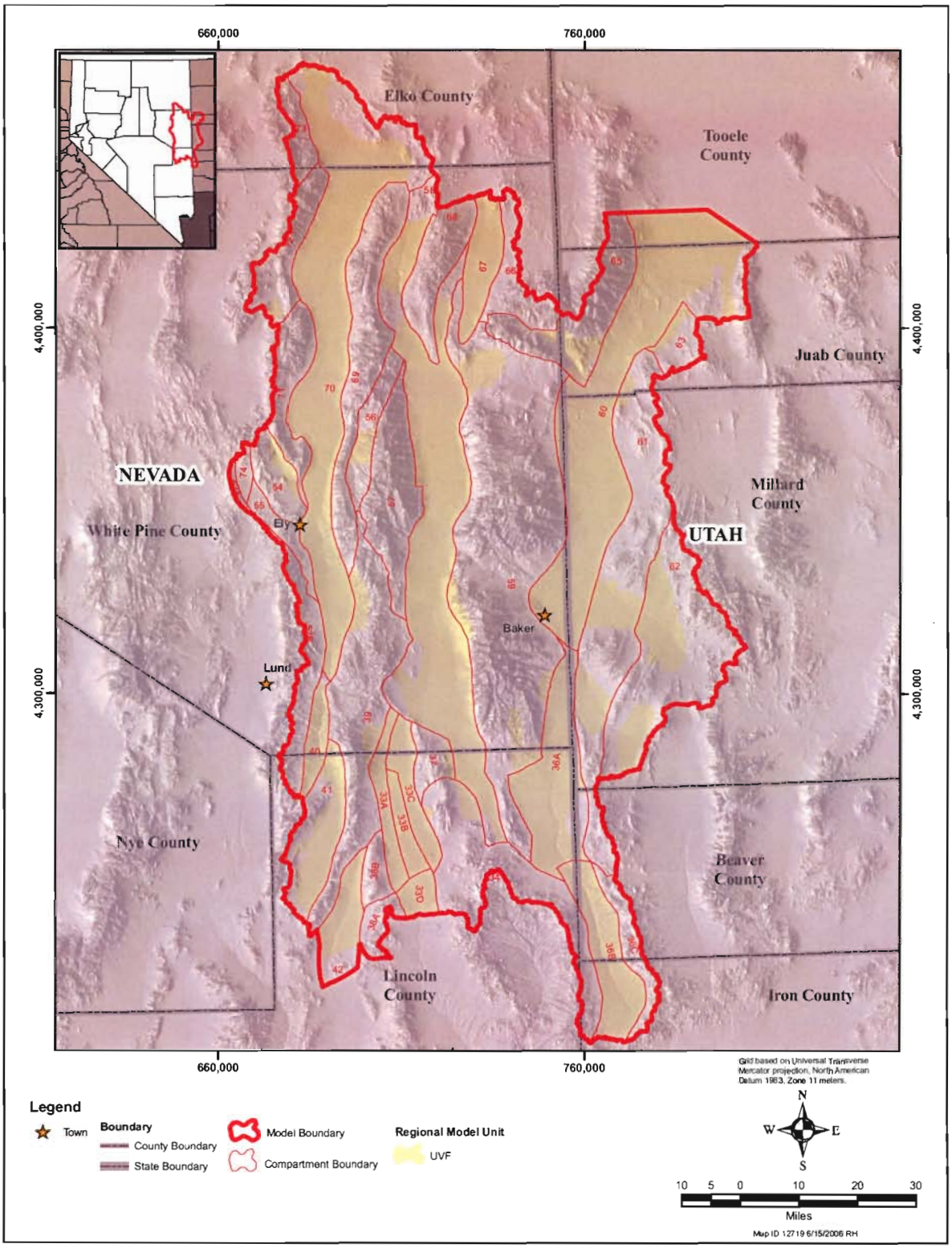

Figure 3-1
Geographic Extents of Hydrogeologic Units: Upper Valley Fill

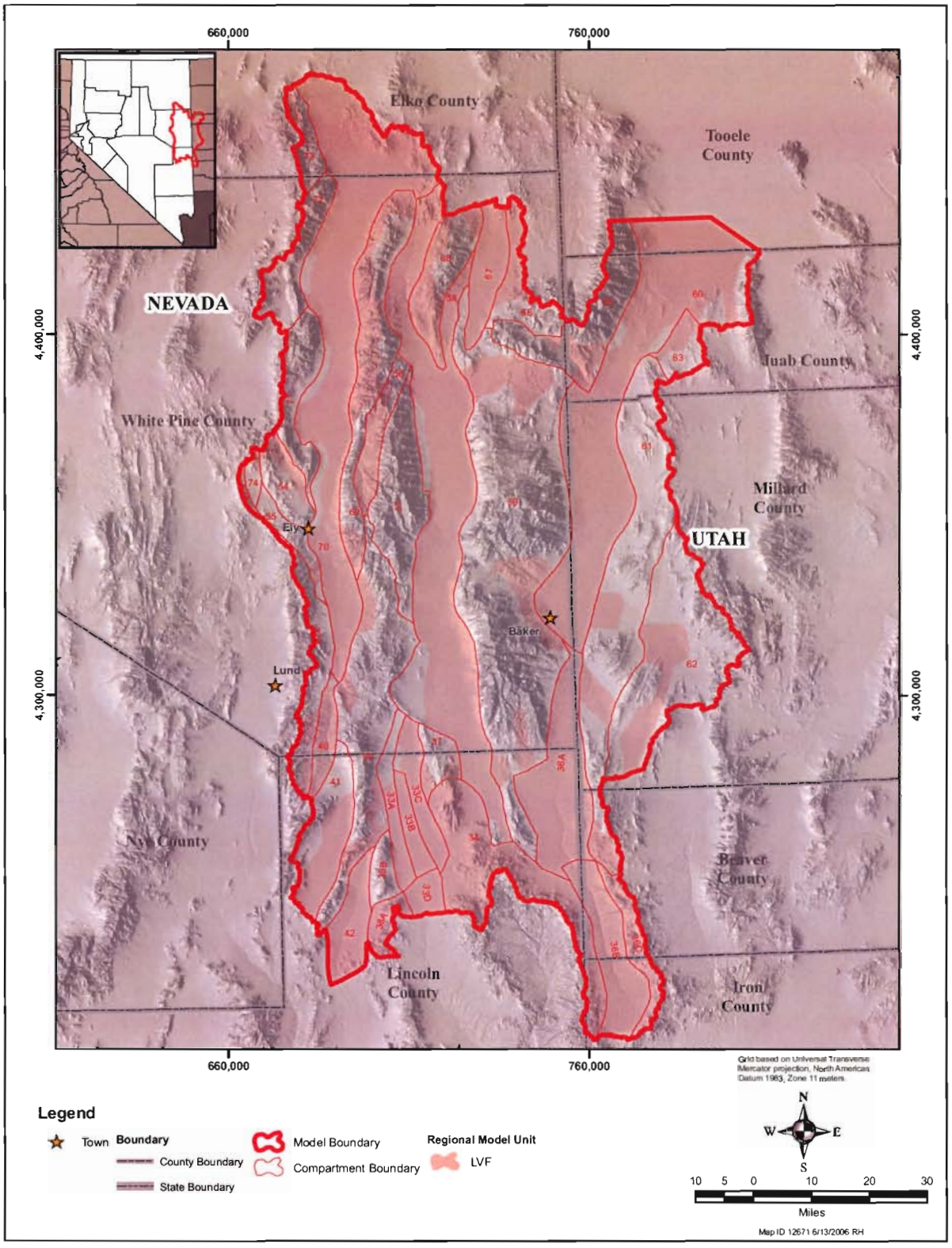

Figure 3-2
Geographic Extents of Hydrogeologic Units: Lower Valley Fill

The carbonate rock RMUs include the upper carbonate RMU and lower carbonate RMU, both of Paleozoic age, each of which are fractured and faulted. At a regional scale, the upper and lower carbonate rocks are moderately to highly permeable. The upper carbonate RMU includes mostly limestones of Permian and Pennsylvanian age. They include the Ely Limestone, Park City Group and other units, and are separated from the lower carbonate rocks by the upper aquitard. The lower carbonate rocks include mostly limestones and dolomites of Mississippian through Cambrian age. They include the Joana Limestone through Pole Canyon Limestone. The Pilot Shale, Eureka Quartzite, and the shales of the Pogonip Group occur within this RMU. Within the Spring Valley area, the upper carbonate rocks are as much as 9,000 ft in thickness and the lower carbonate rocks are as much as 25,000 ft in thickness. The maximum depth to the base of the upper carbonate rocks is about 18,000 ft, and the maximum depth to the base of the lower carbonate rocks is about 32,000 ft. The geographic extent of the upper carbonate rocks is shown on Figure 3-3, and the geographic extent of the lower carbonate rocks is shown on Figure 3-4.

The upper aquitard RMU consists of clastic rocks of Mississippian age. At a regional scale, the upper aquitard is poorly permeable. It includes the Scotty Wash Quartzite, Hamilton Canyon Formation, Chainman Shale, and Peer Spring Formation. However, Chainman Shale is a dominant unit within the upper aquitard. Within the Spring Valley area, the upper aquitard is as much as 6,000 ft in thickness. The maximum depth to the base of the upper aquitard is about 20,000 ft. The geographic extent of the upper aquitard is shown on Figure 3-5.

The basement RMU consists of clastic and metamorphic rocks of Cambrian and Precambrian age. At a regional scale, the basement rocks are nearly impermeable to poorly permeable. The clastic rocks consist mostly of shales and quartzites, including the Pioche Shale, Prospect Mountain Quartzite, and McCoy Creek Group of Cambrian and Precambrian ages. The metamorphic rocks consist of metasediments of Cambrian age. The thickness of the basement rocks is unknown, but it is represented in the model as being 10,000 ft in thickness. The maximum depth to the base of the basement rocks, as represented in the Spring Valley model, is about 40,000 ft. The geographic extent of the basement rocks is shown on Figure 3-6.

The plutonic rock RMU is mostly granitic rocks of Jurassic to Tertiary age. At a regional scale these rocks are poorly permeable. These rocks occur typically within caldera complexes as stocks, dikes, and resurgent domes. The thickness of the plutonic rocks is unknown, but it is assumed to be coincident with the base of the basement rocks at the contact with the plutonic rocks. The maximum depth to the base of the plutonic rocks, as represented in the Spring Valley model, is about 40,000 ft. The geographic extent of the plutonic rocks is shown on Figure 3-7.

3.1.1.1 Identification of Structural Compartments

For the construction of the groundwater model, the modeled area is subdivided into structural compartments as shown on Figure 3-8, where compartment boundaries coincide mostly with important faults within the modeled area (SNWA, 2006c). Where boundary segments coincide with faults, the faults have significant vertical or lateral offsets or have hydrologic importance. However, other boundary segments were located so as to create separate compartments where the fault-based

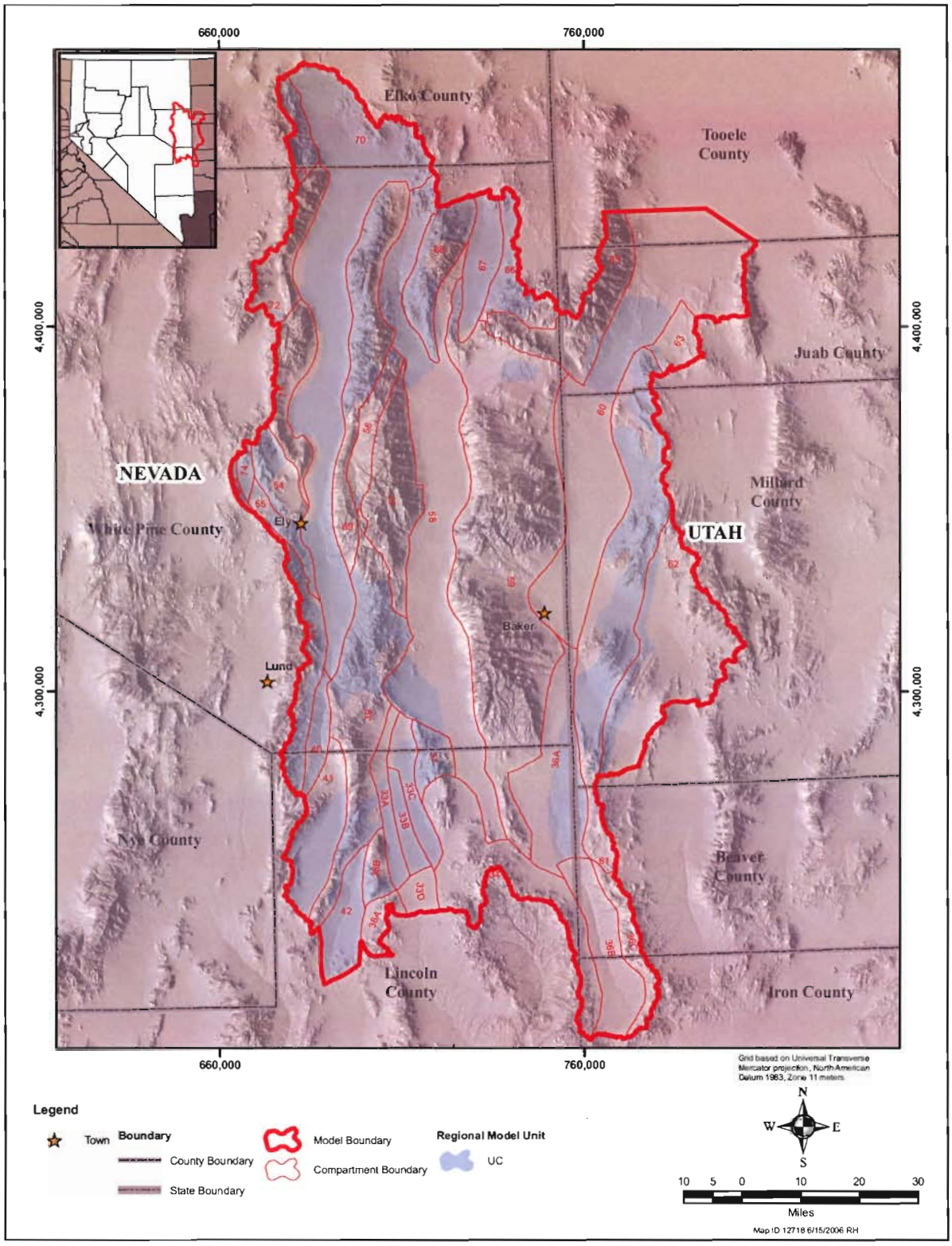

Figure 3-3
Geographic Extents of Hydrogeologic Units: Upper Carbonate Rocks

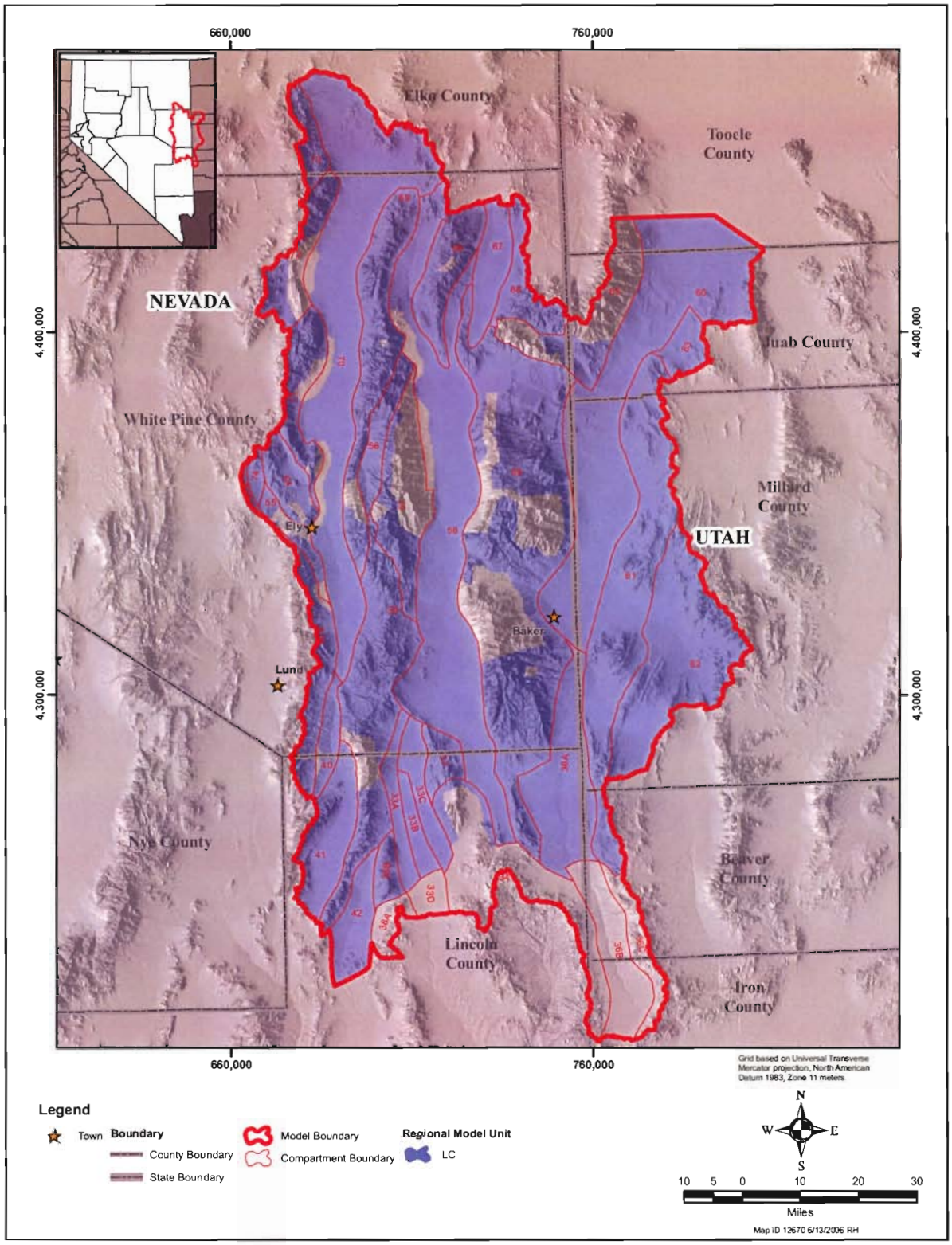

Figure 3-4
Geographic Extents of Hydrogeologic Units: Lower Carbonate Rocks

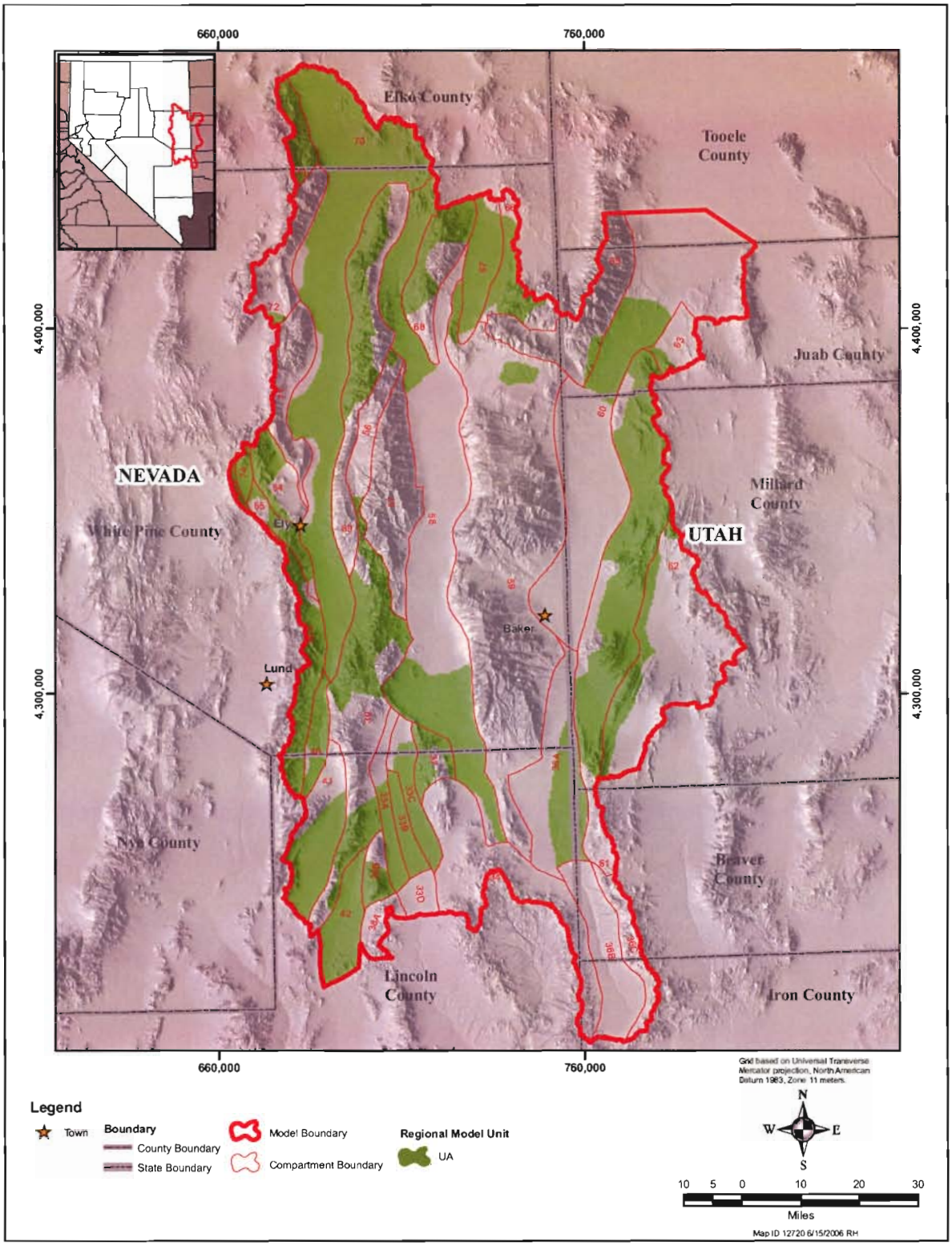

Figure 3-5
Geographic Extents of Hydrogeologic Units: Upper Aquitard

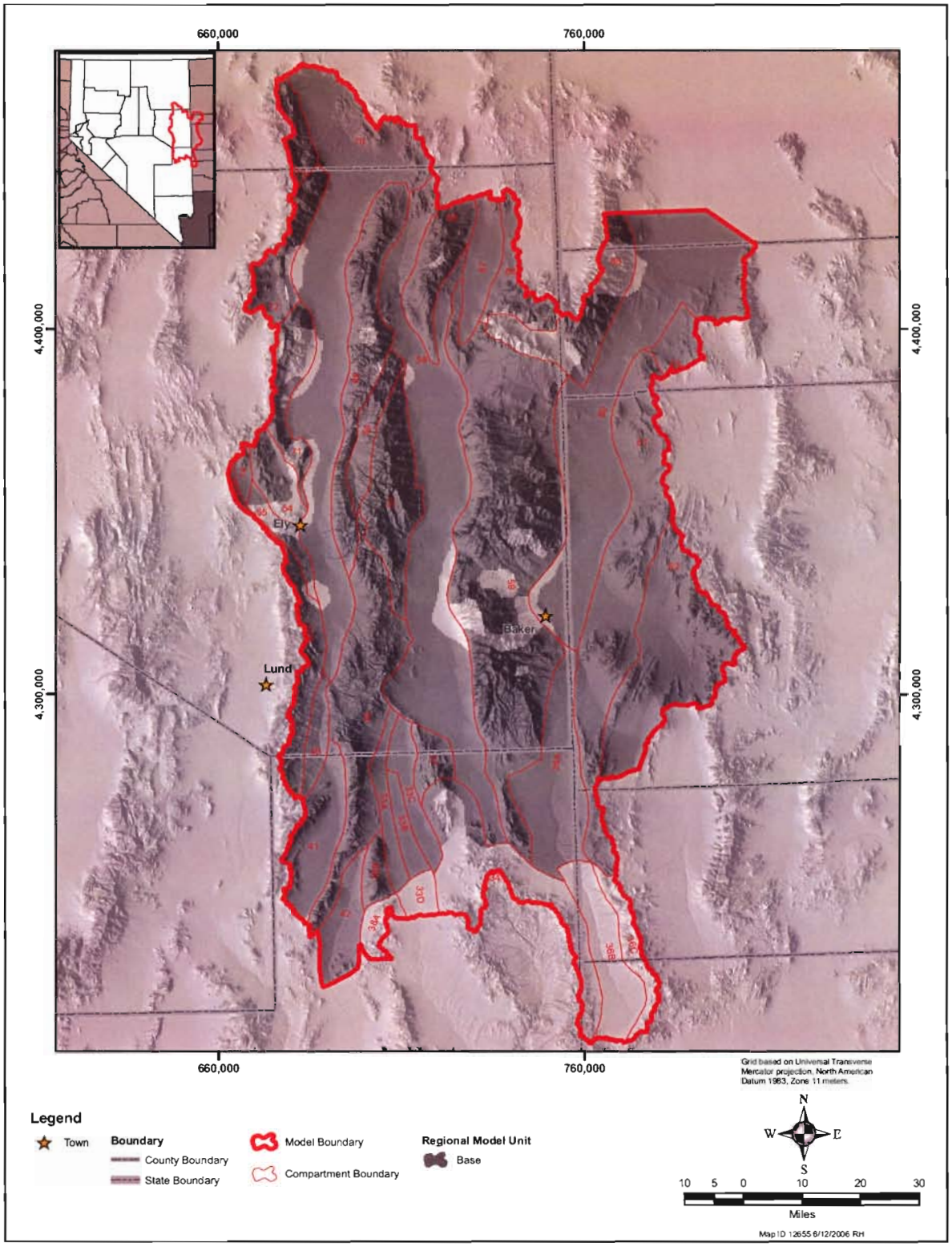

Figure 3-6
Geographic Extents of Hydrogeologic Units: Basement Rocks

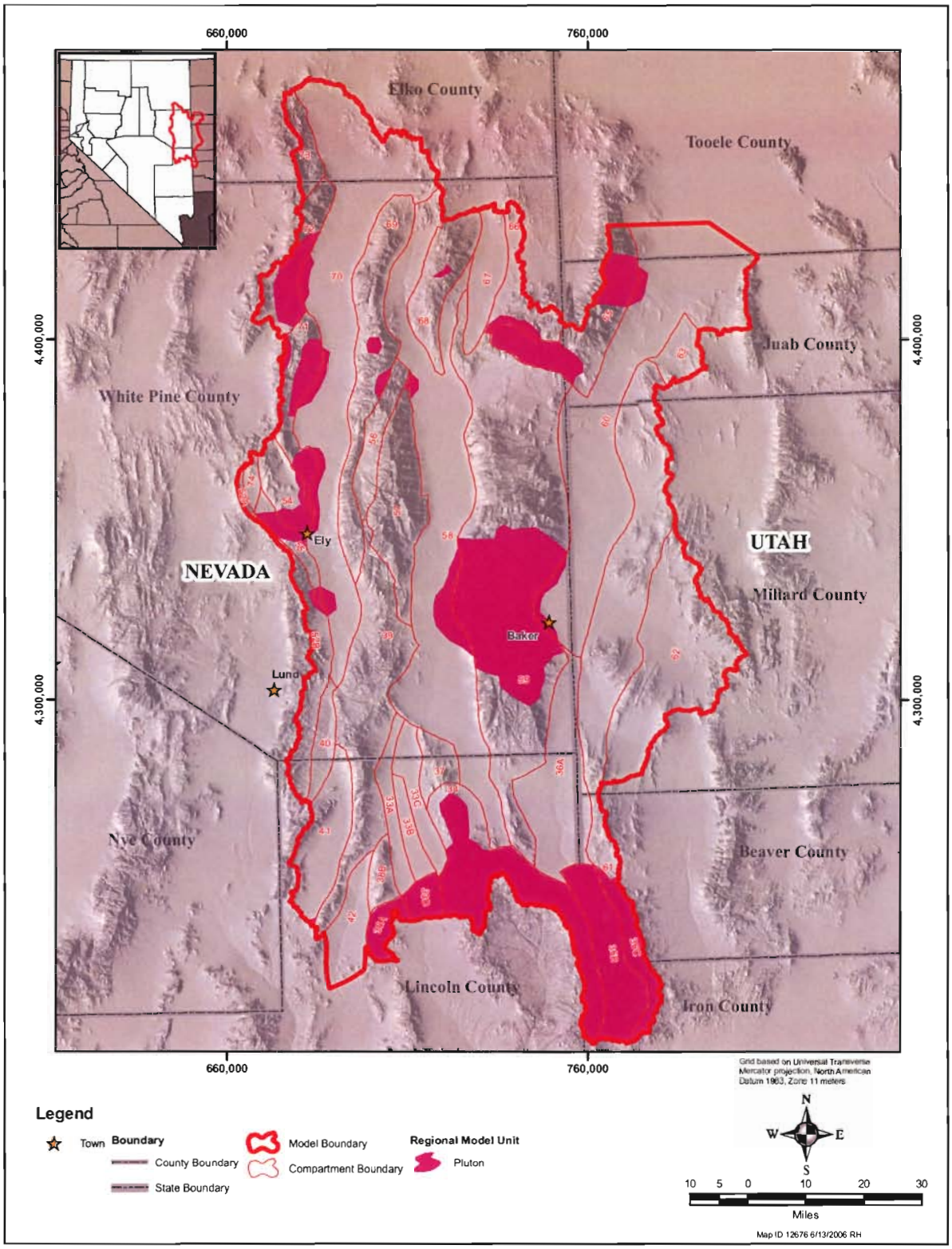

Figure 3-7
Geographic Extents of Hydrogeologic Units: Plutonic Rocks

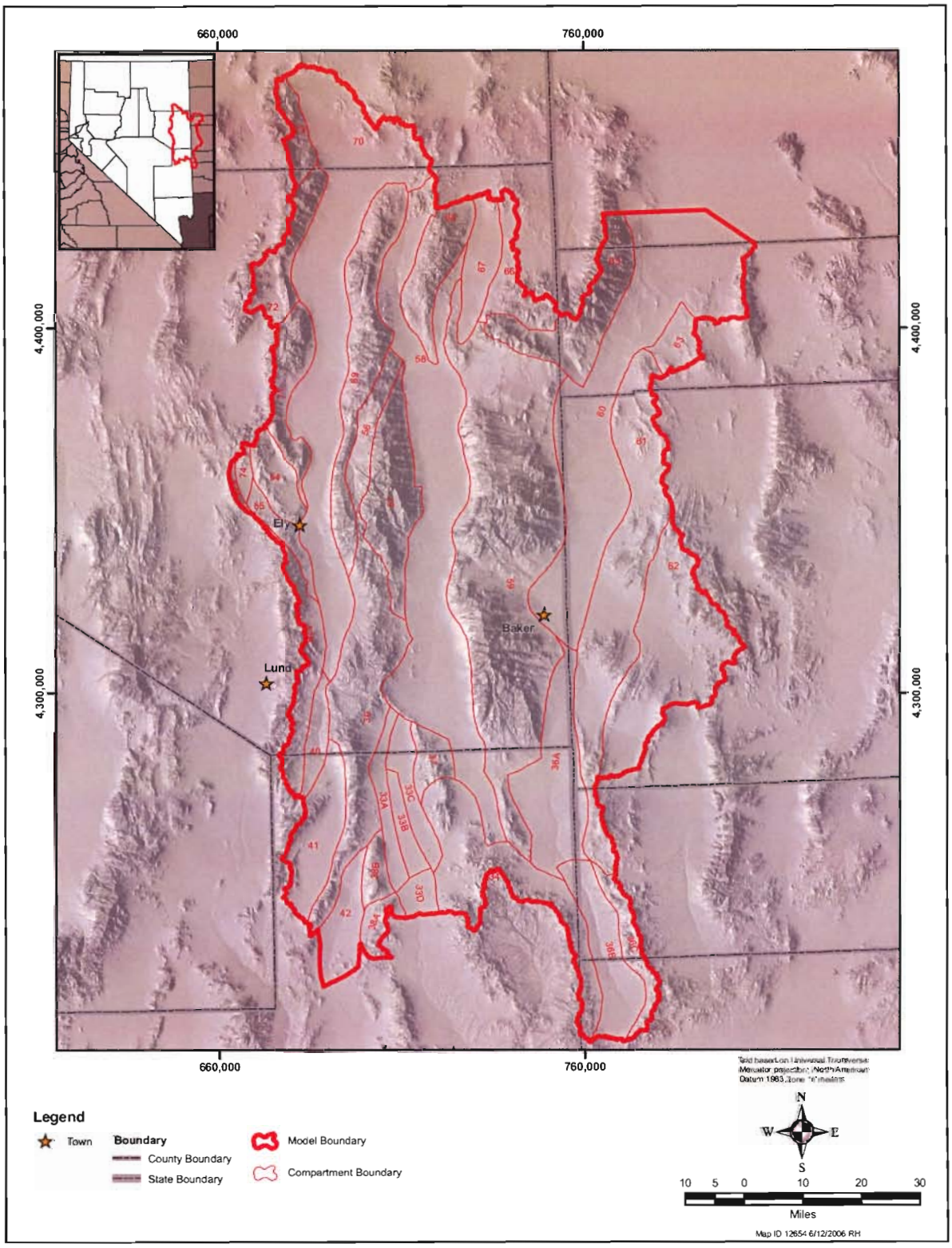

Figure 3-8
Structural Compartments

boundaries are in proximity, but not intersecting. For this situation, a boundary segment is inserted to create a closed compartment polygon where the lateral boundaries are proximate. Still other boundary segments were located to coincide with the margins of the major caldera complexes.

The structural compartments have several purposes in the model. Compartments firstly, are defined in the model to represent lateral or vertical offsets associated with the faults. Figure 3-9 shows a generalized section through adjacent compartments, where the cross section illustrates vertical offsets along the compartment-boundary faults. Because of the offsets, the hydrogeologic units are vertically discontinuous across the modeled area. While the hydrogeologic units are more or less continuous within a compartment, abrupt changes in structural elevations can occur at the faults representing the compartment boundaries. *FEMFLOW3D* accommodates such offsets by making the compartment boundaries coincide with faults representing large offsets.

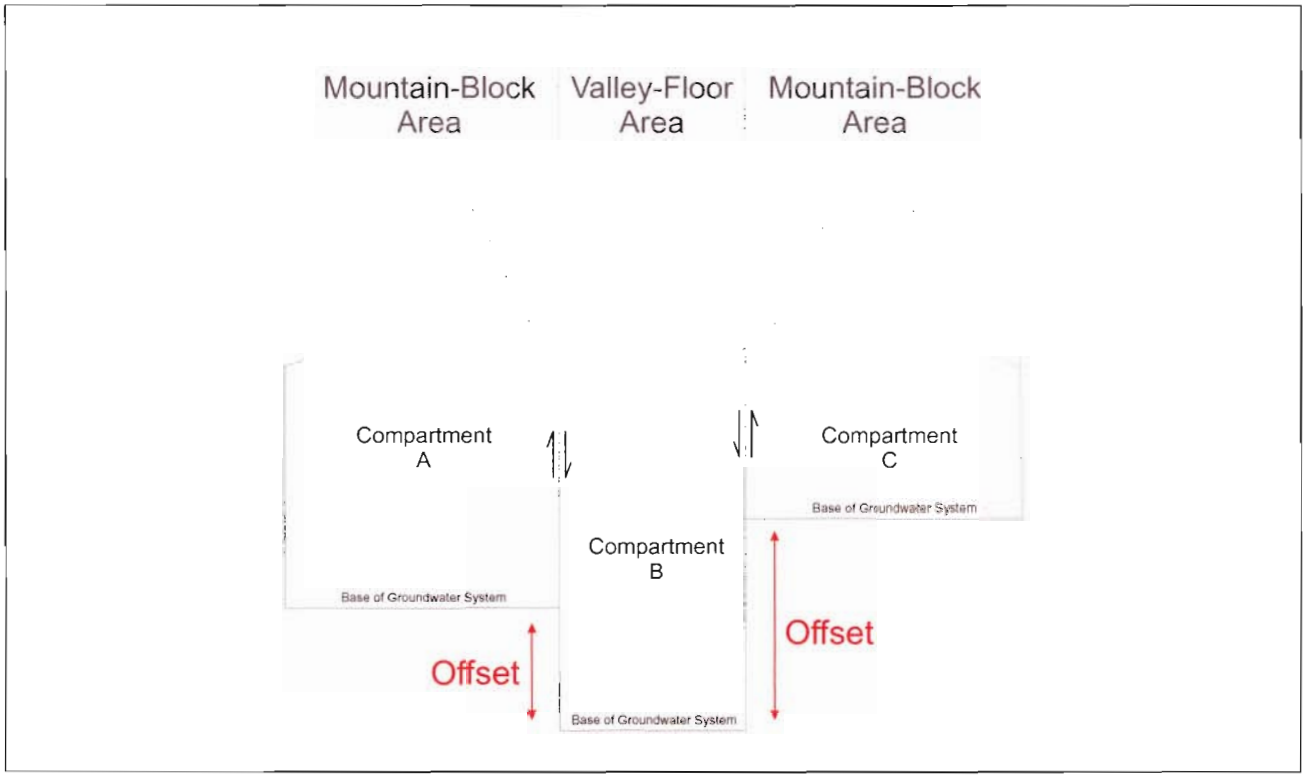

Figure 3-9
Generalized Cross-Section Through Adjacent Compartments

Second, structural compartments are defined in the model to aid in the representation of bimodal groundwater flow (Caine et al., 1996; Kastning, 1977; Faunt, 1997; and Bour and Davy, 1998). One component of groundwater flow occurs within the damage zones of the large-scale faults within the modeled area, where the groundwater flow is essentially two-dimensional. The other component of regional groundwater flow occurs within the structural blocks that occupy the regions between major faults. Within these blocks, groundwater flow occurs in the matrix, fractures, and faults within the individual hydrogeologic units. *FEMFLOW3D* can represent this bimodal groundwater flow by simulating two-dimensional groundwater flow within the compartment-bounding faults,

three-dimensional flow within the compartments themselves, and the groundwater exchanges between the modes.

Third, structural compartments are defined in the model to represent the effect of faults as hydrologic barriers (Antonellini and Aydin, 1994; Heynekamp et al., 1999; Aydin, 1978; Aydin and Johnson, 1978; Bredehoeft, 1997; Sigda et al., 1999). Faults can restrict transverse groundwater flow by juxtaposing a less permeable hydrogeologic unit across a fault with a more permeable unit. The effect is to block groundwater flow in the more permeable unit. Faults also can restrict transverse groundwater flow when the fault zone contains gouge (Heynekamp et al., 1999). Gouge occurs when softer less-permeable beds are dragged along the fault plane. Faults also can restrict transverse groundwater flow when mineral precipitation occurs within the fault zone (Heynekamp et al., 1999). *FEMFLOW3D* can represent these barrier effects by assigning a resistance to transverse groundwater flow across a fault, even when a fault correspondingly is a conduit to groundwater flow.

The model area includes 37 compartments, as shown on Figure 3-8. In general, the principal mountain-front faults are the compartment boundaries. However, some boundary segments represent caldera margins, while still other segments represent the insertion of a boundary to close a compartment polygon.

3.1.1.2 Base Elevations for RMUs

Figure 3-10 through Figure 3-16 show structural contours for each RMU, where the contours represent the elevation at the base of the RMU. Separate contour maps were developed for each structural compartment, and the figures represent the compilation of the contour maps for individual compartments into a contour map for the model area. The compartmental contour maps were developed in part from the hydrogeologic cross sections developed by SNWA (2006c). The locations for the cross sections are shown on Figure 2-1. First, the cross sections were translated from hydrogeologic units to RMUs according to Table 3-1. Second, the lines representing the bases of each RMU on the translated cross section, which have the same jaggedness as shown on the hydrogeologic cross sections, were approximated as a smooth line. Third, additional smoothed cross sections were created to supplement the cross sections developed by SNWA (2006c). Finally, original and supplemental cross sections were use to develop the contour maps.

3.1.2 Construction of Model Meshes

The finite-element mesh for the model consists of individual compartment meshes and a fault mesh. Within *FEMFLOW3D*, the compartment meshes are assembled into an overall mesh. *FEMFLOW3D* automatically outputs a file that can be used for viewing the assembled compartment meshes in Groundwater Modeling System (GMS), which is a computer program developed for the U.S. Corps of Engineers (Environmental Modeling Research Laboratory, 2005) for facilitating the development and use of groundwater models. The *FEMFLOW3D* output file has the extension ".3dm". *FEMFLOW3D* also automatically outputs a file for viewing the fault mesh in GMS, which has the extension ".2dm".

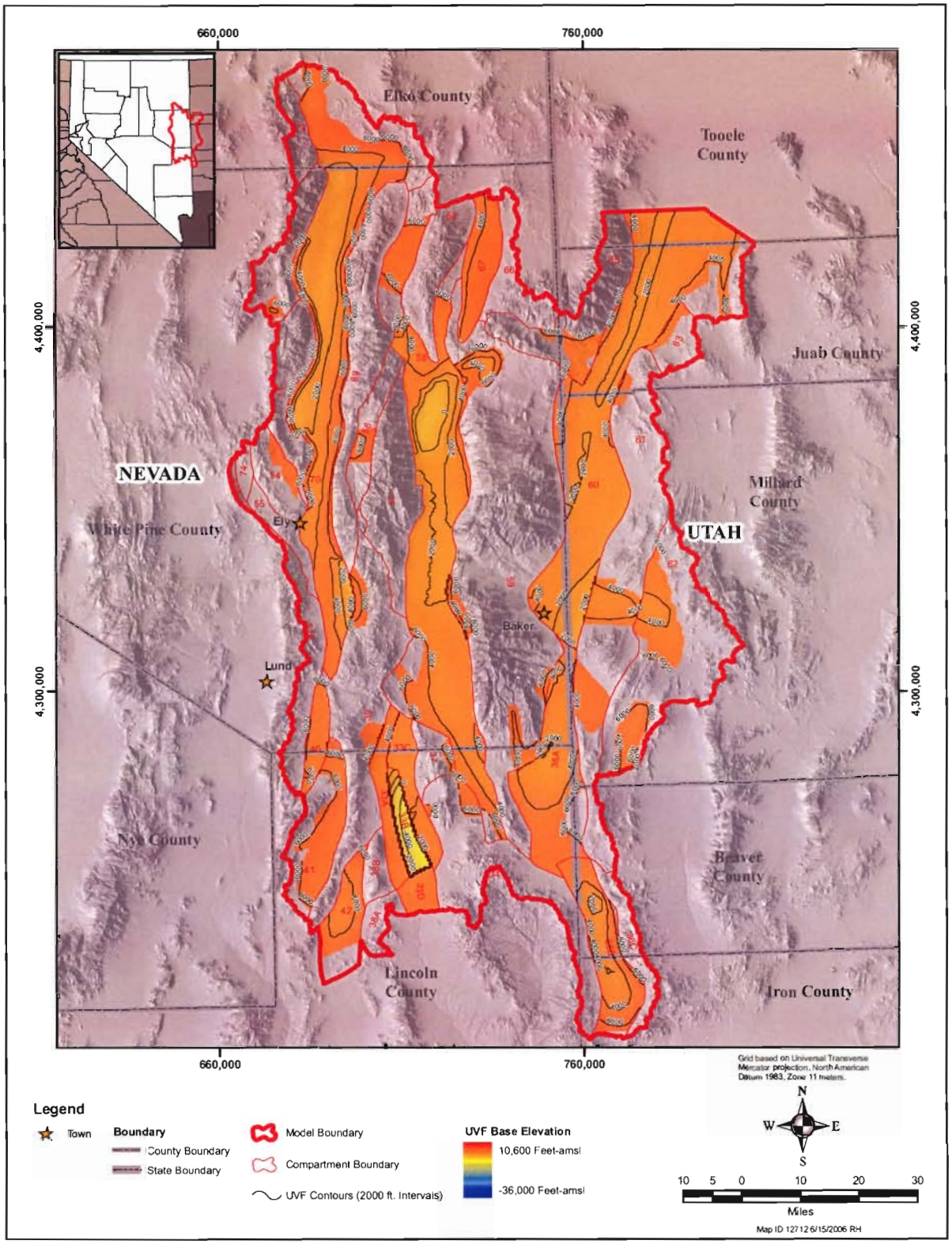

Figure 3-10
Base Elevations For Hydrogeologic Units: Upper Valley Fill

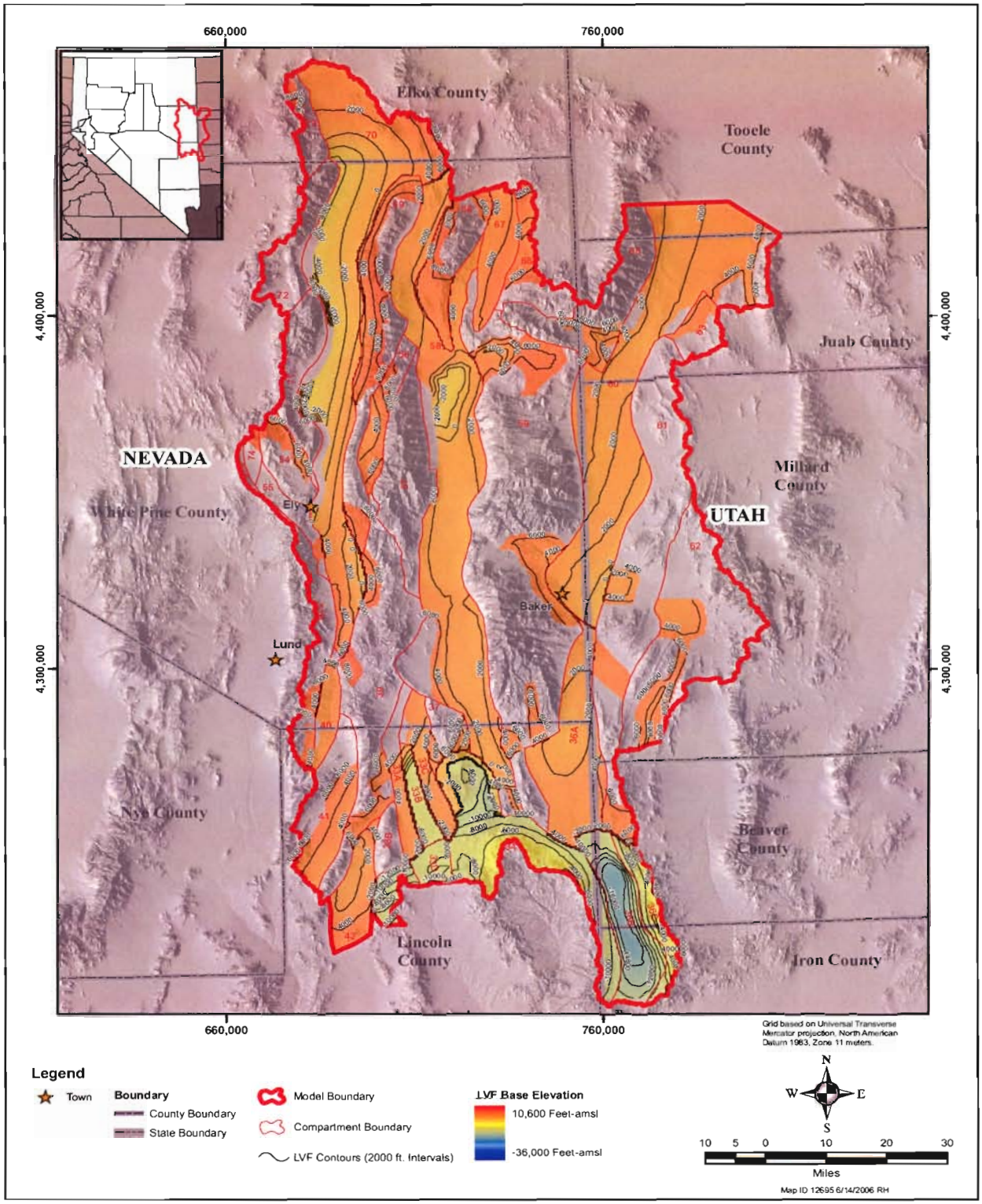

Figure 3-11
Base Elevations for Hydrogeologic Units: Lower Valley Fill

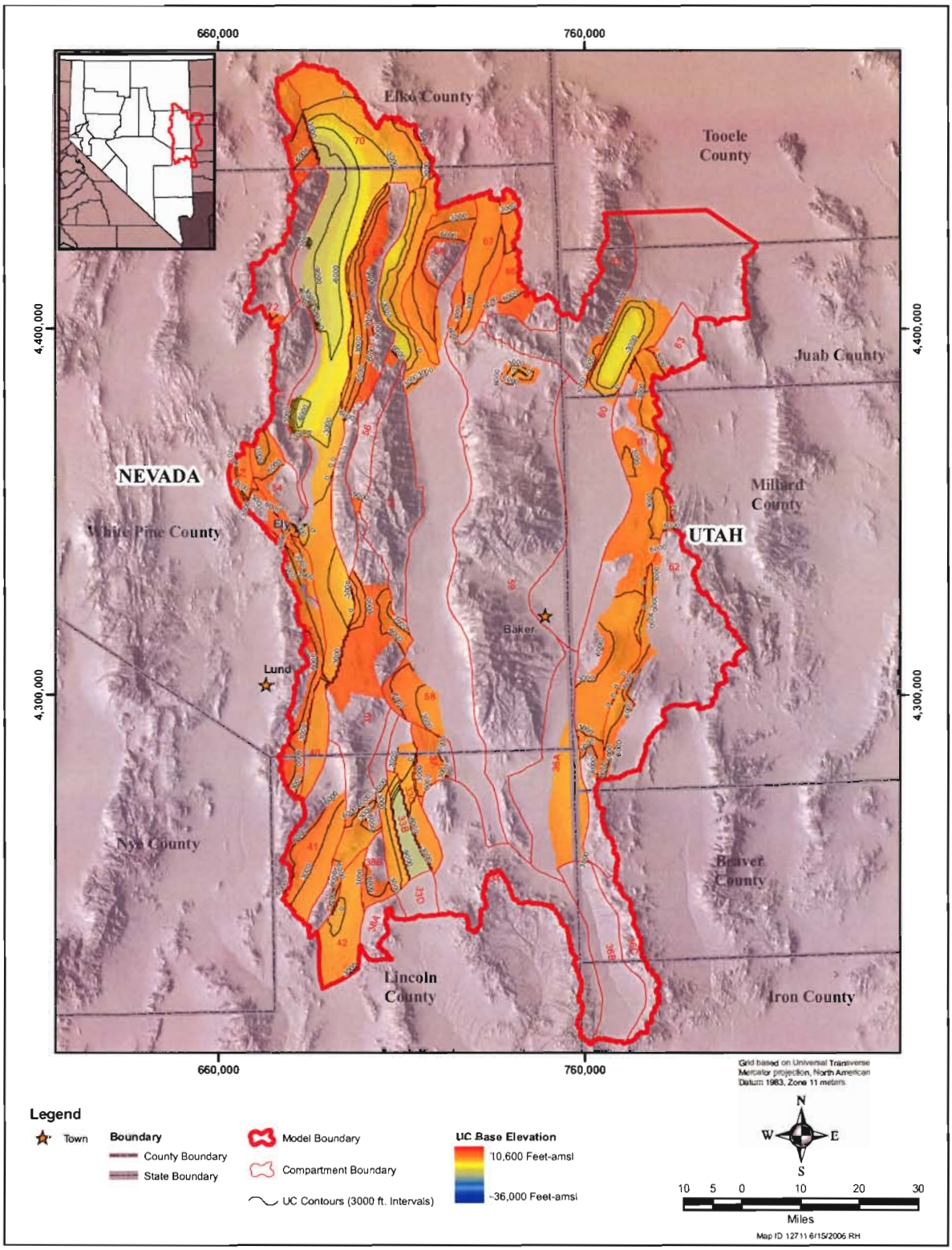

Figure 3-12
Base Elevations for Hydrogeologic Units: Upper Carbonate Rocks

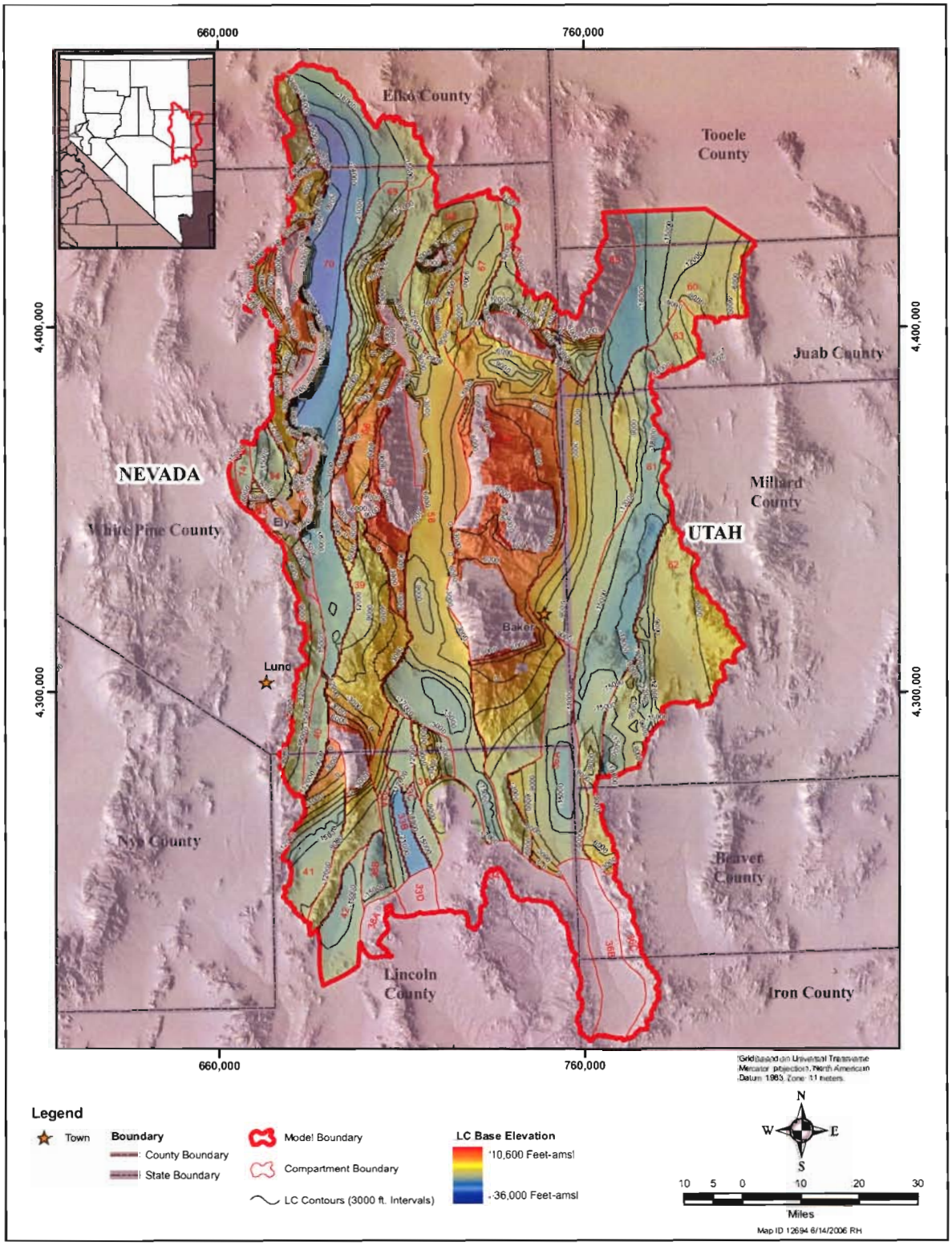

Figure 3-13
Maps Showing Base Elevation for Hydrogeologic Units: Lower Carbonate Rocks

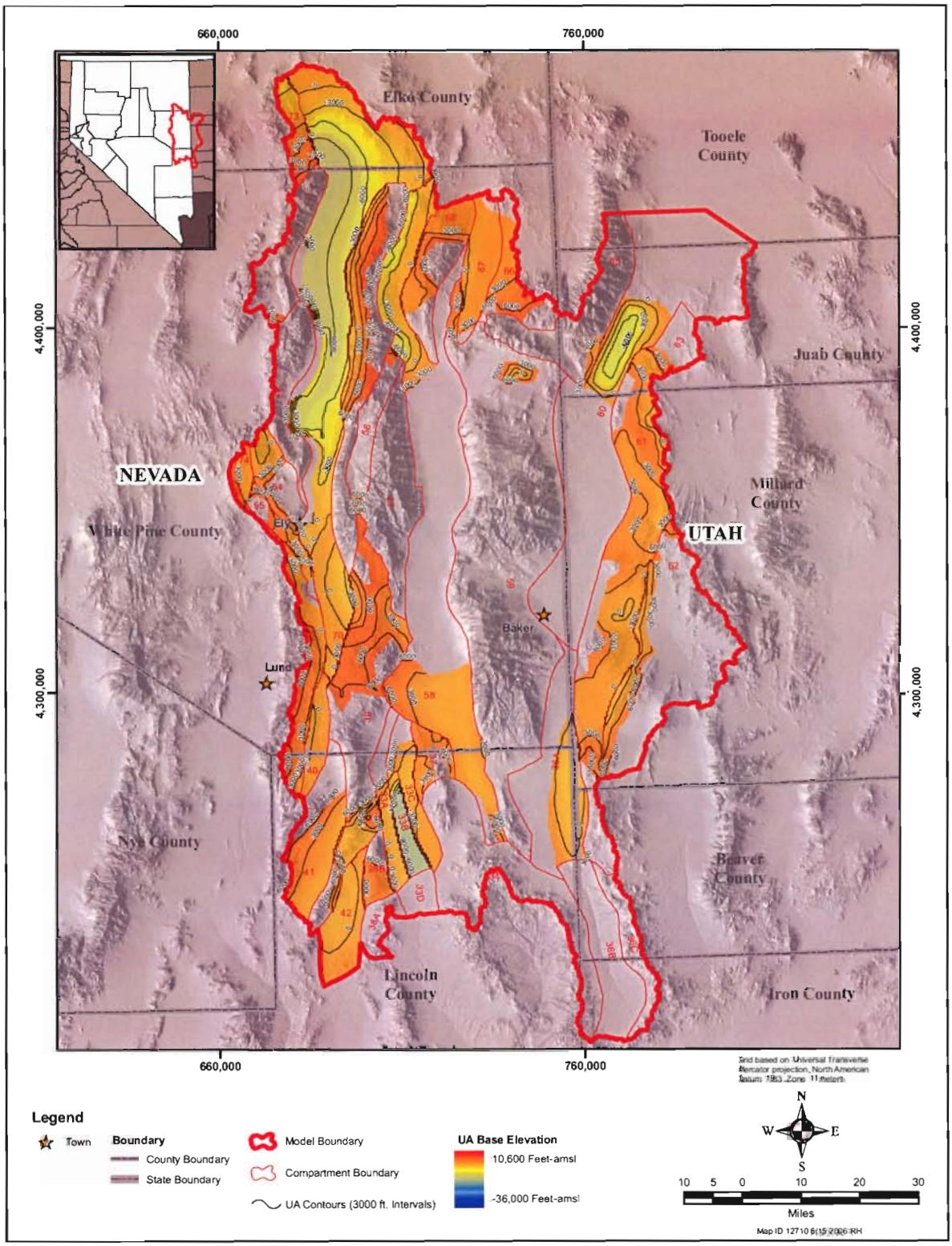

Figure 3-14
Maps Showing Base Elevations for Hydrogeologic Units: Upper Aquitard

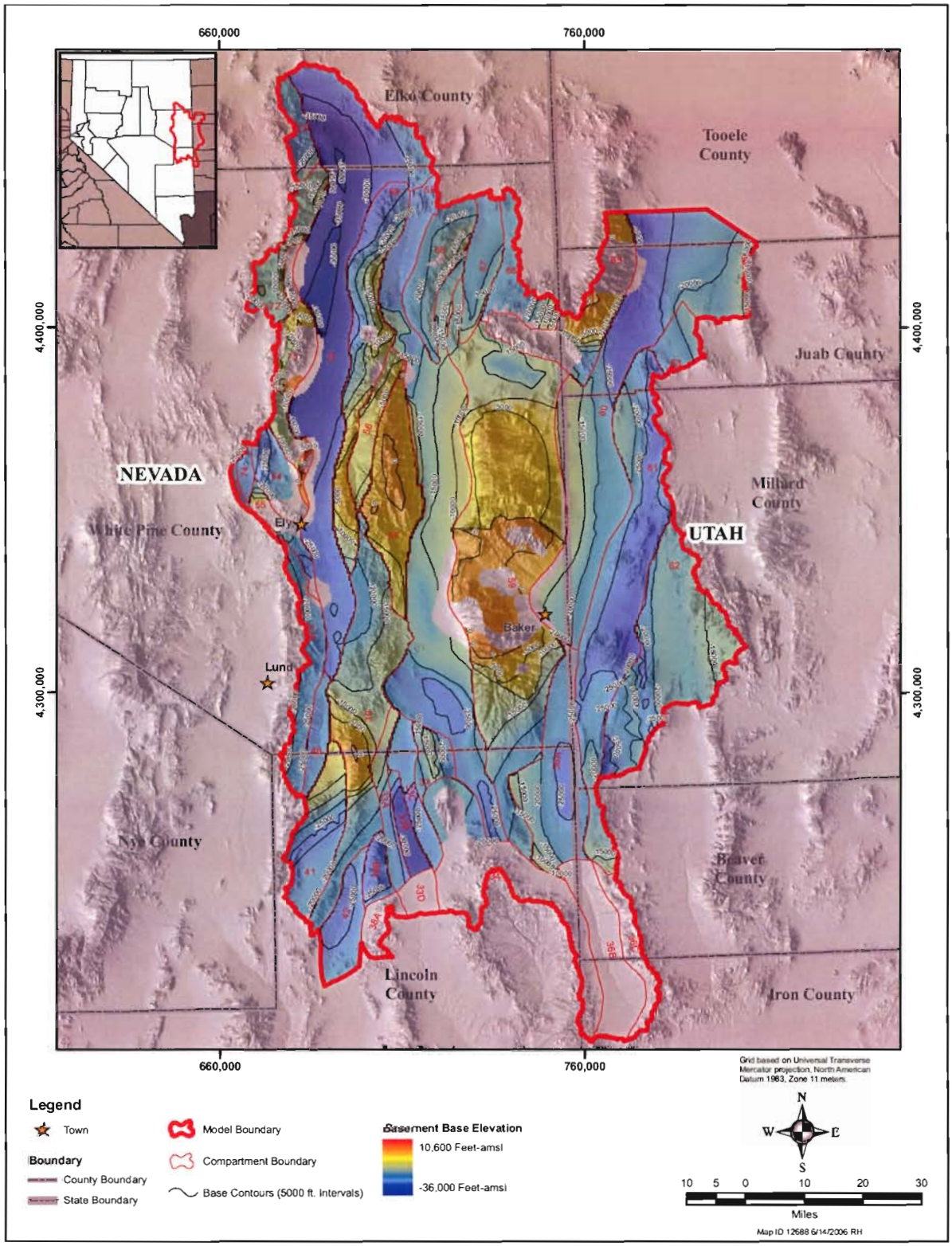

Figure 3-15
Maps Showing Base Elevations for Hydrogeologic Units: Basement Rocks

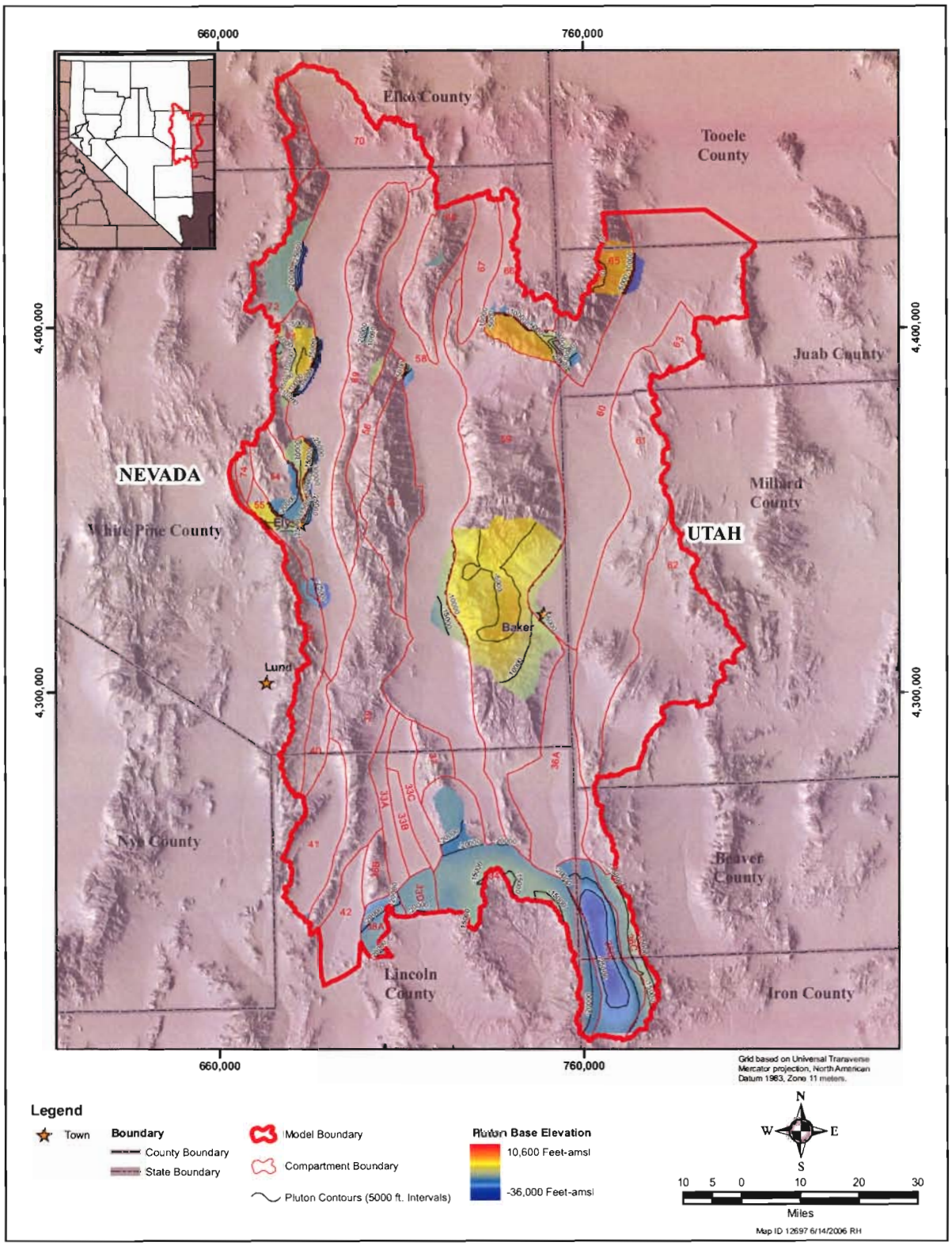

Figure 3-16
Maps Showing Base Elevations for Hydrogeologic Units: Plutonic Rocks

3.1.2.1 Three-Dimensional Compartment Meshes

The RMUs within a compartment are represented by a three-dimensional finite-element mesh. As an example, the mesh for compartment 67 is shown on Figure 3-17 and Figure 3-18, which respectively show plan and oblique views of the mesh. The mesh is comprised of an assemblage of wedge elements, where a typical element is shaped as a blunt wedge, as illustrated on Figure 3-19. The triangular faces of a wedge form the top and bottom of the element. The top and bottom surfaces can deviate from horizontal to represent the local slope of a hydrogeologic structural surface. The quadrilateral faces form vertical sides to the element. Using the vernacular of finite-element modeling, the volume enclosed by the surfaces of the wedge is referred to as an element, and the vertices of the wedge are referred to as nodes.

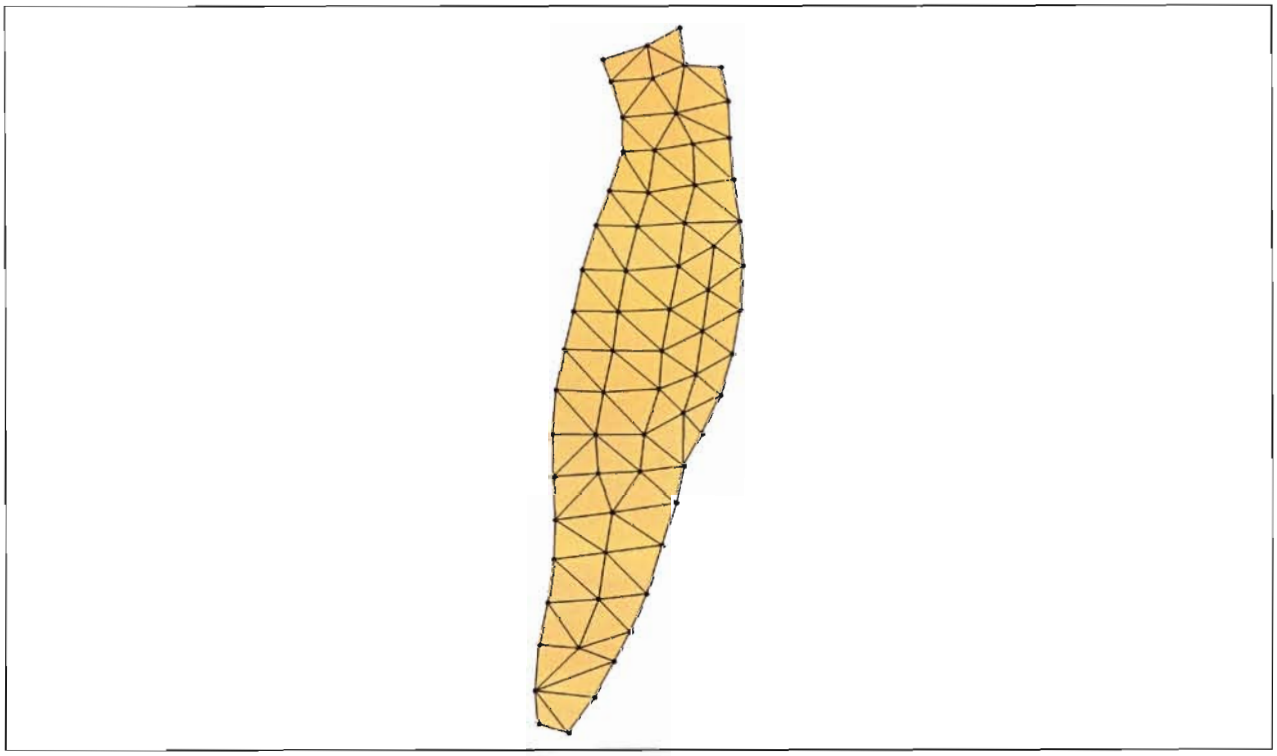

Figure 3-17
Finite-Element Mesh for Compartment 67: Plan View

Within compartment 67, three RMUs pinch out within the compartment. This occurs for the upper carbonate rock, lower carbonate rock, and upper aquitard RMUs. The pinchout of the upper carbonate rock is exposed on the eastern vertical surface of the compartment as shown on Figure 3-18. Those and other pinchouts are accommodated in the finite-element mesh using wedge elements with zero-height edges as shown on Figure 3-20 and Figure 3-21. Elements with zero-height edges retain triangular top and bottom surfaces. However, while an element with one zero-height edge retains three vertical surfaces, two of those surfaces are transformed from quadrilaterals to triangles. An element with two zero-height edges has only two vertical surfaces, and both are a triangle.

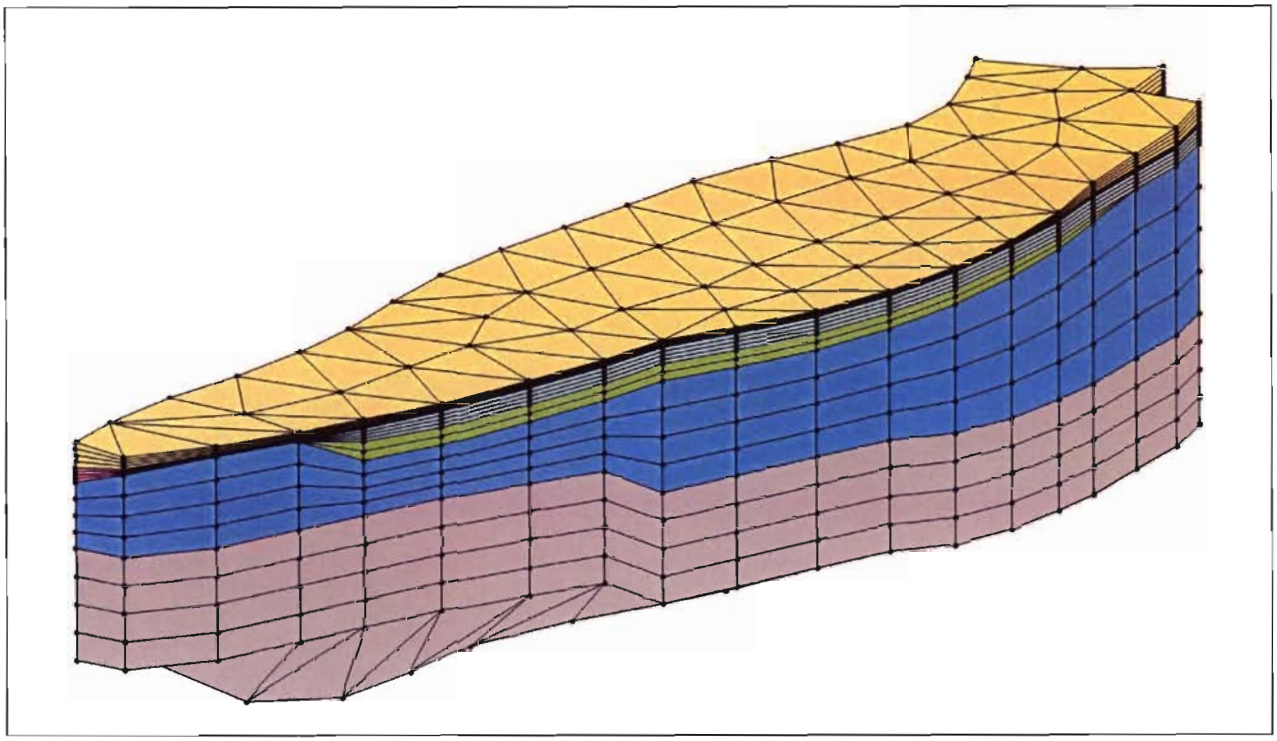

Figure 3-18
Finite-Element Mesh for Compartment 67: Oblique View

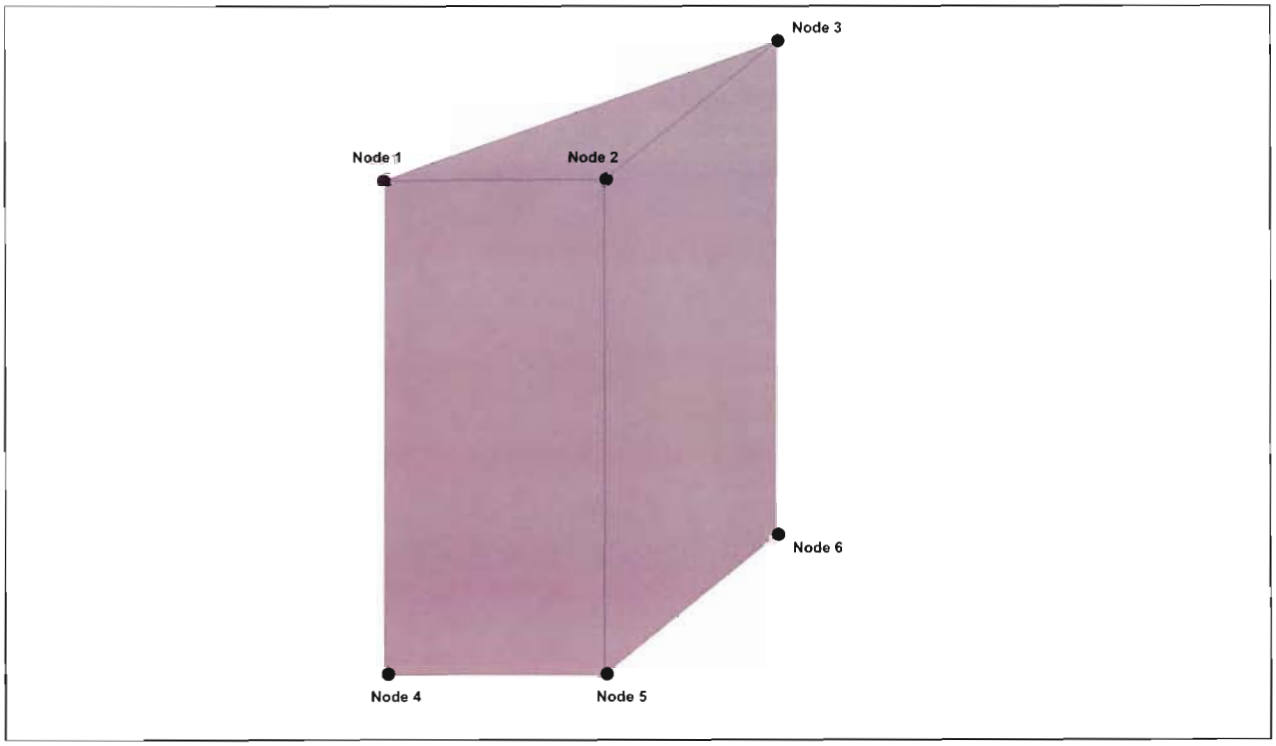

Figure 3-19
Wedge Element Used in Finite-Element Mesh

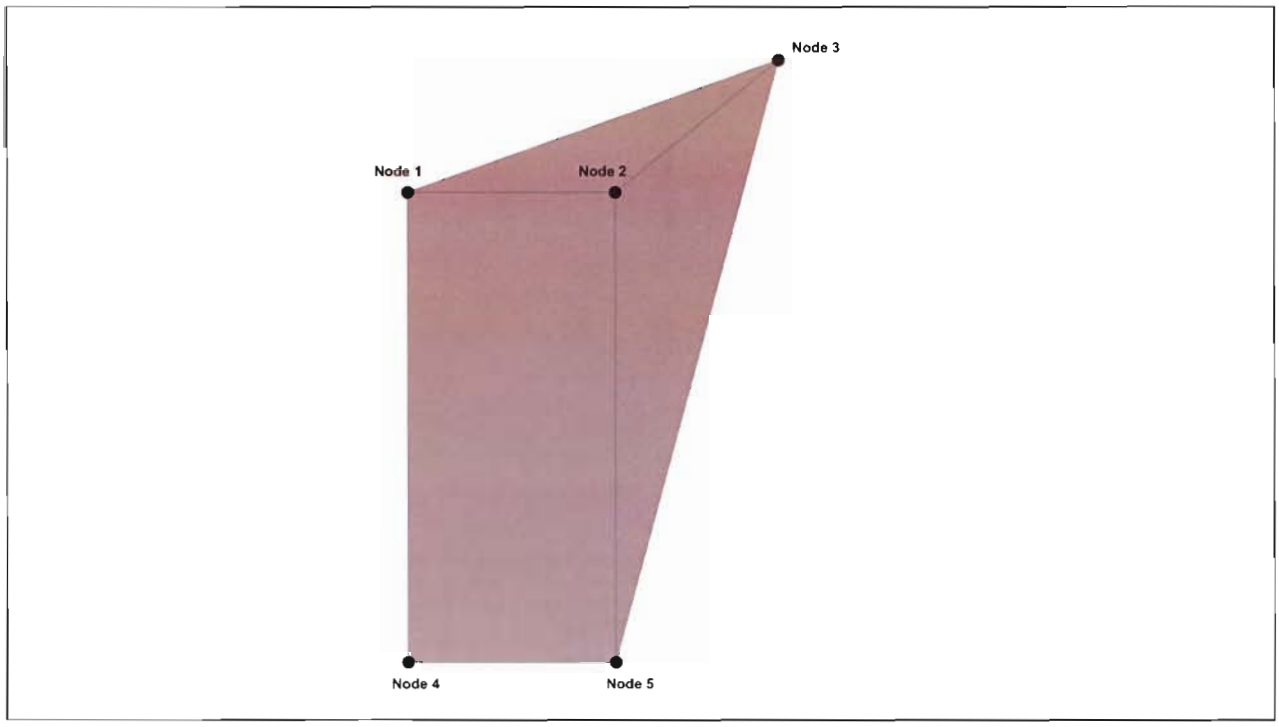

Figure 3-20
Wedge Elements With One Zero-Height Edge

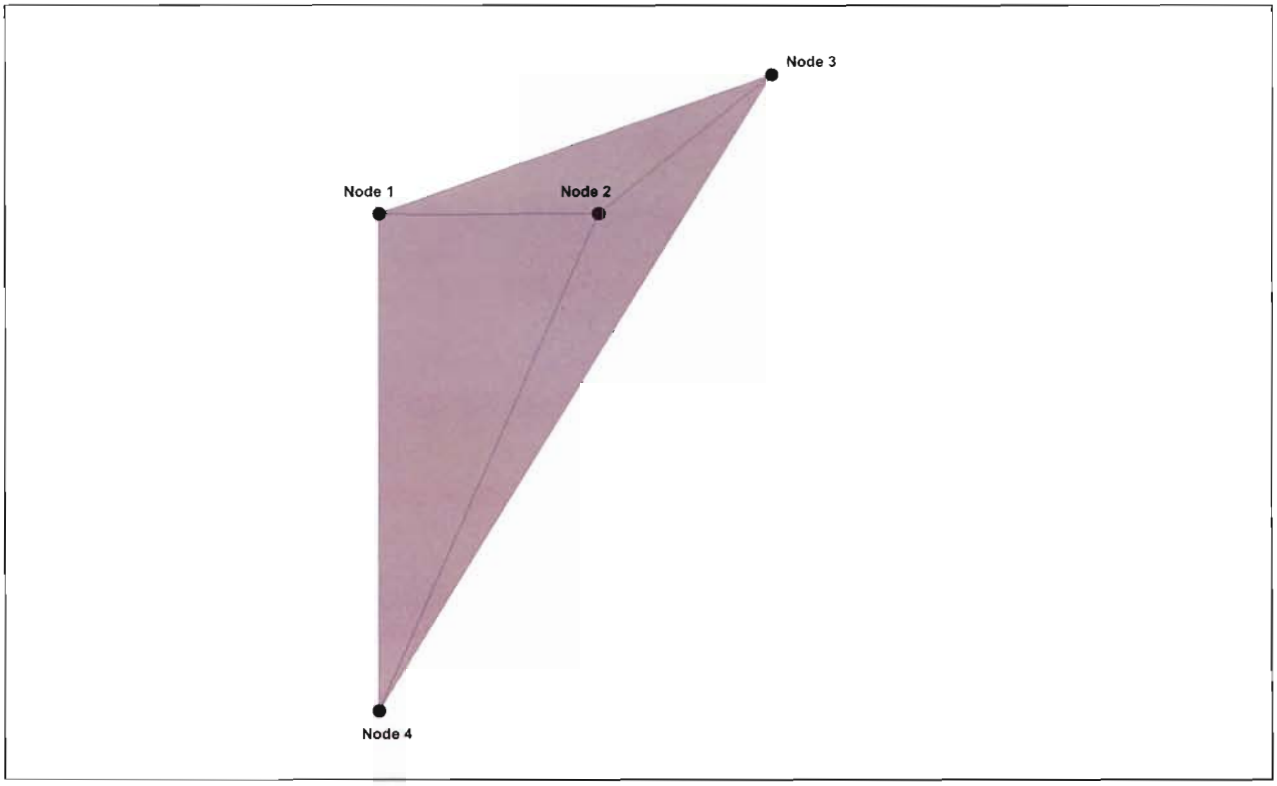

Figure 3-21
Wedge Elements With Two Zero-Height Edges

The mesh structure for compartment 67 and the other compartments has the wedge elements arranged in layers. Each RMU is represented by four layers except for the upper aquitard, which is represented by two layers. The element layers are not horizontal. While the top surface of the upper-most element layer for a particular RMU coincides with top of the unit, the bottom surface of the lower-most element layer coincides with the base of the RMU. The layer surfaces intermediately between the top and base of the hydrogeologic unit are specified so as to subdivide the local thickness of the unit into equal intervals.

The construction of a compartment mesh involves specifying the position and shape of each element within a three-dimensional space. The shape and location of an element is described by specifying which nodes occur at the vertices of a particular wedge element. The three-dimensional location of the nodes in turn is described by specifying the x, y, and z coordinates for a particular node. GMS, GIS software, and other tools were used to construct the meshes. The basic use of these tools was to construct contour maps of the base elevations for each RMU, to construct a two-dimensional map of the finite-element mesh, and to expand the two-dimensional mesh to a three-dimensional mesh based on the contour maps. This approach was repeated for each compartment.

The mesh assembled from the individual compartment meshes is shown on Figure 3-22, Figure 3-23, and Figure 3-24. The mesh is comprised of about 101,000 elements and 68,000 nodes. Figure 3-22 shows the triangular faces of the wedge elements exposed on the upper surface of the mesh. A typical element has a length of 8,000 ft along the side of a triangle. Figure 3-23 and Figure 3-24, respectively, show oblique views of the mesh from the southwest and southeast. Figure 3-25 and Figure 3-26 show cross sections through the mesh, where the section locations are shown on Figure 2-1.

3.1.2.2 Two-Dimensional Fault Meshes

The inter-compartmental faults are represented in *FEMFLOW3D* as two-dimensional vertical features. Correspondingly, a two-dimensional finite-element mesh represents a fault. As shown on Figure 3-27, the faults occurring along the compartment boundaries are included explicitly in the groundwater model. These are the principal faults within the modeled area with respect to vertical or lateral displacements, and they are the principal faults with respect to the potential for groundwater flow within faults. Other faults occur within the modeled area, but they are not represented explicitly within the groundwater model.

The relationship of a fault to the adjacent compartments is shown diagrammatically on Figure 3-28. Figure 3-28 shows a fault segment along the shared boundary of two compartments, a cross sectional perpendicular to the fault, and an oblique view of the fault and adjacent compartments that have been pulled apart to reveal the fault. These three views show two relationships between the fault and adjacent compartments. First, for a compartment node located on a compartment boundary, a compartment node occurs in the adjacent compartment with the same x and y coordinates. Second, for the matched inter-compartmental nodes, fault nodes occur with the same x and y coordinates. Further, a column of fault nodes occurs at the location of the matched inter-compartmental nodes, and

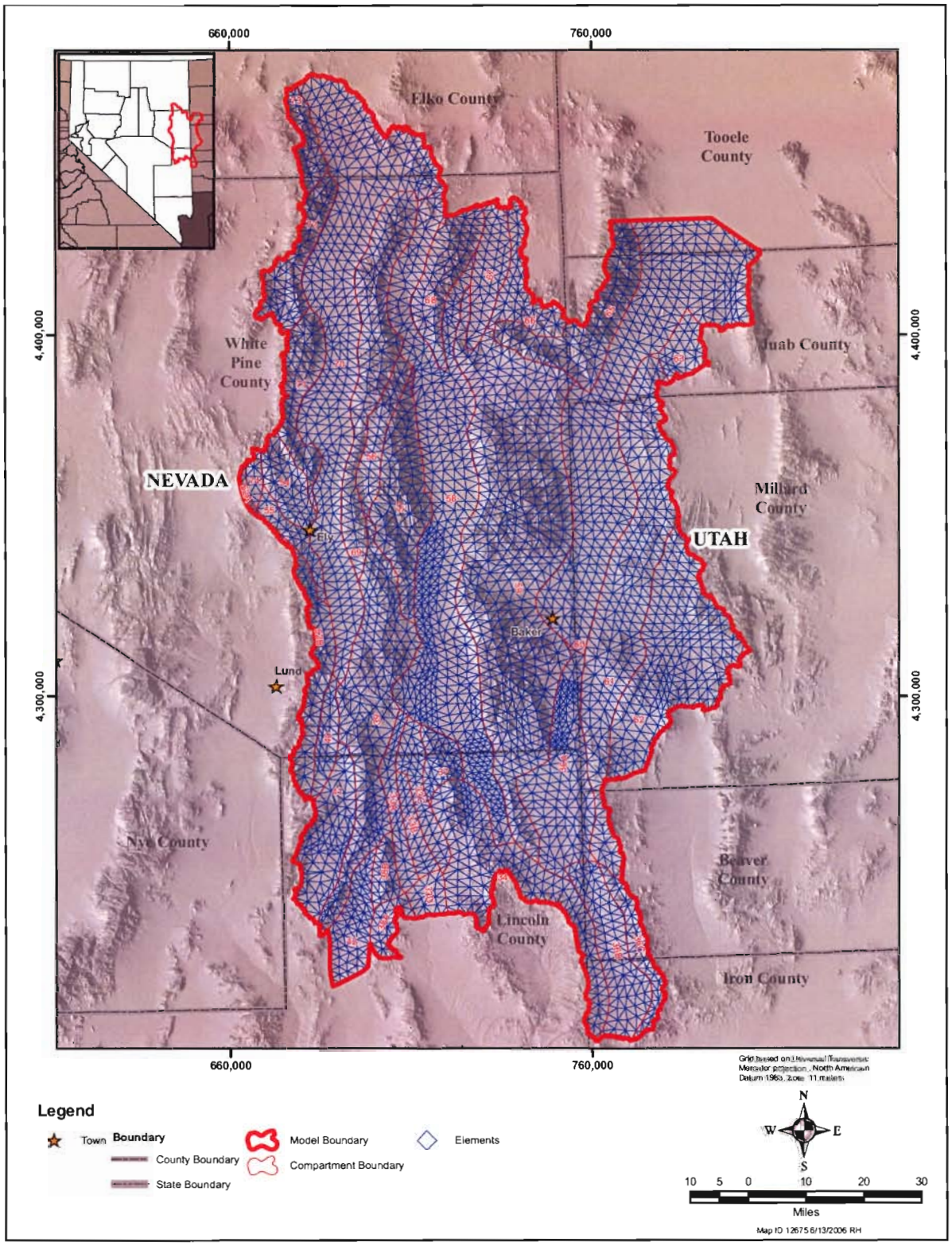

Figure 3-22
View of Finite-Element Mesh

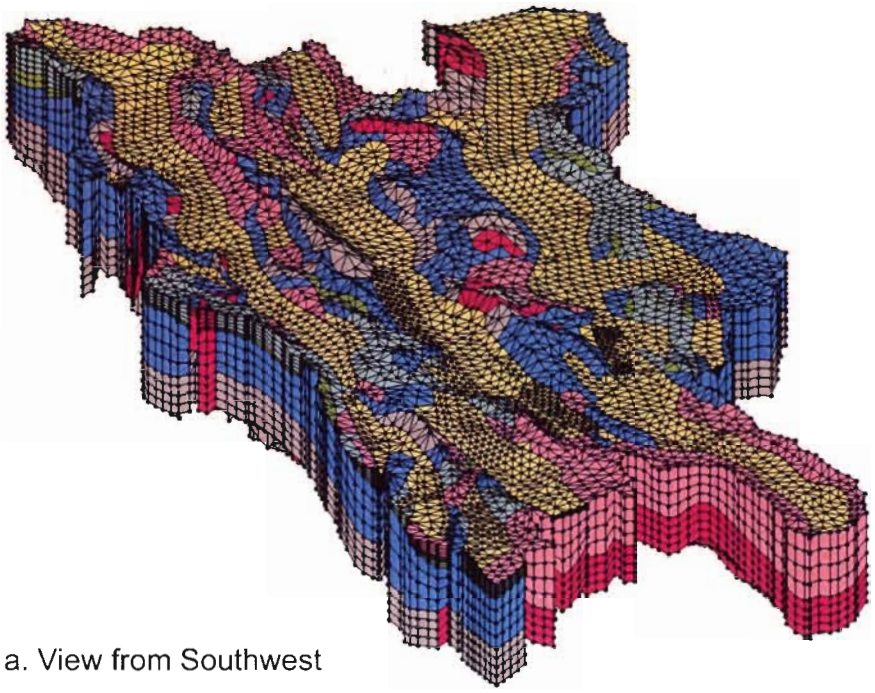

a. View from Southwest

Figure 3-23
Oblique View of Finite-Element Mesh: View from Southwest

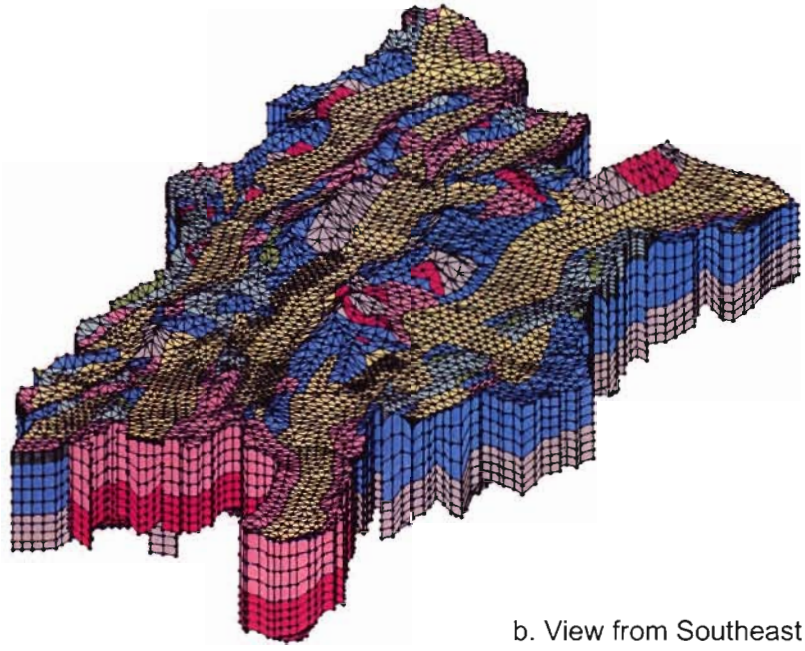

b. View from Southeast

Figure 3-24
Oblique View of Finite-Element Mesh: View from Southeast

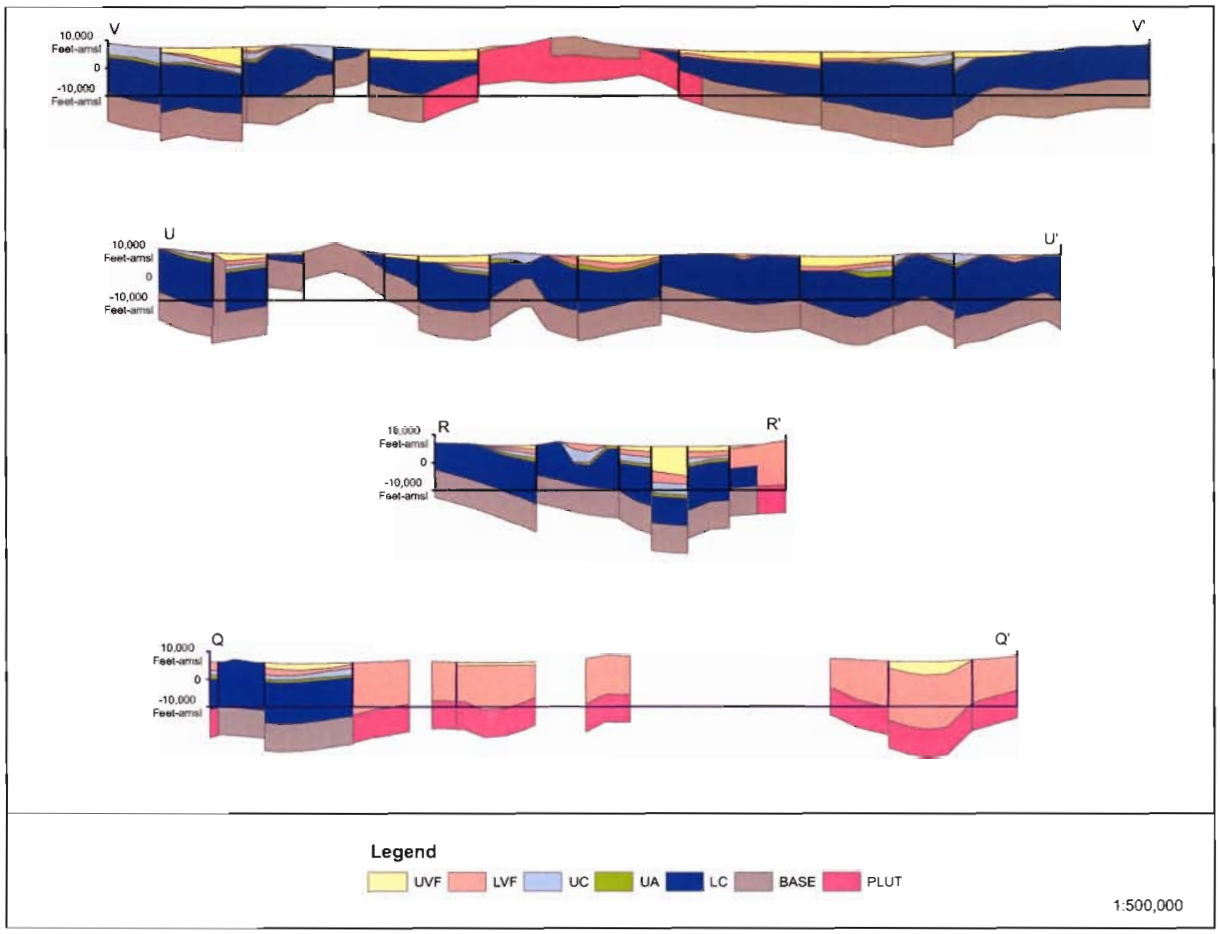

Figure 3-25
Cross Sections Through Three-Dimensional Mesh: Sections V, U, R, and Q

these columns form the basic skeleton of the fault mesh. The fault columns are used to construct a two-dimensional fault mesh by defining triangles to fill the regions between the node columns.

The faults for the groundwater model consist of 78 fault segments corresponding to each boundary segment shown on Figure 3-27. Figure 3-29 shows an oblique view of the corresponding fault mesh. The fault mesh contains 17,000 elements and 9,000 nodes. Including both the compartment and fault meshes, the model has about 118,000 elements and 76,000 nodes.

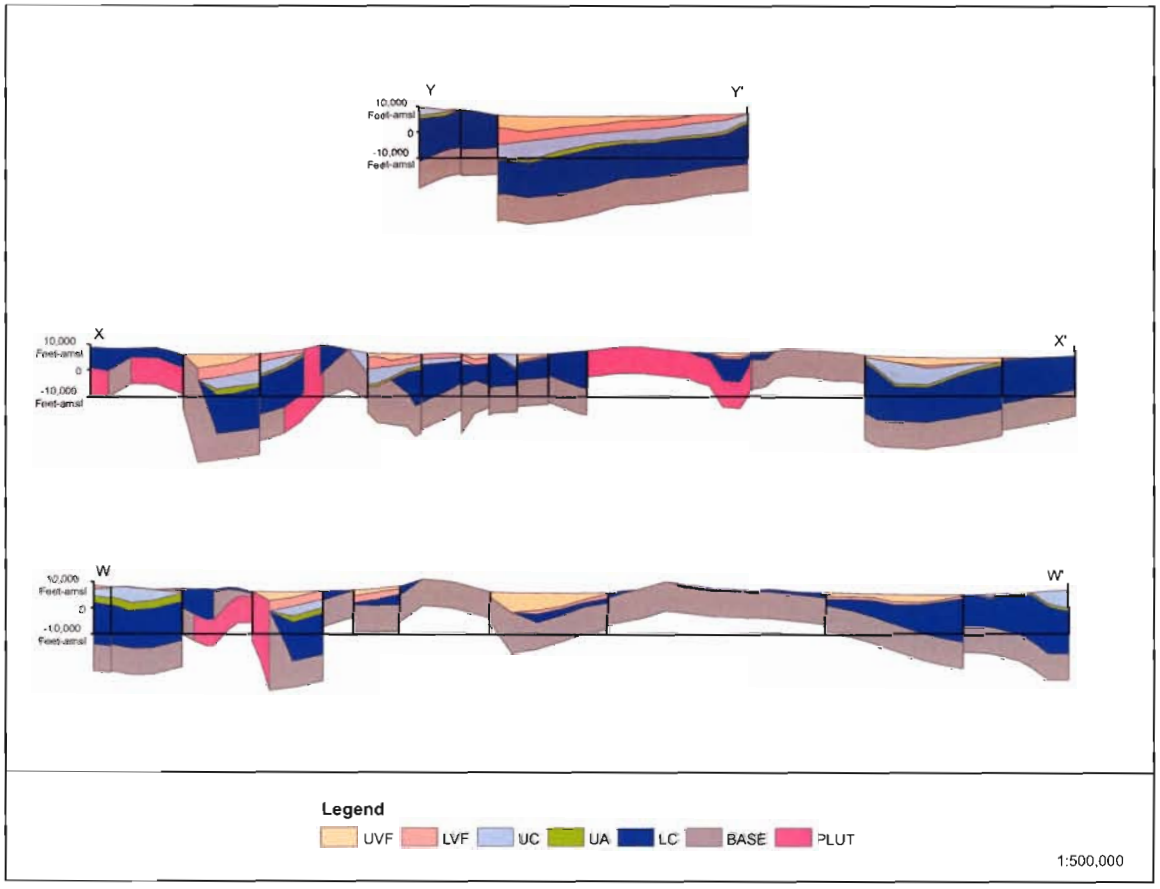

Figure 3-26
Cross Sections Through Three-Dimensional Mesh: Sections Y, X, and W

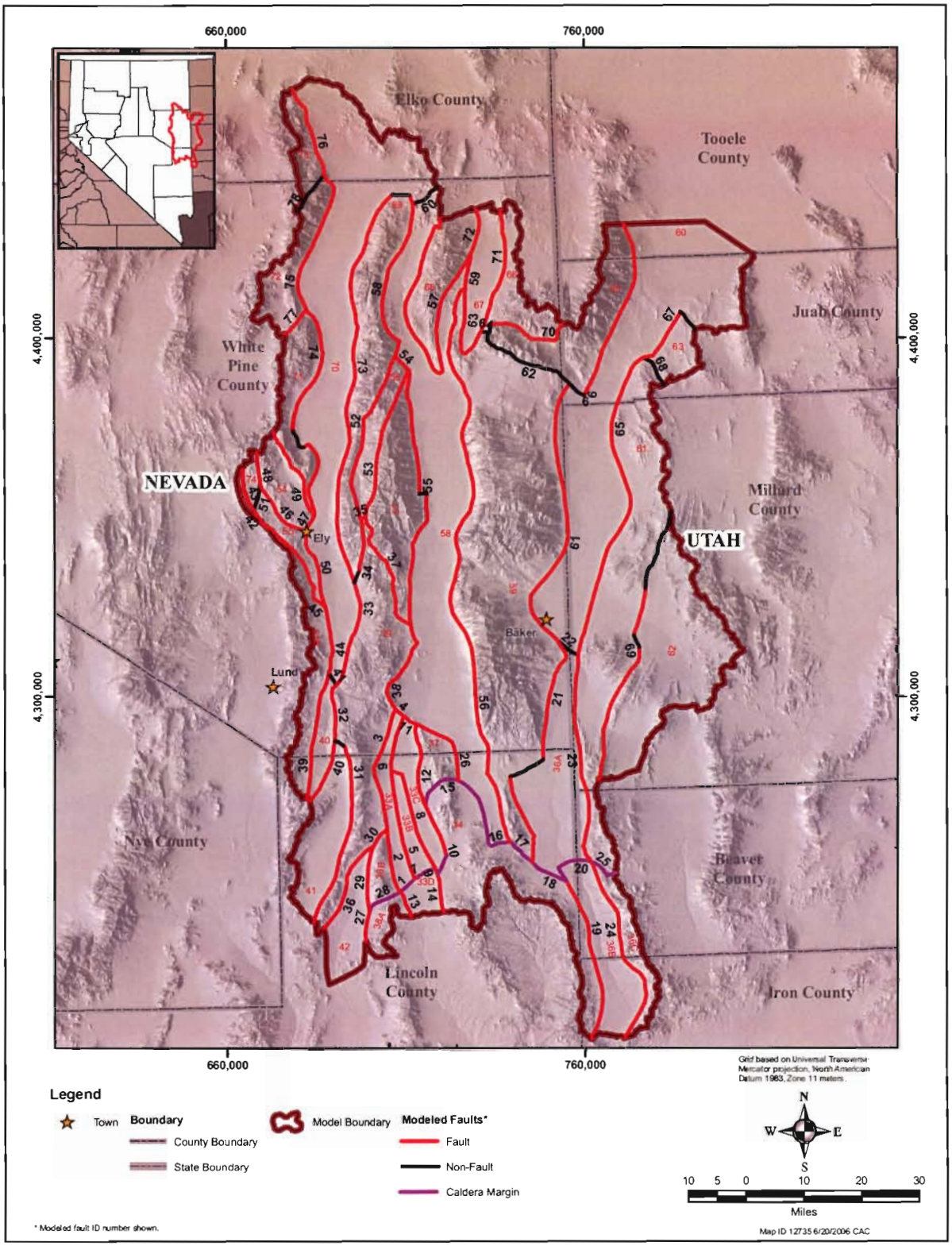

Figure 3-27
Compartment-Boundary Faults

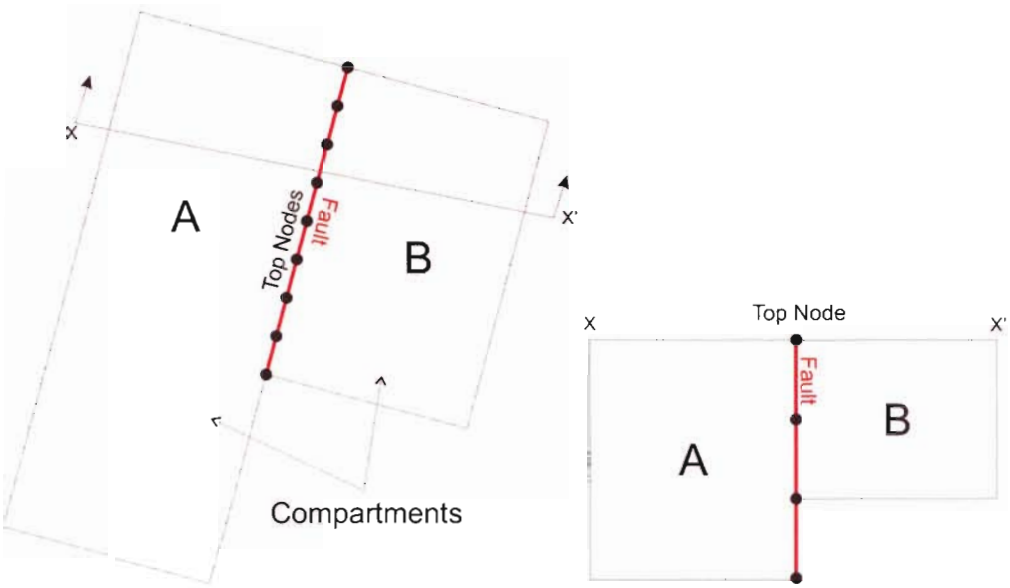

a. Plan View

b. Sectional View

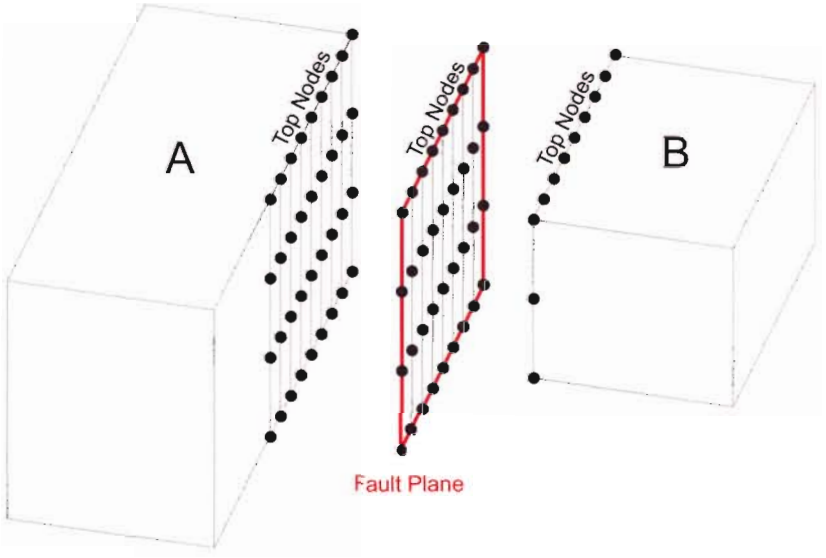

c. Pulled-Apart Oblique View

Figure 3-28
Faults Located Between Boundaries:
A. Plan View B. Section View C. Pulled-apart Oblique View

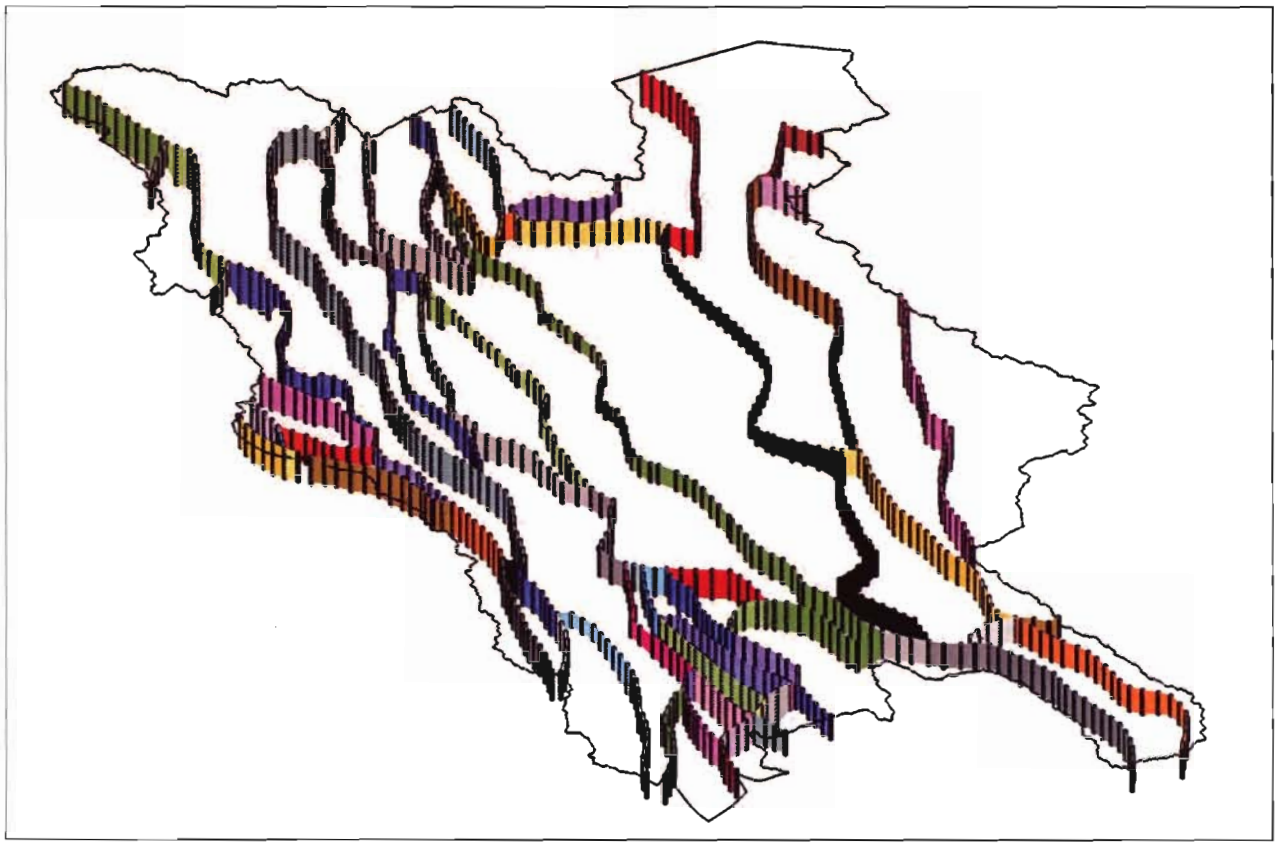

Figure 3-29
Oblique View of Fault Network

This Page Intentionally Left Blank

4.0 HYDRAULIC PARAMETERS

4.1 Background

Hydraulic parameters associated with the Spring Valley model include hydraulic conductivity, hydraulic-conductivity orientation, for the RMUs. Values for hydraulic conductivity are identified from the model calibration, but the available information on hydraulic conductivity is used to constrain the calibration. In terms of a model calibration, the available information on hydraulic parameters is referred to as "prior" information.

Data relating to hydraulic conductivity were compiled into a database. The data sources are Bunch and Harrill (1984), Leeds, Hill, and Jewett (1981a and b; 1983), Berger et al. (1988), Johnson et al. (1998), Converse (2002), Converse (1997, 1998a and b), SRK Consultants (2001), Johnson (2002), URS (2001), Mifflin and Associates (2001), HIS HydroSystems (2002), Belcher et al. (2001), IT Corporation (1997a and b, 1998, 2002a through i), Stoller-Navarro Joint Venture (2004a through e), and Maurer et al. (2004). The geographic coverage includes information on the Spring Valley area, eastern and southern Nevada, western Utah, and other areas as shown on Figure 4-1 through Figure 4-4. The hydrogeologic scope includes information on the upper valley fill, lower valley fill, carbonate rock, and upper aquitard RMUs, but data were not available for the plutonic rock and basement rock RMUs.

Driller's logs for the Spring Valley area were compiled into a database. However, the data are limited to wells constructed within the upper valley fill. The data sources are the Nevada State Engineer and the Utah State Engineer. The geographic coverage includes Steptoe, Spring, and Snake Valleys as shown on Figure 4-5. Data were compiled for about 630 sites within Steptoe Valley, 210 sites within Spring Valley, and 50 within Snake Valley. Among the driller's logs, some contained information on the specific capacity of the well. Specific-capacity data were compiled for about 340 sites as shown on Figure 4-6, including 300 within Steptoe Valley, 20 within Spring Valley, and 20 within Snake Valley.

4.1.1 Upper Valley Fill

The upper valley fill RMU consists mostly of unconsolidated sediments and volcanic rocks as described by SNWA (2006c). The sediments include alluvial and playa deposits.

4.1.1.1 Hydraulic Conductivity

Summary of Aquifer-Test Data. The hydraulic-conductivity data represent results from constant-rate, step-drawdown, and similar tests. Figure 4-7 shows the cumulative distribution of the

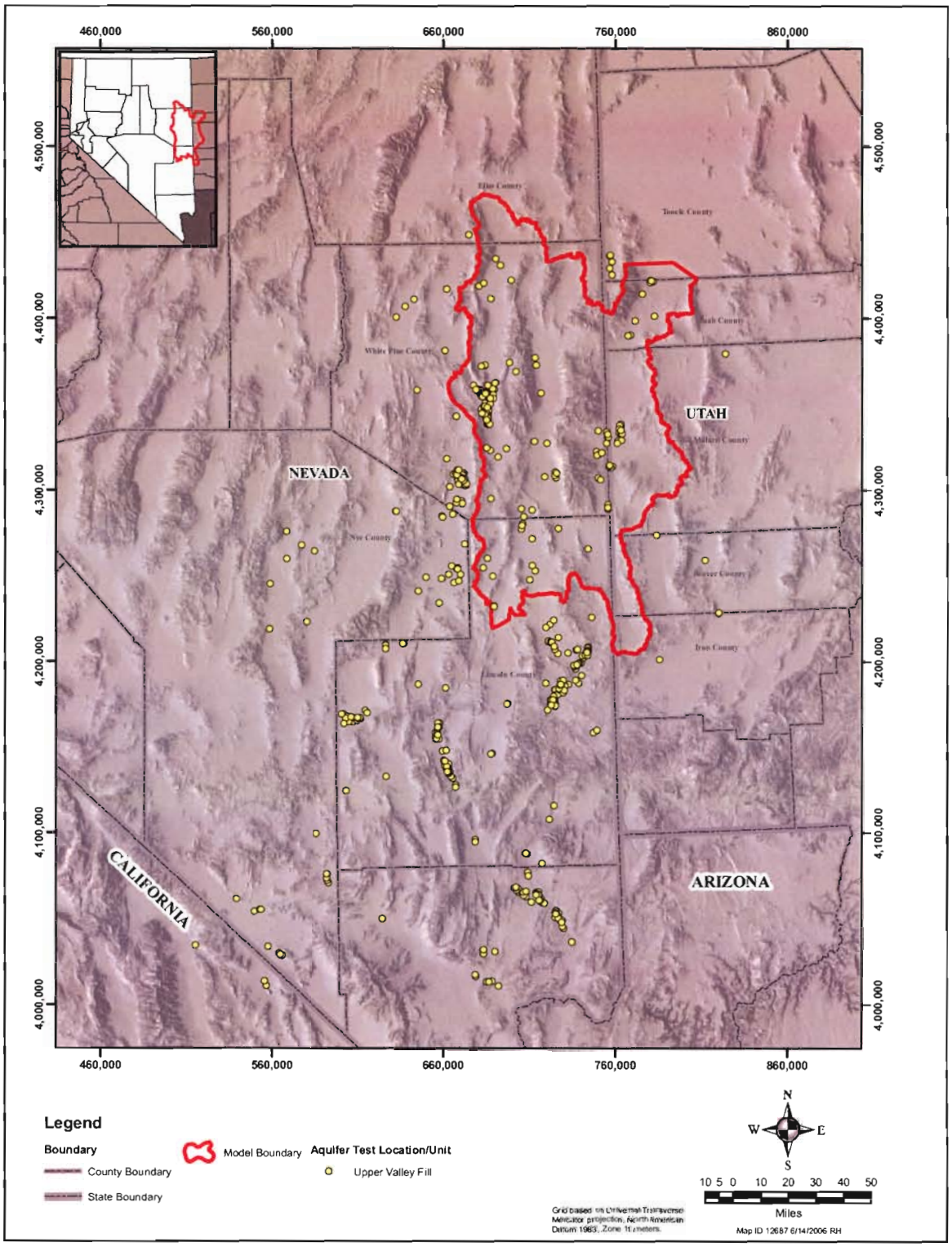

Figure 4-1
Locations of Compiled Aquifer-Test Data: Upper Valley Fill (UVF)

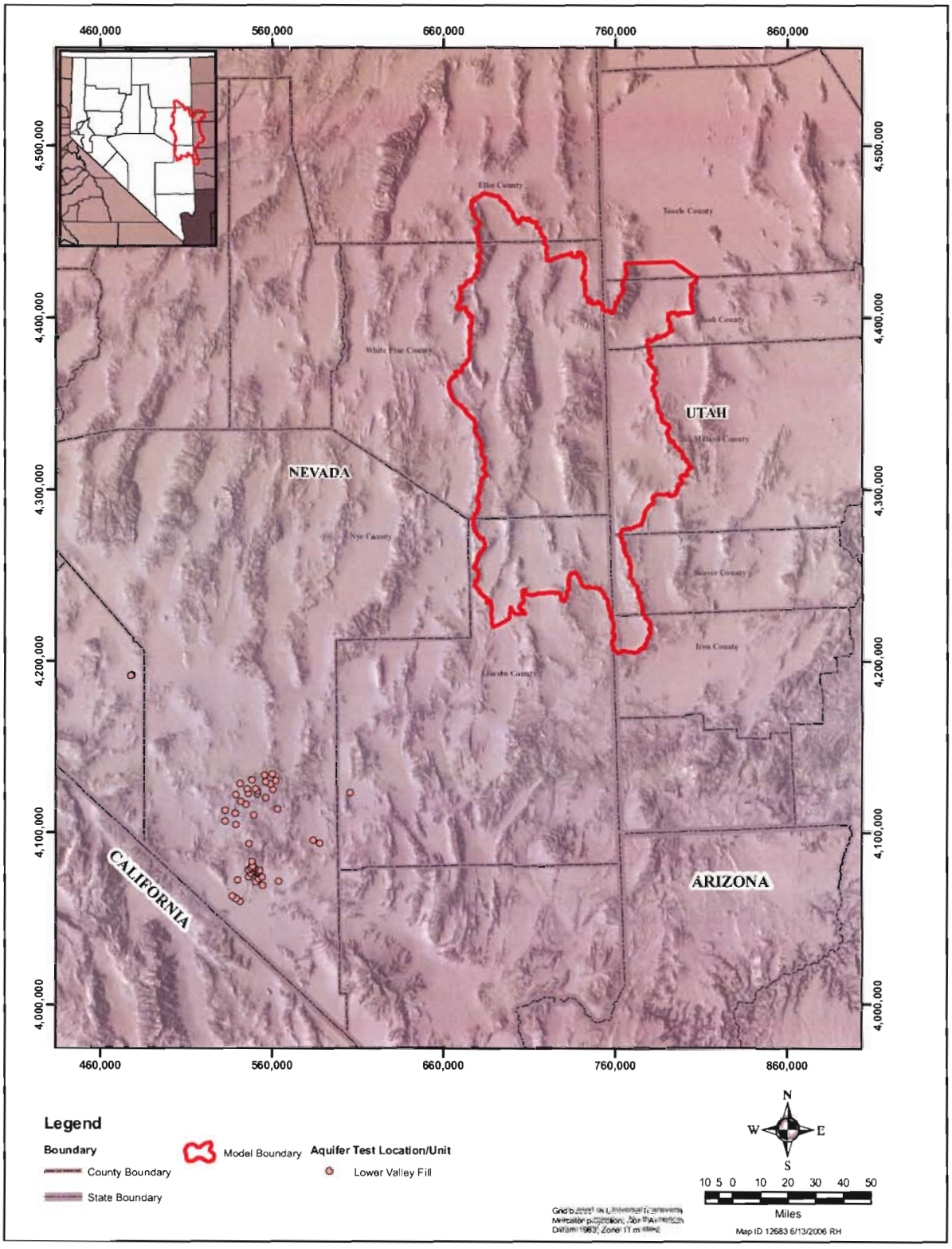

Figure 4-2
Locations of Compiled Aquifer-test Data: Lower Valley Fill (LVF)

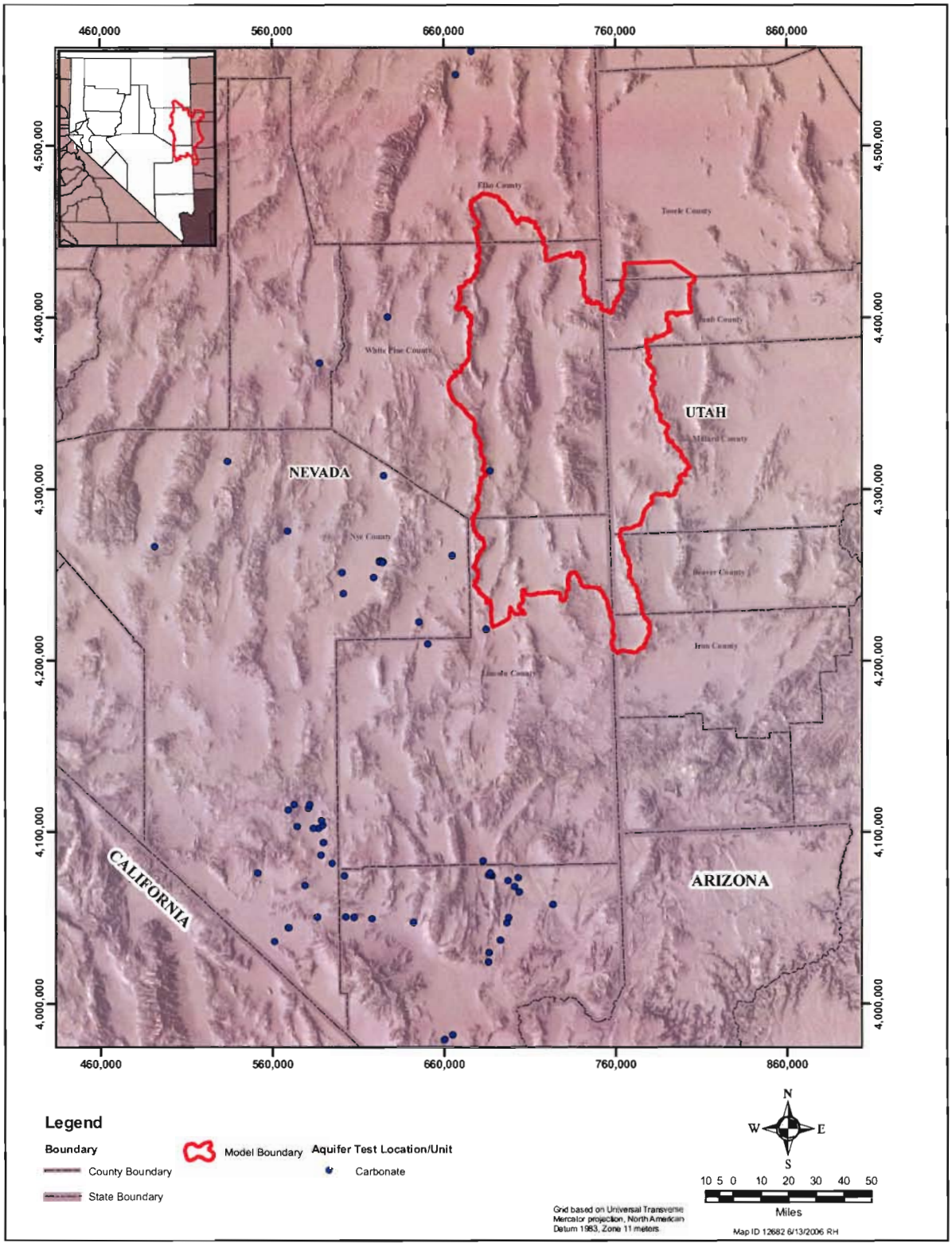

Figure 4-3
Locations of Compiled Aquifer-test Data: Carbonate Rocks (UC/LC)

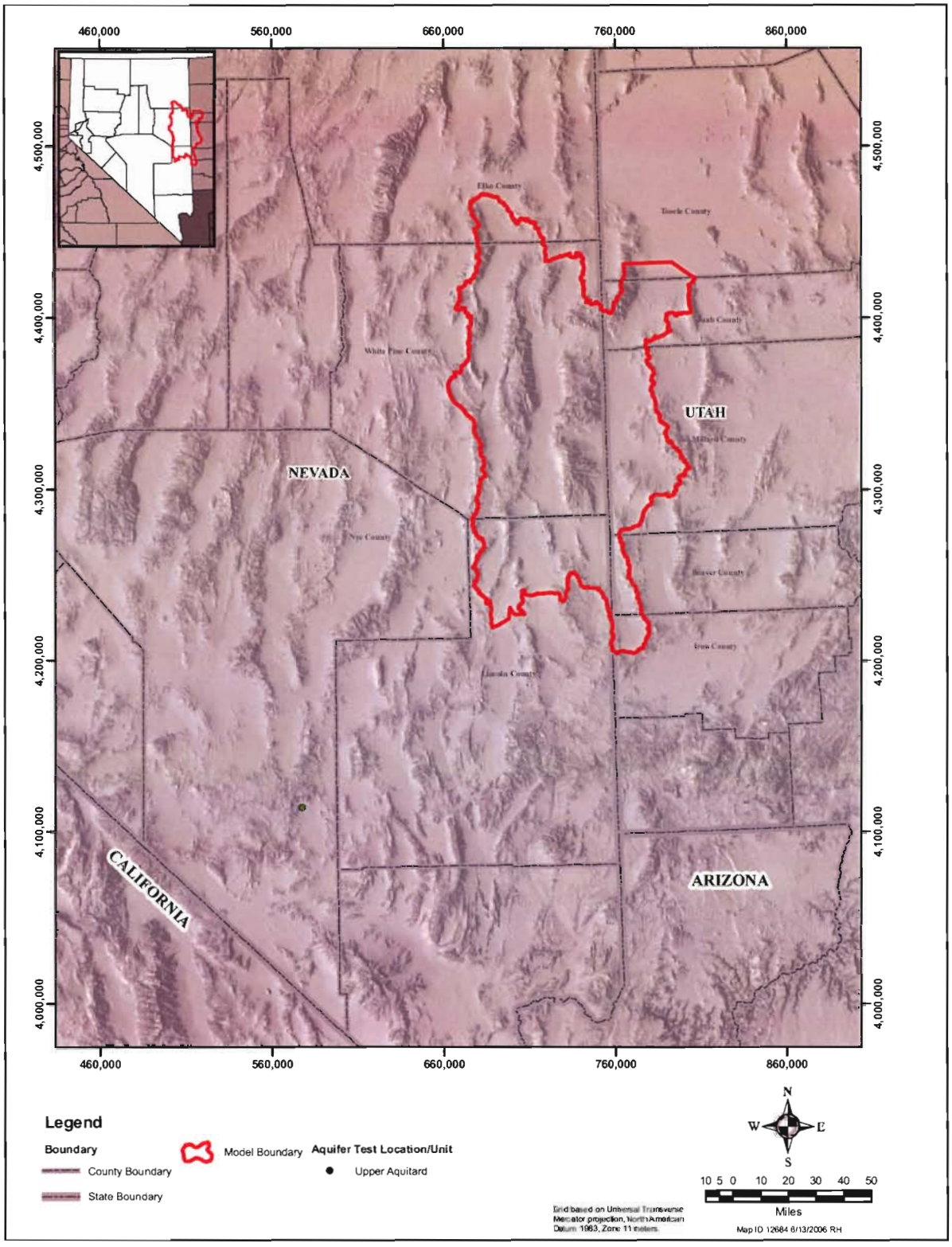

Figure 4-4
Locations of Compiled Aquifer-test Data: Upper Aquitard (UA)

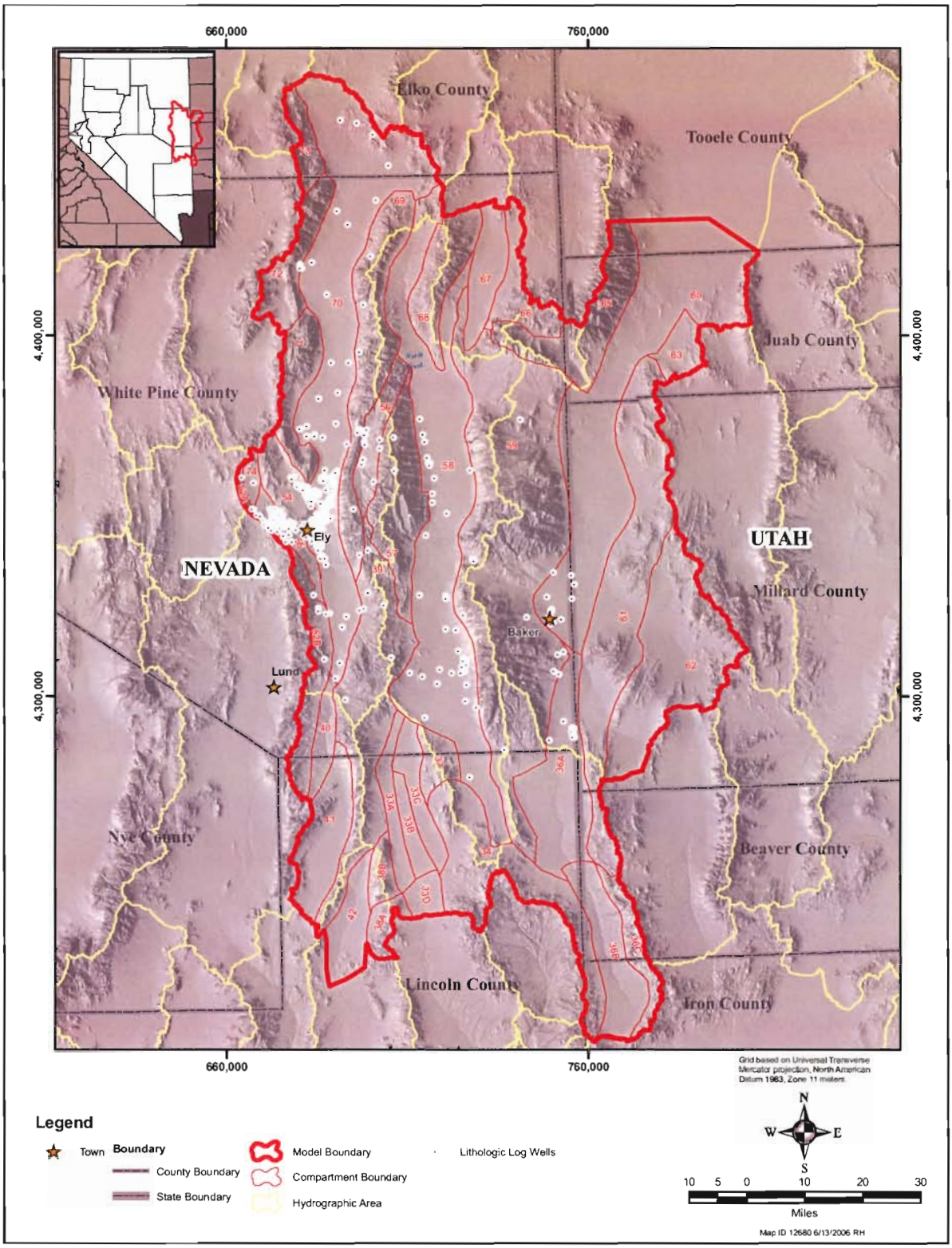

Figure 4-5
Locations of Compiled Drillers Logs

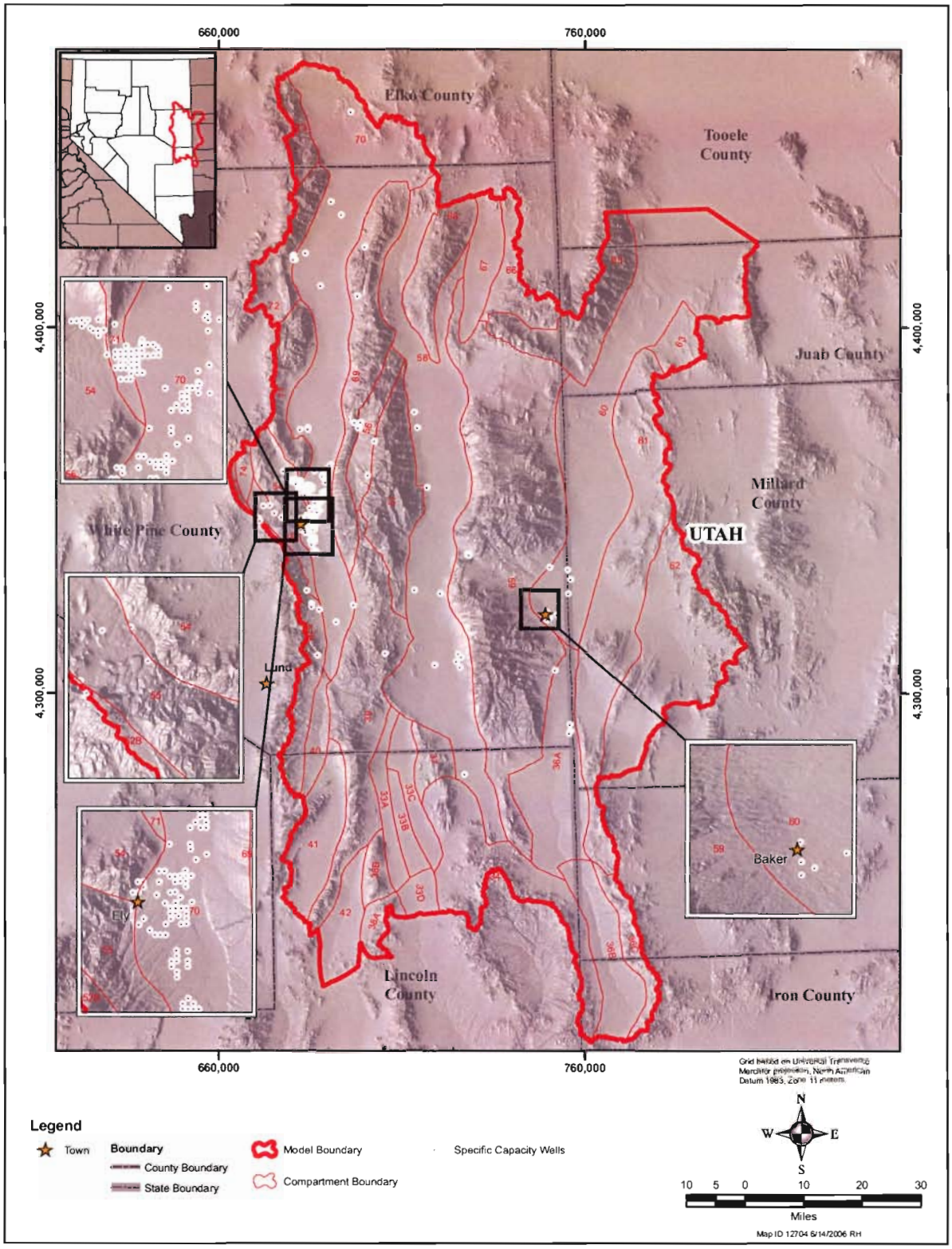

Figure 4-6
Location of Compiled Specific-Capacity Data

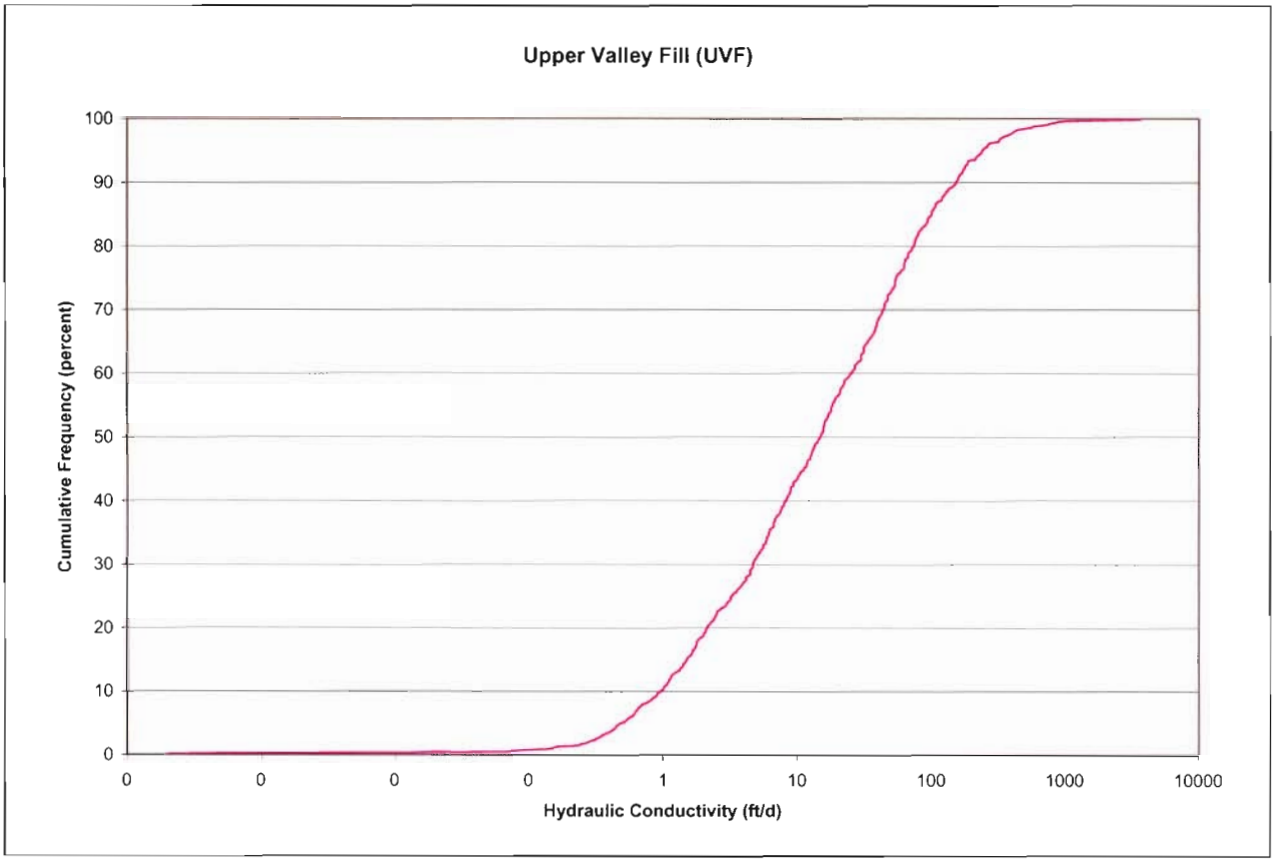

Figure 4-7
Cumulative Distribution of Hydraulic Conductivity: Upper Valley Fill (UVF)

compiled hydraulic conductivities for the upper valley fill RMU. The hydraulic conductivity ranges from 2×10^{-4} to 4×10^{3} ft/d. The average hydraulic conductivity is about 13 ft/d, and the standard deviation is about 0.9 $\log_{10}$ units. The average is based on the logarithmic transformation of the data before calculating the mean and the reverse transformation of the average into a natural value.

The wells represented by the cumulative distribution range in depth from 20 to 3,700 ft, but the average depth is about 300 ft. Figure 4-8 shows the relation of hydraulic conductivity to depth below the land surface. The vertical axis represents the hydraulic conductivity on a $\log_{10}$ scale, and the horizontal axis represents the depth on a linear scale. The depth is the midpoint of the perforated interval for the test well. The data are scattered on the figure, but they do suggest a decrease in log hydraulic conductivity with depth. An interpretation of the conductivity-depth relation is represented on Figure 4-8 as a plotted function, which has the form.

$$\log_{10}(K) = \log_{10}(K_0) + a_1 z + a_2 z^2 \quad \text{for} \quad z < -\frac{a_1}{2a_2} \tag{4-1}$$

and

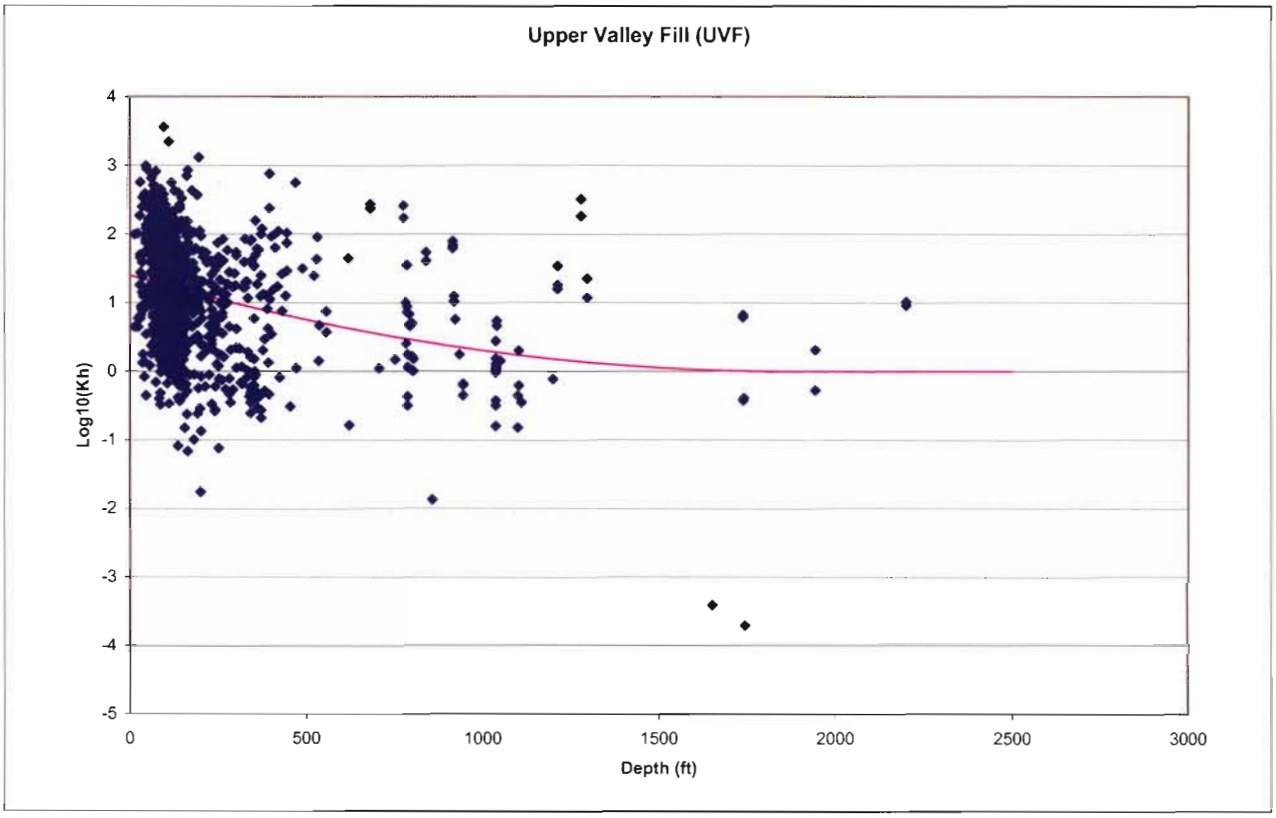

Figure 4-8
Graph Showing Relation Between Hydraulic Conductivity and Depth: Upper Valley Fill

$$\log_{10}(K) = \log_{10}(K_0) - \frac{a_1^2}{4a_2} \quad \text{for} \quad \geq -\frac{a_1}{2a_2} \tag{4-2}$$

where
K is the hydraulic conductivity at depth z [Lt^{-1}],
K_0 is the hydraulic conductivity at depth z = 0 [Lt^{-1}],
z is the depth below the land surface [L],
a_1 is a coefficient [L^{-1}], and
a_2 is a coefficient [L^{-2}].

Equation 4-1 is tangent to a horizontal line, where $z = -a_1/2a_2$, which represents the limiting depth of Equation 4-1. For greater depths, hydraulic conductivity is invariant with depth, as indicated by Equation 4-2.

Equation 4-1 can be rewritten in terms of the relative hydraulic conductivity at depth. The resulting expression is

$$k_R \equiv \frac{K}{K_0} = 10^{a_1 z + a_2 z^2} \tag{4-3}$$

where k_R is the relative hydraulic conductivity with depth [L^0]. Equation 4-3 is similar in form to expressions developed by Saar and Manga (2004), IT Corporation (1996), Belcher et al., (2001), except that Equation 4-3 includes the non-linear term $a_2 z^2$.

The parameters for Equation 4-3 are $a_1 = -1.0 \times 10^{-3}$ ft^{-1} and $a_2 = 2.5 \times 10^{-7}$ ft^{-2}. The minimum value of the relative hydraulic conductivity is 0.1, which occurs at $z = 2000$. The depth-conductivity data for the upper valley fill RMU are so scattered that a specific depth-conductivity relation is difficult to identify. The general existence of a depth-conductivity relation is well established (Ingebritsen and Manning, 1999; Saar and Manga, 2004; Bedinger et al., , 1989, IT Corporation, 1996 and 1997; and D'Agnese et al., 1997), and the available data were used as best possible to incorporate such a relation into the Spring Valley model.

The relation used in the model is consistent with hydraulic-conductivity data collected by Johnson et al., (1968) from alluvial deposits in California. About 300 cores were collected from seven bore holes within the San Joaquin and Santa Clara valleys. The bore holes ranged in depth from 760ft to 2,200 ft, and cores were collected at about 40-ft depth intervals. The data suggests that relative hydraulic conductivity in the California study areas equals about 0.1 at a depth of 2,000 ft. Durbin et al. (1978) estimated that the relative hydraulic conductivity for alluvial deposits in the Salinas Valley, California equals 0.5 at a depth of 2,000 ft. These results from the San Joaquin and Salinas Valleys are relevant because both demonstrate the combined effects of overburden pressure and diagenesis on alluvial deposits that share similarities with the upper valley fill.

Figure 4-9 shows the cumulative distribution of depth-adjusted hydraulic-conductivity values for the upper valley fill. In order to construct the figure, the hydraulic conductivity at depth was translated into the corresponding hydraulic conductivity at zero depth. To accomplish the translation, Equation 4-3 was rearranged to solve for K_0 in terms of K and z, and the resulting expression was used to translate hydraulic-conductivity values representing a particular depth to the corresponding values representing a zero depth. While the unadjusted distribution has a mean of about 13 ft/d, the adjusted cumulative distribution has a mean of about 25 ft/d.

Horizontal Correlations in Texture. The available data do not indicate large-scale horizontal trends with regard to hydraulic conductivity. Figure 4-10 shows the average texture within the upper 500 ft of the upper valley fill based on a binary hydrostratigraphic indicator (Johnson, 1995; Weissmann, 1999; Ritzi, 2000). The indicator is used to classify the calls on driller's logs as either coarse grained or fine grained. The driller's calls were translated into an indicator value based on the Shepard (1954) classification system. The cutoff between a coarse-grained and fine-grained texture is such that the coarse-grained texture is a sand, silty sand, gravely sand, gravel, silty gravel, or sandy gravel. The fine-grained texture consists of clay, silty clay, sandy clay, gravelly clay, clayey silt, sandy silt, or gravelly silt. The cutoff is similar to that used by Johnson (1995).

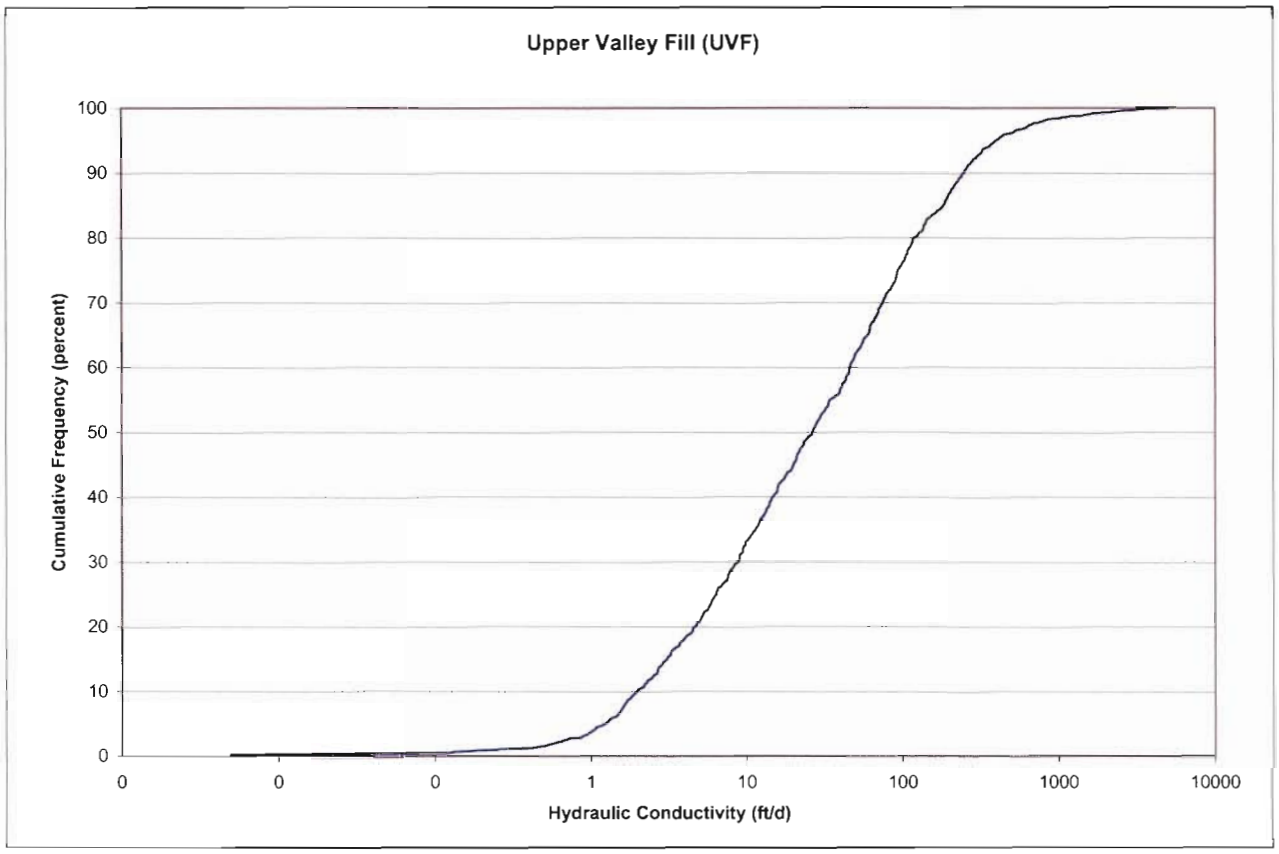

Figure 4-9
Graph Showing Cumulative Distribution of
Depth-Adjusted Hydraulic Conductivity: Upper Valley Fill (UVF)

The texture for each well is posted on Figure 4-10 at each well location as a percentage. The percentage represents the proportion of the interval from the land surface to a depth of 500 ft that is classified as coarse grained. Predominantly coarse-grained textures are indicated where the proportion of coarse-grained textures is greater than 50 percent. Otherwise, predominantly fine-grained textures are indicated. The geographic pattern displayed on Figure 4-10 indicates no large-scale horizontal correlations in texture. Thus, fine-grained and coarse-grained textures each occur throughout particular valleys without any apparent transverse or longitudinal correlation.

Vertical Correlations in Texture. While the upper valley fill does not exhibit a large-scale horizontal structure, it does appear to have a large-scale vertical structure, at least within the upper 500 ft of the upper valley fill. Figures 4-11 through 4-13 show the average percentage of coarse-grained texture with depth respectively for Steptoe, Spring, and Snake valleys. Average textures are plotted for 100-foot intervals from the land surface to a depth corresponding to the deepest well within the valley. Also shown on the figures are the error bars for the estimate of the average percentage of coarse-grained material within a depth interval, where the error-bar length depends in part on the number of wells penetrating an interval. Based on the proportions and error bars plotted on Figures 4-11 through 4-13, the texture-depth relation is similar for shallow depths

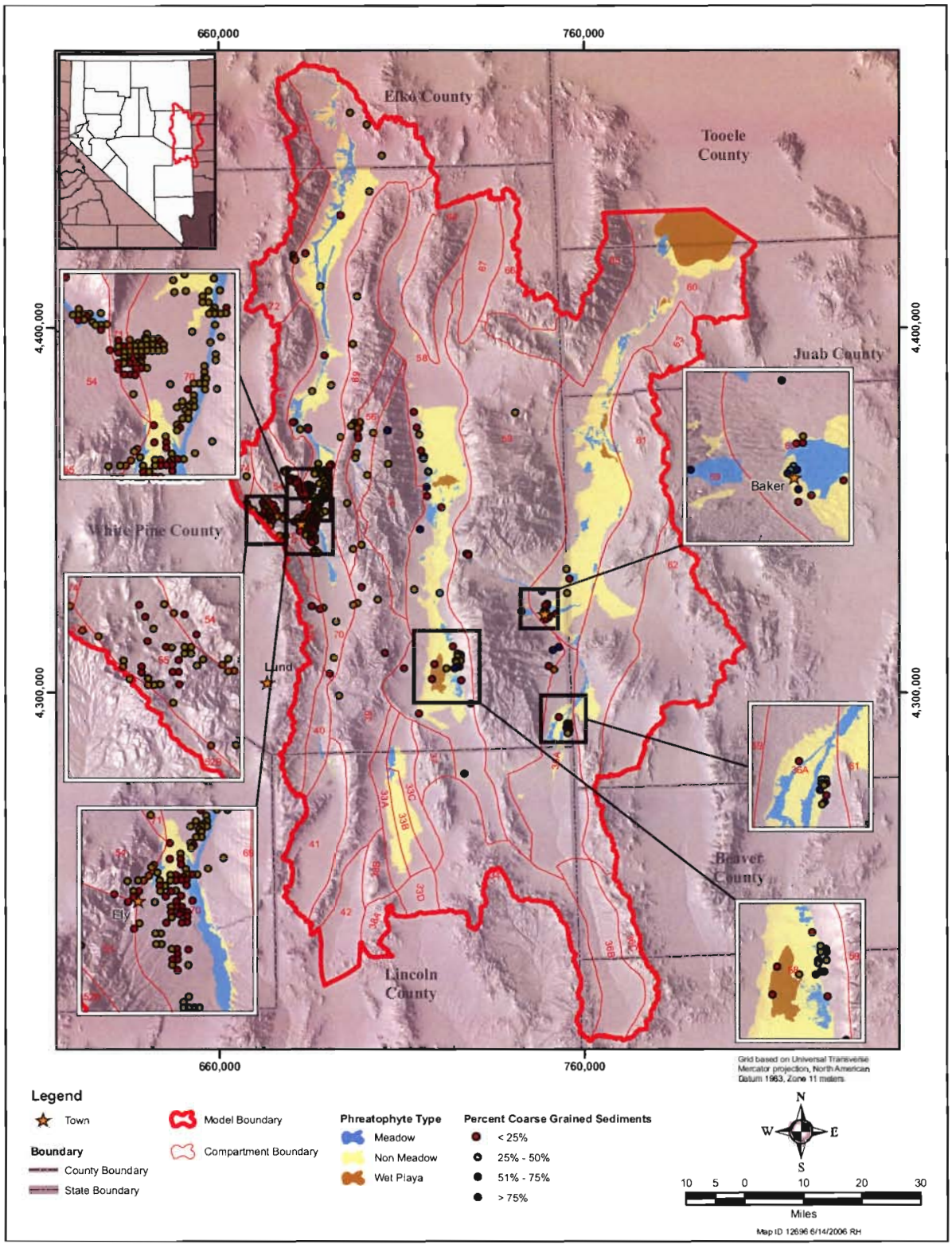

Figure 4-10
Map Showing Texture of Upper Valley Fill Within the Spring Valley Area

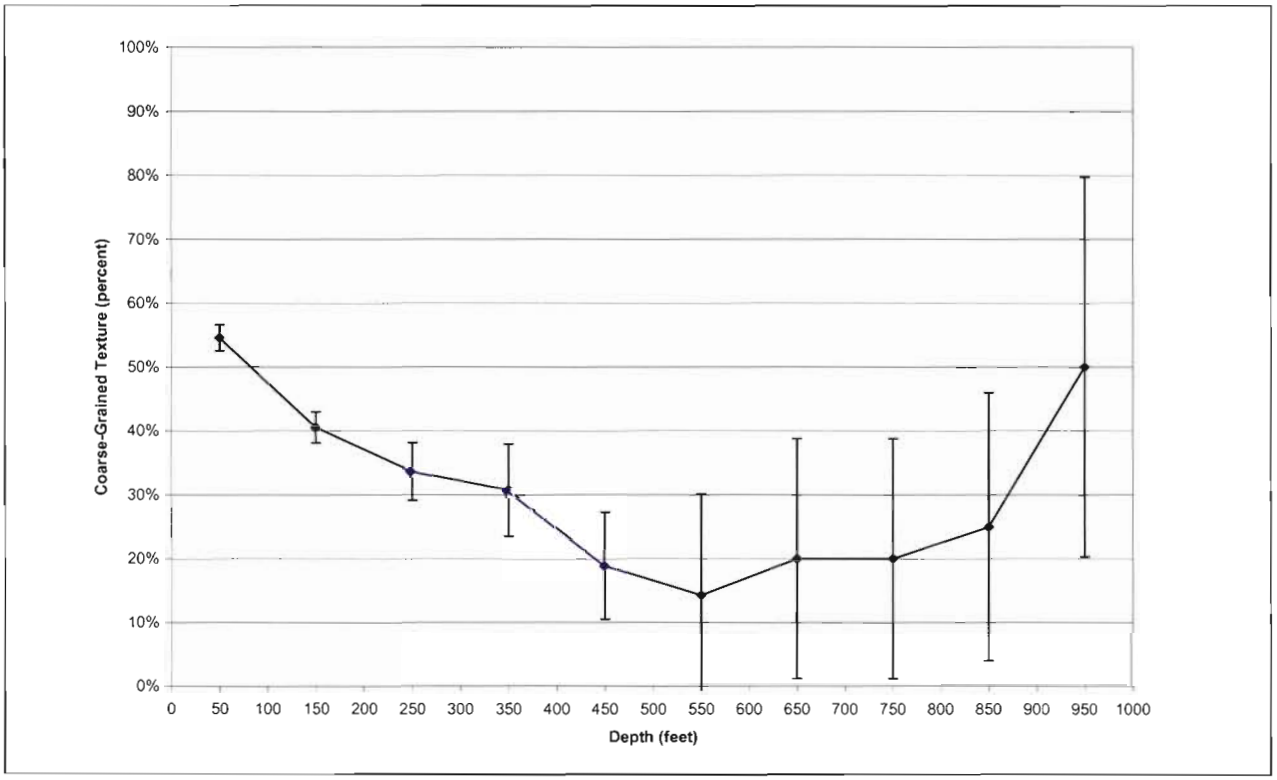

Figure 4-11
Graph Showing Vertical Distribution of Texture for UVF: Steptoe Valley

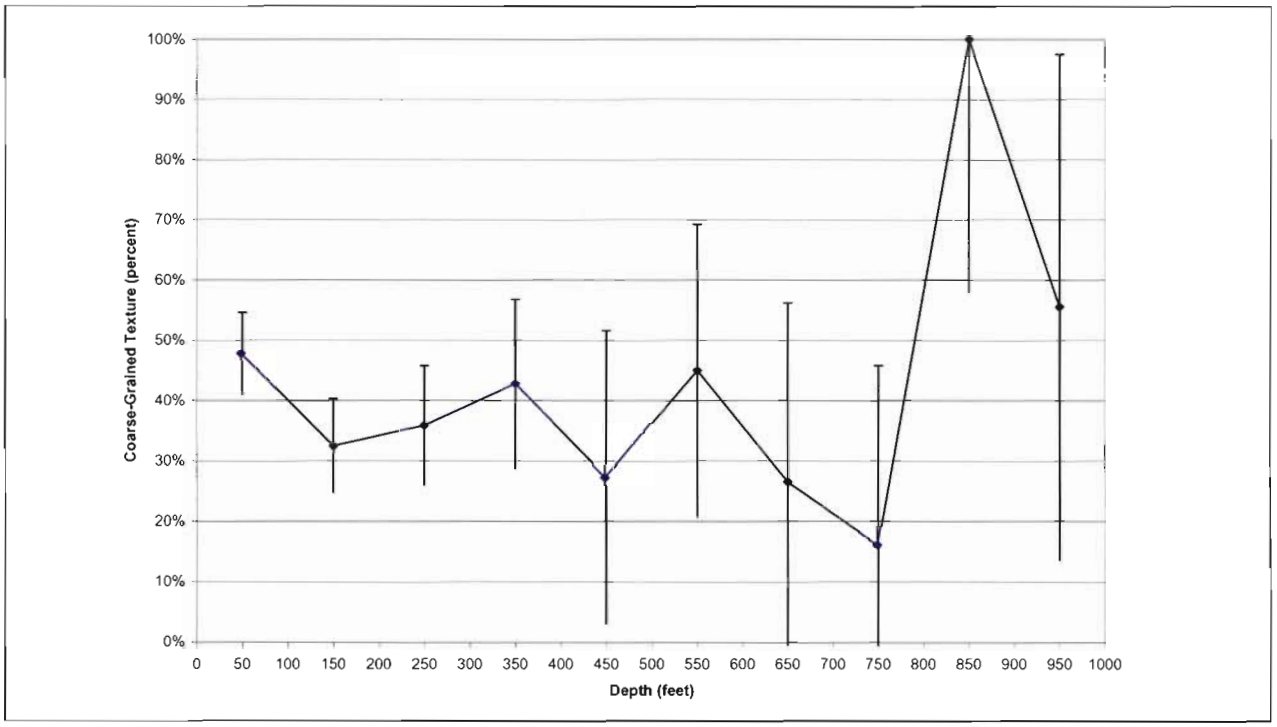

Figure 4-12
Graph Showing Vertical Distribution of Texture for UVF: Spring Valley

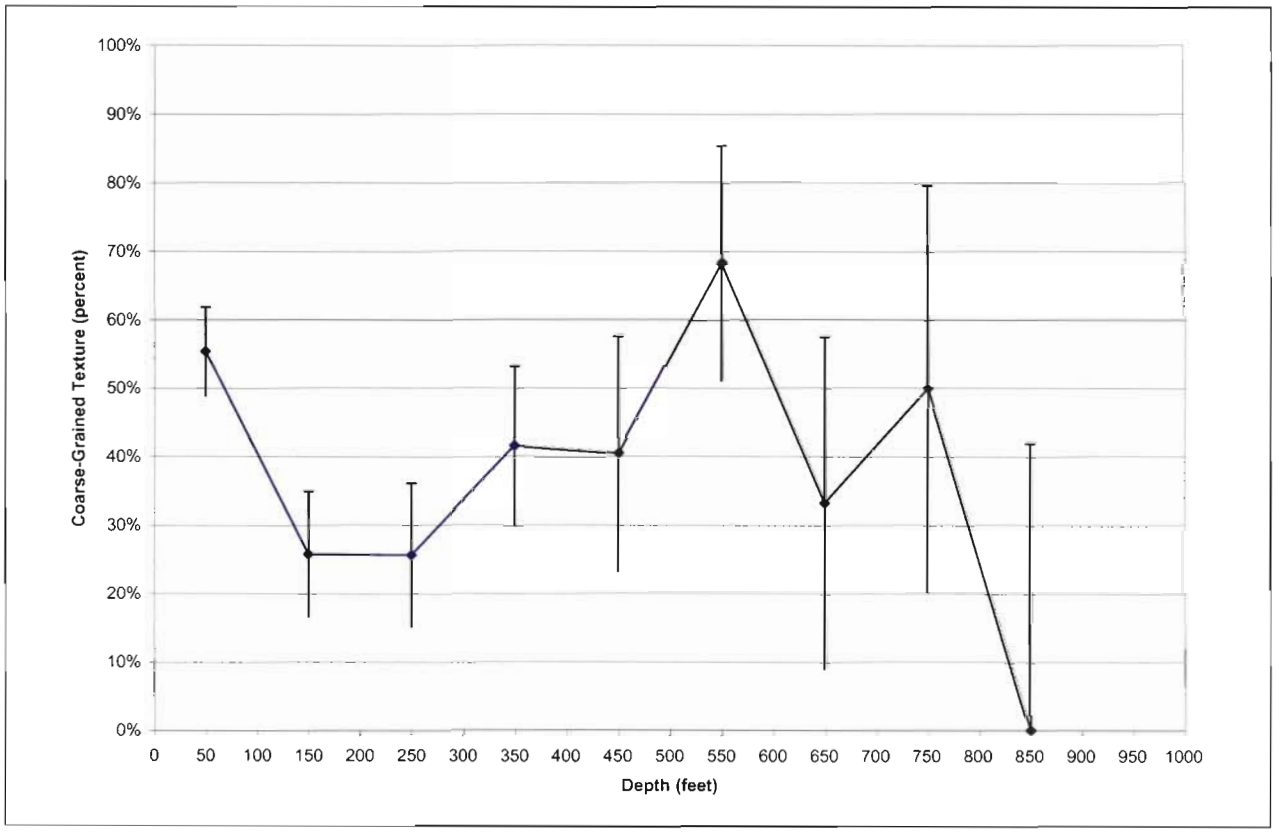

Figure 4-13
Graph Showing Vertical Distribution of Texture for UVF: Snake Valley

among Steptoe, Spring, and Snake valleys. The average proportion of coarse-grained textures decreases with depth for depths ranging from 0 to 500 ft. For greater depths, the trends are dissimilar among the valleys.

Anisotropy in Hydraulic Conductivity. The intermediate-scale textural structure within the upper valley fill indicates a vertical to horizontal anisotropy for hydraulic conductivity. Gelhar (1986) describes that the vertical to horizontal anisotropy within an alluvial groundwater system is related to the respective correlation scales for the hydraulic conductivity in the vertical and horizontal directions. Based on the relation shown on Figure 4-14, which is taken from Gelhar (1986, Figure 2), the anisotropy is about 1:50. The horizontal axis for the relation is variance of the log hydraulic conductivity (σ_f^2). The vertical axis is the ratio of the horizontal hydraulic conductivity over the vertical hydraulic conductivity. The lines within the graph respectively represent a particular ratio of the horizontal correlation scale over the vertical correlation scale (λ_h / λ_v).

The horizontal correlation scale for the upper valley fill was estimated from specific-capacity data for the Spring Valley area. The method described by Lohman (1972) was used to translate specific capacity into transmissivity. The hydraulic conductivity of the screen interval for each well was derived by dividing the transmissivity by the length of the screened interval. The resulting

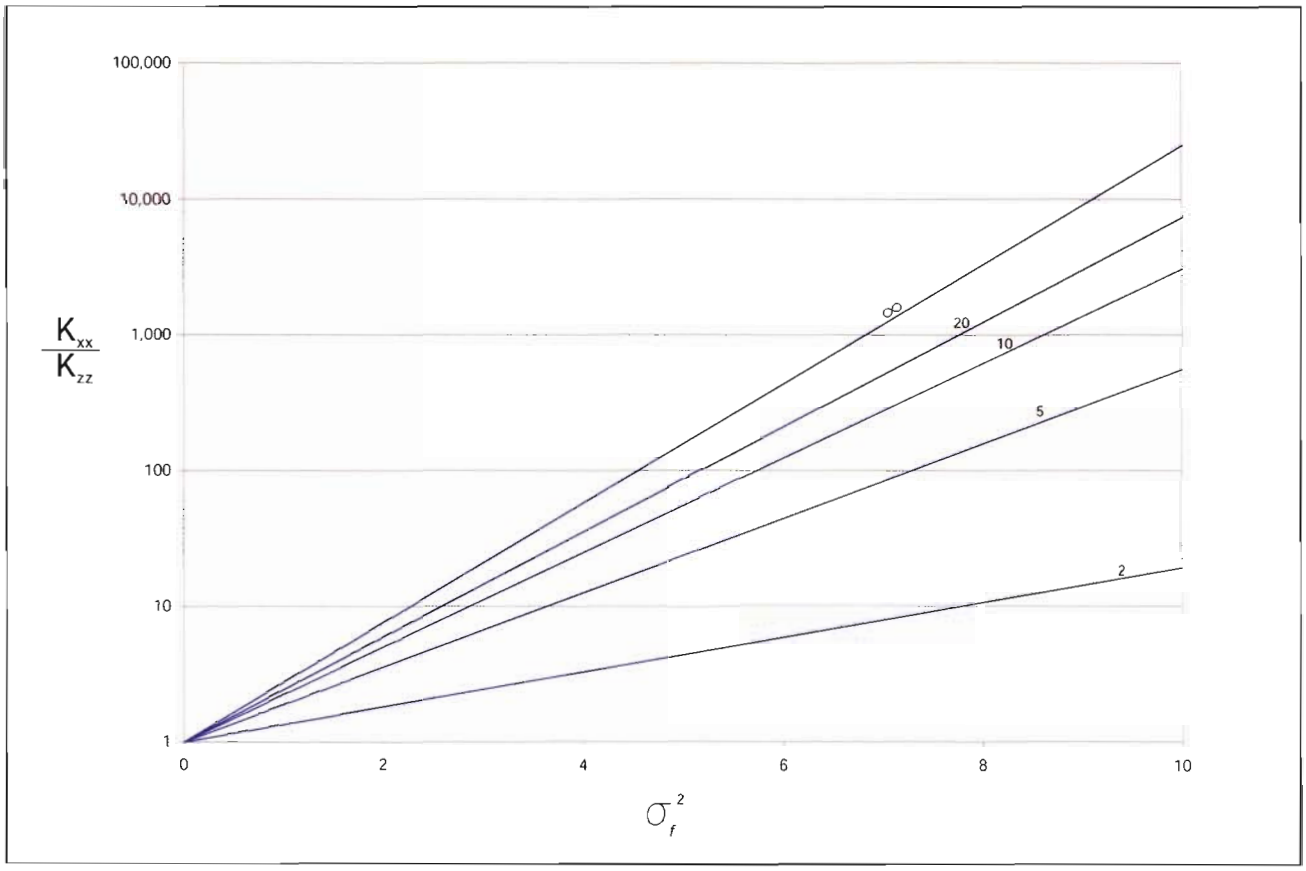

Figure 4-14
Graph Showing the Relation Between Hydraulic Conductivity Anisotropy and Correlation Scales

hydraulic-conductivity values were fitted to an exponential correlation model of the form (Gelhar, 1986)

$$\mathrm{cov}[k(x_1), k(x_2)] = \mathrm{var}[k]\exp\left[-\frac{(x_1 - x_2)^2}{\lambda_h^2}\right] \tag{4-4}$$

where

$$k(x) = \ln[K(x)] \tag{4-5}$$

and where

K is the hydraulic conductivity [Lt^{-1}],
x is the well location vector [L], and
λ_h is the horizontal correlation scale [L^2].

The quantity $x_1 - x_2$ in Equation 4-4 is the separation distance between two wells. Figure 4-15 shows the estimated and fitted correlation models for the upper valley fill within the Spring Valley area. The fitted model has a correlation scale of 3,500 ft, which means the correlation for a separation distance of 3,500 ft equals e^{-1} or 0.37.

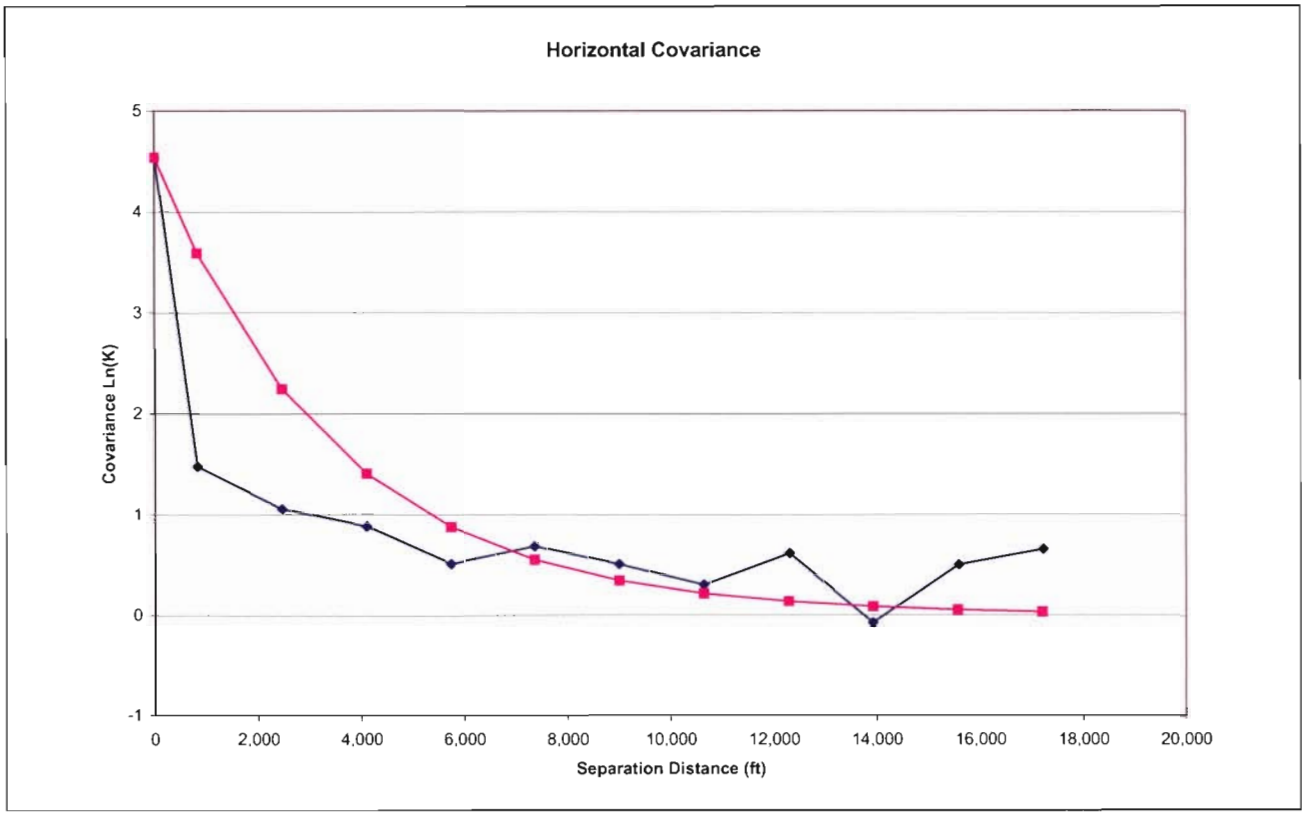

Figure 4-15
Graph Showing the Relation Between Hydraulic Conductivity Anisotropy and Correlation Scales

The vertical correlation scale was estimated for the driller's logs for the Spring Valley area. However, the driller's calls first were translated into hydraulic-conductivity values. This was accomplished by a three-step procedure. Firstly, the driller's calls were translated into a texture class based on the Shepard (1958) trilinear system. Secondly, log hydraulic conductivities were assigned respectively to the sand, silt, and clay end members of the Shepard system. Thirdly, log hydraulic conductivities were derived for each texture class by interpolating over the trilinear system. By this process, each log interval for each well was translated into a log hydraulic-conductivity value. Equation 4-5 then was fitted to the derived values. Figure 4-16 shows the resulting estimated and fitted correlation model. The fitted model has a correlation scale of 100 ft.

The ratio of horizontal to vertical correlation scales was used to estimate the vertical to horizontal anisotropy using the relation developed by Gelhar (1986, Figure 3). The parameters var[ln(K)] = 4.5 an5 $\lambda_h / \lambda_v = 35$ were used in the Gelhar relation, where λ_h and λ_v respectively are the horizontal and vertical correlation scales. The corresponding vertical to horizontal anisotropy is about 1:50. In

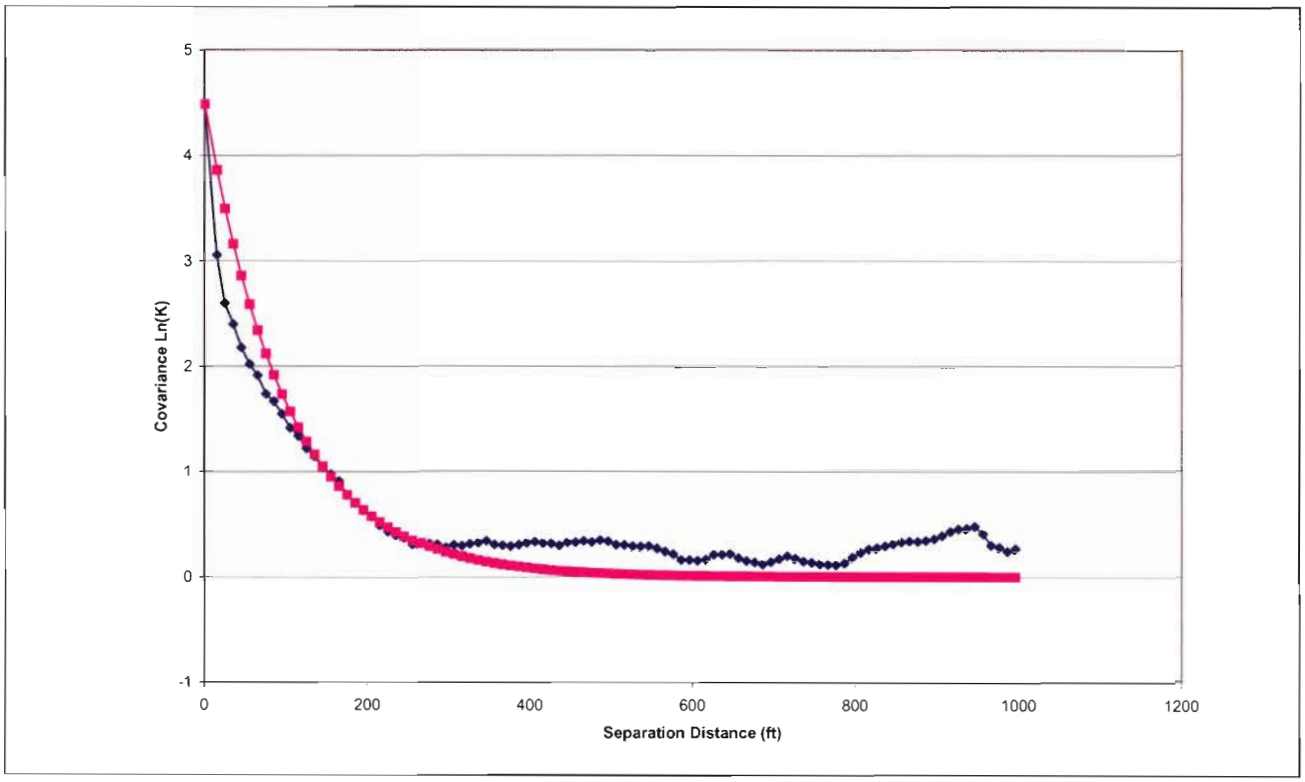

Figure 4-16
Graph Showing Estimated and Fitted Functions for the Vertical Correlation of Hydraulic Conductivity Within the UVF

comparison, Harrill and Preissler (1994) assigned anisotropy of 1:100 to their groundwater model of Stagecoach Valley.

Scaling. For use as prior information in the calibration of the Spring Valley model, the hydraulic-conductivity values derived from aquifer-test data and other information must be scaled. The upper valley fill, as a typical basin deposit, has different degrees of spatial variability at different scales, where the variability tends to decrease with increasing scale (Painter, 2001; Anderson, 1991; Ghilardi et al., 1993; Rovey, 1998, and Proce et al., 2004). On a scale of 0.1 ft, the variability in hydraulic conductivity as measured in individual cores, which represents a sample volume on the order of 10^{-3} ft^3, would exhibit very high variability. On a scale of 100 ft, the variability in hydraulic conductivity as derived from aquifer tests, which represents a sample volume on the order of 10^6 ft^3, exhibit intermediate variability. On a scale of 10,000 ft, which represents a sample volume of 10^{12} ft^3, the variability is low. The available data represent sampling on a scale of tens of feet, but the Spring Valley model represents data on a scale of thousands of feet.

The translation of hydraulic conductivity from the data scale to the model scale involves two considerations: sample bias and interconnectivity. Sample bias relates to the phenomenon that wells tend to be screened in the more conductive units within a groundwater system. While this applies mostly to water-supply wells, it applies also to wells constructed for scientific purposes. The bias is illustrated by the comparison of the average texture within the screened intervals of wells to average

texture over the total depth of the wells. Based on the drillers logs for the Spring Valley area, the proportion of coarse-grained textures within screened intervals of all wells is 50 percent, while the proportion for the total depth of all wells is 40 percent. Based just on this sample bias, a scaling factor of 0.8 should be applied to the aquifer-test data.

Interconnectivity (Proce et al., 2004) is related to the scale of lenses of coarse-grained textures and the hydraulic connections between individual hydrostratigraphic lenses within the groundwater system. The scaling, to account for interconnectivity, ultimately relates to the average spatial scale represented by the aquifer-test data relative to the average scale of the lenses. Four potential conditions exist within the Spring Valley area with respect to scaling: Firstly, if the sample volume of the aquifer tests is small with respect to the hydrostratigraphic structure and the lenses of coarse-grained textures are well interconnected, no scaling is required. Secondly, if the sample volume is large and the lenses are well connected, no scaling is required. Thirdly, if the sample volume is small and the lenses are poorly connected, downward scaling of the aquifer-test data is required. Finally, if the sample volume is large but the lenses are poorly connected, some downward scaling might be required.

Based on the consideration of textural correlation scales and the aquifer-test scales, something between the second case (no scaling) and fourth case (perhaps some downward scaling) probably prevails within the Spring Valley area. The sampling volume of the aquifer tests is relatively large with respect to the horizontal correlation scale, and the individual lenses are moderately connected. The moderate connectivity follows from the greater abundance of fine-grained materials relative to the coarse-grained materials. The horizontal correlation scale suggests that the characteristic scale of hydrostratigraphic lenses is on the order of several thousand feet, and an aquifer test with a six-hour duration or more should reflect the effective hydraulic conductivity at about that scale. Correspondingly, the aquifer-test data do not require scaling to represent the model scale.

4.1.1.2 Conceptual Model

From the discussion above, the conceptual model of the upper valley fill within the Spring Valley area consists of the following elements: Firstly, the upper valley fill is identical within each of the valleys. Secondly, the hydraulic conductivity decreases with depth according to the conductivity-depth relation as shown on Figure 4-8 and represented by Equation 4-3. Thirdly, the hydraulic-conductivity values derived from aquifer tests need to be scaled to account for the sample bias associated with the well-construction practices. The scaling factor is about 0.8, which from the median depth-adjusted aquifer-test data suggests a hydraulic conductivity of about 20 ft/d for the upper valley fill. Fourthly, the vertical to horizontal anisotropy in hydraulic conductivity is 1:50.

4.1.2 Consolidated Rocks

The consolidated-rock RMUs within the Spring Valley area include the lower valley fill, carbonate rock, upper aquitard, plutonic rock, and basement rock RMUs as described by SNWA (2006c).

4.1.2.1 Hydraulic Conductivity

Summary of Aquifer-Test Data. Aquifer-test data are available for the lower valley fill, carbonate rock, and upper aquitard RMUs. Figures 4-17 through 4-19 respectively, show the cumulative distributions of hydraulic conductivity for the lower valley fill, carbonate rock, and upper aquitard RMUs. Figures 4-20 through 4-22 show the cumulative distributions of the depth-adjusted hydraulic conductivity. Aquifer-test data are not available for the plutonic rock and basement rock RMUs (SNWA, 2006b, Volume 1).

Each of the consolidated-rock RMUs has different characteristics with respect to hydraulic conductivity. For the lower valley fill RMU, the hydraulic-conductivity values range from 2×10^{-6} to 1×10^{1} ft/d. The average hydraulic conductivity is 3 ft/d, and the standard deviation is 1.1 $\log_{10}$ units. The average is based on the logarithmic transformation of the data before calculating the average and the reverse transformation of the average into a natural value. For the carbonate rock RMU, the hydraulic-conductivity values range from 4×10^{-6} to 6×10^{3} ft/d. The average hydraulic conductivity is 5 ft/d, and the standard deviation is 1.3 $\log_{10}$ units. For the upper aquitard RMU, the hydraulic-conductivity values range from 9×10^{-4} to 6×10^{-2} ft/d. The average hydraulic conductivity is 0.007 ft/d, and the standard deviation is 0.46 $\log_{10}$ units.

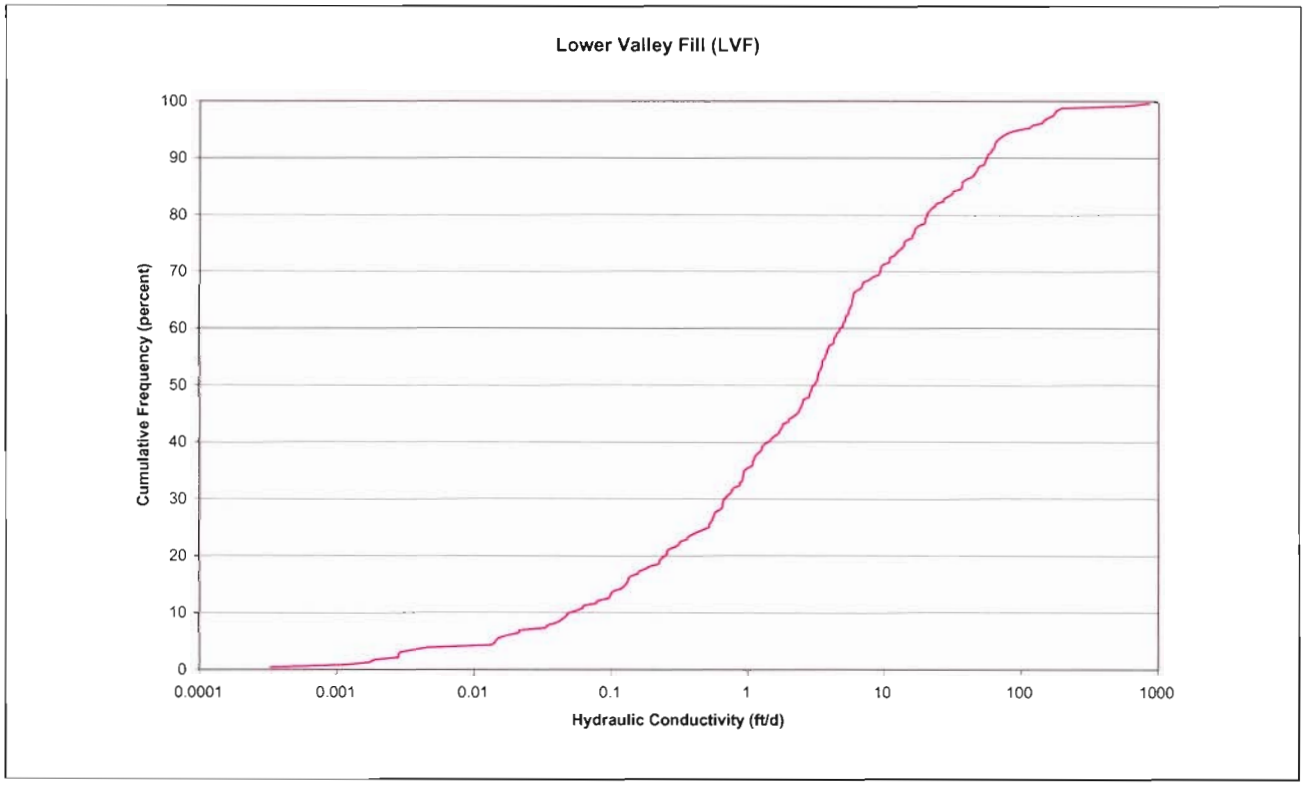

Figure 4-17
Graph Showing Cumulative Distribution of Hydraulic Conductivity: LVF

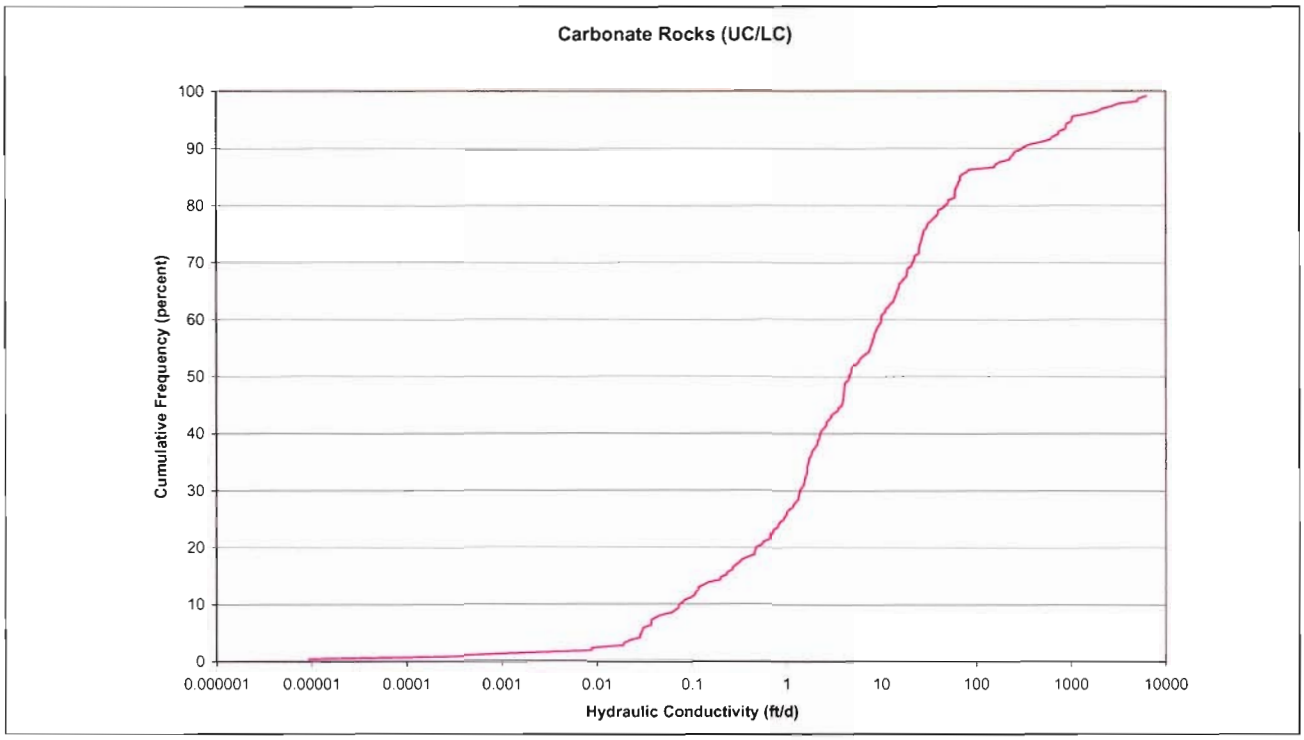

Figure 4-18
Graph Showing Cumulative Distribution of Hydraulic Conductivity: UC/LC

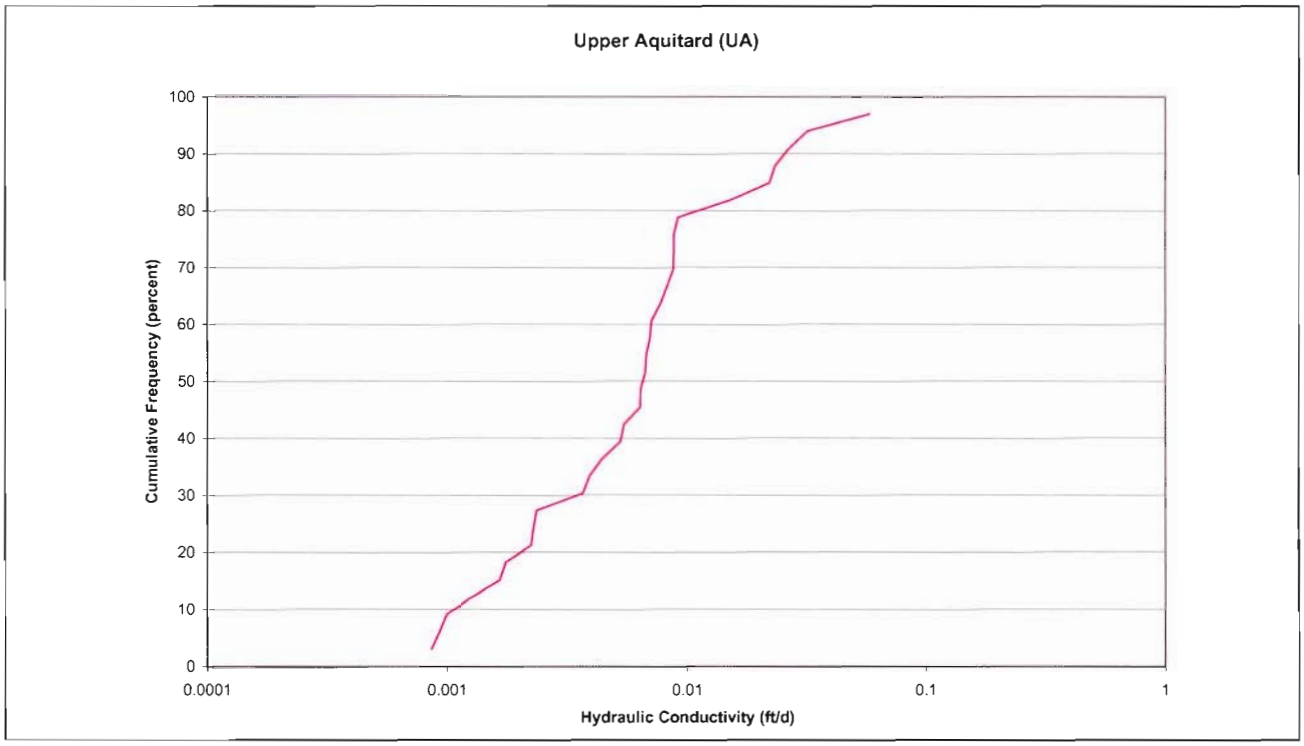

Figure 4-19
Graph Showing Cumulative Distribution of Hydraulic Conductivity: UA

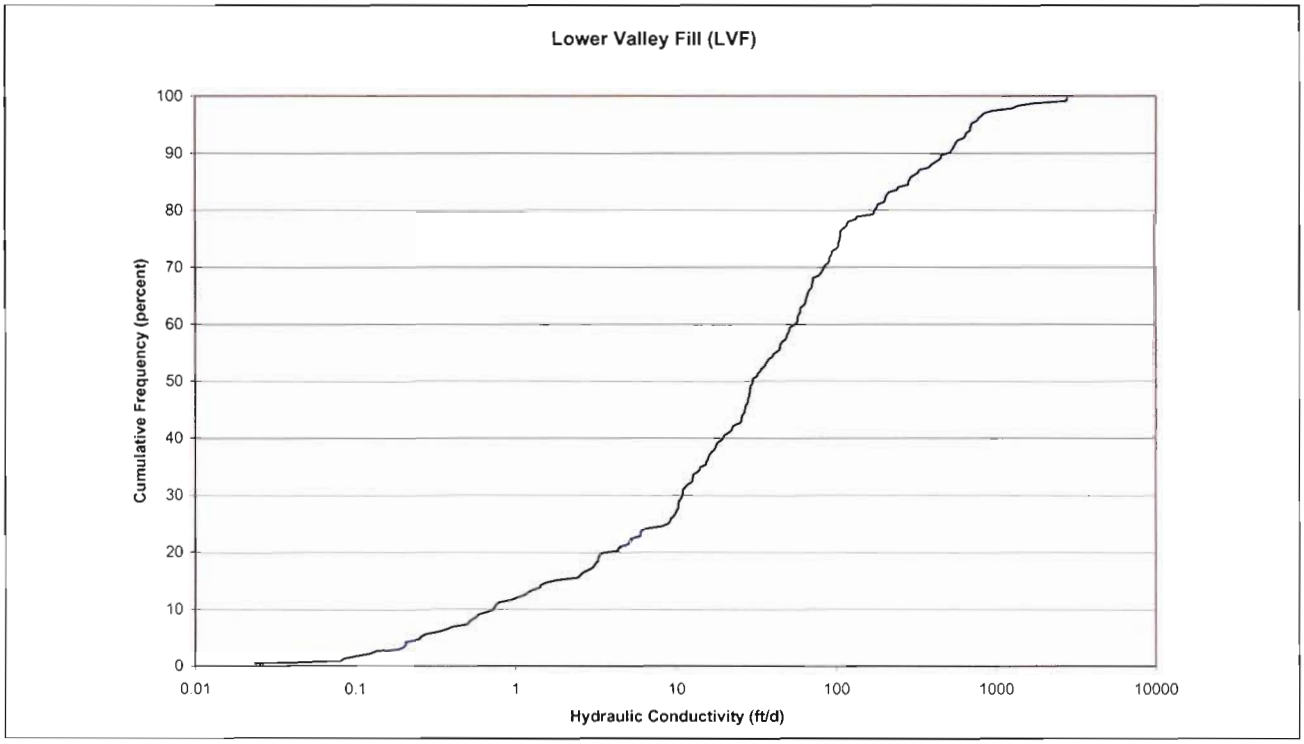

Figure 4-20
Graph Showing Cumulative Distribution of
Depth-Adjusted Hydraulic Conductivity: LVF

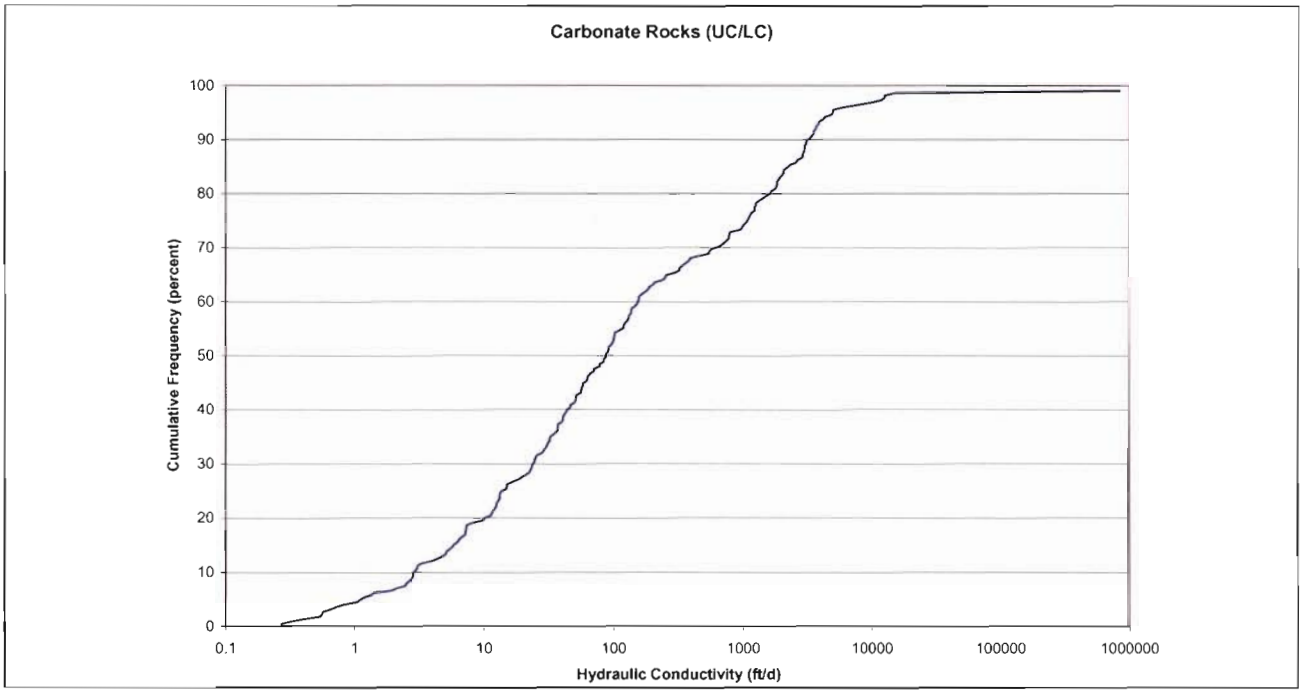

Figure 4-21
Graph Showing Cumulative Distribution of
Depth-Adjusted Hydraulic Conductivity: UC/LC

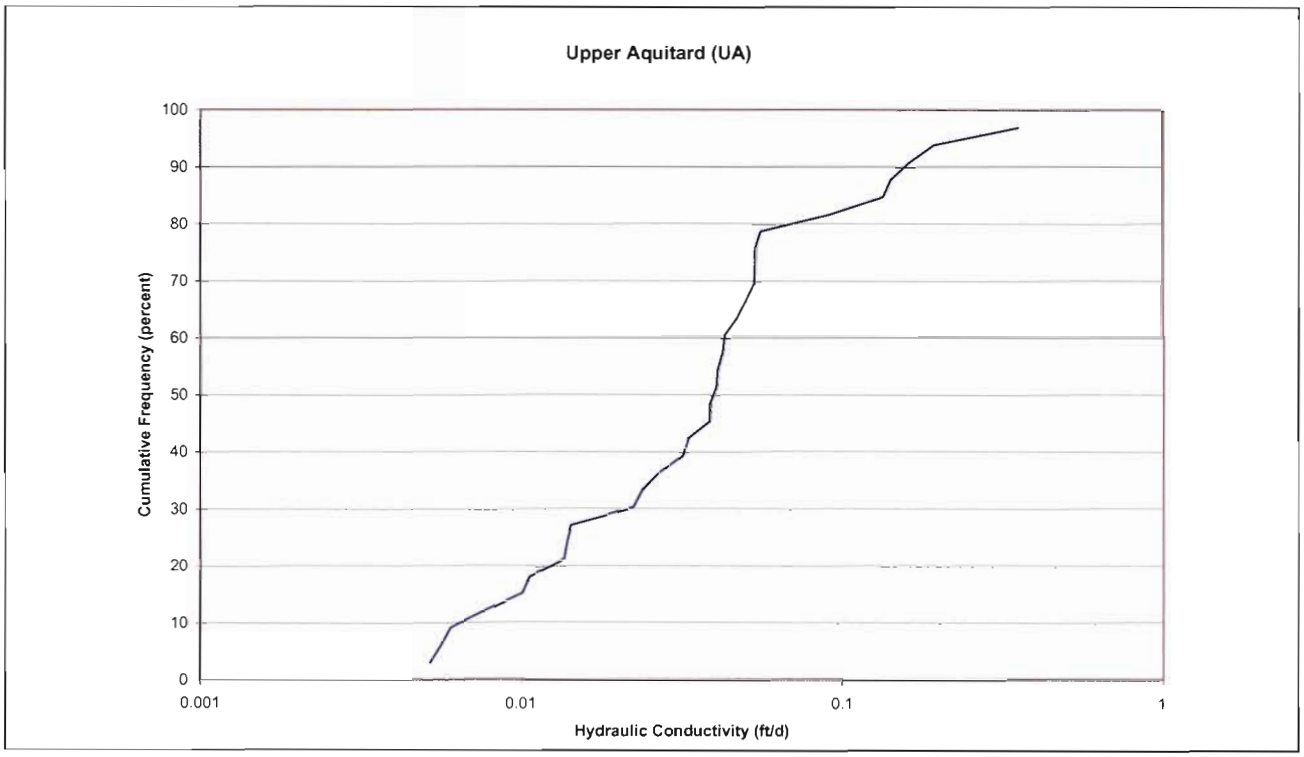

Figure 4-22
Graph Showing Cumulative Distribution of Hydraulic Conductivity: UA

The wells represented by the cumulative distributions range in depth from 300 to 13,700 ft for the lower valley fill, 90 to 7,700 for the carbonate rocks, and 3,000 to 4,600 ft for the upper aquitard. Figures 4-23 through 4-25 show the respective relations of hydraulic conductivity to depth below the land surface. The figures respectively represent the lower valley fill, carbonate rocks, and upper aquitard. The vertical axis represents the hydraulic conductivity on a logarithmic ($\log_{10}$) scale, and the horizontal axis represents the depth on a linear scale. The depth is the midpoint of the perforated interval for the test well. As described previously for the upper valley fill, the data are scattered on the figures, but they do suggest a decrease in log hydraulic conductivity with depth. Interpretations of the respective conductivity-depth relations are shown on Figures 4-23 through 4-25 as plotted functions.

The function is given by Equation 4-1 and Equation 4-2, or Equation 4-3 For the lower valley fill RMU, the parameter values in terms of Equation 4-3 are $a_1 = -7.0\times10^{-7}$ ft^{-1} and $a_2 = 4.0\times10^{-8}$ ft^{-2}. The corresponding tangent depth, which is the depth where hydraulic conductivity becomes invariant with depth, is 8,700 ft. For the carbonate rock and upper aquitard RMUs, the same parameter values were applied. The depth-conductivity data for the consolidated-rock RMUs are so scattered that a specific depth-conductivity relation is difficult to identify. The general existence of a depth-conductivity relation is well established (Ingebritsen and Manning, 1999; Saar and Manga, 2004; Bedinger et al., 1989, IT Corporation, 1996 and 1997; and D'Agnese et al., 1997), and the available data were used as well as possible to incorporate such a relation into the model.

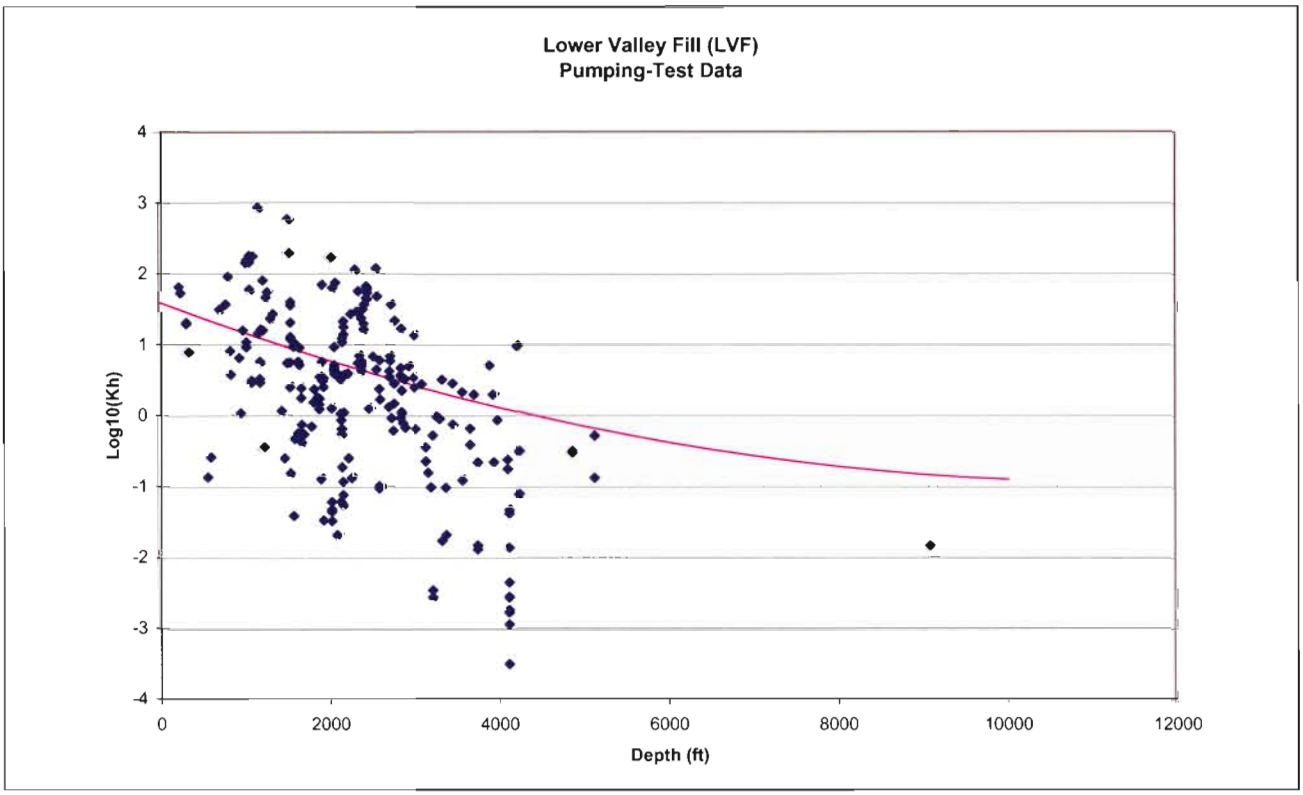

Figure 4-23
Graph Showing Relation Between Hydraulic Conductivity and Depth: LVF

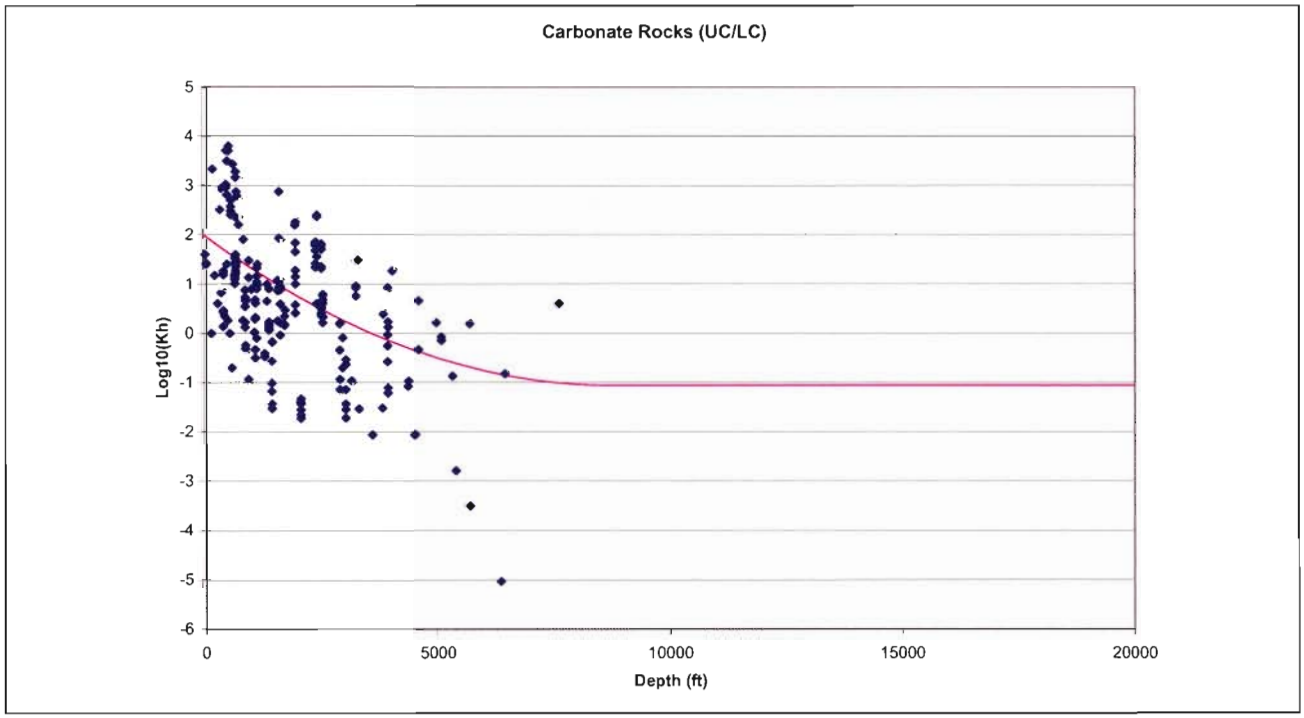

Figure 4-24
Graph Showing Relation Between Hydraulic Conductivity and Depth: UC/LC

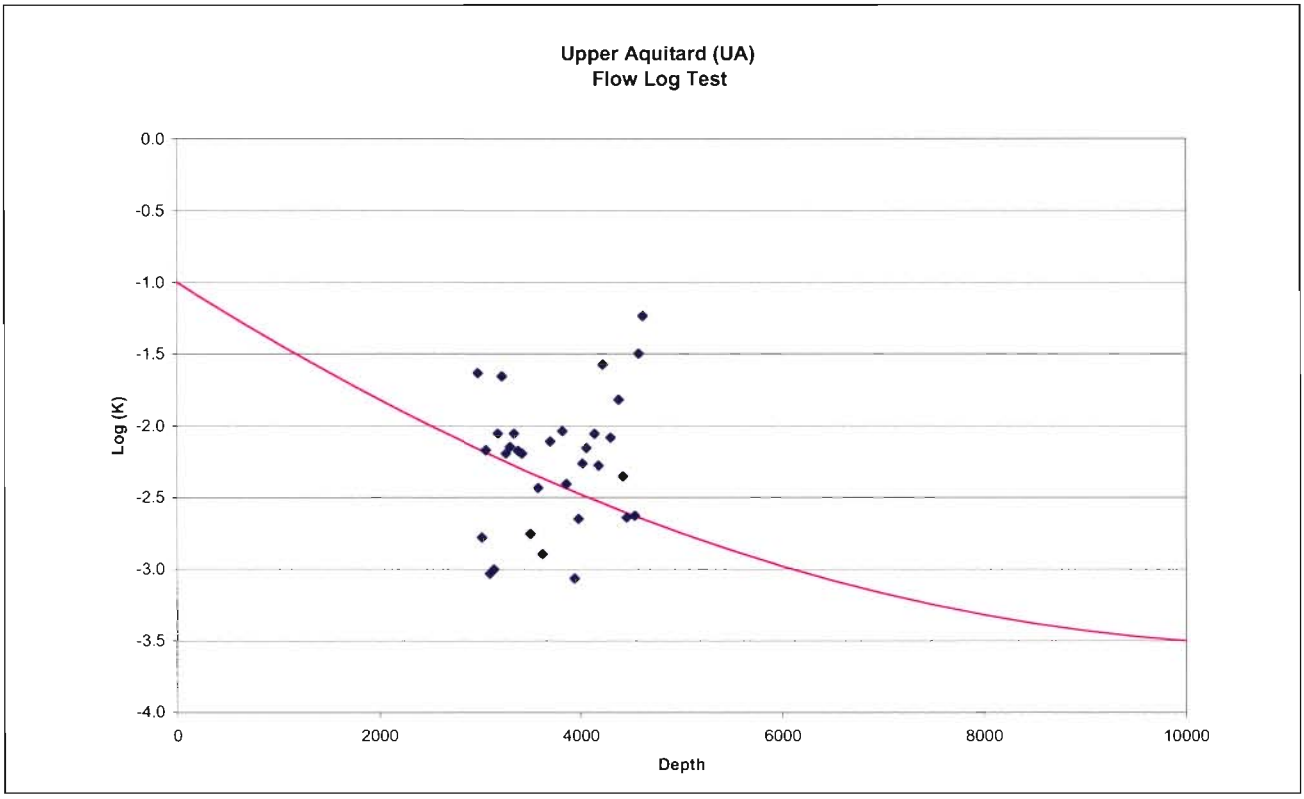

Figure 4-25
Graph Showing Relation Between Hydraulic Conductivity and Depth: UA

Equation 4-3 has a non-zero minimum value of 10^{-3} for the relative hydraulic conductivity. However, Ingebritsen and Manning (1999), Saar and Manga (2004), Bedinger et al., (1989), IT Corporation (1996 and 1997), and D'Agnese et al., (1997) postulated conductivity-depth relations that are either tangent to or asymptotic to a vanishing hydraulic conductivity at depth. At sufficient depth, that most likely is essentially the case, but hydraulic-conductivity data from boreholes within the upper Colorado River basin indicate the occurrence of significant groundwater flow in sandstone and carbonate rocks at depths of 10,000 ft or more. Within Mesozoic sandstones and other rock, active groundwater flow occurs within the Navajo-Nugget aquifer for which burial depths locally exceed 12,000 ft (Freethey and Cordy, 1991). Within Paleozoic sandstones and limestones, artesian wells yield several gallons per minute or more from intervals as much as 16,000 ft below the land surface (Geldon, 1989). Assuming a 100-foot artesian head and 50-foot production interval, such a yield is equivalent to a hydraulic conductivity of 10^{-1} ft/d. For the carbonate rocks within the Spring Valley area, a similar hydraulic conductivity is predicted by the conductivity-depth relation shown on Figure 4-24 for depths exceeding 10,000 ft.

Nevertheless, the minimum relative hydraulic conductivity used in the model is sufficiently small that essentially all the regional groundwater flow occurs at depths less than 8,700 ft. If a lower minimum relative hydraulic conductivity were to be assigned within the groundwater model, the same general partitioning of groundwater flow would occur.

Anisotropy. The consolidated rocks most likely are anisotropic, but the evidence is only indirect. A number of factors can contribute to anisotropic hydraulic conductivity within the consolidated rocks. These include the frequency and orientation of fracturing, the attitude of bedding planes, the frequency and orientation of faulting, and the karstification of the carbonate rocks. However, the importance of individual factors depends in part on the spatial scale that is considered. At scales of a mile or less, fracturing and the attitude of bedding planes may be most important. Structural features at this scale are important to the behavior of individual wells and to the particular occurrence of springs. However, at scales greater than a mile, faulting and karstification may be most important. Hydrogeologic features at this scale are important to the patterns of regional groundwater flow (Greene and Rahn, 1994; Bour and Davy, 1998; and Schulze-Makuch and Cherkauer, 1998).

Within the Spring Valley area, bedding planes are inclined about strikes that have a northward trend. If the hydraulic conductivity of a consolidated rock is different parallel to the bedding plane than perpendicular to the bedding plane, the tilting of the bedding plane will induce horizontal anisotropy along the bedding-plane strike azimuth with respect to the dip azimuth. A 30-degree bedding plane dip is not uncommon, and the overall result of the bedding-plane attitudes within the Spring Valley area is that fracturing causes anisotropic horizontal hydraulic conductivity in the north-south direction relative to the east-west direction. Furthermore, field observations of factures in outcrops suggest a greater frequency and length of fracturing parallel to bedding planes than perpendicular to the bedding planes. Correspondingly, the principal hydraulic conductivity parallel to the bedding plane would be larger than the principal conductivity perpendicular to the bedding plane (Nordqvist et al., 1992; Hester and Long, 1990; Renshaw, 1998; Berkowitz et al., 2000; and Margolin et al., 1998). Were this to be the case, a higher horizontal hydraulic conductivity would occur in the north-south direction than in the east-west direction.

Faulting most likely has imparted horizontal anisotropy to the consolidated rocks at scales greater than a mile. Faults through consolidated rocks can be conduits to groundwater flow. As described by SNWA (2006c), the principal faulting trends northerly parallel to the mountain ranges. However, westerly cross faulting occurs. An analysis by Faunt (1997) of faults within the Death Valley region indicates the frequency of faulting in different orientations, where the northerly orientations are perhaps fivefold more abundant than westerly orientations. An additional analysis by Faunt (1997) of the crustal stress field suggests that faults with northerly orientations would be in tension, while faults with westerly orientations would be in compression. By geographic extrapolation these conditions are expected to prevail within the Spring Valley area.

Faults display a variety of architectures that result in pathways for groundwater flow within the fault plane. However, these pathways tend to occur within a zone of damaged or deformed rock adjacent to the principal plane of displacement (Caine and Forster, 1999 and Caine et al., 1996). Cain and Forster (1999) describe the damage zone as consisting of fractures and small faults that can be characterized in terms of fractures of specified aperture. Additionally, they assumed the transmissivity of an aperture is proportional to the aperture cubed (Snow, 1968 and Snow, 1969). This conceptual model then can be extended to sets of intersecting faults based on the model of Snow (1969).

Using this extension, for two orthogonal sets of vertical faults within the Spring Valley area, Snow (1969) indicates the sets are equivalent to a hydraulic conductivity tensor with principal axes of the

horizontal hydraulic conductivity parallel to traces of the sets. Furthermore, the hydraulic conductivity in a particular direction is proportional the fault frequency and is proportional to the aperture width cubed. Faunt (1997) indicates a fivefold greater frequency of northerly oriented faults relative to the westerly oriented faults. Faunt (1997) additionally suggests that the northerly oriented faults are in tension, while the westerly faults are in compression. Correspondingly, the apertures of the westerly faults are expected to be smaller. If the apertures of the westerly oriented faults were to be just 70 percent of the apertures of the northerly oriented faults, the combined effects of fault frequency and aperture would be exhibited as a hydraulic-conductivity anisotropy of 1:10 (Snow, 1969), with the higher hydraulic conductivity in the northerly direction.

The model of Snow (1969) also indicates a vertical anisotropy. The vertical hydraulic conductivity is the sum of the principal horizontal hydraulic conductivities. North-south groundwater flow occurs only in the northerly oriented faults, east-west flow occurs only in the westerly oriented faults, yet vertical flow occurs in both the northerly and westerly oriented faults. Correspondingly, both fault sets contribute to the vertical hydraulic conductivity. Based on the aperture assumption immediately above, the contribution of the westerly oriented faults is one-tenth the contribution of northerly oriented faults, which means that the vertical hydraulic conductivity is about equal to the northerly hydraulic conductivity. The three-dimensional anisotropy then is 1:10:10 respectively for the westerly, northerly, and vertical hydraulic conductivities.

This anisotropy is confirmed by the model calibration. Early calibration configurations, which are described later, were used to identify the three components of the hydraulic-conductivity tensors for each of the consolidated-rock RMUs. While the confidence intervals on the identified parameters were large, various calibration configurations consistently produced three-dimensional anisotropies similar to the proportions of 1:10:10 respectively for the westerly, northerly, and vertical hydraulic conductivities. This was the case for the lower valley fill, carbonate rock, upper aquitard, plutonic rock, and basement rock RMUs.

The orientation of the hydraulic-conductivity tensors for the consolidated rocks most likely varies regionally in accordance with local changes in the specific azimuth of the northerly oriented faults. Figure 4-26 shows the local orientation of the horizontal principal axes of the hydraulic-conductivity tensor, where the tensor is aligned with the general direction of the mountain-front faults.

Scaling. The hydraulic conductivity of the consolidated rocks depends on the scale of observation (Schulze-Makuch and Cherkauer, 1998; Hester and Long, 1990; Nordqvist et al., 1992; Berkowitz et al., 2000; Renshaw, 1998; Margolin et al., 1998; David et al., 1990; and Dverstorp and Andersson, 1989). The hydraulic conductivity at the scale of the Spring Valley model most likely is dominated by the effects of intermediate-scale but extensive faulting, while the hydraulic conductivity at the scale of an aquifer test most likely is dominated by fracturing. However, a likely conceptual model for scaling the hydraulic conductivity of the consolidate rocks includes both faults and fractures. This conceptual model is comprised of superimposed hierarchal networks. First is the network of orthogonal intermediate-scale faults, which have length scales measured in thousands of feet. Second is a network of large-scale fractures, which have length scales measured in hundreds of feet. Third is a network of intermediate scale fractures, which have length scales measured in tens of feet.

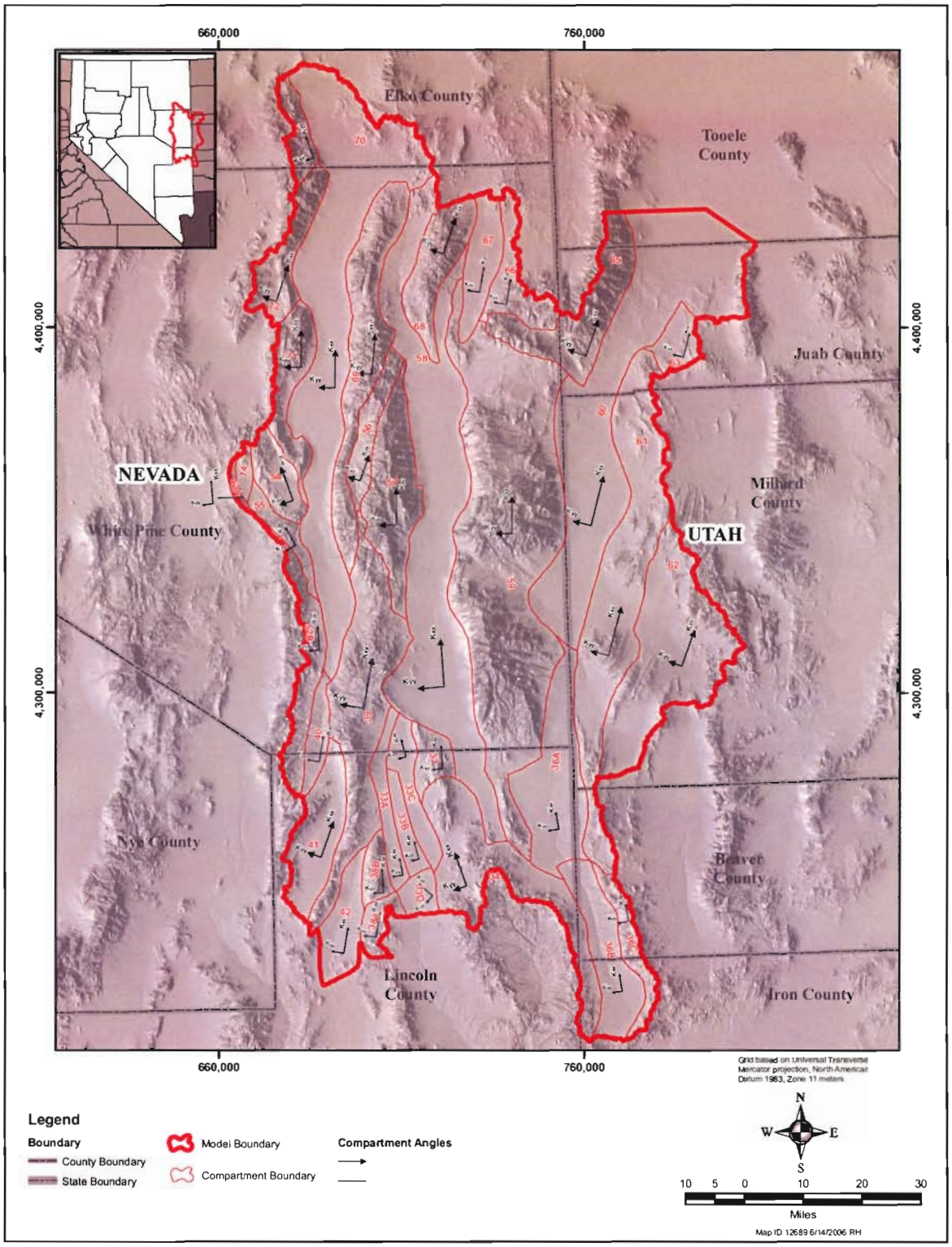

Figure 4-26
Map Showing the Orientation of Hydraulic-Conductivity Tensors for the Consolidated Rocks

The interpretation of a randomly located aquifer test relative to these networks depends on a number of factors. The principal factor is the interconnectivities within a network and between networks. Those interconnectivities in turn depend on the probability distributions describing the abundance, lengths, and apertures of the fractures or faults with different attitudes. Those distributions determine the continuity of flow pathways at each scale, but disparate continuities can occur at different scales. Concomitantly, the scaling factor for the aquifer-test data can range from less than unity to greater than unity, depending on interconnectivities at different scales. However, essentially no information is available at the required scales to estimate a scaling factor for any of the consolidated-rock RMUs.

As a result, the aquifer-test data available for the consolidated-rock RMUs does not provide much information on the model-scale hydraulic conductivities. Those hydraulic conductivities must be identified from the calibration of the model.

4.1.2.2 Conceptual Model

The conceptual model of the consolidated-rock RMUs, which include the lower valley fill, carbonate rocks, upper aquitard, plutonic rocks, and basement rocks, consists of the following elements. Firstly, the hydraulic conductivity for each of the consolidated-rock RMUs decreases with depth identically according to the conductivity-depth relation shown on Figures 4-23 through 4-25. Secondly, the consolidated-rock RMUs are identically anisotropic three-dimensional in hydraulic conductivity with the ratios 1:10:10 with respect to the northerly, westerly, and vertical directions.

5.0 SPECIFIED FLUXES

5.1 Background

The specified fluxes are the head-independent recharges and discharges within the model area. The specified fluxes do not include fluxes represented in the model as head-dependent processes, such as phreatophyte discharges and streamflow-groundwater interactions. For the head-dependent processes, phreatophyte discharges are discussed in Section 6.0 and streamflow-groundwater interactions are discussed in Section 7.0. The specified fluxes within the model area include mountain-block precipitation recharge, some occurrences of mountain-front streamflow recharge, boundary groundwater underflows, and cultural water use. The mountain-block recharge represents the direct infiltration of precipitation within interfluvial areas and the net recharge owing to streamflow-groundwater interactions along the channel reaches within mountain-block areas. The mountain-front streamflow recharge is groundwater recharge that in the model is accounted for neither in the mountain-block recharge nor in the explicit simulation of streamflow as described in Section 7.0. The groundwater underflows are groundwater flows from the model area to adjacent areas. The cultural water use includes the consumptive use of groundwater and surface water by the largest communities within the model area and the consumptive use of groundwater by agricultural irrigators.

The specified fluxes represent a net groundwater recharge for the model area. The mountain-block recharge (an inflow) averages about 285,600 acre-ft/yr (Table 2-1). The mountain-front streamflow recharge (an inflow) averages about 2,700 acre-ft/yr (Table 2-1). The groundwater underflows (an outflow) average 45,700 acre-ft/yr (Table 2-1). The cultural water use (outflows) was about 1,400 acre-ft/yr in 1960 (Table 2-1) and about 15,100 acre-ft/yr in 2005. The net recharge for all the specified fluxes within the model area (inflows less outflows) is 241,200 acre-ft/yr for 1960 and 227,500 acre-ft/yr for 2005.

The specified fluxes are simulated using the module *WFLUX* within *FEMFLOW3D*. The respective specified fluxes represent either time-invariant or time-variant groundwater recharge or discharge. The mountain-block precipitation recharge, mountain-front streamflow recharge, and boundary underflows are treated as time-invariant model inputs. The community and agricultural water use is treated as a time-variant input. The development of these inputs is described below.

5.1.1 Mountain-Block Precipitation Recharge

The mountain-block precipitation recharge used in the model is based on an evaluation by SNWA (2006b, Volume 2) of Maxey-Eakin recharge estimates (Eakin and others, 1951) developed by Eakin (1962), Eakin (1963), Rush and Eakin (1963), Rush and Kazmi (1965), Hood and Rush (1965), and

Eakin and others (1967). Except for Spring, Steptoe, and Snake valleys, the mountain-block recharges assigned to the model are the Maxey-Eakin recharges estimated by these investigators (Table 2.4-1). Spring, Steptoe, and Snake valleys are more complicated because the investigators also estimated mountain-front streamflow that is partly accounted for in the Maxey-Eakin recharge estimates.

The translation of Figure 5-1 into model inputs involves calculating nodal fluxes for nodes representing the top surface of the three-dimensional finite-element mesh. In other words, Figure 5-1 expresses the recharge in units of depth per unit time. That must be translated into nodal fluxes in units of volume per unit time. The translation is given by the relations (Pinder and Gray, 1977)

$$q_{i,e} = \frac{1}{3}\iint_{A_e} r(x, y)dxdy \tag{5-1}$$

and

$$Q_i = \sum_e q_{i,e} \tag{5-2}$$

where

$q_{i,e}$ is the flux at node i due to the recharge within the area of element e [L^3t^{-1}],
r is the recharge per unit area represented by Figure 5-1 [Lt^{-1}],
A_e is the geographic limits of element e [L^2], and
Q_i is the cumulative flux at node i due to all the elements connected to node i [L^3t^{-1}].

Equation 5-1 and Equation 5-2 together state that a nodal flux equals one-third of the area recharge occurring on all the elements connected to the node.

5.1.2 Mountain-Front Streamflow and Recharge

The data used is described in SNWA (2006a) to estimate the additional recharge from mountain-front runoff. The mountain-front runoff from streamflows are modeled at approximately 47,000 acre-ft/yr for Spring Valley with a corresponding recharge calculated from the model as 18,400 acre-ft/yr (Tables 2.1-1 and 2.1-2).

While the mountain-front streamflow within Spring Valley is treated in the simulation of streamflow-groundwater interactions as described in Section 7.0 the streamflow within Snake Valley is treated in the model as a specified flux. Using the module *WFLUX* in *FEMFLOW3D*, the Snake Valley streamflow is reflected as valley-floor recharge along Big Springs Wash immediately downstream from the mountain front (Figure 5-2). The average recharge is 2,700 acre-ft/yr.

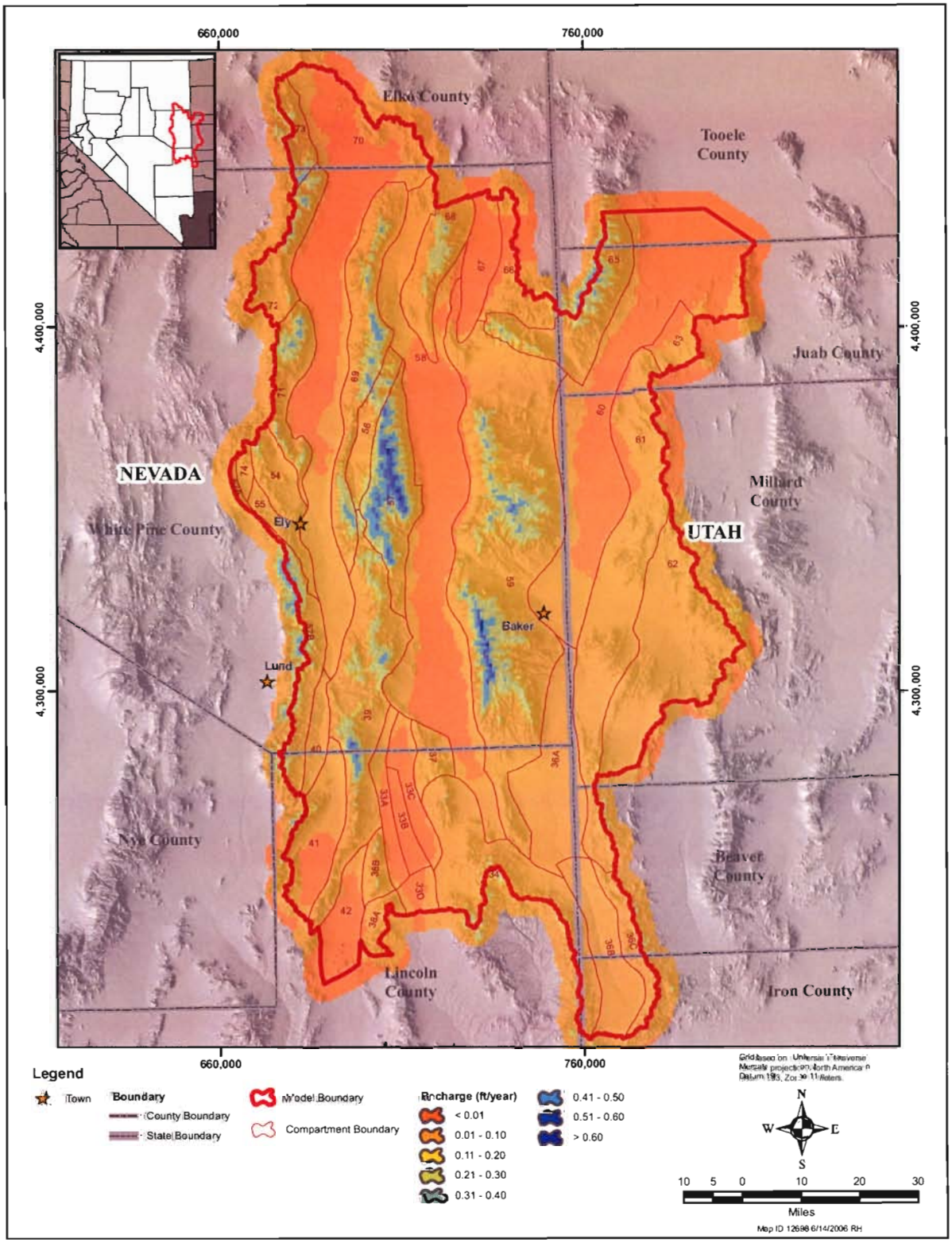

Figure 5-1
Map Showing Precipitation Recharge Within the Spring Valley Area

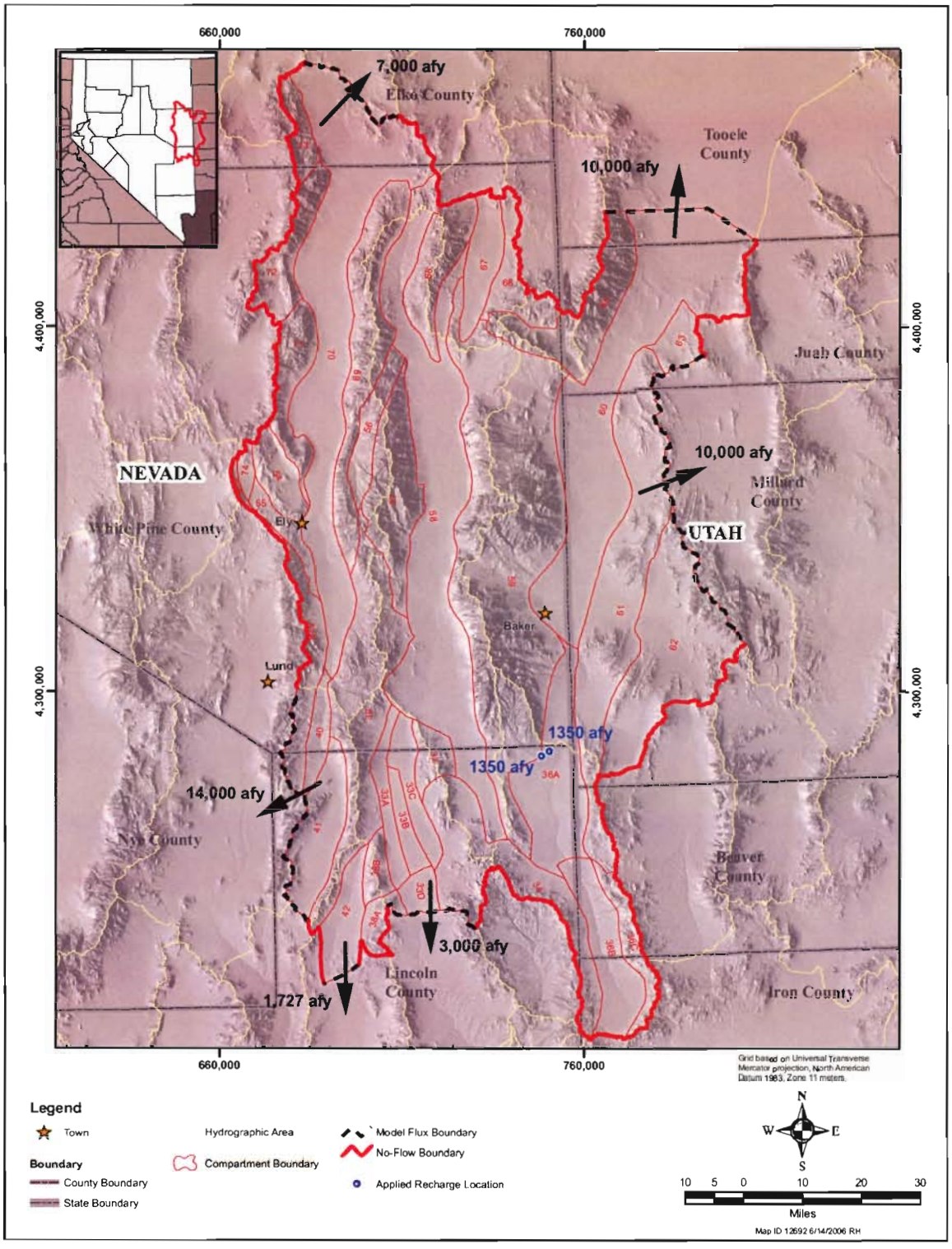

Figure 5-2
Map Showing Locations of Groundwater Recharge From Streams and Boundary Underflows

5.1.3 Boundary Underflows

Eakin (1962), Rush and Eakin (1963), Rush and Kazmi (1965), Hood and Rush (1965), and Eakin and others (1967) estimated the inter-basin groundwater underflows within the Spring Valley area, including underflows at the boundary of the area. Based on the review of these estimates as described by SNWA (2006b, Volume 7), boundary underflows were assigned to the Spring Valley model at the locations shown on Figure 5-2. At each location, the underflows are outflows from the Spring Valley area. The cumulative average outflow is 45,700 acre-ft/yr. The average underflows at specific locations are 10,000 acre-ft/yr from Snake Valley eastward into Tule Valley, 10,000 acre-ft/yr from Snake Valley northward into the Great Salt Lake basin, 7,000 acre-ft/yr from Steptoe Valley northward into Goshute Valley, 14,000 acre-ft/yr from Cave Valley westward into White River Valley, and 3,000 acre-ft/yr from Lake Valley southward into Patterson Valley.

According to Eakin (1963) and Rush and Eakin (1963) underflows do not occur from either Cave Valley or Lake Valley into Dry Lake Valley. Correspondingly, the underflow assigned to the Dry Lake Valley boundary of the model equals only the mountain-block recharge within that part of Dry Lake Valley included in the Spring Valley model. SNWA (2006b, Volume 2) estimates that the recharge within the northern part of Dry Lake Valley is 1,700 acre-ft/yr, and an underflow of that value is assigned within the model to represent southward groundwater flow at the model boundary.

5.1.4 Cultural Water Use

The cultural water use includes water use for community, agricultural, industrial, and mining purposes. However, the Spring Valley model represents implicitly only the water use of the largest communities within the Spring Valley area and the groundwater use by agriculture. These are represented in the model as specified fluxes representing the consumptive uses. The consumptive-use component of any water use is the hydrologically significant component, because it is the consumptive-use component that can cause large-scale responsive changes in groundwater system. Correspondingly, water uses that do not have a large consumptive-use component are not important to the hydrologic system. This is the case for consumptive uses that are small with respect to the head-dependent discharges from the groundwater system. For the Spring Valley area, industrial and mining uses both fall into this category, and they are not represented in the model.

5.1.4.1 Surface-Water Use for Agricultural Irrigation

Even though agricultural use of surface water has had some impact on consumptive use within the model area, that consumptive use does not need to be represented in the model. The reasons are as follows: Firstly, the surface water use for irrigation mostly has been to irrigate lands that under pre-development conditions were covered with native phreatophytes. Under the pre-development conditions, the native vegetation often represented meadows of various classifications. Correspondingly, irrigation of these lands created only an increment of additional consumption equal to the difference between the pre-development and post-development consumptive uses.

Secondly, the development of surface water occurred mostly during the early part of the modern cultural history of the model area. Consequently, the hydrologic system has equilibrated with that development through modification of the pre-development rate and geographic distribution of water use by phreatophytes. This modification occurred because cultural consumptive uses, owing to either groundwater or surface-water development, eventually always translate into groundwater impacts. Furthermore, the impacts ultimately are expressed as changes in the natural head-dependent discharges from the groundwater system, such as the water use by phreatophytes.

Thirdly, because the historical surface-water development is expressed in the steady-state water use by phreatophytes, that development is represented implicitly in the model through the simulation of the phreatophytic consumptive use. Eakin (1962), Rush and Eakin (1963), Rush and Kazmi (1965), Hood and Rush (1965), and Eakin, Hughes, and Moore (1967) estimated the phreatophytic consumptive use within the model area in about 1960. The estimated consumptive use reflects the pre-1960 surface-water development. Therefore, the Spring Valley model, in effect, uses the 1960 phreatophytic consumptive use as an initial condition. Correspondingly, the historical surface-water development is represented in the model.

The relation of surface-water development to phreatophytic consumptive use is shown on Figure 5-3 for a closed hydrologic system. This figure shows two diagrams. Figure 5-3 represents the pre-development and post-development steady-state condition. Based on the control volume delineated on Figure 5-3 the water budget for the pre-development condition is given by the relation

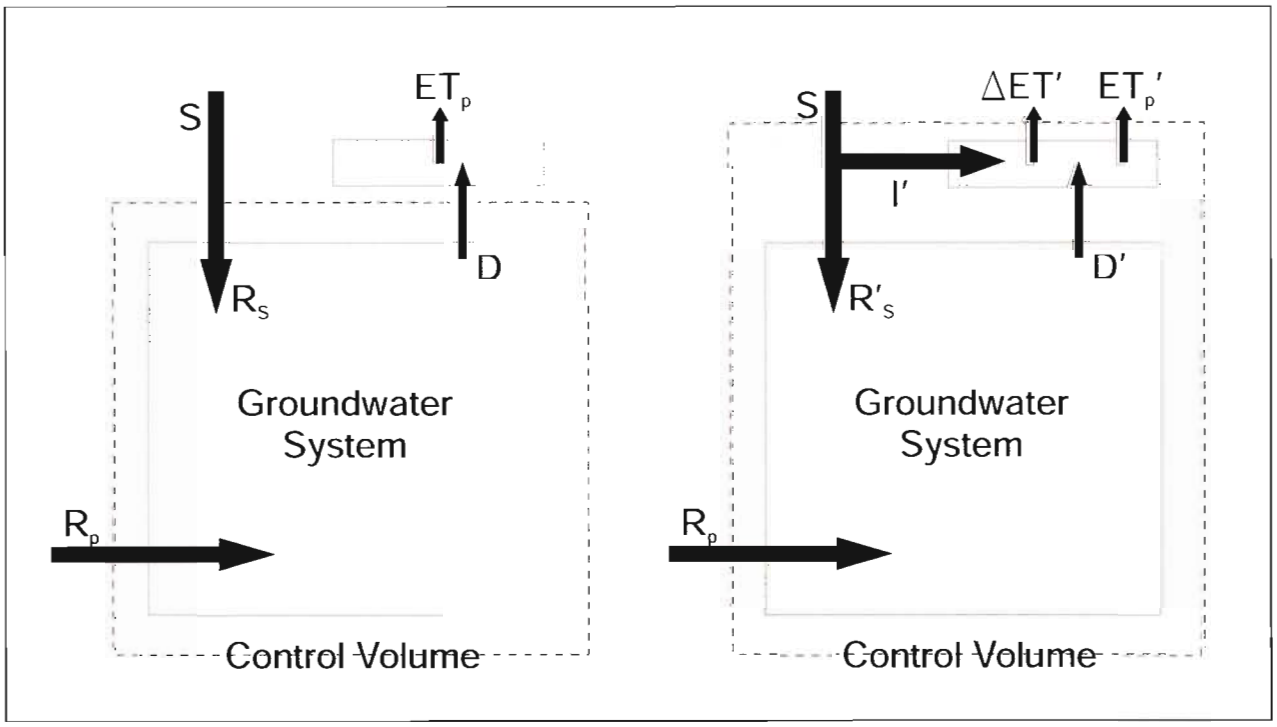

Figure 5-3
Diagram Showing Impact of Surface-Water Development on a Groundwater System: Pre-Development and Post-Development

$$R_S + R_P = D \tag{5-3}$$

or alternatively

$$S + R_P = ET_P \tag{5-4}$$

where
R_S is the recharge from streamflow [L^3t^{-1}],
R_P is the recharge from mountain-block precipitation [L^3t^{-1}],
D is the groundwater discharge to phreatophytes [L^3t^{-1}],
ET_P is the consumptive use by phreatophytes [L^3t^{-1}], and
S is the mountain-front streamflow [L^3t^{-1}].

The corresponding water budget for the post-development condition is given by the relation

$$R_S' + I' + R_P = \Delta ET' + ET_P' \tag{5-5}$$

or alternatively

$$S + R_P = \Delta ET' + ET_P' \tag{5-6}$$

where

R_S' is the streamflow recharge after the irrigation diversion [L^3t^{-1}],
I' is the surface-water diversion for irrigation [L^3t^{-1}],
$\Delta ET'$ is the change in agricultural consumptive use due to irrigation [L^3t^{-1}], and
ET_P' is the phreatophytic consumptive use after the irrigation [L^3t^{-1}],

and where the prime notation indicates a quantity that changes in the post-development condition.

The pre-development water budget (Equation 5-4) and the post-development water budget (Equation 5-6) can be combined to yield an expression for the change in the hydrologic system due to the surface-water development. The resulting expression is

$$\Delta ET' + ET_P' = ET_P \tag{5-7}$$

which indicates that agricultural plus natural consumptive use under the post-development condition equals the natural consumptive use under the pre-development condition.

The model uses the condition expressed by Equation 5-7 as an initial steady-state condition and thereby incorporates the historical surface-water development.

5.1.4.2 Groundwater Use for Agricultural Irrigation

Groundwater has been developed for agricultural irrigation within the Spring Valley area. However, that development occurred much later than the surface-water development. Eakin (1962), Rush and Eakin (1963), Rush and Kazmi (1965), Hood and Rush (1965), and Eakin and others (1967) indicate that as late as the early 1960's, very little groundwater development had occurred. While Hood and Rush (1965) suggest for Snake Valley that some groundwater irrigation was occurring in 1967, elsewhere within the Spring Valley area the consumptive uses of groundwater were minor and have not been included. However, since the mid 1960's, groundwater has been developed for irrigation within the Spring Valley area.

The consumptive-use component of groundwater use for irrigation, which is quantitatively equivalent to the pumping less the returns to the groundwater system, is the water-use component that can have large-scale impacts on the groundwater system. Furthermore, the consumptive-use component of relevance is the change in the groundwater consumptive use relative to pre-development conditions. For the new irrigation of previously non-phreatophytic areas, the change is the consumptive use of the crop. For the new irrigation of phreatophytic areas, the change is the consumptive use of the crop less the previous consumptive use of the phreatophytes.

The consumptive use associated with agricultural irrigation depends on the acreage actually irrigated, the potential evapotranspiration for the crop, the crop water-use coefficient, the effective precipitation, the crop uniformity within the irrigated acreage, and the previous groundwater consumptive use for the irrigated acreage. Furthermore, to estimate the long-term average consumptive use, the consumptive use depends on the year-to-year continuity of irrigation, which is influenced by energy costs and the local and regional markets for the produced crops. The factors are related by the expression

$$\Delta ET = A\left(k_U k_C k_O PET - P_e - ET_p\right) \tag{5-8}$$

where

ΔET is the change in consumptive use due to groundwater irrigation [L^3t^{-1}],
PET is the potential evapotranspiration [Lt^{-1}],
P_e is the effective precipitation [Lt^{-1}],
ET_p is the prior evapotranspiration of native phreatophytes [Lt^{-1}],
A is the irrigated acreage [L^2],
k_U is the crop uniformity coefficient [L^0],
k_C is the crop water-use coefficient [L^0], and
k_O is the crop coefficient for other factors [L^0].

The application of Equation 5-8 to the model area yields the consumptive-use estimates listed in Table 2.4-2, which indicates the agricultural consumptive use was about 300 acre-ft/yr in 1960 and about 13,100 acre-ft/yr in 2005. The parameter values used in Equation 5-8 are described below.

The irrigated acreage is based on the interpretation of imagery and water-rights information. Firstly, the estimate is based in part on the interpretation of a false-infrared satellite image of the Spring Valley area representing 2002 as shown on Figure 5-4. Secondly, the estimate is based on the interpretation of the U.S. Geological Survey 7.5-minute ortho-photographic quadrangles for the Spring Valley area. The satellite image was used to identify irrigated areas, and the ortho-photo quadrangles were used to enhance the interpretation of the satellite image. Water-rights information (SNWA, 2006b, Volume 5) was used to discriminate, as best possible, amongst areas irrigated solely with groundwater or surface water. This information was used concurrently to identify probable areas of agricultural irrigation with groundwater as shown on Figure 5-5.

Information on potential evapotranspiration and precipitation was obtained from SNWA (2006b, Volumes 2 and 3). SNWA (2006b, Volume 3) developed a relation between potential evapotranspiration, latitude, and elevation, and that relation SNWA used to identify a potential evapotranspiration for each valley within the model area. SNWA (2006b, Volume 2) prepared a map of annual precipitation, and that map was used to identify a precipitation for each valley.

The water-use and uniformity coefficients were selected based on a literature review. The water-use coefficient, which relates to a crop with full coverage and uniform irrigation, probably equals about 0.9 (Doorenbos and Pruitt, 1977; California Department of Water Resources, 1967; California Department of Water Resources, 1986; and American Society of Civil Engineers, 1990). The uniformity coefficient, which relates to a crop with less than full coverage and non-uniform irrigation, probably equals about 0.7 (American Society of Civil Engineers, 1990 and American Society of Agricultural Engineers, 1990). The likely combined effect of the water-use and uniformity coefficients is to reduce the consumptive use to about 80 percent of the potential evapotranspiration.

The coefficient for the other factors, which includes the continuity of production, was assumed to be about 0.7, based on observations of abandoned areas of previous irrigation in the field, on ortho-photographic quadrangles, and on satellite images.

5.1.4.3 Surface-Water and Groundwater Use for Community Uses

Ely and McGill are the largest communities within the Spring Valley area. Both groundwater and surface water are used by these communities to satisfy water-supply requirements. The values were estimated from the community populations, per capita water use, and a consumptive-use fraction as described by SNWA (2006b, Volume 5) The consumptive-use fraction is estimated to equal 50 percent, which means that 50 percent of the water supply is consumed owing to either landscape irrigation or wastewater disposal practices.

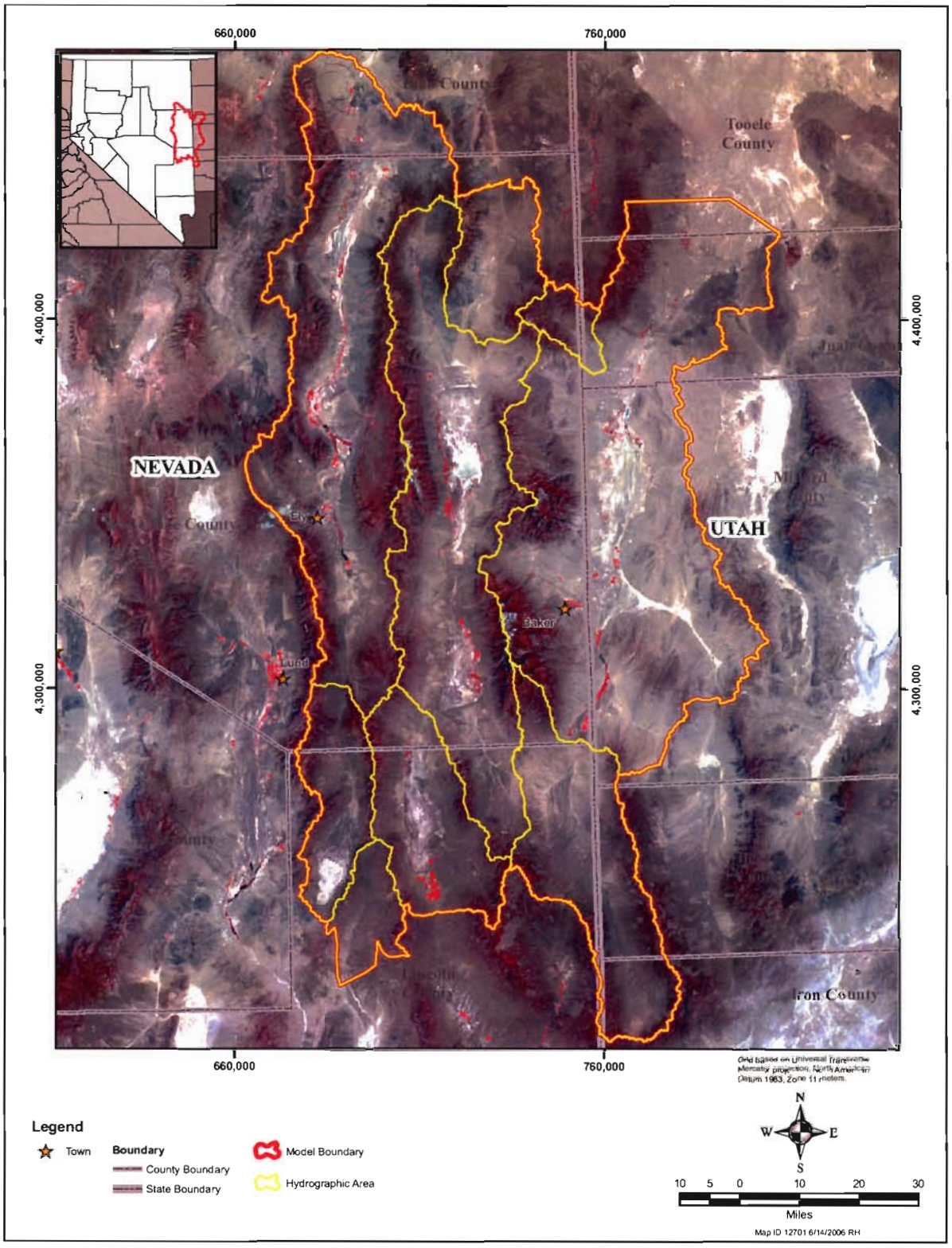

Figure 5-4
Map Showing Satellite Image of the Spring Valley for 2002

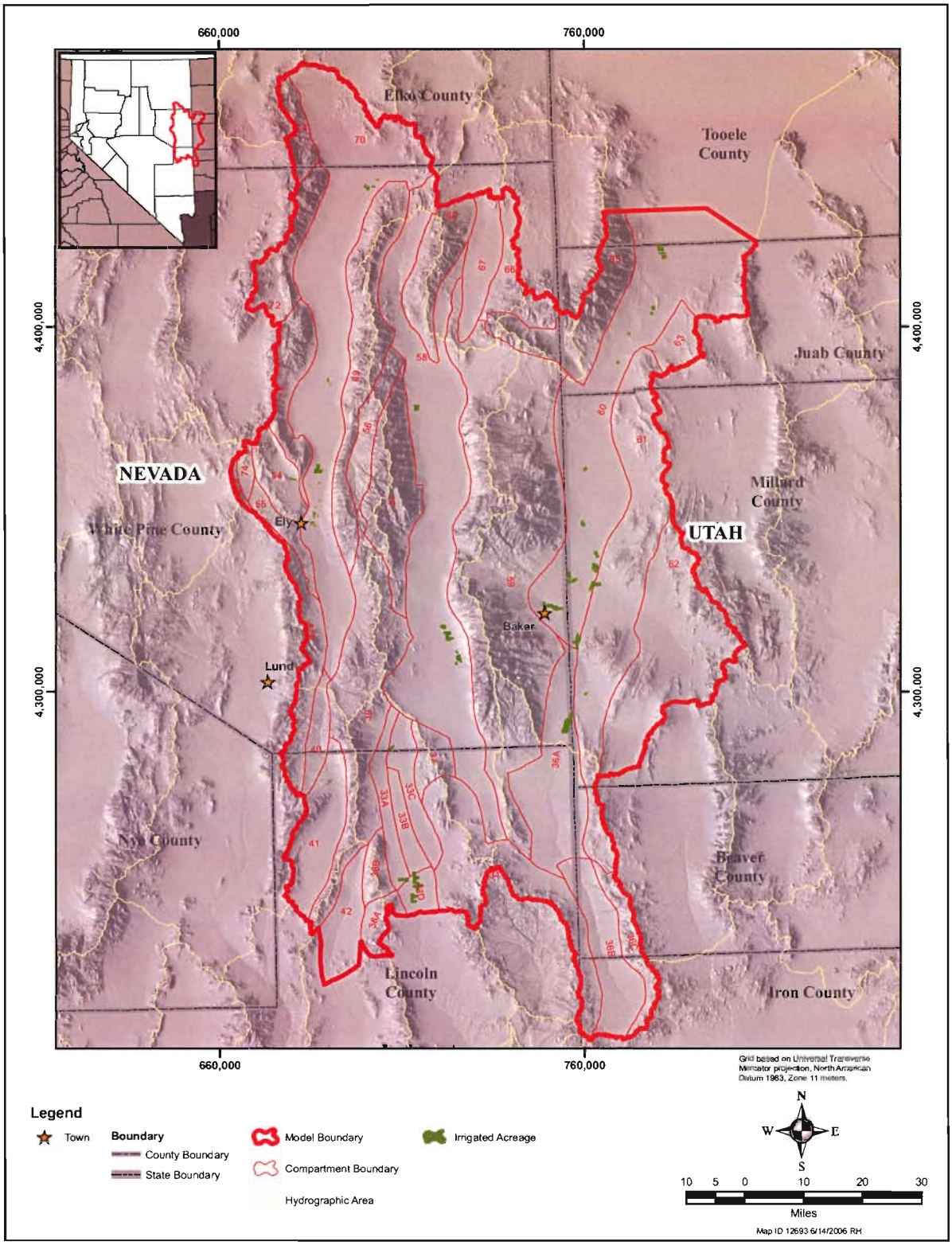

Figure 5-5
Map Showing Areas Irrigated With Groundwater in 2002

This Page Intentionally Left Blank

6.0 GROUNDWATER DISCHARGES TO PHREATOPHYTE AREAS AND PLAYA SURFACES

6.1 Background

The consumptive use of groundwater by phreatophytes represents the largest groundwater discharge within the model area. The average consumptive use is about 245,000 acre-ft/yr, based on the discharges estimated by Eakin (1962), Rush and Eakin (1963), Rush and Kazmi (1965), Hood and Rush (1965), and Eakin, Hughes, and Moore (1967). This discharge occurs over an area of 700,000 acres, with a corresponding average consumptive use rate of 0.35 ft/yr. As described by SNWA (2006b, Volume 3), the phreatophyte areas are comprised of meadow, non-meadow, and bare-soil areas. The meadow areas cover about 99,000 acres (Table 6-1) and mostly represent saltgrass and saltgrass-rabbitbrush vegetation communities. The non-meadow areas cover about 525,000 acres (Table 6-1) and mostly represent greasewood and greasewood-rabbitbrush communities. The bare-soil areas cover about 76,000 acres (Table 6-1) and mostly represent playa areas.

The particular phreatophyte associations tend to occur in areas where the depth to the groundwater table is within a specific range. The saltgrass tends to occur where the depth to groundwater is less than 8 ft, but it is observed where the depth to groundwater is as much as 12 ft (Robinson, 1958; Young and Blaney, 1942; and Blaney and others, 1933). Data collected in the Owens Valley, California (Manning, 2001 and Harrington and Howard, 2000) indicates that saltgrass occurs where the groundwater depth is less than 10 ft, yet it has been observed where the depth to groundwater is as much as 20 ft. Rabbitbrush tends to occur where the depth to groundwater is less than 15 ft. However, data collected in the Owens Valley (Manning, 2001 and Harrington and Howard, 2000) indicates rabbitbrush occurs where the depth to groundwater is as much as 20 ft. Greasewood tends to occur where the depth to groundwater is less than 50 ft (Robinson, 1958). While this represents the typical groundwater conditions for these species, other factors influence the habitable groundwater depth within a particular location. These factors include soil texture, soil-water quality, and climate. Where the soil texture is finer, the soil-water salinity is lower, and the climate is wetter, particular species can occur in association with a deeper groundwater table.

The consumptive use of groundwater depends in part on the depth to the groundwater table (White, 1932; Young and Blaney; 1942; Robinson, 1958; Blaney, 1958; and Rantz, 1968). Furthermore, the relation of consumptive use to the groundwater depth can be approximated by a linear function (Robinson, 1958 and Rantz, 1968). Consumptive use decreases with groundwater depth and goes to zero when the groundwater depth equals the maximum depth tolerated by the vegetation species for a particular setting. Studies by Lee (1912), Duell (1990), Wilson and others (1992), Harrington and others (2004), and Harrington and Steinwand (2003) and others within the Owens Valley, California related to the dependence of phreatophyte discharge to the groundwater depth. Studies by Robinson,

Table 6-1
Simulated Steady-State Phreatophyte Discharges

Parameter		Location				
		Cave Valley	Lake Valley	Snake Valley	Spring Valley	Steptoe Valley
Reported Evapotranspiration[a] (afy)		200	10,000	88,000	71,000	76,000
Potential Evapotranspiration (ft/yr)		3.86	3.97	4.06	3.93	3.87
ET_{max}[b] (ft/yr)	Meadow	3.86	3.97	4.06	3.93	3.87
	Non-Meadow	0.07	0.21	0.16	0.49	0.55
	Wet Playa			0.41	0.39	
ComputedET (afy)	Meadow	160	5,300	50,200	19,100	31,700
	Non-Meadow	40	4,700	22,400	49,900	44,400
	Wet Playa	-	-	15,500	2,200	-
	Total	**200**	**10,000**	**88,100**	**71,200**	**76,100**
Area (acres)	Meadow	1,100	3,500	33,600	14,300	46,800
	Non-Meadow	900	43,900	219,500	146,300	114,700
	Wet Playa	-	-	64,300	11,500	-
	Total	**2,000**	**47,400**	**317,400**	**172,100**	**161,500**
Extinction Depth (ft)	Meadow	10	10	10	10	10
	Non-Meadow	50	50	50	50	50
	Wet Playa	10	10	10	10	10

[a]SNWA (2006a), Volume 3)
[b]See Equations 6-1 or 6-3

1970: Nichols and others (1997), Nichols (2000), Czarnecki (1997), Reiner and others (2002), Laczniak and others (1999), Laczniak and others (2001), Nichols and others (1997), Berger and others, 2001; Carman (1989), Robinson (1970), Berger and others (2001), and Stannard and Weaver (1995) within the Great Basin and elsewhere also relate to the depth-dependence of phreatophyte discharges.

The groundwater evaporation from bare soil also depends on the depth to the groundwater table (Gardner, 1958; Gardner and Fireman, 1958; Ripple and others, 1972; Menking and others, 2000; Thorn, 1995; Tyler and others, 1997; Allison and Barnes, 1985; Jacobson and Jankowski, 1989; and Malek and McCurdy, 1990). The evaporation of groundwater increases with a decreased depth to the groundwater table. For fine-grained soils, groundwater evaporation will occur from a bare-soil surface where the depth to the groundwater table is as much 10 ft. Evaporation can occur at greater depths, but the rate will tend to be very small. Where the evaporation rate is significant, the discharge can be approximated with a linear relation (Ripple et al., 1972).

Groundwater discharges to phreatophytes and playa surfaces are simulated using the module *WEVAP* within *FEMFLOW3D*. These discharges are represented within the module as piecewise linear functions of head. With the local head greater than a specified threshold value, a phreatophyte or playa discharge increases with a greater head above the threshold. With the local head less than or equal to the threshold value, the discharge equals zero. These conditions are represented in the module *WEVAP* by the relation shown on Figure 6-1 and represented by the equations.

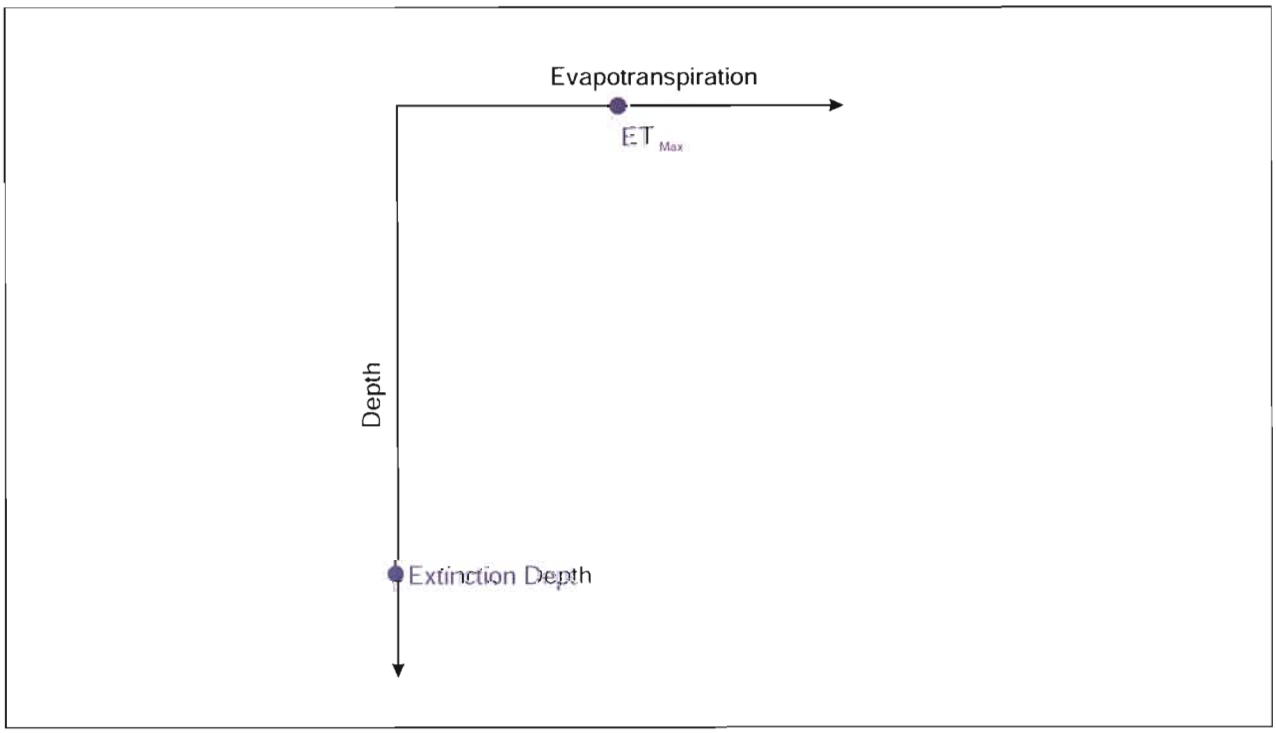

Figure 6-1
Diagram Showing Relation Between Groundwater Discharge and Groundwater Depth Within Phreatophyte Areas

$$ET = ET_{max} - d\frac{ET_{max}}{d_0} \quad \text{for} \quad d < d_0 \tag{6-1}$$

and

$$ET = 0 \quad \text{for} \quad d \geq d_0 \tag{6-2}$$

or

or

$$ET = ET_{max} - (z_L - h)\frac{ET_{max}}{d_0} \quad \text{for} \quad h > z_L - d_0 \tag{6-3}$$

and

$$ET = 0 \quad \text{for} \quad h \le z_L - d_0 \tag{6-4}$$

where

ET_{max} is the evapotranspiration rate when the groundwater table is at the land surface (Lt^{-1}),
ET is the evapotranspiration rate (Lt^{-1}),
d is the depth to the groundwater table (L),
z_L is the land-surface altitude (L),
h is the groundwater-table altitude (L), and
d_0 is the extinction depth (L).

and where the altitude of the groundwater table is represented by the relation

$$h = z_L - d \tag{6-5}$$

Equation 6-1 and Equation 6-2 or Equation 6-3 and Equation 6-4 represent the phreatophyte or playa-surface discharge per unit area. The overall discharge from a specified area is given by the integral

$$Q_{ET} = \iint_A ET(d(x,y))dxdy \tag{6-6}$$

where

Q_{ET} is the discharge from the specified area (L^3t^{-1}), and
A is the limits of the specified area.

The simulation of the phreatophyte and playa discharges for the Spring Valley model requires inputs related to Equation 6-3 through Equation 6-6. The inputs include the specification of the locations and areas of phreatophytes and discharging playas, the altitude of the land surface within the phreatophyte and playa locations, the local extinction depths for the phreatophyte and playa discharges, and the local maximum evapotranspiration rate for the discharges. The development of these inputs is described below.

6.1.1 Geographic Extent of Phreatophyte and Playa Areas

The geographic extents for phreatophytes and discharging playas are shown on Figure 6-2, and the corresponding acreages are listed in Table 6-1. The extents for the phreatophytes are shown as

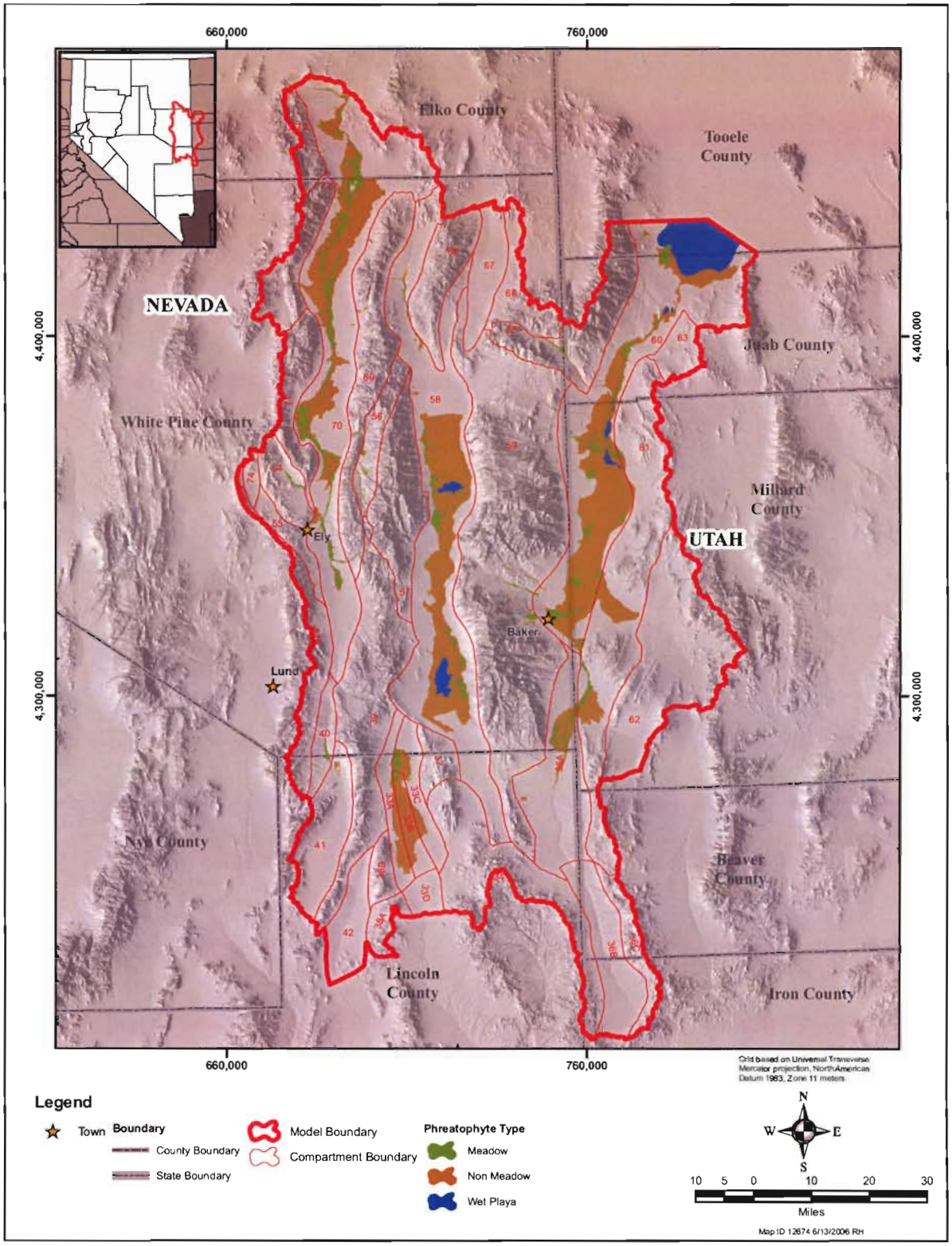

Figure 6-2
Map Showing Location of Areas With Phreatophytes

separate extents for meadow and non-meadow areas. The meadows represent saltgrass and saltgrass-rabbitbrush vegetation communities. The non-meadows represent greasewood and greasewood-rabbitbrush communities. The geographic extents of the meadow, non-meadow, and playa areas were delineated based on the work of Rush and Kazmi (1965), Eakin et al. (1967), Rush and Eakin (1963), Eakin (1962), Hood and Rush (1965), Nichols (2000), and other sources. The procedures used to compile the extents from these sources are described by SNWA (2006b, Volume 3).

6.1.2 Extinction Depths for Discharge Relations

As represented in Equation 6-3, the depth-discharge relation for phreatophyte and playa discharges depends in part on the assignment of an extinction depth. Specific extinction depths were assigned in the Spring Valley model to represent the meadow, non-meadow, and playa areas. The selected depths are 10 ft for meadows, 50 ft for non-meadow phreatophyte areas, and 10 ft for wet playas.

The extinction depths for the meadow and non-meadow phreatophyte areas are based on the reported occurrences of phreatophytes within the Spring Valley area and elsewhere (Robinson, 1958; Eakin, 1962; Rush and Eakin, 1963; Eakin and others, 1967; Rush and Kazmi, 1965; Hood and Rush, 1965; Manning, 2001; and Harrington and Howard, 2000). As listed in Table 6-1, the extinction depths used in the model are 10 ft for meadows and 50 ft for non-meadows. The extinction depth for groundwater evaporation from playas was derived from Ripple and others (1972). The extinction depth used in the model is 10 ft.

6.1.3 Groundwater Depth within Phreatophyte and Playa Areas

The groundwater depth within the phreatophyte and playa areas is shown on Figure 6-3. The map was developed based on the geographic distribution of meadow, non-meadow, and playa areas. The distribution of these areas is an indicator of the groundwater depth (Robinson, 1958, Rantz, 1968; Nichols, 2000; Manning, 2001; and Harrington and Howard, 2000). Meadow phreatophytes occur in areas where the groundwater depth is less than about 10 ft. Likewise, playa discharges occur where the groundwater depth is less than about 10 ft. Non-meadow phreatophytes occur where the groundwater depth is less than about 50 ft. Based on these extinction depths, Figure 6-4 was constructed by assuming that the boundaries of meadow, non-meadow, and playa areas coincided with a contour of equal groundwater depth and that intermediate contours can be interpolated from the boundary contours.

A depth slightly less than the corresponding extinction depth was assigned to the boundary contours so that the resulting contour map would indicate the incipient termination of the corresponding meadow, non-meadow, or playa area. The boundaries of the meadow and non-meadow areas represent a groundwater depth of 8 ft. The outer boundaries of the non-meadow areas represent a groundwater depth of 48 ft. Finally, the central region of large meadow areas was assumed to represent a groundwater-depth of 4 ft.

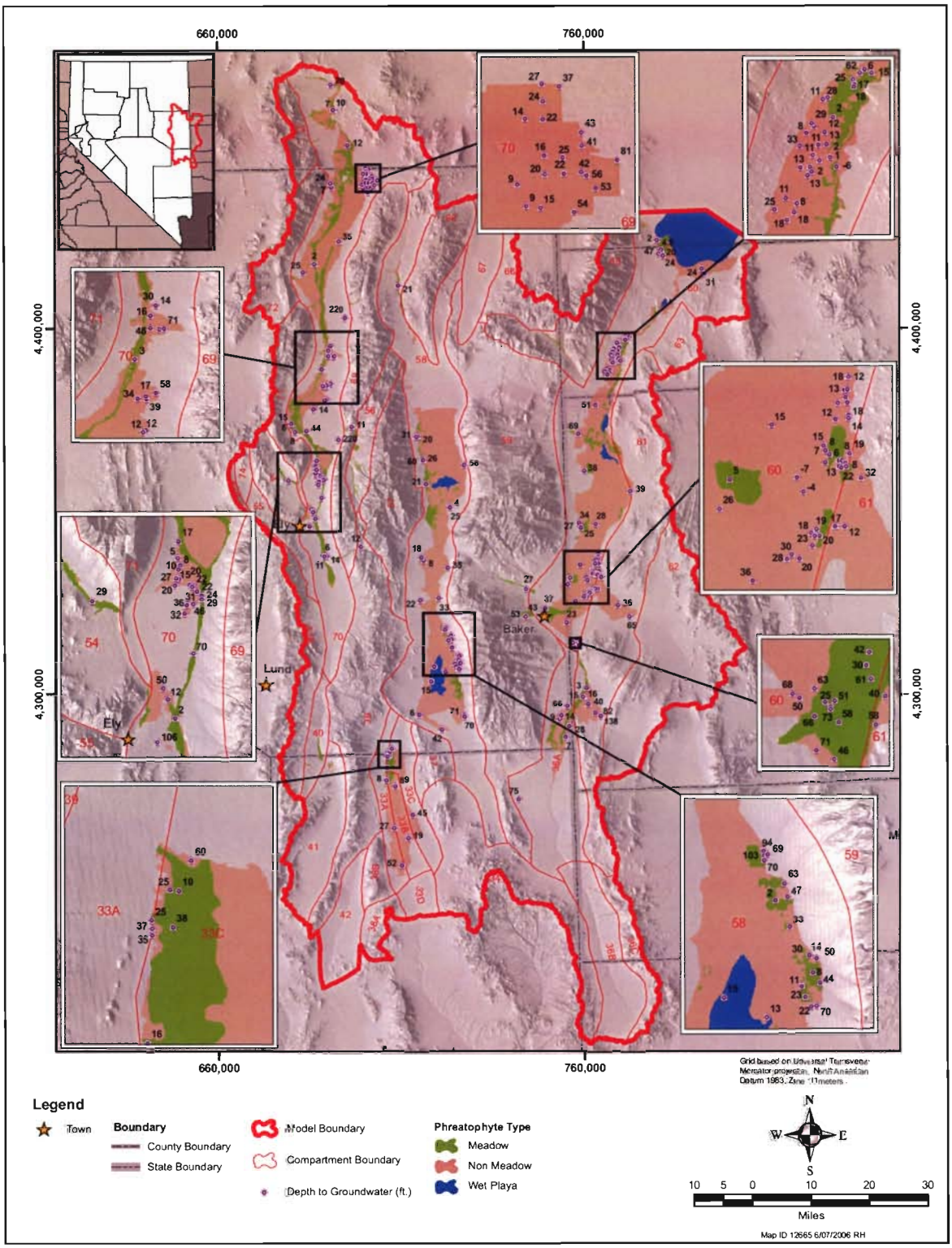

Figure 6-3
Map Showing Measured Groundwater Depth Within Phreatophyte and Playa Areas

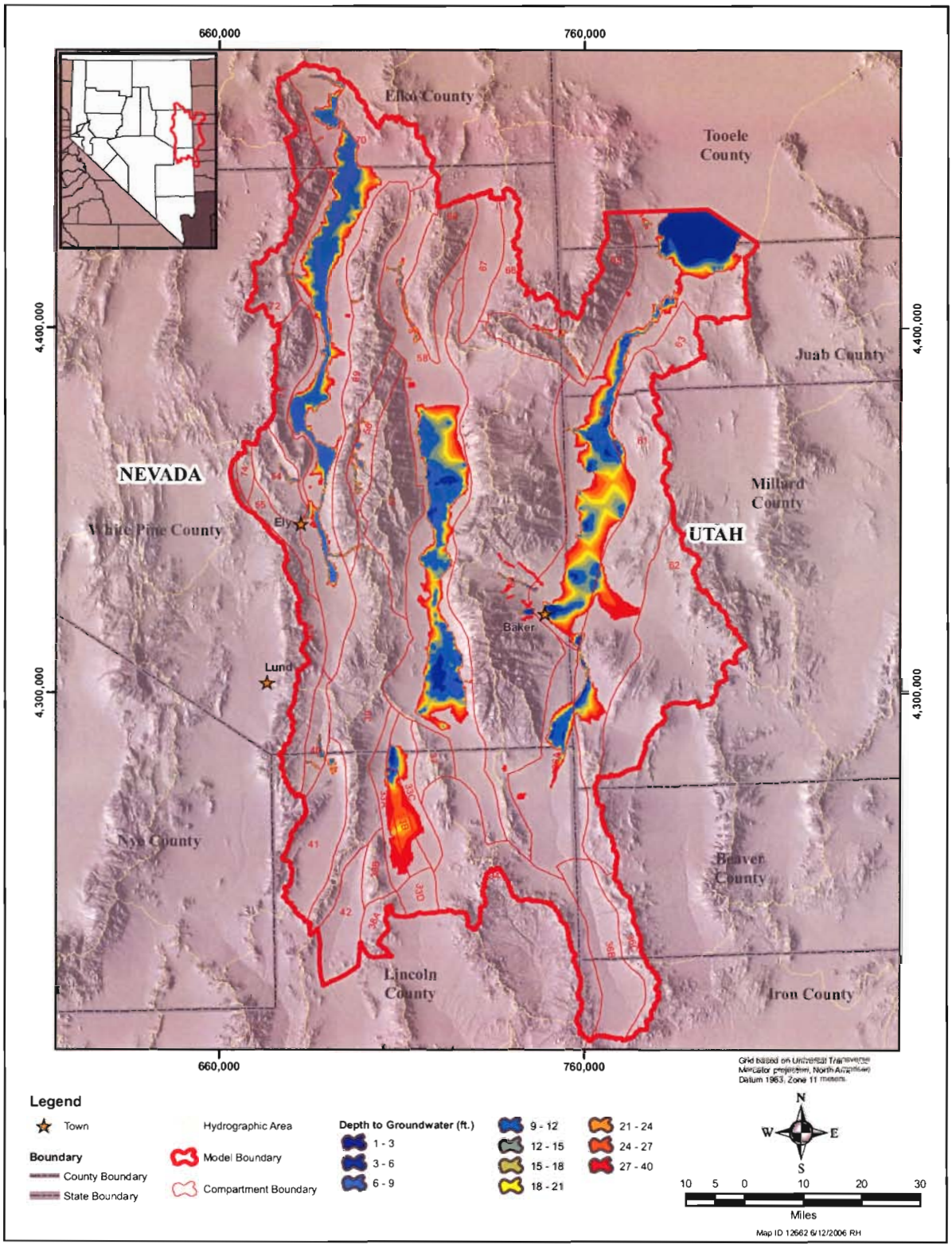

Figure 6-4
Map Showing Depth-to-Groundwater Within Phreatophyte Areas

6.1.4 Maximum Evapotranspiration Rates for Discharge Relations

As represented in Equation 6-3, the depth-discharge relation for phreatophyte and playa discharges depends in part on the assignment of a maximum evapotranspiration rate. Specific rates were assigned to each discharge category and each valley within the Spring Valley model containing phreatophytes. The assigned maximum evapotranspiration rates are listed in Table 6-1.

The rates were assigned on the basis of a calibration process. The calibration involved identifying rates such that the total phreatophyte and playa discharges for a valley best matched the estimated discharge for the valley. The estimated discharges are those listed in Table 6-1, which are the estimates developed by Eakin (1962), Rush and Eakin (1963), Rush and Kazmi (1965), Hood and Rush (1965), and Eakin, Hughes, and Moore (1967) respectively for Cave, Lake, Spring, Snake, and Steptoe valleys. While these estimates represent five separate discharge values, the specification of maximum evapotranspiration rates requires the identification of 12 values (Table 6-1). Accordingly, because the number of parameters exceeds the number of discharge estimates, the calibration is indeterminate without the introduction of additional information. That additional information was introduced by directly assigning maximum evapotranspiration rates for the meadow and playa depth-discharge relations. The assigned rate for meadows was the potential evapotranspiration rate for a particular valley. The assigned rate for playa discharges was a tenth of the potential evapotranspiration rate for a particular valley. Correspondingly, the calibration was reduced to identifying the maximum evapotranspiration rates for the non-meadow phreatophytes in each valley. Figure 6-5 shows the comparison between the calibrated and estimated discharge for each valley, while Table 6-1 lists the maximum evapotranspiration rate.

The maximum evapotranspiration rates for the non-meadow phreatophytes in each case are less than the potential evaporation rate. This is the case because the rates represent the vegetation density corresponding to the existing groundwater depth. Then, the maximum evapotranspiration rate, in effect, represents the discharge that would occur with existing density were the groundwater table to be at the land surface.

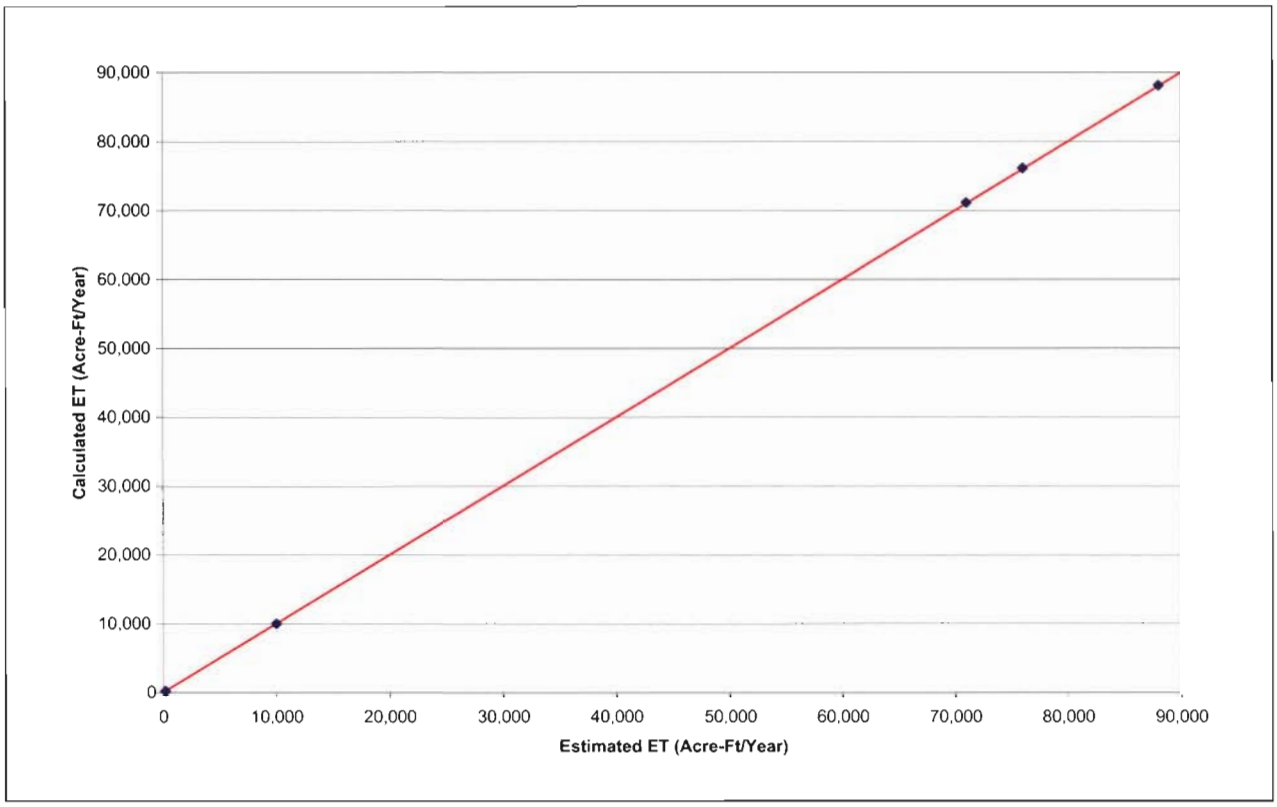

Figure 6-5
Graph Comparing Estimated and Modeled Groundwater Discharges From Phreatophyte Areas

7.0 GROUNDWATER RECHARGE FROM STREAMS AND SURFACE-WATER DISCHARGES TO PLAYAS

7.1 Background

The water yield from precipitation within the Spring Valley area is represented in the model by precipitation recharge within mountain-block areas, recharge from streamflow within valley-floor areas, and streamflow discharge onto playa surfaces. In their water-resource appraisals of the model area, Eakin (1962), Rush and Eakin (1963), Rush and Kazmi (1965), Hood and Rush (1965), and Eakin, Hughes, and Moore (1967) use the Maxey-Eakin method (Eakin and others, 1951) to estimate recharge within mountain-block areas. For Spring, Steptoe, and Snake valleys, the investigators also estimated the mountain-front streamflow. However, they did consider some mountain-front streamflow was accounted for in the Maxey-Eakin recharge.

Additional water yield due to streamflow was attributed to only some of the valleys within the model area. For Spring Valley, Rush and Kazmi (1965) presumed water yield, in addition to the Maxey-Eakin recharge, occurs as mountain-front streamflow. They estimated the additional water yield due to streamflow is 36,000 acre-ft/yr. For Snake Valley, Hood and Rush (1965) presumed also that water yield in addition to the Maxey-Eakin recharge occurs. They did not quantify the additional water yield due to streamflow, but they did estimate the additional recharge due the streamflow is 2,700 acre-ft/yr.

While the streamflow recharge for Snake Valley is represented in the model as a specified flux as described in Section 5.0, the mountain-front streamflow for Spring Valley is represented in the model as specified streamflow inputs to the simulation of streamflow-groundwater interactions. However, instead of using the streamflow estimates of Rush and Kazmi (1965) as the model inputs, revised estimates were used. Considerable additional streamflow information has been collected since 1965. That information has been evaluated by SNWA (2006a) to re-estimate the additional water yield represented by mountain-front streamflow. The mountain-front streamflow input to the model is approximately 47,000 acre-ft/yr (Table 7-1) (SNWA, 2006a).

The groundwater recharge associated with mountain-front streamflow is simulated using the module *WRIVER* within *FEMFLOW3D*. Recharge is simulated by routing streamflow through a network of channels and calculating the local recharge based on the elevation of the streamflow surface, the groundwater level beneath the stream channel, and the hydraulic characterization of the channel bed.

The stream-channel network for Spring Valley is shown on Figure 7-1. The network represents the valley-floor portions of the simulated streams within Spring Valley. The network also represents two streams within Snake Valley. The Snake Valley channels are included in order to simulate the return

Table 7-1
Assignment of Streamflow Inputs (afy) within Model

Stream	Discharge
Bassett Creek	3,300
Bastian Creek	2,700
Cleve Creek	7,300
Eightmile Creek	1,000
Frenchman Creek	300
Garden Creek	400
Kalamazoo Creek	4,400
Little Negro Creek	600
McCoy Creek	5,200
Muncy Creek	1,800
Negro Creek	2,000
North Creek	1,000
Odgers Creek	1,800
Piermont Creek	1,300
Pine Creek	2,200
Siegel Creek	900
Stephens Creek	600
Swallow Creek	6,100
Taft Creek	2,100
Willard Creek	300
Williams Creek	2,200

or potential return of springflows to the groundwater system. Warm Spring and Big Spring within Snake Valley are explicitly represented within the Spring Valley model as head-dependent discharges, and the dispositions of the spring discharges are simulated by including the springs within the stream-channel network. The locations of Warm and Big springs are shown on Figure 7-1, and their discharges are listed in Table 7-2.

Stream-aquifer interactions are simulated within the module *WRIVER* based on two principles. Firstly, the simulation is based on the steady-state water budget for the stream-channel network. The network is defined in term of reaches and links. The network consists of connected reaches. A reach consists of connected links, where the links represent the basic spatial discretization of the overall network. For a specified reach link, the water budget can be expressed as

$$Q_{up} + Q_{tr} = Q_{gw} + Q_{dn} \qquad (7\text{-}7)$$

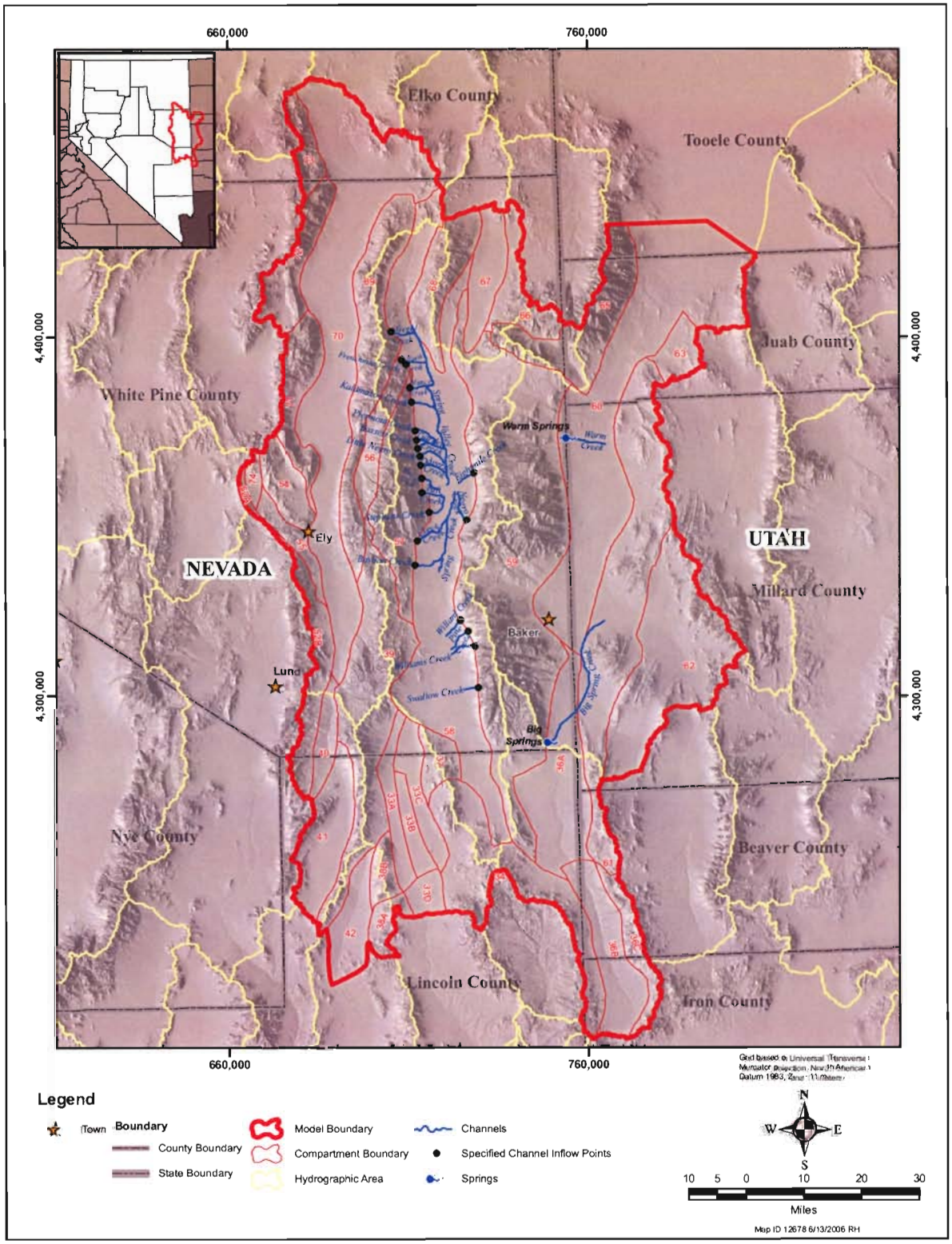

Figure 7-1
Map Showing Spring, Streams, and Specified Streamflows Represented in Mode

Table 7-2
Description of Monitored Springs within Modeled Area

Hydrographic Area	Site Name	Discharge (afy)	Orfice Elevation (ft)	Calculated Source Depth (ft)
Cave Valley	Cave Spring	400	6,488	2,300
Lake Valley	Geyser Spring	700	6,494	6,000
Snake Valley	Big Springs	6,700	5,568	600
	Caine Spring	7	5,028	3,700
	Rowland Spring	2,500	6,570	6,000
	Spring Creek Spring	3,300	6,087	6,000
	Warm Springs	12,400	5,248	4,600
Spring Valley	North Millick Spring	400	5,590	6,000
	North Spring	0	5,763	6,000
	South Bastian Spring	0	5,660	6,000
	South Millick Spring	700	5,592	6,000
	Swallow Springs	600	6,080	6,000
	Swallow Canyon Spring	13,600	6,290	6,000
	The Cedars	100	5,783	6,000
	Willow Spring	2	5,982	6,200
Steptoe Valley	Cherry Creek Hot Springs	100	6,797	17,200
	Monte Neva Hot Springs	1,000	6,011	10,400

where

Q_{up} is the stream inflow to the upper end of the link (ft^3/s),
Q_{tr} is the tributary inflow along the link (ft^3/s),
Q_{gw} is the groundwater recharge along the link (ft^3/s), and
Q_{dn} is the stream outflow from the lower end of the link (ft^3/s).

When applied to every link and reach in the network, Equation 7-7 simulates the steady-state distribution of streamflow within the network. This formulation presumes the travel time through the network for the propagation of a streamflow change is small compared to the temporal discretization used. This condition is satisfied for both steady-state and transient-state simulations with the Spring Valley model. A streamflow change will propagate through the network within a timeframe of days. However, the time-step durations used in the model have a timeframe of years.

The groundwater-recharge term depends on several factors. Firstly, the recharge depends on the relation of the local groundwater table to the local streamflow surface. Secondly, the recharge

depends on the hydraulic characteristics of the channel bed. Thirdly, the recharge depends on the wetted area of the channel. These factors are represented in the expression

$$Q_{gw} = wLK'\frac{\Delta h}{B'} \tag{7-8}$$

where

$$\Delta h = z_S - h \tag{7-9}$$

or

$$\Delta h = z_B + d - h \tag{7-10}$$

and where

w is the wetted streamflow width,
L is the wetted length of the link,
K' is the vertical hydraulic conductivity of the channel-bed material,
Δh is the elevation difference between the streamflow surface and the groundwater table,
B' is the thickness of the channel-bed material,
z_S is the elevation of the streamflow surface,
h is the elevation of the groundwater table,
z_B is the elevation of the channel bed, and
d is the streamflow depth.

The streamflow width and depth are functions of the streamflow within the link, and those functions are evaluated based on the streamflow at the upstream end of a link. The wetted length is less than or equal to the physical length of the link. The wetted length will be less than the physical length when the stream inflows are less than the infiltration capacity of the link.

The relations between the quantities in Equation 7-8 through Equation 7-10 are shown on Figure 7-2, which represents the case of a hydraulically connected stream and underlying groundwater system. A hydraulic connection occurs when the groundwater table is sufficiently high that the recharge from the stream is dependent on the groundwater-table elevation. For a lower groundwater table, the stream is separated by an unsaturated interval beneath the stream such that the recharge from the stream is independent of the groundwater-table elevation.

For the case of a hydraulically disconnected stream and underlying groundwater system, Equation 7-8 becomes

$$Q_{gw} = wLK'\frac{(d + B')}{B'} \tag{7-11}$$

where

$$d + B' = \Delta h \tag{7-12}$$

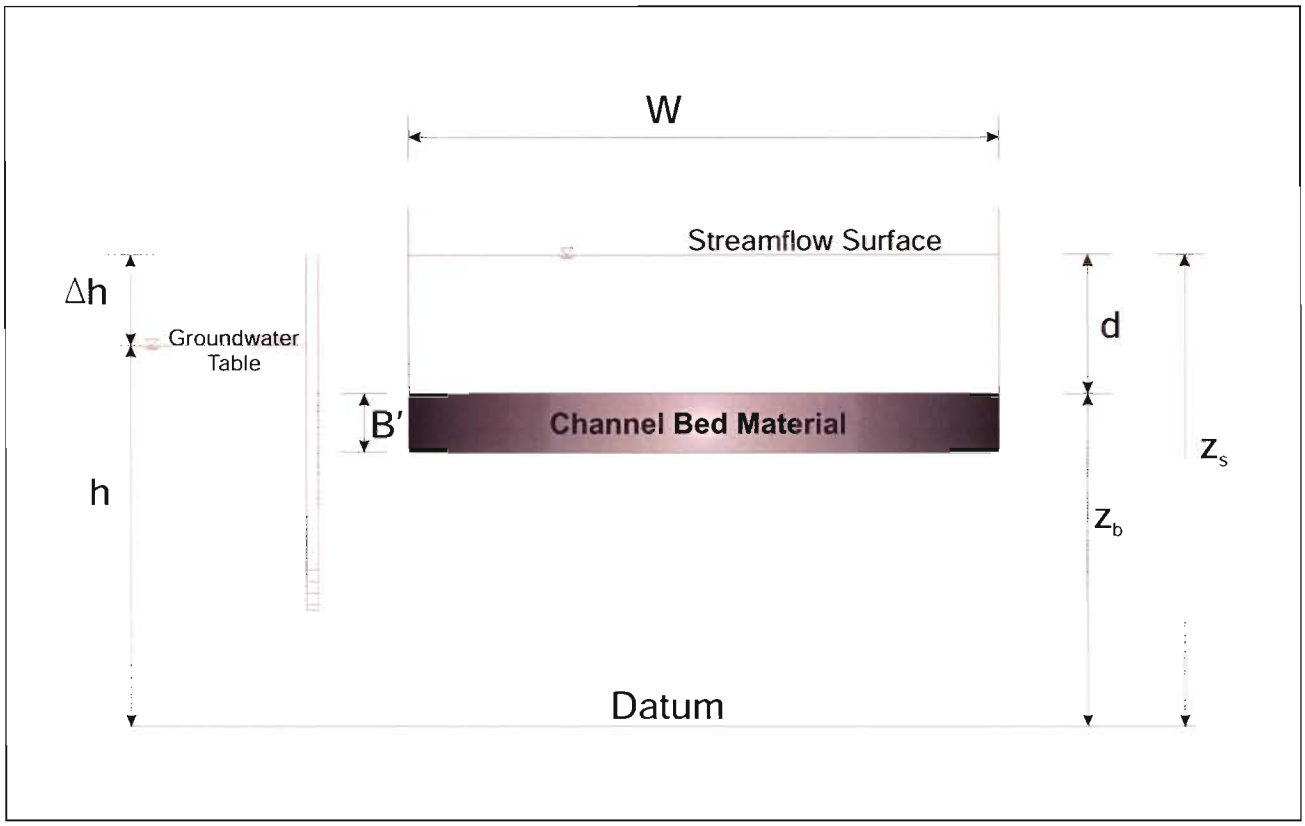

Figure 7-2
Diagram Showing Quantities Used to Simulate Groundwater Recharge From Streams; Hydraulically Connected

and

$$\Delta h = (z_B + d) - (z_B - B') \tag{7-13}$$

Equation 7-11 is derived based on the assumption that the pressure head at the bottom of the bed material is zero when and after a hydraulic disconnection occurs, which is shown on Figure 7-3.

For both the connected and disconnected cases, the quantity L is the wetted length within the channel link, which can be shorter than the overall link length. The wetted length will be less than the link length if the recharge capacity of the link exceeds the stream inflows, including both the upstream and tributary inflows. This case occurs when

$$wL_L K' \frac{\Delta h}{B'} > Q_{up} + Q_{tr} \tag{7-14}$$

where L_L is the length of the reach. Then,

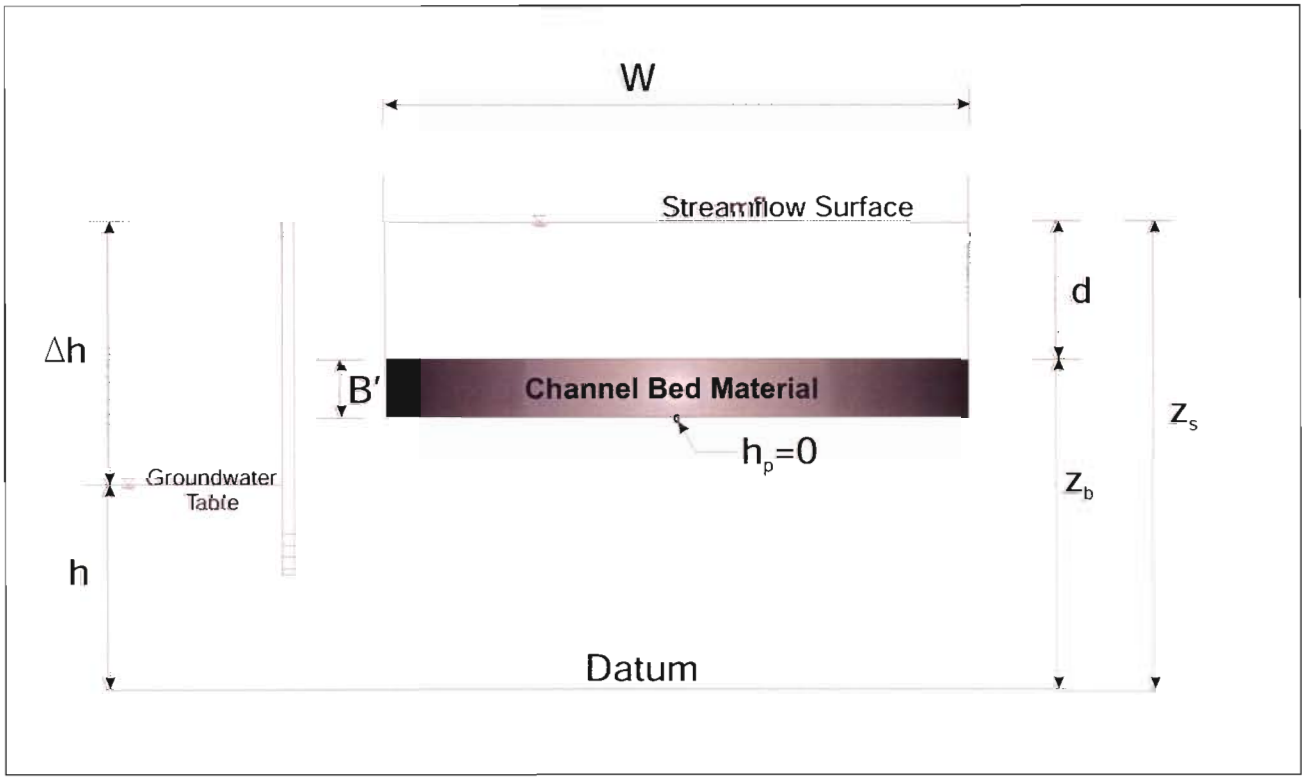

Figure 7-3
Diagram Showing Quantities Used to Simulate Groundwater Recharge From Streams; Hydraulically Disconnected

$$Q_{gw} = Q_{up} + Q_{tr} \tag{7-15}$$

and

$$L = \left(Q_{up} + Q_{tr}\right)\left(\frac{B'}{wK'\Delta h}\right) \tag{7-16}$$

where again L is the wetted length within the link.

The simulation of stream-aquifer interactions using the module *WRIVER* in *FEMFLOW3D* requires the specification of values for the parameters contained in Equation 7-8 and Equation 7-11 These parameters include the link length, the relations between streamflow and streamflow width and depth, the specified mountain-flow stream inflows to the channel network, and the hydraulic characteristics of the channel-bed material. The development of these inputs is described below.

7.1.1 Network Configuration

The stream-channel network consists of 25 reaches and two springs as shown on Figure 7-1 and listed in Table 7-1. Individual channel reaches include from 2 to 20 links. A separate reach is used to represent each of the streams that contribute additional precipitation water yield as mountain-front streamflow to the hydrologic system and streams to which mountain-front streams are tributary. On the east slope of the Schell Creek Range, the streams include Siegel, North, Frenchman, Muncy, Kalamazo, Piermont, Garden, Bassett, Little Negro, Odgers, McCoy, Taft, Stephens, Cleve, and Bastian creeks. On the west slope of the Snake Range, the streams include Eightmile, Negro, Willard, Pine, Williams, and Swallow creeks. On the Spring Valley floor, the streams include Spring Valley and Spring creeks. On the Snake Valley floor, the streams include Warm and Big Spring creeks. Warm and Big springs within Snake Valley also are a component of the stream-channel network. Within Spring Valley, the streamflow that does not become groundwater recharge discharges either to the Yelland Lake playa or the south playa. Within Snake Valley, such streamflow discharges onto the Snake Valley playas.

The parameters for the stream-channel network include the link length, channel-bed elevation, and the spatial relation of the network to the finite-element mesh representing the groundwater system. Reaches are subdivided into links based on the nodes in the finite-element mesh. Accordingly, a link spans the geographic interval from the midpoints between the nodes located along the reach, and the link length is the channel length over the span. Correspondingly, each link has a node located near its midpoint. The channel-bed elevation assigned to the link is the land-surface elevation near the node.

7.1.2 Channel-Geometry Relations

The streamflow depth to streamflow and the streamflow width to streamflow relations are represented in the Spring Valley model in the form

$$d = \alpha_d Q^{\beta_d} \tag{7-17}$$

and

$$w = \alpha_w Q^{\beta_w} \tag{7-18}$$

where

Q is the local streamflow (L^3t^{-1}),
w is the streamflow width (L),
d is the streamflow depth (L),
α_w is the coefficient of the width-discharge relation [$L^{-2\beta} t^{\beta}$],
α_d is the coefficient of the depth-discharge relation [$L^{-2\beta} t^{\beta}$],
β_w is the exponent of the width-discharge relation [L^0], and

β_d is the exponent of the depth-discharge relation [L^0].

The form of these equations is based on that presented by Leopold and Maddock (1953), which has been used extensively by Parrett and others (1983), Omang and others (1982), Hedman and others (1972), Osterkamp and Hedman (1982), Hedman and Osterkamp (1983), Osterkamp (1979), Harenberg (1980), and Hedman (1970). Based on this work, the exponent of the width relation for a particular site can range from 0.1 to 0.4, and the coefficient can range from 2 to 8 with the discharge expressed in cubic feet per second. Correspondingly, the exponent of the depth relation can range from 0.3 to 0.5, and the coefficient can range from 0.8 to 2

The coefficients and exponents applicable to the Spring Valley area were estimated from streamgaging information at the U.S. Geological Survey sites listed in Table 7-3. At those sites information is readily available on discharge, streamflow width, and streamflow depth. The resulting depth-discharge relation is shown on Figure 7-4. The parameters are 0.28 for the exponent and 5.8 for the coefficient. The width-discharge relation is shown on Figure 7-5. The parameters are 0.28 for the exponent and 508 for the coefficient. These relations are those used in the model.

Table 7-3
Streamgaging Stations Used to Identify Channel-Geomerty Parameters

Station ID	Station Name
09416000	Muddy River near Moapa, NV
09417500	Meadow Valley Wash at Eagle Canyon, near Ursine, NV
09418500	Meadow Valley Wash near Caliente, NV
09419000	Muddy River near Glendale, NV
09415460	White River near Red Mountain near Preston, NV
10243700	Cleve Creek near Ely, NV
10244950	Steptoe Creek near Ely, NV
10245445	Illipah Creek near Hamilton, NV
10243260	Lehman Creek near Baker, NV
09415515	Water Canyon Creek near Preston, NV
09415460	White River near Red Mountain near Preston, NV
10242875	Granite Creek near Callao, UT
10242870	Trout Creek near Callao, UT

7.1.3 Specified Mountain-Front Streamflows

Streamflows are specified as inflows to channel reaches at the mountain front. Figure 7-1 shows the locations where such streamflows are specified, and Table 7-1 lists the particular streamflows. Streamflows are assigned as steady-state mean annual discharges, where the cumulative discharge is approximately 47,000 acre-ft/yr. The specified streamflows were estimated from the streamgaging

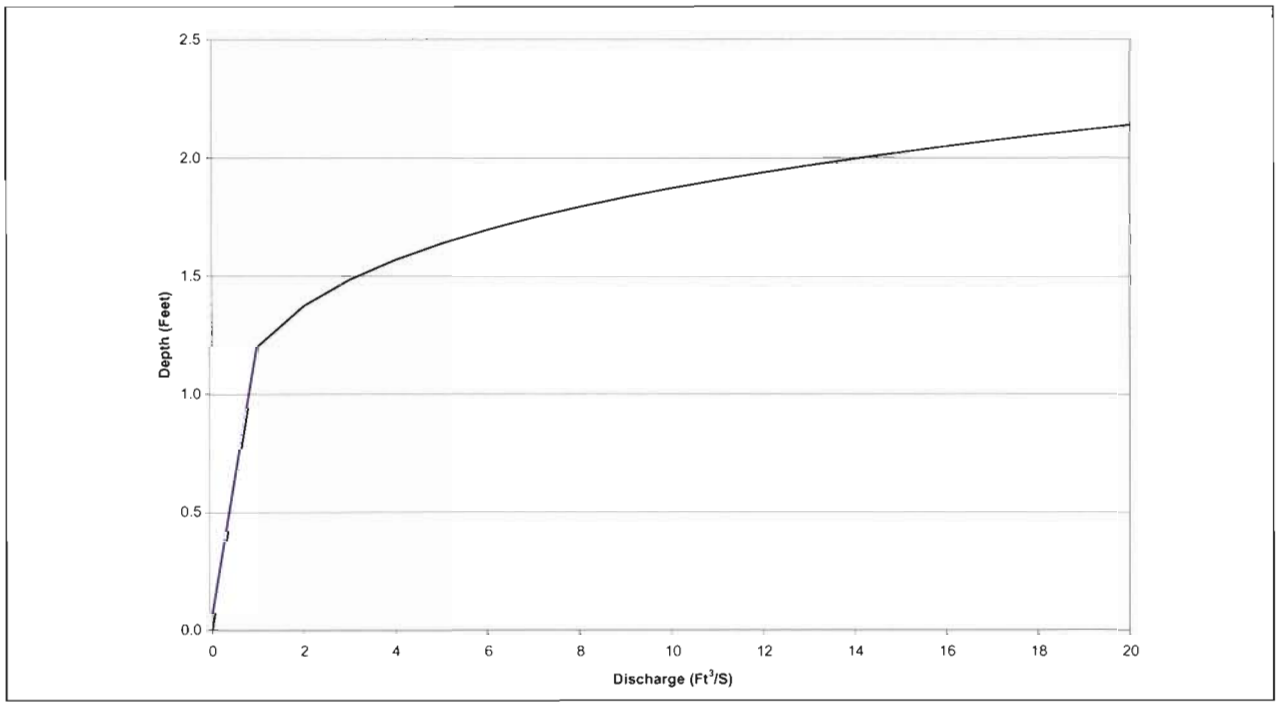

Figure 7-4
Graph Showing Relation Used in Model Between Streamflow and Streamflow Depth

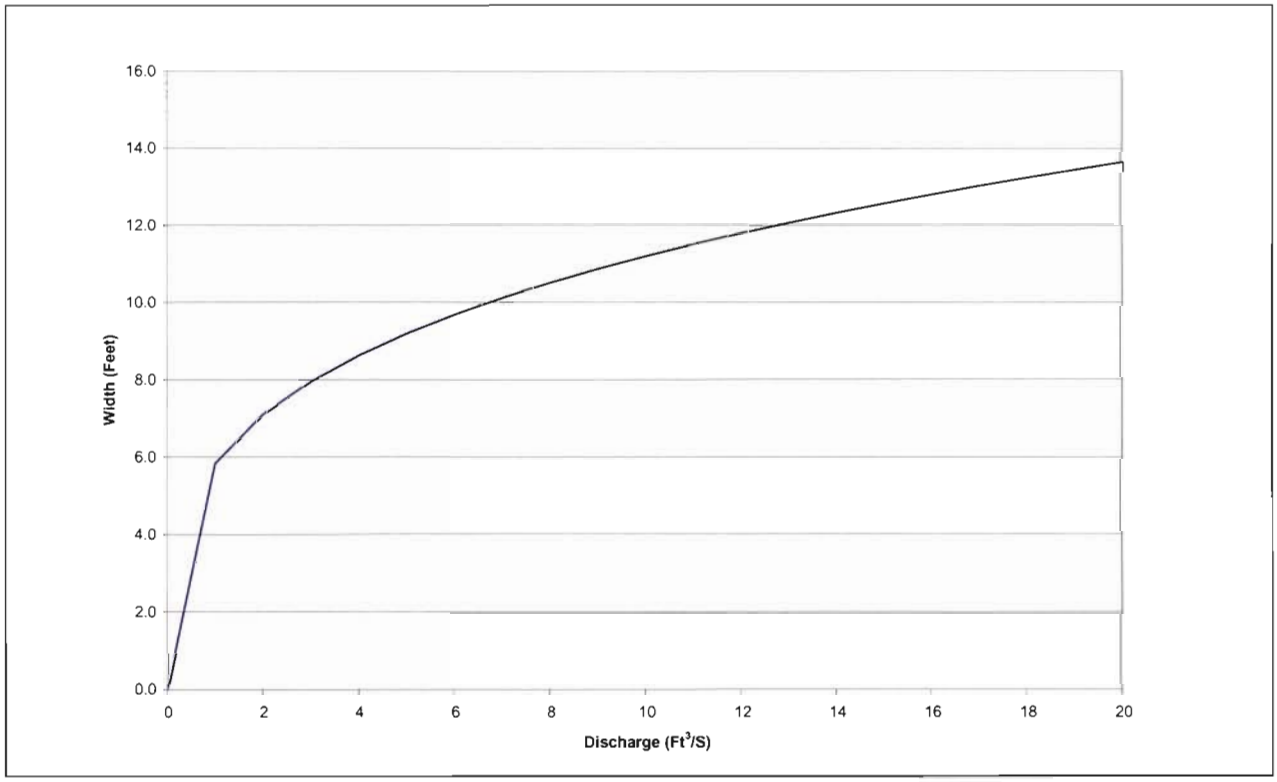

Figure 7-5
Graph Showing Relation Used in Model Between Streamflow and Streamflow Width

records and miscellaneous streamflow measurements for the Spring Valley area. Streamflows were estimated from these data using the method of Moore (1968) as described in SNWA (2006a).

7.1.4 Spring Inflows

The discharges from Warm and Big springs are incorporated within the stream-channel network. Warm Spring discharges into Warm Creek (Figure 7-1), and Big Spring discharges into Big Spring Creek (Figure 7-1). The measured spring discharges are 12,400 acre-ft/yr for Warm Spring and 6,700 acre-ft/yr for Big Spring. The spring discharges are represented by a stream-channel reach that has special properties. Firstly, Equation 7-11 is restated in the form

$$Q_{sp} = C\Delta h \tag{7-19}$$

and

$$\Delta h = h - z_{sp} \tag{7-20}$$

where

Q_{sp} is the spring discharge [L^3t^{-1}],
C is the spring leakance [L^2t^{-1}],
Δh is the driving head for the spring discharge [L],
z_{sp} is the spring-orifice elevation [L], and
h is the head at the spring-source point within the groundwater system [L].

The spring leakance in Equation 7-19 is equivalent to the term

$$\frac{wLK'}{B'}$$

in Equation 7-11.

The leakance cannot be identified without knowing both the spring discharge and head at the source-water depth. As described by SNWA (2006b, Volume 4), both springs have a source within the carbonate rocks. Based on a geothermal-geochemical evaluation, the source of Warm Spring occurs at a depth of 4,600 ft within the carbonate rocks. Likewise, the source of Big Springs occurs at a depth of 600 ft. Because the heads in the groundwater system at these depths are unknown, leakances were identified respectively for Warm and Big springs during the calibration of the groundwater model. That process results in leakance values that are consistent with the spring discharges and the computed heads at the spring-source locations and depths.

Hundreds of springs occur within the Spring Valley area, but only Warm and Big springs are included. From among the hundreds of springs, Table 7-2 lists springs for which discharge information has been available to SNWA, while Figure 7-6 shows their locations. Except for Warm and Big springs,

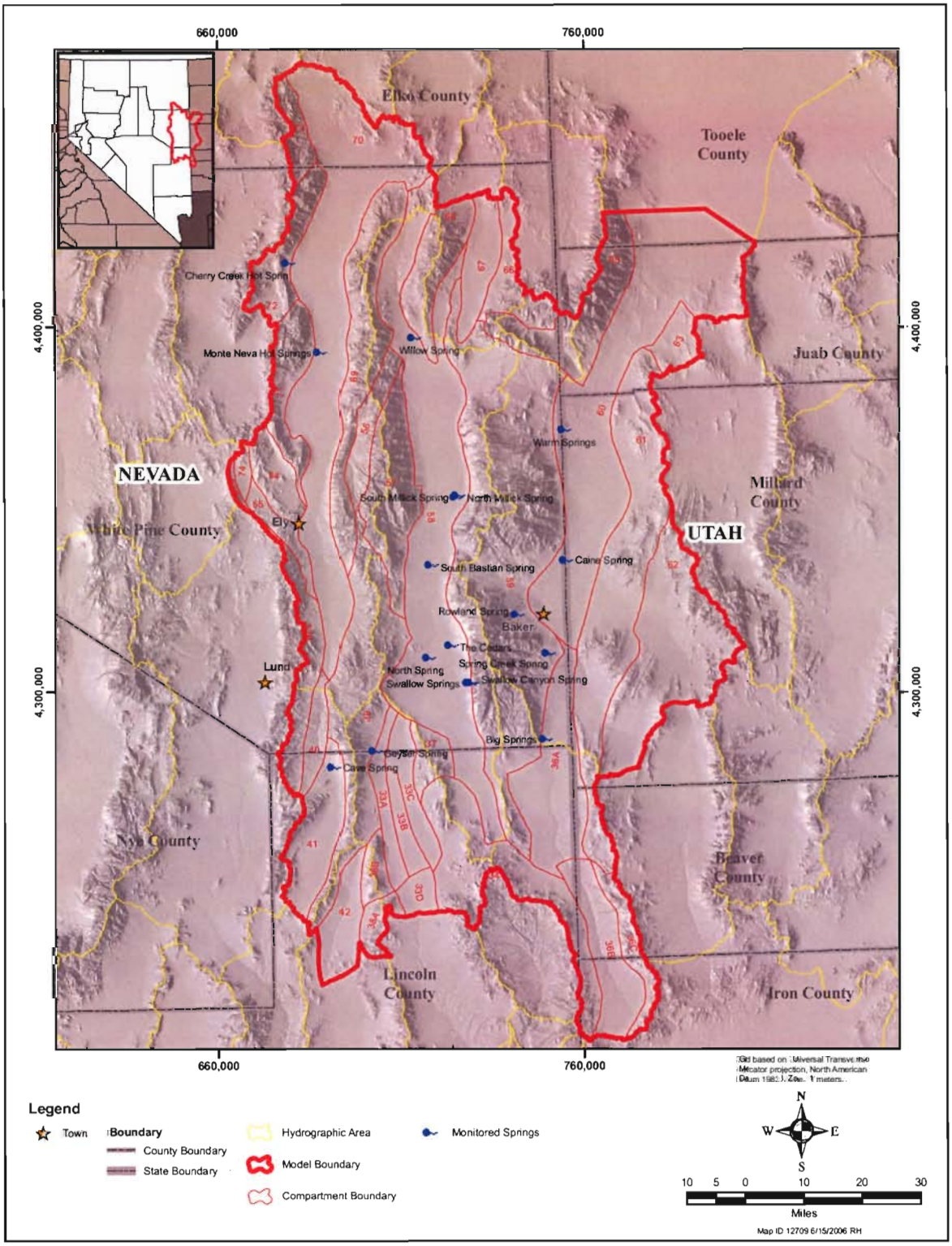

Figure 7-6
Map Showing Monitored Springs Within Study Area

neither the listed wells nor other wells were included in the Spring Valley model. They were not included due to one or more evaluation factors. Firstly, a spring was excluded if the discharge is small. Secondly, a spring was excluded if it is classified as a mountain-block spring for which the discharge is independent of regional groundwater conditions. Thirdly, a spring was excluded if it is located within a phreatophyte area and could be lumped with the simulation of the phreatophytes discharge. After considering these criteria, only Warm and Big springs are represented explicitly within the Spring Valley model. All other springs are represented implicitly within the model by the specification of mountain-block recharge, the specification of mountain-front streamflow, or the simulation of phreatophyte and playa discharges.

7.1.5 Channel-Bed Hydraulic Characteristics

The channel-bed thickness and hydraulic conductivity are specified for each link within the stream-channel network. The channel-bed thickness specifies the groundwater depth below a channel at which the stream becomes hydraulically disconnected from the groundwater system. While this is only one influence of this parameter, the relation of the channel-bed thickness to this phenomenon is the most important consideration in its specification. Muskat and Wyckoff (1946), Bouwer (1988), Bouwer (1989), Bouwer (1990) discuss the hydraulics of stream-aquifer, canal-aquifer, and pond-aquifer interactions. Based on this work, a channel-bed thickness of 10 ft is assigned to all links within the stream-channel network.

The hydraulic conductivity for the channel-bed material was derived by calibrating the stream-channel networks to the estimated streamflow discharges within the Spring Valley area. Based on the overall water budget for the Spring Valley area, the cumulative streamflow evaporation on Snake and Spring valley playas averages 43,500 acre-ft/yr. This evaporation is equal to the cumulative streamflow discharge onto the playas. From the single value for the discharge from the stream-channel network, a single value of channel-bed hydraulic conductivity can be identified. However, in order to accomplish the calibration, it was necessary to specify the groundwater depth for those reaches where the depth to groundwater is less than 10 ft, which is the specified channel-bed thickness. With this additional information, a channel-bed hydraulic conductivity of 0.38 ft/d was identified.

The calibrated hydraulic conductivity is within the range of values associated with other studies within the Great Basin and other areas. SNWA (Gavin Kistinger, 2006, written communication) collected streamflow-recharge data representing four channels within Spring Valley. When the streamflow recharge relations described by Equation 7-8 through Equation 7-16 are applied to the data, along with channel-geometry relations, the resulting channel-bed hydraulic conductivities range from 0.1 to 3 ft/d. Niswonger and others (2004) collected streamflow-recharge data on Trout Creek within the Humboldt River basin. Those data indicate a channel-bed hydraulic conductivity of 0.2 ft/d. Burkham (1970) collected streamflow-recharge data on streams within the Tucson area, Arizona. Those data indicate hydraulic conductivities that range from 0.02 to 0.2 ft/d for selected individual streams. Lee (1912) collected streamflow-recharge data within the Owens Valley, California. Those data indicate hydraulic conductivities that range from 0.9 to 3 ft/d for selected individual streams.

The calibrated bed-material hydraulic conductivity results in a particular partitioning of the cumulative streamflow discharge to individual playas. In other words, the calibrated conductivity results in particular discharges going to particular playas. The streamflow discharge onto the playas within Spring Valley is 29,100 acre-ft/yr, which includes 21,300 acre-ft/yr to the Yelland Lake playa and 7,800 acre-ft/yr to the south-valley playa. The streamflow discharge onto the playas within Snake Valley is 14,400 acre-ft/yr, which includes 2,500 acre-ft/yr to the Baker Creek Sink and 11,900 acre-ft/yr to the north-valley playa. Table 7-4 lists these simulated streamflow discharges onto playas.

The groundwater recharge from the stream-channel network also is listed in Table 7-4. The recharge within Spring Valley is 18,400 acre-ft/yr. The recharge in Snake Valley is 7,400 acre-ft/yr, which represents returns to the groundwater system of the discharges from Warm and Big Springs.

Table 7-4
Simulated Steady-State Water Budgets (afy) for Streams

Stream	Inflow		Recharge	Outflow
	Type	Rate		
Spring Valley				
Bassett Creek	Assigned	3,300	300	3,000
Bastian Creek	Assigned	2,700	700	2,000
Cleve Creek	Assigned	7,300	1,500	5,800
Eightmile Creek	Assigned	1,000	400	600
Frenchman Creek	Assigned	300	100	200
Garden Creek	Assigned	400	800	3,300
Garden Creek	Tributary	3,700	--	--
Kalamazoo Creek	Assigned	4,400	800	3,600
Little Negro Creek	Assigned	600	500	100
McCoy Creek	Assigned	5,100	800	4,300
Muncy Creek	Assigned	1,800	400	1,400
Negro Creek	Assigned	2,000	800	1,200
North Creek	Assigned	1,000	600	600
North Creek	Tributary	200	--	--
Odgers Creek	Assigned	1,800	700	1,100
Piermont Creek	Assigned	1,300	600	700
Pine Creek	Assigned	2,300	700	1,600
Siegel Creek	Assigned	900	400	500
Spring Creek	Tributary	7,800	2,000	5,800
Spring Valley Creek	Tributary	10,600	4,400	6,200
Stephens Creek	Assigned	600	400	200
Swallow Creek	Assigned	6,000	500	5,500
Taft Creek	Assigned	2,100	300	1,800
Willard Creek	Assigned	300	200	100
Williams Creek	Assigned	2,300	700	1,600
Total			**18,600**	
Snake Valley				
Big Spring Creek	Spring	6,700	4,200	2,500
Warm Creek	Spring	13,200	1,600	11,600
Total			**5,800**	
Total			**24,400**	

8.0 MODEL CALIBRATION

8.1 Background

8.1.1 Model Purpose and Calibration Design

Model calibration is the process of identifying parameter values within a model such that the model represents essential features of the actual system. Models always represent simplifications of actual systems, and the appropriate level of simplification depends in large part on the model use. Correspondingly, a simplification that is appropriate for one use might be inappropriate for another use. The purpose of the groundwater model of the Spring Valley area is to provide a decision-making framework for managing and monitoring groundwater development in Spring Valley.

8.1.2 Calibration and Parameter Evaluation Approaches

A steady-state model calibration was used to identify values for the hydraulic properties of the RMUs, faults, stream channels, and spring conduits. The calibration software PEST (Waterloo Hydrogeologic, 2002) was used to calibrate the groundwater model. PEST uses a version of the Gauss-Levenberg method to iteratively identify model parameters that minimize a least-squares objective function. The approach is similar to those used by Cooley and Naff (1990), Durbin (1983), Durbin and Bond (1998), and Poeter and Hill (1998). However, PEST does not output some desirable statistics on the model calibration, and post-calibration processing of the PEST results was performed.

The hydraulic characteristics of the RMUs and faults are the primary calibration parameters. The parameters identified for the RMUs are the principal components of the hydraulic-conductivity tensor, where each RMU was treated as being anisotropic but homogeneous with respect to the magnitude of principal components of the hydraulic conductivity tensor. However, the orientation of the hydraulic-conductivity tensor varies geographically as indicated on Figure 4-26. While the tensor orientation was fixed within the calibration, the calibration was used to identify the magnitudes of principal components of the hydraulic-conductivity tensor for each RMU. The identified magnitudes for an RMU represent the hydraulic conductivity at zero depth, where the hydraulic conductivity at depth is represented by the depth relations described in Section 4.0. The parameters identified for the faults are transmissivity and leakance. With respect to transmissivity, faults were treated as homogeneous. With respect to leakance, however, the faults were treated as heterogeneous. While the leakances assigned within a fault link are homogeneous, different leakance values are assigned to different fault segments.

The characteristics of the stream-channels and springs are secondary calibration parameters. The parameter identified for the stream channels is the channel-bed hydraulic conductivity. The stream channels are treated as homogeneous with respect to hydraulic conductivity. The parameter identified for the springs is the spring-conduit leakance. Individual values were identified for the two springs.

Even though PEST was used to facilitate the identification of parameter values, the calibration required trying different parameterizations. The differences mostly involved considering alternative geographic zonations, but they also involved differences in the weight given to the prior parameter estimates. While the incorporation of prior information into the model calibration improves the calibration (Cooley, 1982), difficulty arises in the assignment of relative weights to the prior information with respect to the groundwater levels, phreatophyte discharges, and springflows. This is an ongoing research topic (Gupta and others, 1998; Yapo and others, 1998; and Khadam and Kalurachchi, 2004) without much resolution, and practical problems continue to be solved by introducing a subjective element into the weighting. This was the case for the calibration of the Spring Valley model. Based on consideration of the model purpose, the prior information on the hydraulic conductivity was given weight so as to contribute to the calibration objective function about equally to the groundwater levels. Furthermore, the phreatophyte discharges and springflows were given weights so as to contribute about equally to the groundwater levels.

8.1.2.1 Mathematical Formulation of Parameter Identification Problem

The calibration is formulated as a maximum *a posteriori* non-linear regression (Durbin and Bond, 1998). As implemented in PEST, this formulization has an objective function in the form

$$S = \left[\overline{Y} - \overline{\eta}(\overline{\beta})\right]^T \overline{\psi}^{-1} \left[\overline{Y} - \overline{\eta}(\overline{\beta})\right] + \left[\overline{\mu} - \overline{\beta}\right]^T \overline{V}^{-1} \left[\overline{\mu} - \overline{\beta}\right] \tag{8-1}$$

where

S is the scalar sum of squared residuals,

$\overline{Y}$ is a vector of observed values,
$\overline{\eta}$ is a vector of computed values corresponding to the observed values,
$\overline{\beta}$ is a vector of parameter values,
$\overline{\psi}$ is the covariance matrix associated with the observed values,
$\overline{\mu}$ is a vector of prior estimates of the parameter values, and
$\overline{V}$ is the covariance matrix associated with the prior estimates of the parameter values.

The covariance matrix for the observations in turn is expressed as (Beck and Arnold, 1977)

$$\overline{\psi} = \sigma^2 \overline{\Omega} \tag{8-2}$$

where

σ^2 is an unknown constant variance associated with the observations and
$\overline{\Omega}$ is the known part of the observation covariance matrix.

The estimator for the parameter vector $\overline{\beta}$ is given by the relation (Beck and Arnold, 1977)

$$\overline{b} = \overline{\mu} + \overline{P}\left[\overline{X}^T \overline{\Omega}^{-1} \left(\overline{Y} - \overline{X}\overline{\mu}\right)\right] \tag{8-3}$$

where

$$\overline{P} \equiv \left[\overline{X}^T \overline{\Omega}^{-1} \overline{X} + \sigma^2 \overline{V}\right]^{-1} \tag{8-4}$$

where

$$\sigma^2 = \frac{1}{n}\left(\overline{Y} - \overline{X}\overline{b}\right)^T \overline{\Omega}^{-1} \left(\overline{Y} - \overline{X}\overline{b}\right) \tag{8-5}$$

and where

$\overline{b}$ is the estimate of the parameter vector $\overline{\beta}$,
$\overline{X}$ is the sensitivity matrix of the computed heads with respect to the model parameters, and
n is the number of observations.

The sensitivity matrix, which sometimes is referred to in its transposed form as the Jacobian matrix (Beck and Arnold, 1977), has the form

$$\overline{X} \equiv \begin{bmatrix} \frac{\partial \eta_1}{\partial \beta_1} & \cdots & \frac{\partial \eta_1}{\partial \beta_p} \\ \vdots & & \vdots \\ \frac{\partial \eta_n}{\partial \beta_1} & \cdots & \frac{\partial \eta_n}{\partial \beta_p} \end{bmatrix} \tag{8-6}$$

where p is the number of model parameters.

The uncertainty in the estimated parameters is given by the relation (Beck and Arnold, 1977)

$$\mathrm{cov}\left[\overline{b} - \overline{\beta}\right] = \overline{P}$$

or

$$\mathrm{cov}\left[\underline{b}-\underline{\beta}\right]=\left[\underline{\underline{X}}^{T}\underline{\underline{\Omega}}^{-1}\underline{\underline{X}}+\sigma^{2}\underline{\underline{V}}^{-1}\right]^{-1} \tag{8-7}$$

where $\mathrm{cov}\left[\underline{b}-\underline{\beta}\right]$ is the covariance of the deviation of the estimated parameter values from their true values. The standard errors of parameters are the square roots of the diagonal terms of the covariance matrix (Draper and Smith, 1998). PEST computes and outputs a parameter covariance matrix. However, the computation does not include the quantity $\underline{\underline{V}}$ in Equation 8-7, and the covariance was calculated from Equation 8-7 in post processing.

The uncertainty in the parameter estimates as given by Equation 8-8 translates into uncertainty in the model predictions. The translation is given by the relation

$$\mathrm{cov}\left[\underline{\hat{Y}}\right]=\underline{\underline{X}}_{1}\,\mathrm{cov}\left[\underline{b}-\underline{\beta}\right]\underline{\underline{X}}_{1}^{T} \tag{8-8}$$

where

$\underline{\hat{Y}}$ is a vector of model values corresponding to the predictions and
$\underline{\underline{X}}_{1}$ is the sensitivity matrix for the model predictions with respect to the model parameters.

The standard errors of prediction are the square roots of the diagonal terms of the covariance matrix (Draper and Smith, 1998).

8.1.2.2 Model-Evaluation Statistics

A suite of statistics was used to evaluate the model calibration and subsequent predictions (Hill, 1998). Those statistics include the standard error of the estimate, coefficient of determination, and standard errors of the parameters. They also include the composite parameter sensitivities and composite observation sensitivities. However, the most important statistics are the standard errors of the predictions, which are a quantification of the predictive reliability of the model with respect to its use in assessing the proposed pumping and alternatives.

Standard Error of Estimate. The standard error of the estimate is the standard deviation of the divergence between the observed groundwater levels and other observations and the corresponding simulated values. This weighted standard error is given by the relation

$$s_{e}^{2}=\frac{1}{n}\left(\underline{Y}-\underline{\underline{X}}\,\underline{b}\right)^{T}\underline{\underline{\Omega}}^{-1}\left(\underline{Y}-\underline{\underline{X}}\,\underline{b}\right) \tag{8-9}$$

where

s_e is the standard error of the estimate and
n is the number of observations.

Coefficient of Determination. The coefficient of determination, which often is referred to as the r-squared statistic, assesses the portion of the total variance in the observations explained by the model. This statistic is given by the relation (Cooley and Naff, 1990)

$$r^2 = \frac{\left(\underline{\psi}^{-1/2}\underline{Y} - m_Y\right)^T\left(\psi^{-1/2}\hat{Y} - m_{\hat{Y}}\right)}{\left[\left(\underline{\psi}^{-1/2}\underline{Y} - m_Y\right)^T\left(\underline{\psi}^{-1/2}\underline{Y} - m_Y\right)\left(\underline{\psi}^{-1/2}\underline{Y} - m_{\hat{Y}}\right)^T\left(\underline{\psi}^{-1/2}\underline{Y} - m_{\hat{Y}}\right)\right]^{1/2}} \tag{8-10}$$

where

$\underline{r}^2$ is the coefficient of determination,
$\underline{Y}$ is a vector of observed values,
m_Y is the mean of the observations,
$\hat{Y}$ is a vector of model values corresponding to the observations, and
$m_{\hat{Y}}$ is the mean of the model values.

Standard Errors of the Parameters. The standard errors of the parameters assess the uncertainty in the estimated parameter values. This statistic is given by the relation

$$s_b^2 = \mathrm{cov}[b_i, b_i] \tag{8-11}$$

where (Beck and Arnold, 1977)

$$\mathrm{cov}[\underline{b}] = \left[\underline{X}^T\underline{\Omega}^{-1}\underline{X} + \sigma^2\underline{V}\right]^{-1} \tag{8-12}$$

and where s_b is the standard error of the parameter b_i.

Composite Parameter Sensitivities. The composite parameter sensitivities assess the sensitivity of each parameter with respect to all observations. The parameter sensitivities are given by the relation (Waterloo Hydrogeologic, 2002)

$$s_i = \frac{1}{n}\left(\underline{X}_i^T\underline{\psi}^{-1}\underline{X}_i\right)^{1/2} \tag{8-13}$$

where

$$\overline{X}_i \equiv \begin{bmatrix} \dfrac{\partial \eta_1}{\partial \beta_i} \\ \vdots \\ \dfrac{\partial \eta_n}{\partial \beta_i} \end{bmatrix}$$

and where

N_j is the computed value of corresponding observations
s_i is the composite parameter sensitivity for parameter i,
$\overline{X}_i$ is a vector representing column i of the sensitivity matrix, and
n is the number of observations.

The composite parameter sensitivity represents the magnitude of column i within the sensitivity matrix, weighted by the inverse of the observation covariance matrix, then normalized by the number of observations. The resulting value quantifies the sensitivity of the computed groundwater levels and other model outputs to a change in a parameter value.

Composite Observation Sensitivities. The composite observation sensitivities assess the sensitivity of the calibrated parameter values to a change in an observation value. The observation sensitivities are given by the relation (Waterloo Hydrogeologic, 2002)

$$s_j = \frac{1}{p}\left(\psi_{jj}^{-1}\overline{X}_j\overline{X}_j^T\right)^{1/2} \tag{8-14}$$

where

$$\overline{X}_j \equiv \begin{bmatrix} \dfrac{\partial \eta_j}{\partial \beta_1} & \cdots & \dfrac{\partial \eta_j}{\partial \beta_p} \end{bmatrix} \tag{8-15}$$

and where

s_j is the composite observation sensitivity for observation j,
$\overline{X}_j$ is a vector representing row j of the sensitivity matrix, and
p is the number of parameters.

The composite observation sensitivity represents the magnitude of row j within the sensitivity matrix, weighted by the inverse of the variance for observation j, then normalized by the number of parameters. The resulting value quantifies the sensitivity of the parameter values to a change in an observation value.

Standard Error of Prediction. The standard error of prediction assesses the reliability of the model predictions.

$$s_p^2 = \mathrm{cov}\left[\hat{Y}_i, \hat{Y}_i\right] \tag{8-16}$$

where

$$\mathrm{cov}\left[\hat{Y}\right] = \overline{X}_1 \, \mathrm{cov}\left[\bar{b} - \overline{\beta}\right] \overline{X}_1^T \tag{8-17}$$

and where

s_p is the standard error of prediction at location i,
$\hat{Y}$ is a vector of predicted groundwater levels or other model outputs, and
$\overline{X}_1$ is the sensitivity of the predictions relative to the parameter values.

The standard error of prediction quantifies the reliability of the predicted groundwater levels or other model outputs. The reliability is expressed in terms of the probability that the actual future condition will be within the range of one standard deviation above or below the predicted value. For example, if the prediction is for a groundwater-level change of Δh, the range would be $\Delta h \pm s_p$, for which there is about a 67 percent probability the actual groundwater level will be in that range. More precisely, the probability would be expressed in terms of the student t-distribution, but the standard error of prediction and the normal distribution associated with that statistic is an adequate substitute and more easily understood.

8.1.3 Calibration Targets and Uncertainties

The calibration targets include estimated groundwater levels, estimated springflows, estimated streamflows, estimated phreatophyte discharges, and prior parameter estimates of hydraulic conductivity. The setup of the calibration involved estimating the target values and the corresponding uncertainty in the estimated values in terms of an observation variance. The weights assigned within an observation group, such as groundwater levels, equal the inverse of the error variance. However, additional weighting was assigned among groups such that each group contributes about equally to the objective function (Equation 8-1) near the optimal parameter values.

8.1.3.1 Groundwater-Level Observations

The groundwater-level observations are estimates of the predevelopment steady-state conditions within the groundwater system. That steady-state condition existed until about the 1960's. Groundwater-level data are sparse for the pre-development period, but more data is available for the post-development period. The 500 well locations used in the calibration, and the monitoring locations are shown on Figure 8-1. Those locations represent sites for which both groundwater-level data and

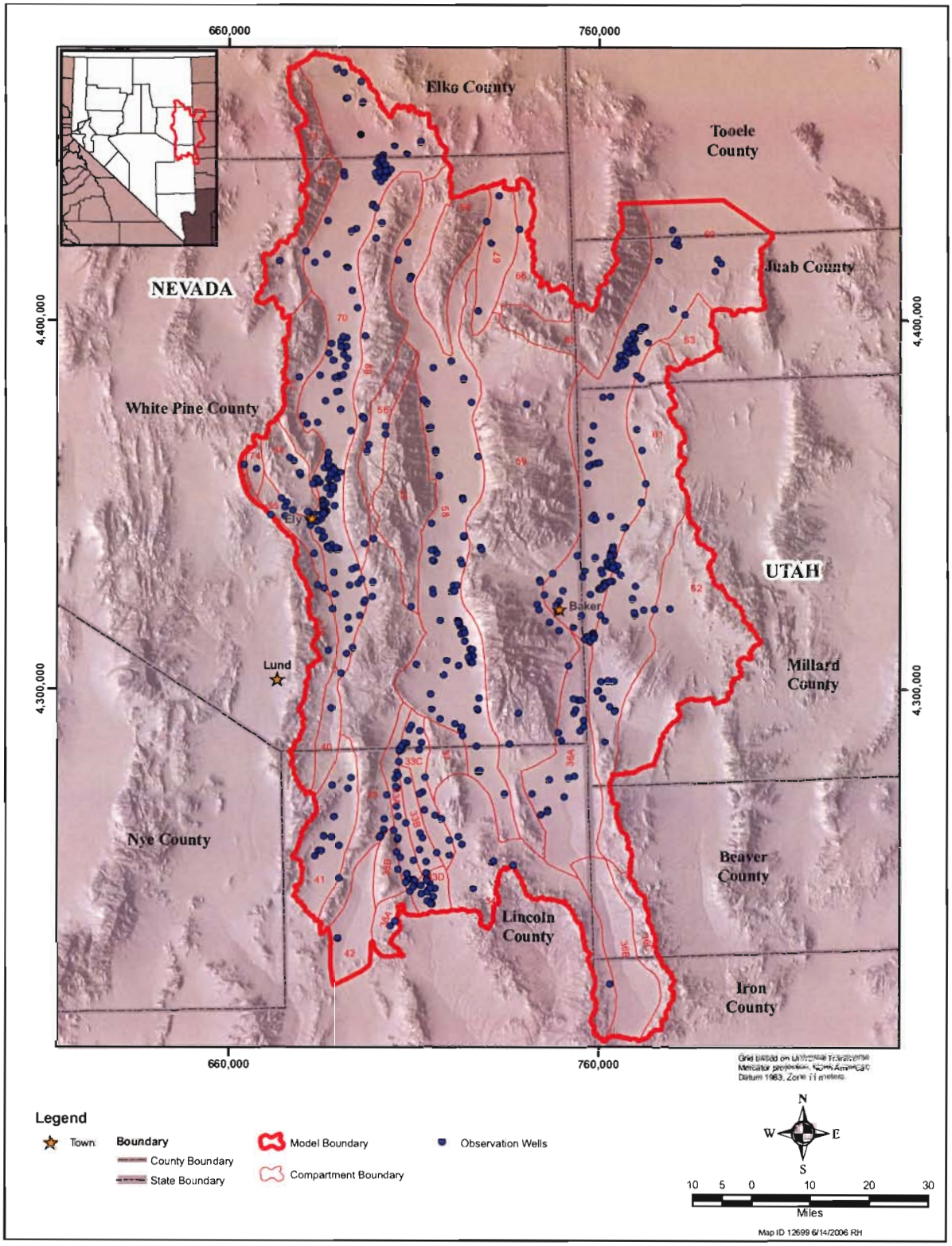

Figure 8-1
Map Showing Location of Observation Wells Used in Calibration

well-construction information are available. Sites lacking well-construction information were not used in the calibration.

The target groundwater levels were estimated as described in SNWA (2006b, Volume 6), steady-state groundwater levels were estimated not only from water-level measurements made during the 1960's and earlier, but also from the backward extrapolation of more recent measurements. The estimator for the steady-state groundwater levels was the average of the available measurements. However, wells with hydrographs displaying a trend were treated differently. Either the well was eliminated as an observation point or the earliest data were averaged.

An uncertainty was assigned to each estimated groundwater level. The uncertainty represents the random departures of the estimated groundwater level from the actual level. The estimated groundwater levels are represented by the random function

$$h_i = H_i + \varepsilon_{1i} + \varepsilon_{2i} + \varepsilon_{3i} \tag{8-18}$$

where

$$\text{var}[h_i] = \text{var}[\varepsilon_{1i}] + \text{var}[\varepsilon_{2i}] + \text{var}[\varepsilon_{3i}] \tag{8-19}$$

and where

$$s_h^2 = \text{var}[h_i] \tag{8-20}$$

and finally where

h_i is the estimated steady-state groundwater level for well i [L],
s_h is the standard error of the estimated groundwater level [L],
H_i is the actual steady-state groundwater level [L],
ε_{1i} is the error associated with the measuring-point elevation for the well [L],
ε_{2i} is the error associated with the temporal variability in groundwater levels [L], and
ε_{3i} is the error associated with the conceptual fit to the groundwater model [L].

The error terms are random variables assumed to be distributed normally with zero mean.

Well-Location Uncertainty. A measuring-point error causes a groundwater-level error when a groundwater-depth measurement is translated into a corresponding groundwater elevation. The error associated with the measuring-point elevation is mostly an error associated with the well location. For most of the observation wells in the database, the measuring-point elevation was interpolated from a topographic map based on the assumed well location. However, for most of the wells in the database, the true location is uncertain, and the uncertainty ranges from tens of feet to thousands of feet. The location uncertainty translates into elevation uncertainty depending on the slope of the topographic surface in the vicinity of the well. For the wells used in the model calibration, the standard error of the measuring-point uncertainty ranges from 0 to 300 ft. The average standard error is 50 ft, where the

average is the square root of the average of the variances $\text{var}[\varepsilon_{1i}]$. The standard error for each observation well is listed in SNWA (2006b, Volume 6), along with the computations used to derive the standard error.

Groundwater-Variability Uncertainty. The groundwater-variability error relates to how well the data characterize the variability within a well of groundwater levels. Groundwater levels fluctuate seasonally and inter-annually, but groundwater levels are measured intermittently with periods ranging typically from months to years. The estimator for the steady-state groundwater level is the average groundwater elevation for the well. If long-term continuous monitoring data were available for the well, the average would represent a very reliable estimate of the actual long-term average. However, the data typically available for a well represent only periodic samplings of a temporally fluctuating random variable. Correspondingly, the computed average is an uncertain estimate of the mean. As described in SNWA (2006b, Volume 6), the standard error of the estimate depends on the number of measurements and the variability among the measurements. For the wells used in the model calibration, the standard error of the groundwater-variability uncertainty ranges from 0 to 50 ft. The average standard error is 5 ft, where the average is the square root of the average of the variances $\text{var}[\varepsilon_{2i}]$. The standard error for each observation well is listed in SNWA (2006b, Volume 6), along with the computations used to derive the standard error.

Conceptualization Uncertainty. The conceptualization error relates to the differences in spatial scales associated with the groundwater-level measurements and the model. The groundwater-level data represent point measurements. The measurements reflect groundwater conditions within a particular three-dimensional vicinity of the well. The dimensions of that vicinity depend on at least four factors. The first is the conductiveness of the groundwater system, where the representative vicinity is larger for more conductive systems. The second is the intermediate-scale heterogeneity of the groundwater system, where the representative vicinity is larger for less heterogeneous systems. The third is the anisotropy of the groundwater system, where the representative vicinity is larger for less anisotropic systems. The fourth is the hydraulic gradient within the groundwater system, where the representative vicinity is larger for hydraulically flatter groundwater system.

The representative vicinity can have scales ranging from many thousands of feet down to tens of feet. The model scale is at many thousands of feet. While large scales occur where the groundwater system is highly conductive, homogeneous, isotropic, and of low gradient, small scales occur where the system is poorly conductive, highly heterogeneous, highly anisotropic, and has a large gradient. The groundwater system throughout much of the Spring Valley area is characteristic of the conditions associated with small representative vicinities. This is especially the case for the consolidated-rock hydrogeologic unit, but it applies also to the upper valley fill, only to a slightly lesser degree. Therefore, the use of the model to represent small scale processes is inappropriate.

Different conceptual models of carbonate-rock hydraulic conductivity apply at the model and observations scales. The groundwater-level measurements for wells constructed in carbonate rocks have a conceptual uncertainty that is expressed as a standard error (Anderson and Woessner, 2002, and Gelhar, 1986). This standard error describes the random difference between a groundwater-level measurement at a point and the geographic distribution of groundwater levels over an area with dimensions of several miles and more. For wells in mountain-block areas, including wells in

consolidated rock or in areas underlain at shallow depths by consolidated rock, the standard error most likely has a magnitude on the order of hundreds of feet. For wells in valley-floor areas, including wells either in the upper valley fill or in adjacent or underlying consolidated rock, the standard error of conceptual uncertainty is smaller. That standard error most likely has a magnitude on the order of tens of feet. The contrasting standard errors between the mountain-block and valley-floor areas are due mostly to the contrasting conductivities and hydraulic gradients.

The conceptual uncertainty is much lower for the valley-floor wells than for the mountain-block wells. Correspondingly, a standard error of 10 ft was assigned the valley-floor wells, and a standard error of 500 ft was assigned to the mountain-block wells. The standard error for the mountain-block wells is such that those wells essentially have no weight in the calibration. This is appropriate because the mountain-block groundwater-level measurements not only are highly uncertain but also are biased. Bias occurs because the groundwater-flow vector tends to be nearly vertical, and the vertical hydraulic gradients are high. Consequently, the mountain-block monitoring wells tend to reflect only the highest heads along the nearly vertical flow paths. Additionally, there is considerable variability in the depth of these wells and the sources of water to these wells, whether it be perched, semi-perched or regional in origin.

Overall Groundwater-Level Uncertainty. Figure 8-2 shows, for each well used in the calibration, the combined standard error for each observation, where the standard error represents the combined effects of uncertain well locations, temporally varying groundwater levels and disparate representative scales. The standard error ranges from 10 to 300 ft for the valley-floor wells. The average standard error is about 50 ft, where the average is the square root of the average of the variances $\mathrm{var}[h_i]$. The mountain-block wells each are assigned a combined standard error of 500 ft, which equals the standard error for the conceptual uncertainty.

8.1.3.2 Phreatophyte Discharge Estimates

In addition to groundwater levels, the estimated phreatophyte discharges (as described in Section 6.0) are used as calibration targets. The target values are the basin scale phreatophyte discharges estimated by Eakin (1962), Rush and Eakin (1963), Rush and Kazmi (1965), Hood and Rush (1965), and Eakin, Hughes, and Moore (1967). The coefficient of variation for the phreatophyte discharge from a particular valley most likely is on the order of 30 percent. The groundwater appraisals by Eakin and Rush, including those in the Spring Valley area, tended to use similar techniques throughout Nevada for estimating phreatophyte discharges. While their work represents the beginning of quantitative hydrology in Nevada, subsequent work by other investigators has been consistent with the earlier work with respect to the stated coefficient of variation. Correspondingly, the estimated phreatophyte discharges were used in the calibration with a standard error based on a coefficient of variation of 30 percent.

8.1.3.3 Springflow and Streamflow Estimates

The estimated average discharges from two regional spring systems within the model area, Warm Spring and Big Spring in Snake Valley, were used as calibration targets (as described in Section 7.0).

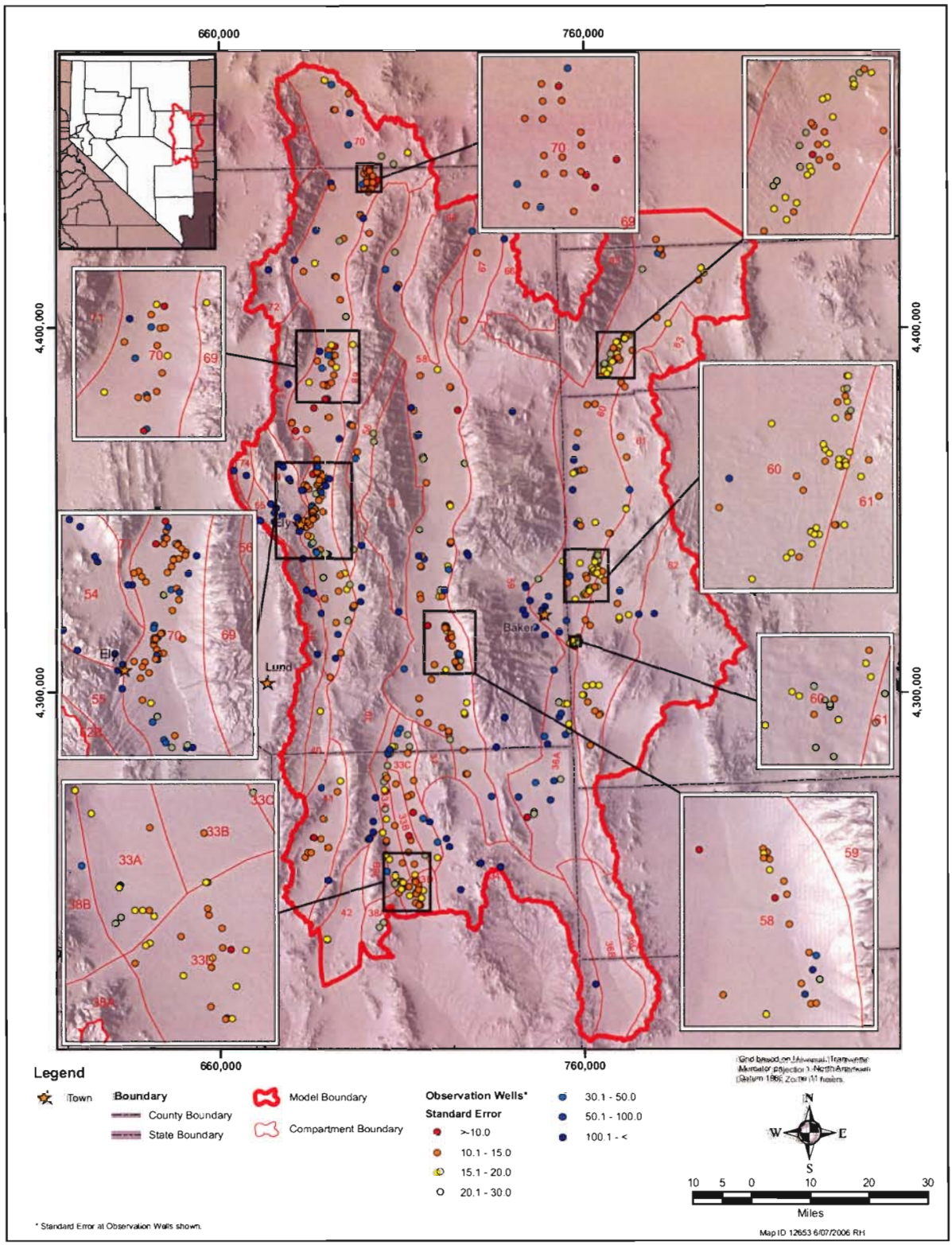

Figure 8-2
Map Showing Standard Error of Observations

The limited discharges measurements for the springs each display certain fluctuations. These fluctuations reflect both the temporal variability of the springflows and the variability of the measurement locations. The springflow measurements represent inconsistent measuring locations. While both springs have a principal orifice or a principal group of orifices, additional groundwater discharges are distributed along a surface-water channel downstream from the principal discharge. Accordingly, the measured springflow depends on the location of the measuring point along the channel. Nevertheless, the average springflow for each spring was used in the calibration with a standard error based on a coefficient of variation of 10 percent.

8.1.3.4 Streamflow Discharges onto Playas

The estimated streamflow discharges onto playas within Spring and Snake valleys (as described in Section 7.0) were used as calibration targets within the calibration. The combined streamflow onto playas, where the streamflow evaporates, is the streamflow required to close the steady-state hydrologic budget for the model area. Then, the uncertainty in the streamflow is the uncertainty that propagates through the calculation of the closure value. As described in Section 2.0, the hydrologic budget has the form

$$Q_{MB} + Q_{MF} = Q_{ET} + Q_U + Q_{EP} + Q_{CU} \tag{8-21}$$

or, by rearranging terms,

$$Q_{EP} = Q_{MB} + Q_{MF} - Q_{ET} - Q_U - Q_{CU}$$

where

Q_{MB} is the mountain-block recharge [L^3t^{-1}],
Q_{MF} is the mountain-front streamflow [L^3t^{-1}],
Q_{ET} is the phreatophyte discharge [L^3t^{-1}],
Q_U is the groundwater underflow from the modeled area [L^3t^{-1}],
Q_{EP} is the streamflow discharge onto the playas and subsequent evaporation [L^3t^{-1}], and
Q_{CU} is the cultural consumptive use of groundwater [L^3t^{-1}].

Based on the procedure for calculating the variance of function of random variables (Benjamin and Cornell, 1970), the uncertainty in the streamflow discharges to the playas is given by the relation

$$\text{var}[Q_{EP}] = \sum_i \sum_j \text{cov}[Q_i, Q_j] \tag{8-22}$$

where i and j correspond to each of the subscripts in Equation 8-21. Equation 8-22 has a correlation structure such that the random components on the two sides of Equation 8-21 balance for any realization. In order to preserve the water-budget, the algebraic summation of the random components

on the righthand side of Equation 8-21 must equal the random component of the streamflow discharges to the playas. In mathematical terms,

$$\varepsilon_{EP} = \sum_i \varepsilon_i \tag{8-23}$$

where

ε_{EP} is the random component of the streamflow discharge [L^3t^{-1}] and
ε_i is the random component of the righthand-side quantities [L^3t^{-1}].

The coefficients of variation for streamflow discharges onto playas is assumed to be 30 percent.

8.1.3.5 Prior Parameter-Value Estimates

The calibrated parameter values include the hydraulic conductivities of the hydrogeologic units, the transmissivities of the faults, the leakances of the faults, the streambed hydraulic conductivities, and the spring leakances. The model calibration is structured in terms of the log-transformation of these parameters. PEST is used to estimate the logarithms of the hydraulic parameters. The uncertainties in the prior estimates of those parameters are expressed in PEST in logarithmic form.

The uncertainty in the prior estimate of hydraulic conductivity of the upper valley fill can be derived from the aquifer-test data. While the aquifer-test data represent point values, the calibration requires an assessment of the uncertainty in the average hydraulic conductivity of the upper valley fill at the model scale. However, the variance of the average hydraulic conductivity can be derived from the relation (Vanmarcke, 1983)

$$\text{var}[\log K_A] = \gamma(A)\sigma^2_{\log K} \tag{8-24}$$

where

K_A is the average hydraulic conductivity within the area A [Lt^{-1}],
$\gamma(A)$ is the variance function evaluated for the area A [L^0], and
$\sigma^2_{\log K}$ is the variance of the point $\log_{10}$ hydraulic conductivities [L^0].

As described by Vanmarcke (1983), the variance function is given by an integral involving the correlation structure associated with the point hydraulic conductivities. Furthermore, for the average over a very large area with respect to the correlation scale of the point process, the variance function is approximately equal to the correlation scale divided by the characteristic model scale. As described in Section 2.3, the correlation scale for the log hydraulic conductivity of the upper valley fill is on the order of several thousand feet. The characteristic model scale is on the order of many thousands of

feet. Concomitantly, the variance function at the model scale has a value of about 10^{-1}. The variance of the point log hydraulic conductivities is about 2.0 $\log_{10}$ units, and the corresponding variance of the average log hydraulic conductivity is about 0.2 $\log_{10}$ units.

The variances for the prior estimates of the other model parameters are larger than that for the hydraulic conductivity of the upper valley fill. Furthermore, the estimation of the variances relies on more subjective information. In particular, the variance of a prior estimate was derived from the relation

$$\mathrm{var}[\log b] = \left[\frac{(\log(b_{max}) - \log(b_{min}))}{4}\right]^2 \qquad (8\text{-}25)$$

where

b_{max} is the maximum probable value of the parameter,
b_{min} is the minimum probable value of the parameter.

Equation 8-25 implies the range between the maximum and minimum probable values of the parameter represents a range of four standard deviations, which is equivalent to stating that the probability of the true value is in the range of 95 percent. The variances derived from Equation 8-25 are listed in Table 8-1.

8.1.4 Calibration Results

The calibration results are shown on Figures 8-3 through 8-6 and Tables 8-2 through 8-6. Figure 8-3 through Figure 8-6 show scatter diagrams comparing weighted observations and the corresponding weighted simulated values. Figure 8-7 shows the geographic distribution of the weighted residuals for the groundwater-level observations. Figure 8-8 shows the composite observation sensitivities for the wells used in the calibration. Figure 8-9 shows a diagram representing the correlation structure among the calibrated parameters. Figure 8-10 shows the simulated steady-state groundwater elevations for the simulation, and Figure 8-11 shows the phreatophyte discharge areas for the simulation. Tables 8-2 through 8-4 list the parameter estimates and their standard errors. Table 8-5 lists the simulated steady-state water budget for the hydrologic system, and Table 8-6 lists the simulated steady-state water budget for the groundwater system.

Table 8-1
Prior Estimates and Uncertainties for Calibration Parameters

Unit	Parameter	Prior Estimate	Standard Error (Log_{10} units)
Upper valley fill RMU	Northerly hydraulic conductivity (ft/d)	20	0.2
	Vertical to northerly anisotropy	1:50	0.5
	Westerly to northerly anistropy	1:20	0.5
Lower valley fill RMU	Northerly hydraulic conductivity (ft/d)	20	0.5
	Vertical to northerly anisotropy	1:50	0.5
	Westerly to northerly anistropy	1:20	0.5
Carbonate rock RMU	Northerly hydraulic conductivity (ft/d)	150	0.8
	Westerly to northerly anisotropy	1:10	0.5
	Vertical to northerly anisotropy	1:1	0.5
Upper aquitard RMU	Northerly hydraulic conductivity (ft/d)	0.3	2.0
	Westerly to northerly anisotropy	1:10	0.5
	Vertical to northerly anisotropy	1:1	0.5
Plutonic rock RMU	Northerly hydraulic conductivity (ft/d)	5	0.8
	Westerly to northerly anisotropy	1:10	0.5
	Vertical to northerly anisotropy	1:1	0.5
Basement rock RMU	Northerly hydraulic conductivity (ft/d)	10	0.8
	Westerly to northerly anisotropy	1:10	0.5
	Vertical to northerly anisotropy	1:1	0.5
Fault	Transmissivity (ft^2/dy)	--	--
Fault	Leakance (ft/d)	--	--
Stream channels	Channel-bed hydraulic conductivity (ft/d)	0.4	0.3
Spring conduits	Warm Spring leakance (ft/d)	8x104	0.5
	Big Spring leakance (ft/d)	4x104	0.5

The scatter diagrams indicate the fits between the observations and the corresponding simulated values. The horizontal axis for each diagram represents the weighted observation, and the vertical axis represents the weighted simulated value. A diagonal line is plotted on each diagram to represent the match line. Figure 8-3 shows a scatter diagram for the groundwater-elevation observations used in the calibration. The coefficient of determination is 0.99, which means the model represents 99 percent of the variability in the observations. The standard error of the estimate is 8.9, which represents 1 percent of the maximum weighted observation. Figure 8-4 shows a scatter diagram for the phreatophyte-discharge observations used in the calibration. The coefficient of determination is 0.98. The standard error of the estimate is 35, which represents 6 percent of the maximum weighted observation. Figure 8-5 shows a scatter diagram for the spring-discharge observations used in the calibration. The coefficient of determination is essentially zero because the number and range of observations is small. The standard error of the estimate is 780, which represents 40 percent of the range of weighted observations. Figure 8-6 shows a scatter diagram for the streamflow-discharge

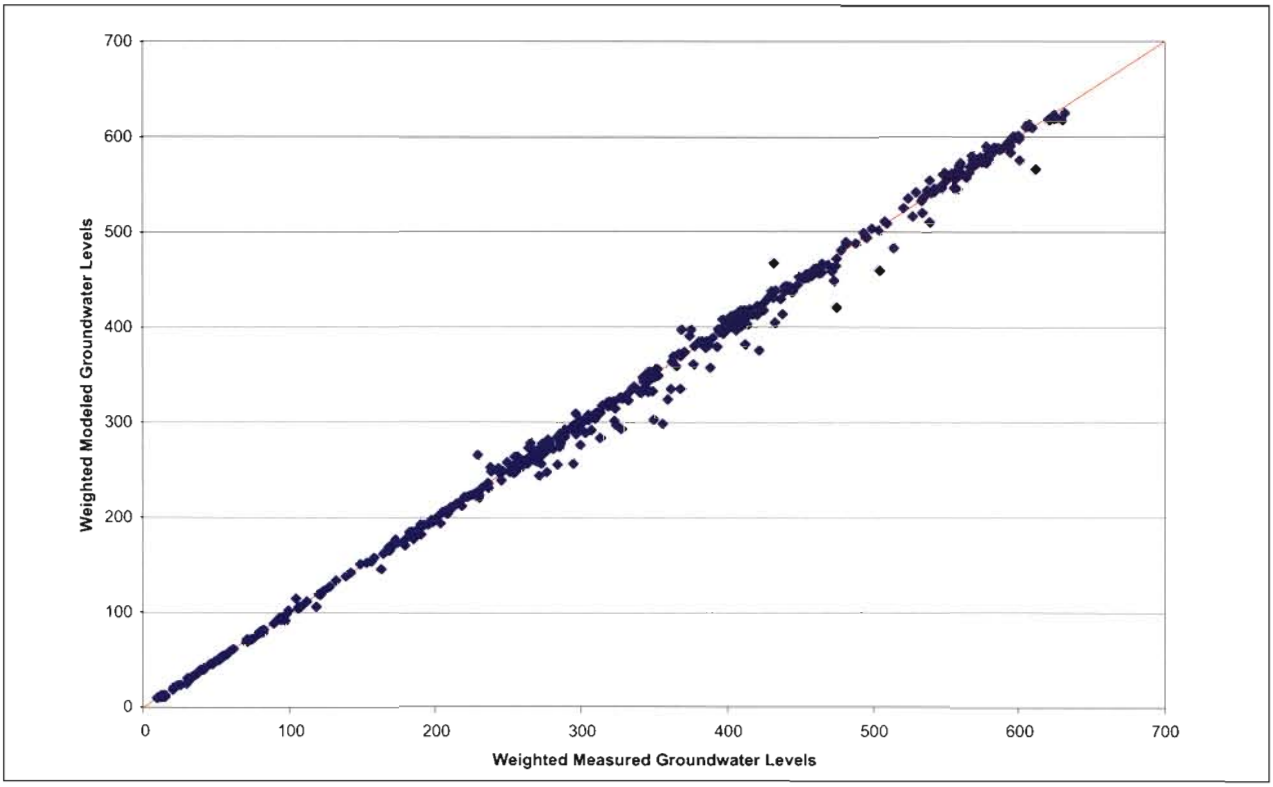

Figure 8-3
Graphs Showing Comparison of Weighted Measured and Computed Observations: Groundwater Levels

observations used in the calibration. The coefficient of determination also is essentially zero because the number and range of observations is small. The standard error of the estimate is 630, which represents 7 percent of the maximum weighted observation.

The cumulative distribution of the weighted groundwater-level residuals (Figure 8-12) also indicate the model fit to the groundwater-level observations. The horizontal axis indicates the magnitude of the weighted residual. The vertical axis is the probability that a residual would be less than or equal to a particular residual value, where probability assigned to a residual is based on the Weibull equation (Haan, 1977). The probability that a residual is within a specified range is the difference between the probability value corresponding to the residual values representing the top and bottom of the range. Figure 8-12 shows the cumulative distribution for all the observation wells used in the calibration. The range of residuals is from -36 to +57, which are dimensionless values because the residuals have the unit of feet and the weights have the unit of inverse feet. However, 67 percent of the residuals are within the range ± 5, which indicates the standard error of the residuals also is 5. The range of residuals for Steptoe Valley are from -12 to 58, but the standard error is 3. The range of residuals for Spring Valley is from -8 to +45, but the standard error is 3. The range of residuals for Snake Valley is from -36 to +47 ft, but the standard error is 5. The range of residuals for Lake Valley is from -0.5 to +0.5 ft, and the standard error is 0.4.

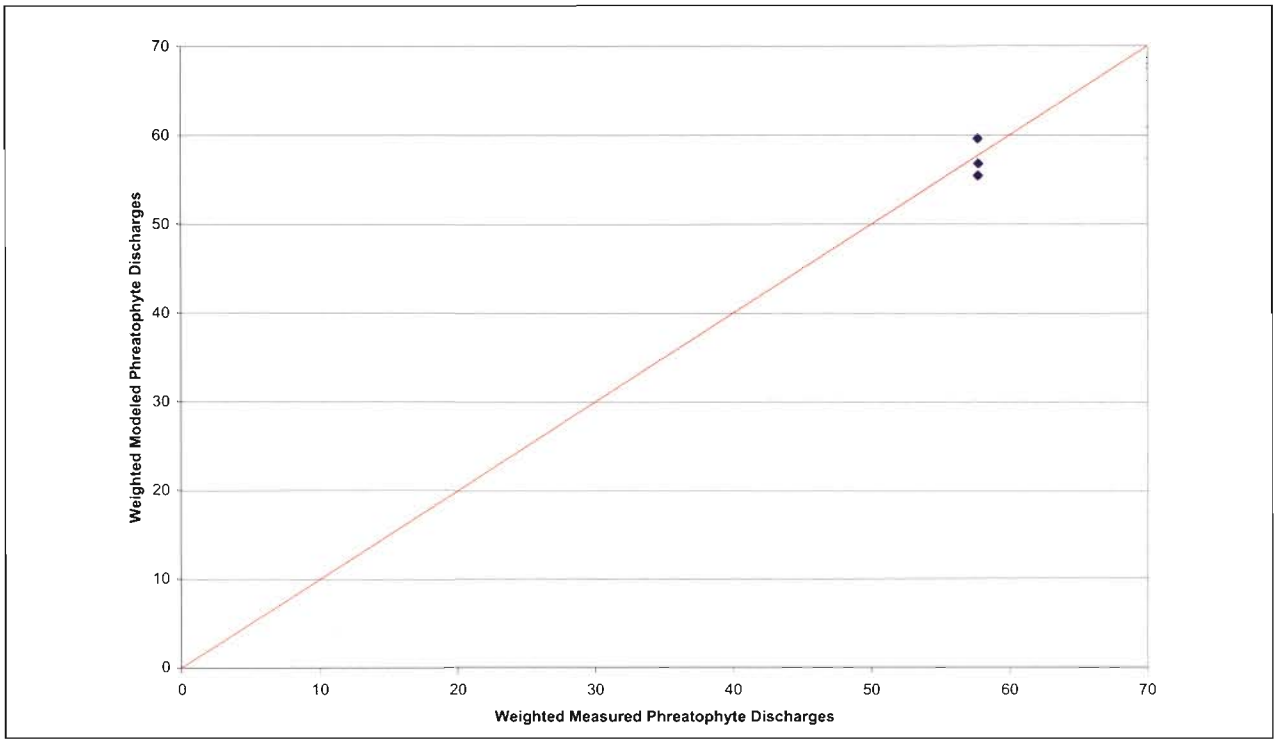

Figure 8-4
Graphs Showing Comparison of Weighted Measured and Computed Observations: Phreatophyte DIscharges

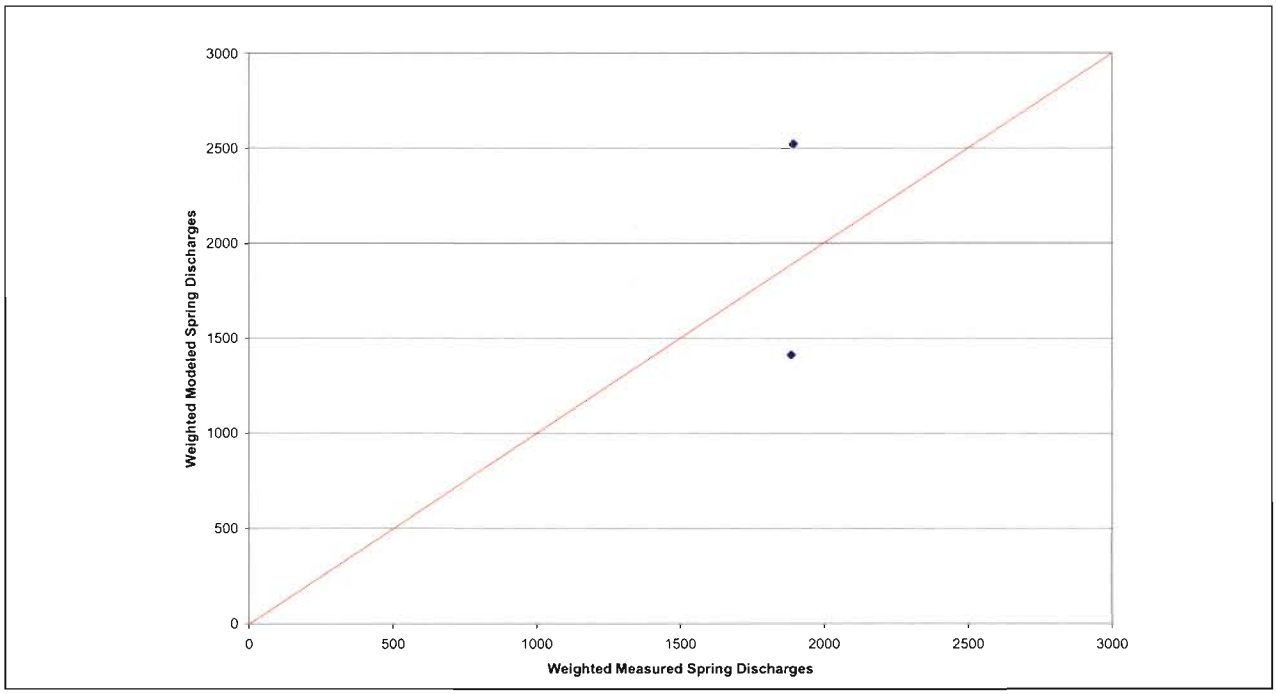

Figure 8-5
Graphs Showing Comparison of Weighted Measured and Computed Observations: Spring Discharges

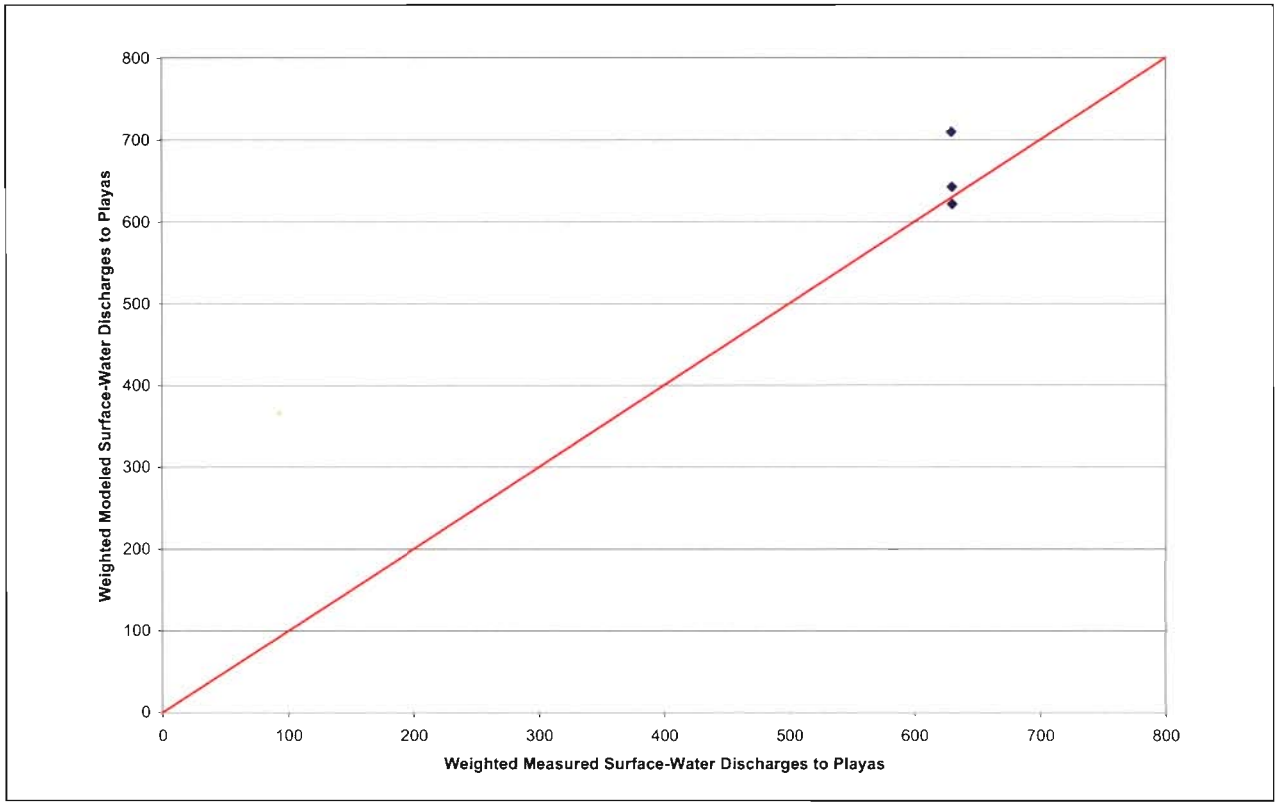

Figure 8-6
Graphs Showing Comparison of Weighted Measured and Computed Observations: Surface Water Discharges to Playas

The composite observation sensitivities indicate the relative importance of particular observations in the identification of the parameter values: the more sensitive the parameters are to a particular observation, the more important is the observation in the calibration. Figure 8-8 shows the weighted composite observation sensitivities for the wells used in the calibration. The figure does not indicate anything anomalous with respect to the observation sensitivities. Because the observation sensitivities are weighted, they tend to be greater for observations with less uncertainty. Additionally, the sensitivities have some tendency to be greater where the number of wells within a compartment is limited.

The composite parameter sensitivities indicate the relative sensitivity of the simulated groundwater levels and other model outputs to a change in a model parameter. Model parameters that have a greater effect on the model outputs will be associated with larger composite parameter sensitivities. Furthermore, the larger the sensitivity the more identifiable is the parameter from the calibration. Tables 8-7 to 8-9 list the composite parameter sensitivities for each parameter in the calibration configuration. The inspection of the tables indicates the sensitivities range over five orders of magnitude. The sensitivities for the hydraulic conductivities (Table 8-7) range from 10^{0} to 10^{-3}. The sensitivity for the fault transmissivity (Table 8-9) is 10^{-1}, and sensitivities for the fault leakances range from 10^{-1} to 10^{-5}. The sensitivity for the Warm Spring leakances (Table 8-8) is 10^{0}, while the sensitivity for the Big Spring leakance is 10^{0}. Finally, the sensitivity for the channel-bed hydraulic

Table 8-2
Regional Model Units Parameter Estimates and Standard Errors

Regional Model Unit	Parameter	Value	Standard Error
Upper valley fill RMU	Horizontal hydraulic conductivity (K_x)	20	2.7
	Westerly hydraulic conductivity (*Ky*)	1.0	0.15
	Vertical hydraulic conductivity (*Kz*)	0.40	18
Lower valley fill RMU	Horizontal hydraulic conductivity (*Kx*)	20	6.7
	Westerly hydraulic conductivity (*Ky*)	1.0	0.15
	Vertical hydraulic conductivity (*Kz*)	0.40	19
Carbonate rock RMU	Horizontal hydraulic conductivity (*Kx*)	140	3.1
	Westerly hydraulic conductivity (*Ky*)	14	3.6
	Vertical hydraulic conductivity (*Kz*)	140	18
Upper aquitard RMU	Horizontal hydraulic conductivity (*Kx*)	0.31	7.2
	Westerly hydraulic conductivity (*Ky*)	0.031	18
	Vertical hydraulic conductivity (*Kz*)	0.31	20
Plutonic rock RMU	Horizontal hydraulic conductivity (*Kx*)	4.4	26
	Westerly hydraulic conductivity (*Ky*)	0.44	30
	Vertical hydraulic conductivity (*Kz*)	4.4	32
Basement rock RMU	Horizontal hydraulic conductivity (*Kx*)	10	17
	Westerly hydraulic conductivity (*Ky*)	1.0	23
	Vertical hydraulic conductivity (*Kz*)	10	25

Table 8-3
Streams and Springs Parameter Estimates and Standard Errors (ft/day)

Unit	Parameter	Value	Standard Error
Stream channels	Channel-bed hydraulic conductivity	0.44	0.051
Spring conduits	Warm Spring leakance	$8.9x10^3$	0.012
	Big Spring leakance	4.6x106	18

Table 8-4
Fault Parameter Estimates and Standard Errors (ft^2/day)

Unit	Parameter	Value	Standard Error	Unit	Parameter	Value	Standard Error
Faults	Transmissivity	9.3	210	Fault 40	Leakance	1	730
Fault 01	Leakance	2,000	240	Fault 41		1,700	1,500
Fault 02		1,900	84	Fault 42		2,000	12,000
Fault 03		1,600	32	Fault 43		2,000	3,000
Fault 04		5,300	170	Fault 44		1,700	420
Fault 05		4,000	110	Fault 45		9,000	1,200
Fault 06		1,600	70	Fault 46		5,400	320
Fault 07		2,100	270	Fault 47		3,800	260
Fault 08		3,700	150	Fault 48		2,100	2,000
Fault 09		1,700	1,100	Fault 49		720	32
Fault 10		1,800	930	Fault 50		830	120
Fault 11		6,000	210	Fault 51		1,900	12,000
Fault 12		1,200	130	Fault 52		78	11
Fault 13		1,800	490	Fault 53		15,000	820
Fault 14		2,100	1,000	Fault 54		20	21
Fault 15		3,100	1,100	Fault 55		0	230
Fault 16		2,000	300	Fault 56		360	8
Fault 17		670	290	Fault 57		92	57
Fault 18		6,500	460	Fault 58		6	100
Fault 19		1,500	4,500	Fault 59		2	1,800
Fault 20		4,500	4,000	Fault 60		3,400	520
Fault 21		5,300	170	Fault 61		7	6
Fault 22		2	93	Fault 62		3	1,000
Fault 23		8,500	61	Fault 63		3	430
Fault 24		820	1,500	Fault 64		2	18,000
Fault 25		27	2,100	Fault 65		10,000	38
Fault 26		8,200	80	Fault 66		39,000	420
Fault 27		1	1,200	Fault 67		800	50
Fault 28		2,300	430	Fault 68		2,300	57
Fault 29		1	880	Fault 69		1,000	83
Fault 30		2,200	260	Fault 70		9,200	1,700
Fault 31		150	19	Fault 71		10,000	14,000
Fault 32		9,800	1,200	Fault 72		3	560
Fault 33		930	98	Fault 73		1,800	13
Fault 34		1,300	130	Fault 74		1,900	26
Fault 35		1,300	2,300	Fault 75		6,700	400
Fault 36		1	280	Fault 76		2,500	830
Fault 37		2,900	200	Fault 77		3,100	1,500
Fault 38		61	11	Fault 78		2,300	6,300
Fault 39		3,800	1,400				

Table 8-5
Simulated Steady-State Water Budget (afy) for Hydrologic System

Budget Component	Simulated	Simulated	Estimated Rate
Inflows			
Mountain-block recharge (A)			
Steptoe Valley	85,000	85,000	0
Tippett Valley	6,900	6,900	0
Spring Valley	65,000	65,000	0
Snake Valley	71,000	71,000	0
Pleasant Valley	5,000	5,000	0
Hamlin Valley	24,000	24,000	0
Cave Valley	14,000	14,000	0
Lake Valley	13,000	13,000	0
Dry Lake Valley (northern part)	1,700	1,700	0
Spring Valley Streamflow (B)	47,500	47,500	0
Snake Valley streamflow	2,700	2,700	0
Total	**335,800**	**335,800**	**0**
Outflows			
Phreatophyte ET (C)	73,300	71,000	2,300
Spring Valley	74,700	76,000	-1,300
Steptoe Valley	0	200	-200
Cave Valley	10,800	10,000	800
Snake Valley	84,600	88,000	-3,400
Boundary underflows (D)			
Steptoe Valley	7,000	7,000	0
Lake Valley	3,000	3,000	0
Cave Valley	14,000	14,000	0
Snake Valley	20,000	20,000	0
Dry Lake Valley	1,700	1,700	0
Playa evaporation (E)			
Spring Valley Yelland Lake	21,600	21,300	300
Spring Valley South Playa	8,400	7,800	600
Snake Valley	14,800	14,400	400
Agricultural and community consumptive use (F)			
Steptoe Valley	0	0	0
Spring Valley	0	0	0
Snake Valley	300	300	0
Lake Valley	0	0	0
Ely		700	700
McGil	400	400	0
Total	**335,300**	**335,800**	**-500**
Residual	**500**	**0**	

Table 8-6
Simulated Steady-State Water Budget (afy) for Groundwater System

Budget Component	Simulated	Simulated	Estimated Rate
Inflows			
Mountain-block recharge (A)			
Steptoe Valley	85,000	85,000	0
Tippett Valley	6,900	6,900	0
Spring Valley	65,000	65,000	0
Snake Valley	71,000	71,000	0
Pleasant Valley	5,000	5,000	0
Hamlin Valley	24,000	24,000	0
Cave Valley	14,000	14,000	0
Lake Valley	13,000	13,000	0
Dry Lake Valley (northern part)	1,700	1,700	0
Spring Valley valley-floor streamflow recharge	17,500	18,500	-900
Snake Valley valley-floor streamflow recharge	9,400	7,00	2,000
Total	**312,500**	**311,400**	**1,100**
Outflows			
Phreatophyte ET	73,300	71,000	2,300
Spring Valley	74,700	76,000	-1,300
Steptoe Valley	0	200	-200
Cave Valley	10,800	10,000	800
Snake Valley	84,600	88,000	-3,400
Boundary underflows (D)			
Steptoe Valley	7,000	7,000	0
Lake Valley	3,000	3,000	0
Cave Valley	14,000	14,000	0
Snake Valley	20,000	20,000	0
Dry Lake Valley	1,700	1,700	0
Spring Discharges			
Warm Sping	17,000	12,400	4,600
Big Spring	5,000	6,700	-1,700
Agricultural and community consumptive use			
Groundwater use in Steptoe Valley	0	0	0
Groundwater use in Spring Valley	0	0	0
Groundwater use in Snake Valley	300	300	0
Groundwater use in Lake Valley	0	0	0
Ely	700	700	700
McGill	400	400	0
Total	**312,500**	**311,400**	**1,100**
Residual	**0**	**0**	

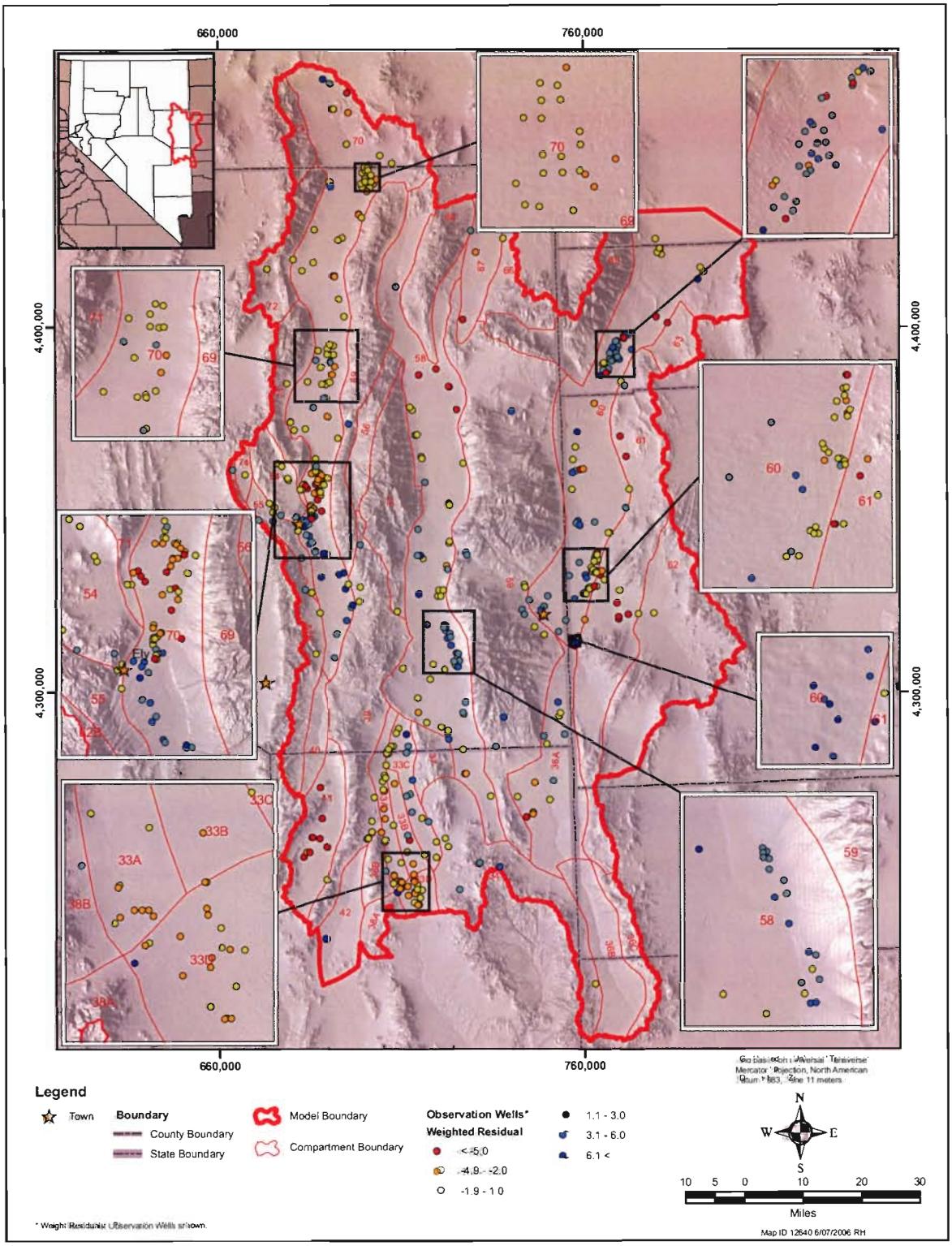

Figure 8-7
Map Showing Weighted Residuals at Observation Wells Used in Calibration

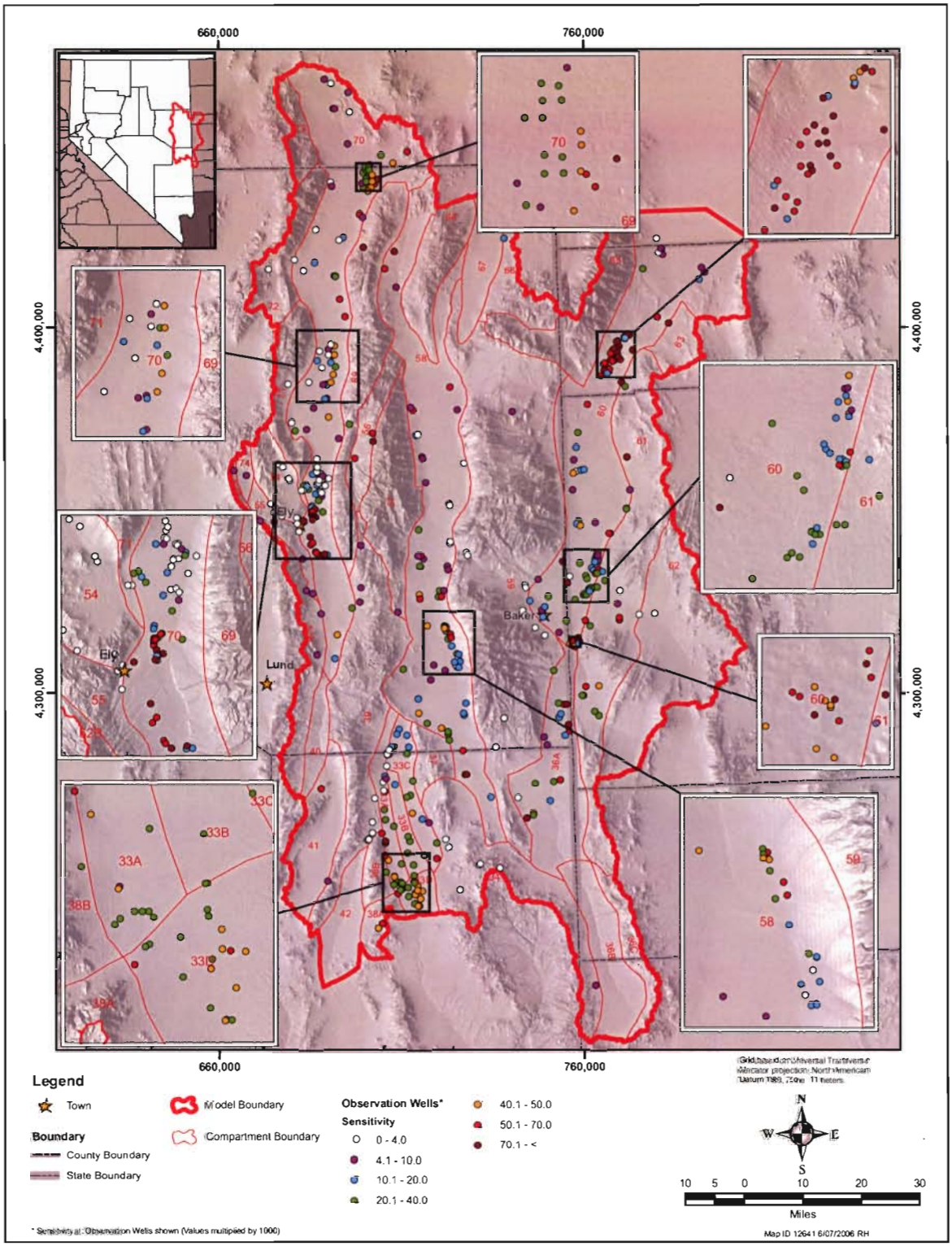

Figure 8-8
Map Showing Composite Observation Sensitivities for Wells Used in the Calibration

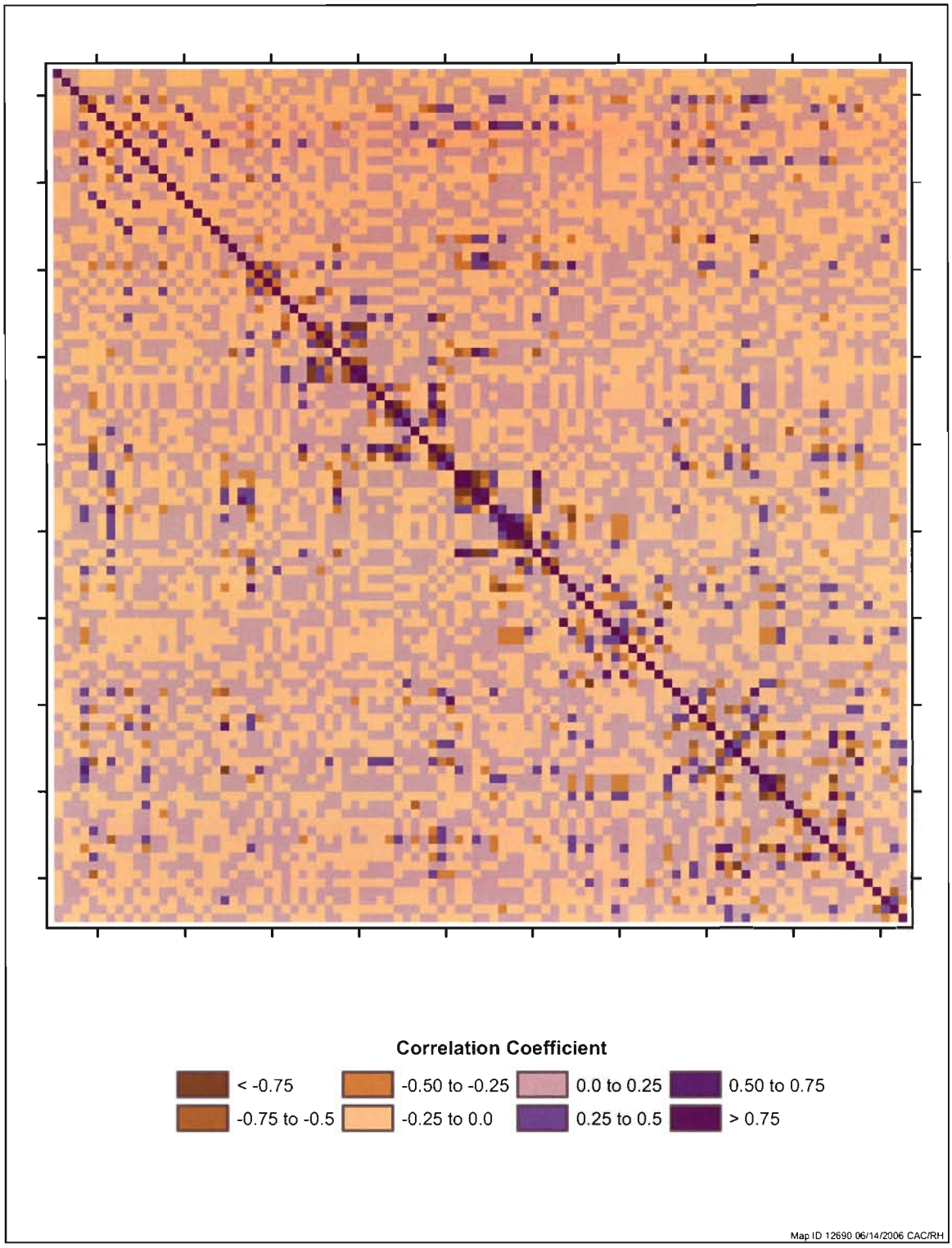

Figure 8-9
Diagram Showing Structure of Correlations Between Parameters

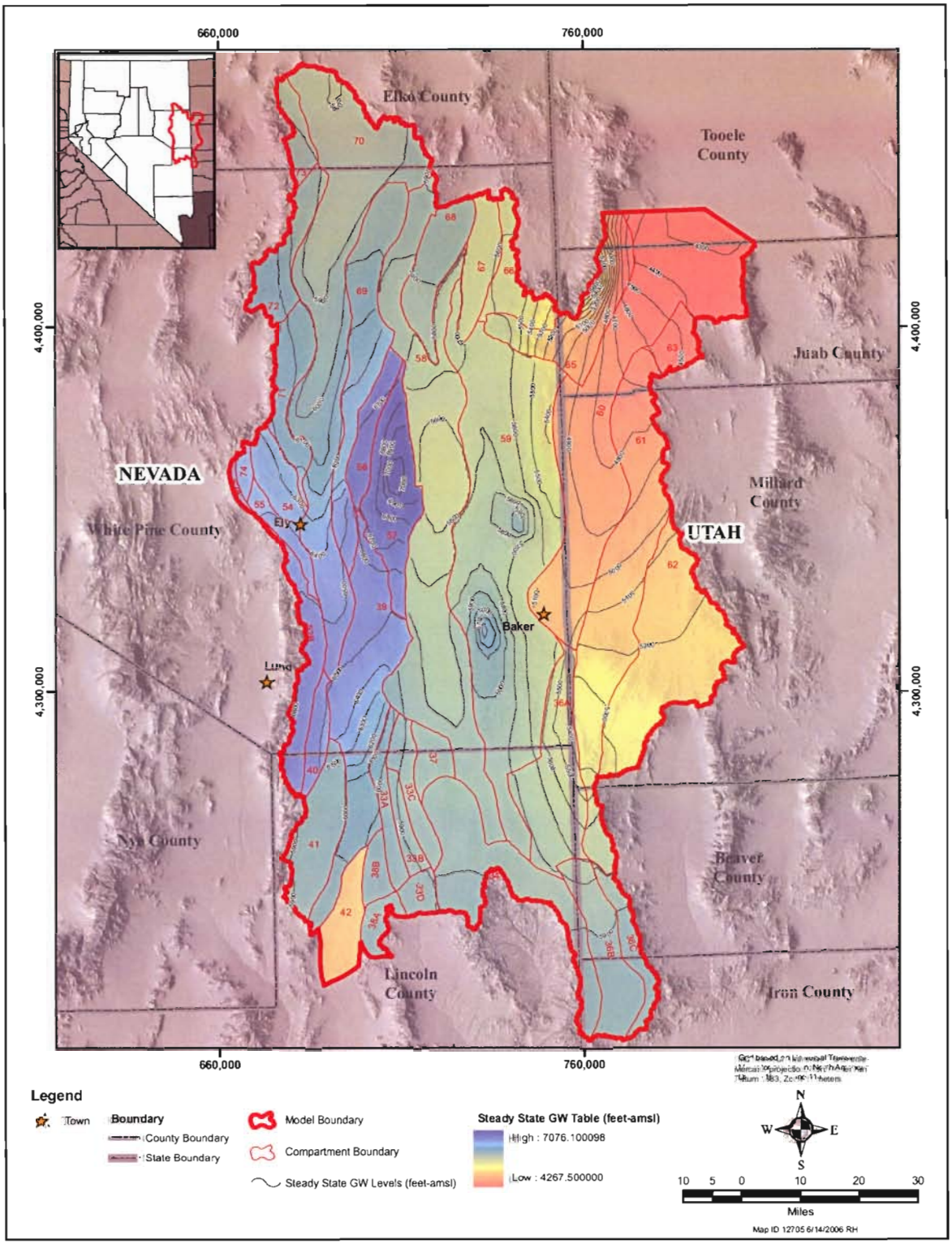

Figure 8-10
Map Showing Simulated Steady-State Groundwater-Table Elevations

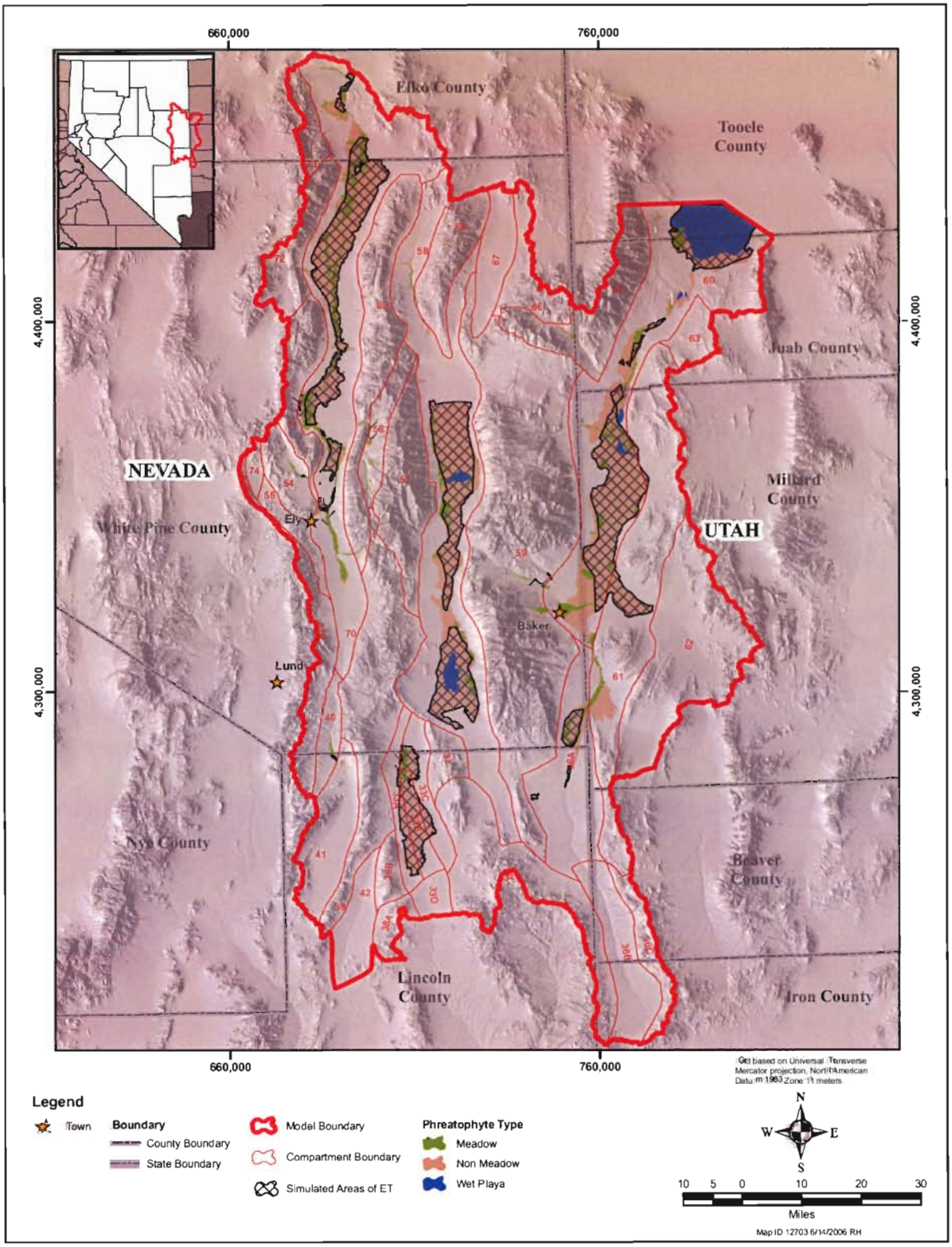

Figure 8-11
Map Showing Areas of Simulated Steady-State Phreatophyte Discharges

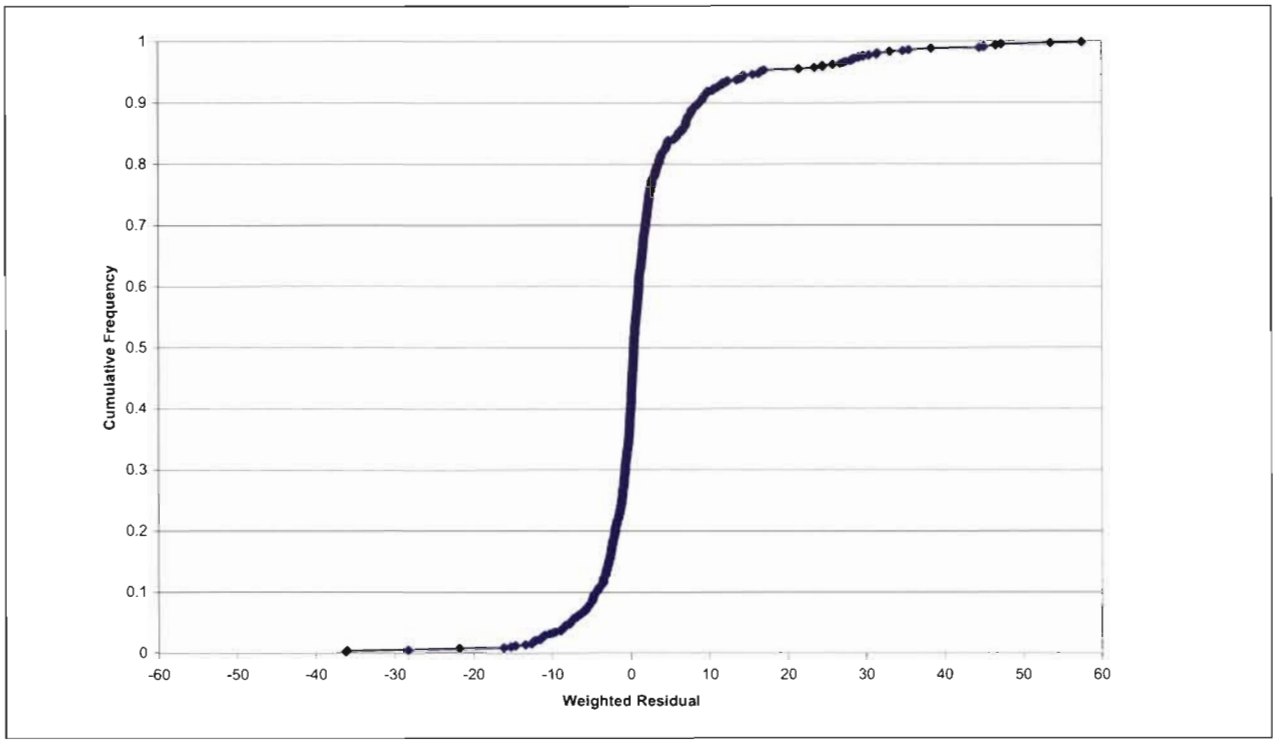

Figure 8-12
Graphs Showing Cumulative Distributions of Weighted Residuals for Groundwater Levels: Entire Model Area

conductivity is 10^{-3}. Overall, Tables 8-7 through 8-9 indicate the highest parameter sensitivities are for the hydraulic conductivity of the upper valley fill and carbonate rock RMUs, which means that those parameters are the most identifiable from the calibration.

The scatter diagrams, cumulative distributions of residuals, composite observation sensitivities, and composite parameter sensitivities are descriptive of the internal working of the calibration process and are important for utilizing the model as a monitoring and management tool. The covariance matrix of the parameter estimates is directly related to the predictive reliability of the model. The standard errors of the parameter estimates are listed in Tables 8-2 to 8-4 where the standard errors are the square roots of the diagonal terms within the covariance matrix. Figure 8-9 is a diagram that shows the covariance matrix in terms of its correlation structure. While the diagonal elements of the correlation matrix equal one, the off-diagonal elements range from zero to one. A zero value for an off-diagonal element means the uncertainties in the parameter estimates are completely uncorrelated. A unit value indicates the uncertainties are perfectly correlated. Figure 8-9 shows the pattern of correlations within the covariance matrix. An inspection of the figure indicates little correlation occurs among the parameters.

Tables 8-2 to 8-4 and Figure 8-9 represent only part of the uncertainty in the calibrated parameters. The represented part is that part associated with the identifiability of the parameters based on the observations and prior parameter information. Not represented is parameter uncertainty resulting from uncertainty in the water-budget inputs to the model (Dawdy, Lichty, and Bergmann, 1972). The

effects of such uncertainties are not recognized in the formulation of the calibration. The principal source of the additional parameter uncertainty is the uncertainty in the estimates of recharge and discharge by Eakin (1962), Rush and Eakin (1963), Rush and Kazmi (1965), Hood and Rush (1965), and Eakin, Hughes, and Moore (1967).

That uncertainty translates into parameter uncertainty. However, based on the prior information on the hydraulic conductivity of the upper valley fill, there is less uncertainty associated with this parameter, and subsequently more uncertainty is distributed to the other hydrogeologic units. As the observation weights squared ($\overline{\Omega}^{-1}$) become small relative to the parameter weights squared ($\sigma^2 \overline{V}^{-1}$), the parameter covariance matrix is dominated by the uncertainty in the prior parameter estimates.

Figure 8-10 and Figure 8-11 and Table 8-5 and Table 8-6 show simulation results corresponding to the calibrated parameter values. Figure 8-10 shows the simulated groundwater levels respectively for the groundwater table. Figure 8-11 shows the simulated areas of phreatophyte discharges. Table 8-5 lists the simulated water-budget components for the hydrologic system. Table 8-6 lists the simulated water-budget components for the groundwater system. In both tables, the simulated water-budget components are compared with the corresponding budgets based in part on the early work by Eakin (1962), Rush and Eakin (1963), Rush and Kazmi (1965), Hood and Rush (1965), and Eakin, Hughes, and Moore (1967).

The simulated and estimated water budgets for the hydrologic and groundwater systems are nearly identical for the cumulative inflows and outflows. However, for the hydrologic system, the individual water-budget components generally differ by less than 5 percent between the simulated and estimated budgets. For the groundwater system, that holds for the water-budget components except for the spring discharges. The simulated spring discharges differ by as much as 30 percent from the estimated discharge.

Table 8-7
Regional Model Units Composite Parameter Sensitivities

Regional Model Unit	Parameter	Sensitivity
Upper valley fill RMU	Horizontal hydraulic conductivity	$2.5x10^{0}$
	Vertical hydraulic conductivity	$3.3x10^{-3}$
Lower valley fill RMU	Horizontal hydraulic conductivity	$6.4x10^{-1}$
	Vertical hydraulic conductivity	$3.3x10^{-3}$
Carbonate rock RMU	Northerly hydraulic conductivity	$1.2x10^{0}$
	Westerly hydraulic conductivity	$1.8x10^{0}$
	Vertical hydraulic conductivity	$3.3x10^{-3}$
Upper aquitard RMU	Northerly hydraulic conductivity	$9.7x10^{-3}$
	Westerly hydraulic conductivity	$2.4x10^{-1}$
	Vertical hydraulic conductivity	$3.3x10^{-3}$
Plutonic rock RMU	Northerly hydraulic conductivity	$1.9x10^{-1}$
	Westerly hydraulic conductivity	$6.6x10^{-3}$
	Vertical hydraulic conductivity	$3.3x10^{-3}$
Basement rock RMU	Northerly hydraulic conductivity	$2.2x10^{-1}$
	Westerly hydraulic conductivity	$2.3x10^{-1}$
	Vertical hydraulic conductivity	$3.3x10^{-3}$

Table 8-8
Streams and Springs Composite Parameter Sensitivities

Unit	Parameter	Sensitivity
Stream channels	Channel-bed hydraulic conductivity	$1.9x10^{0}$
Spring conduits	Warm Spring leakance	$4.8x10^{0}$
	Big Spring leakance	$3.3x10^{-3}$

Table 8-9
Fault Parameter Estimates and Standard Errors
(Page 1 of 2)

Unit	Parameter	Sensitivity	Unit	Parameter	Sensitivity
Faults	Transmissivity	$1.9x10^{-1}$	Fault 40	Leakance	$5.4x10^{-3}$
Fault 01	Leakance	$6.6x10^{-4}$	Fault 41		$1.2x10^{-4}$
Fault 02		$2.5x10^{-3}$	Fault 42		$5.7x10^{-5}$
Fault 03		$3.4x10^{-2}$	Fault 43		$6.2x10^{-5}$
Fault 04		$2.3x10^{-1}$	Fault 44		$1.0x10^{-3}$
Fault 05		$1.5x10^{-1}$	Fault 45		$3.8x10^{-4}$

Table 8-9
Fault Parameter Estimates and Standard Errors
(Page 2 of 2)

Unit	Parameter	Sensitivity	Unit	Parameter	Sensitivity
Fault 06		$1.1x10^{-1}$	Fault 46		$1.9x10^{-3}$
Fault 07		$4.9x10^{-4}$	Fault 47		$1.3x10^{-3}$
Fault 08		$1.6x10^{-1}$	Fault 48		$2.1x10^{-4}$
Fault 09		$3.0x10^{-4}$	Fault 49		$5.6x10^{-3}$
Fault 10		$6.6x10^{-3}$	Fault 50		$2.2x10^{-3}$
Fault 11		$2.4x10^{-2}$	Fault 51		$5.2x10^{-5}$
Fault 12		$2.2x10^{-2}$	Fault 52		$1.9x10^{-1}$
Fault 13		$3.9x10^{-4}$	Fault 53		$3.8x10^{-4}$
Fault 14		$2.2x10^{-4}$	Fault 54		$1.9x10^{-1}$
Fault 15		$2.2x10^{-3}$	Fault 55		$1.8x10^{-1}$
Fault 16		$8.8x10^{-3}$	Fault 56		$1.5x10^{0}$
Fault 17		$8.8x10^{-3}$	Fault 57		$5.8x10^{-3}$
Fault 18		$6.6x10^{-3}$	Fault 58		$5.8x10^{-3}$
Fault 19		$2.0x10^{-2}$	Fault 59		$8.0x10^{-3}$
Fault 20		$2.0x10^{-2}$	Fault 60		$6.6x10^{-4}$
Fault 21		$1.1x10^{-2}$	Fault 61		$1.5x10^{0}$
Fault 22		$1.4x10^{-3}$	Fault 62		$2.4x10^{-3}$
Fault 23		$2.0x10^{-2}$	Fault 63		$1.1x10^{-2}$
Fault 24		$2.0x10^{-2}$	Fault 64		$7.0x10^{-4}$
Fault 25		$2.0x10^{-2}$	Fault 65		$2.4x10^{-3}$
Fault 26		$1.5x10^{-2}$	Fault 66		$4.3x10^{-4}$
Fault 27		$4.3x10^{-2}$	Fault 67		$4.8x10^{-3}$
Fault 28		$8.4x10^{-4}$	Fault 68		$1.9x10^{-3}$
Fault 29		$8.7x10^{-2}$	Fault 69		$2.8x10^{-3}$
Fault 30		$1.6x10^{-1}$	Fault 70		$3.4x10^{-3}$
Fault 31		$2.7x10^{-1}$	Fault 71		$9.0x10^{-5}$
Fault 32		$1.0x10^{-3}$	Fault 72		$1.5x10^{-2}$
Fault 33		$2.0x10^{-3}$	Fault 73		$1.9x10^{-1}$
Fault 34		$3.2x10^{-3}$	Fault 74		$1.9x10^{-1}$
Fault 35		$2.6x10^{-4}$	Fault 75		$2.7x10^{-4}$
Fault 36		$1.9x10^{-1}$	Fault 76		$4.7x10^{-4}$
Fault 37		$4.6x10^{-3}$	Fault 77		$2.7x10^{-4}$
Fault 38		$4.5x10^{-1}$	Fault 78		$4.6x10^{-5}$
Fault 39		$3.1x10^{-4}$			

Table 8-10
Regional Model Units Parameter Estimates and Standard Errors

Regional Model Unit	Parameter	Value	Standard Error
Upper valley fill RMU	Horizontal hydraulic conductivity (K_x)	20	2.7
	Westerly hydraulic conductivity (K_y)	1.0	0.15
	Vertical hydraulic conductivity (K_z)	0.40	18
Lower valley fill RMU	Horizontal hydraulic conductivity (K_x)	20	6.7
	Westerly hydraulic conductivity (K_y)	1.0	0.15
	Vertical hydraulic conductivity (K_z)	0.40	19
Carbonate rock RMU	Horizontal hydraulic conductivity (K_x)	140	3.1
	Westerly hydraulic conductivity (K_y)	14	3.6
	Vertical hydraulic conductivity (K_z)	140	18
Upper aquitard RMU	Horizontal hydraulic conductivity (K_x)	0.31	7.2
	Westerly hydraulic conductivity (K_y)	0.031	18
	Vertical hydraulic conductivity (K_z)	0.31	20
Plutonic rock RMU	Horizontal hydraulic conductivity (K_x)	4.4	26
	Westerly hydraulic conductivity (K_y)	0.44	30
	Vertical hydraulic conductivity (K_z)	4.4	32
Basement rock RMU	Horizontal hydraulic conductivity (K_x)	10	17
	Westerly hydraulic conductivity (K_y)	1.0	23
	Vertical hydraulic conductivity (K_z)	10	25

9.0 REFERENCES

Allison G.B. and Barnes, C.J., 1985, Estimation of evaporation from the normally "dry" Lake Frome in south Australia: Journal of Hydrology, Vol. 78, pp. 229-242.

American Society of Agricultural Engineers, 1990, Management of farm irrigation systems: St. Joseph, Missouri, American Society of Agricultural Engineers, 1040 p.

American Society of Civil Engineers, 1990, Evapotranspiration and Irrigation Water Requirements: New York, American Society of Civil Engineers, 332 p.

Anderson, Mary P., 1991, Comment on "Universal Scaling of Hydraulic Conductivities and Dispersivities in Geologic Media" by S. P. Neuman: Water Resources Research, Vol. 27, No. 6, pp. 1381-1382.

Anderson, Mary P., and Woessner, William W., 2002, Applied groundwater modeling: Simulation of flow and advective transport: San Diego, California, Academic Press, 381 p.

Antonellini, M., and Aydin, A., 1994, Effect of faulting on fluid flow in porous sandstones: petrophysical properties: American Association of Petroleum Geologists Bulletin, Vol. 78, No. 3, pp. 355-377.

Avon, Lizanne, and Durbin, Timothy J., 1994, Evaluation of the Maxey-Eakin method for estimating recharge to groundwater basins in Nevada: American Water Resources Association, Water Resources Bulletin, Vol. 30, No. 1, pp. 99-111.

Aydin, A., 1978, Small faults formed as zones of deformation bands and as slip surfaces in sandstone: Pure and Applied Geophysics, Vol. 16, pp. 931-942.

Aydin, A., and Johnson, A. M., 1978, Development of faults as zones of deformation bands and as slip surfaces in sandstone: Pure and Applied Geophysics, Vol. 116, pp. 913-930.

Batu, Vedat, 1998, Aquifer hydraulics: A comprehensive guide to hydrogeologic data analysis: New York, John Wiley & Sons, Inc., 727 p.

Beck, James V. and Arnold, Kenneth J., 1977, Parameter estimation in engineering and science: New York, John Wiley & Sons, Inc., 501 p.

Bedinger, M.S., Sargent, K.A., and Langer W.H., 1989, Studies of geology and hydrology in the Basin and Range Province, southwestern United States, for isolation of high-level radioactive waste – characterization of the Rio Grande region, New Mexico and Texas: U.S. Geological Survey Professional Paper 1370-C, 42 p.

Belcher, W. R., Elliott, P. E., and Geldon, A. L., 2001, Hydraulic-property estimates for use with a transient ground-water flow model of the Death Valley regional ground-water flow system, Nevada and California: U. S. Geological Survey Water-Resources Investigations Report 01-4120, 28 p.

Benjamin, Jack R., and Cornell, C. Allin, 1970, Probability, statistics, and decision for civil engineers: New York, McGraw-Hill, 684 p.

Berger, D. L., Kilroy, K. C., Schafer, D. H., 1988, geophysical logs and hydrologic data for eight wells in the Coyote Spring area, Clark and Lincoln Counties, Nevada: U. S. Geological Survey Open-File Report 87-679, 59 p.

Berger, David L., Johnson, Michael J., Tumbusch, Mary L., and Mackay, Jeffrey, 2001, Estimates of evapotranspiration from the Ruby Lake National Wildlife Refuge Area, Ruby Valley, northeastern Nevada, May 1999-October 2000: U.S. Geological Survey Water-Resources Investigations Report 01-4234, 38 p.

Berkowitz, Brian, Bour, Olivier, Davy, Philippe, and Odling, Noelle, 2000, Scaling of fracture connectivity in geological formations: Geophysical Research Letters, Vol. 27, No. 14, pp. 2061-2064.

Blaney, H.F., Taylor, C.A., Nickle, H.G., and Young, A.A., 1933, Water losses under natural conditions from wet areas in southern California: California Department of Public Works, Division of Water Resources, Bulletin 44, 176 p.

Blaney, Harry F., 1958, Consumptive use of ground water by phreatophytes and hydrophytes in New Mexico Water; Present Use and New Sources: New Mexico Annual Water Conference Proceedings, Vol. 3, pp. 98-110.

Bour, Olivier, and Davy, Philippe, 1998, On the connectivity of three-dimensional fault networks: Water Resources Research, Vol. 34 (10), pp. 2611-2622.

Bouwer, Herman, 1988, Surface water-groundwater relations for open channels *in* Proceedings of the Irrigation and Drainage Division Specialty Conference: American Society of Civil Engineers, Irrigation and Drainage Division, pp. 149-156.

Bouwer, Herman, 1989, Effect of water depth and groundwater table on infiltration: Journal of Irrigation and Drainage Engineers, Vol. 115, No. 4, pp. 556-567.

Bouwer, Herman, 1990, Effect of water depth and groundwater table on infiltration from recharge basins *in* Harris, Steven C. (editor) Proceedings of the 1990 National Conference, Durango Colorado: American Society of Civil Engineers, Irrigation and Drainage Division, pp. 377-384.

Bredehoeft, John D., 1997, Fault permeability near Yucca Mountain: Water Resources Research, Vol. 33, No. 11, pp. 2459-2463.

Broadbent, R., Katzer, T., and Brothers, K., 1995, Mountain-front runoff and ground-water recharge in east central Nevada: Las Vegas Valley Water District Cooperative Water Project report No. 17, 16 p.

Brothers, Kay, Bernholtz, Alan J., Buqo, Thomas S., and Tracy, James V., 1994, Hydrology and steady state ground-water model of Spring Valley, White Pine and Lincoln counties, Nevada: Las Vegas Valley Water District Cooperative Water Project Report No. 13, Hydrographic Basin 184, 116 p.

Brothers, Kay, Buqo, Thomas S., and Tracy, James V., 1993a, Hydrology and steady state ground-water model of Snake Valley, east-central Nevada, and west-central Nevada: Las Vegas Valley Water District Cooperative Water Project Report No. 9, Hydrographic Basin 195, 85 p.

Brothers, K., Buqo, T.S., Tracy, James V., Stock, Mark, Bentley, Craig, Zdon, Andrew, and Kepper, John, 1993b, Hydrology and steady state ground-water model of Cave Valley, Lincoln and White Pine counties, Nevada: Las Vegas Valley Water District Cooperative Water Project Report No. 11, Hydrographic Basin 180, 78 p.

Bunch, R.L., and Harrill, J. R., 1984, Compilation of selected hydrologic data from the MX missile-siting investigation, East-central Nevada and western Utah: U. S. Geological Survey Open-File Report 84-702, 123 p.

Burbey, T.J., 1997, Hydrogeology and potential for ground-water development, carbonate-rock aquifers in southern Nevada and southeastern California: U.S. Geological Survey Water-Resources Investigation 95-4168, 65 p.

Burbey, Thomas J., and Prudic, David E., 1991, Conceptual evaluation of regional groundwater flow in the carbonate-rock province of the Great Basin, Nevada, Utah, and adjacent states; Regional aquifer-system analysis: U. S. Geological Survey Professional Paper 1409-D, 84 p.

Burkham, D.E., 1970, Depletion of streamflow by infiltration in the main channels of the Tucson Basin, southeastern Arizona: U.S. Geological Survey Water-Supply Paper 1939-B. 36 p.

Caine, Jonathan Saul, and Forster, Craig B., 1999, Fault zone architecture and fluid flow: Insights from field data and numerical modeling *in* William C. Haneberg and others (editors) Faults and Subsurface Fluid Flow in the Shallow Crust: American Geophysical Union Geophysical Monograph Series No. 113, pp. 101-127.

Caine, Jonathan Saul, Evans, James P., and Forster, Craig B., 1996, Fault zone architecture and permeability structure: Geology, Vol. 24, No. 11, pp. 1025-1028.

California Department of Water Resources, 1967, Vegetative water use: California Department of Water Resources Bulletin 113-2.

California Department of Water Resources, 1986, Crop water use in California: California Department of Water Resources Bulletin 113-4, 116 p.

Carman, R. L., 1989, Measurement of evapotranspiration in phreatophyte areas, Smith Creek Valley and Carson Desert, west-central Nevada, 1983: U. S. Geological Survey Water-Resources Investigations Report 89-4118, 18 p.

Carr, P. A., and Van Der Camp, G. S., 1969, Determining aquifer characteristics by the tidal method: Water Resources Research, Vol. 5, No. 5, pp. 1023-1031.

Cohen, Philip, 1963, Specific-yield and particle-size relations of Quaternary alluvium, Humboldt River Valley, Nevada: U.S. Geological Survey Water-Supply Paper 1669-M, pp. 20-23.

Cooley, R.L. and Naff, R.L., 1990, Regression modeling of ground-water flow: U.S. Geological Survey Techniques in Water-Resources Investigations TWRI 93-B4, 232 p.

Corbet, T., Ho, C., Knupp, P., and Ramsey, J., 1998, Review and verification of the *MINEDW* groundwater flow code: Sandia National Laboratories, 30 p.

Czarnecki, John B., 1997, Geohydrology and evapotranspiration at Franklin Lake Playa, Inyo County, California: U. S. Geological Survey Water-Supply Paper 2377, 75 p.

D'Agnese, Frank A., Faunt, Claudia C., Turner, A. Keith, and Hill, Mary C., 1997, Hydrogeologic evaluation and numerical simulation of the Death Valley regional ground-water flow system, Nevada and California: U.S. Geological Survey Water-Resources Investigations Report 96-4300, 124 p.

David, Christian, Gueguen, Yves, and Pampoukis, Georges, 1990, Effective medium theory and network theory applied to the transport properties of rock: Journal of Geophysical Research, Vol. 95, No. B5, pp. 6993-7005.

Dawdy, David, R., Lichty, Robert W., and Bergmann, James M., 1972, A rainfall-runoff simulation model for estimation of flood peaks for small drainage basins: U.S. Geological Survey Professional Paper 506-B, 31 p.

Dettinger, M.D., 1989, Reconnaissance estimates of natural recharge to desert basins in Nevada, USA using chloride-balance calculations: Journal of Hydrology, Vol. 106, pp. 55-78.

Dettinger, M D., 1992, Geohydrology of areas being considered for exploratory drilling and development of the carbonate-rock aquifers in southern Nevada; preliminary assessment: U.S. Geological Survey Water-Resources Investigation 90-4077, 35 p.

Dettinger, M.D., Harrill, J. R., Schmidt, D. L., and Hess, J. W., 1995, Distribution of carbonate-rock aquifers and the potential for their development, southern Nevada and adjacent parts of California, Arizona, and Utah: U.S. Geological Survey Water-Resources Investigations 91-4146, 100 p., 2 plates.

Doorenbos, J., and Pruitt, W.O., 1977, Guidelines for predicting crop water requirements: Food and Agriculture Organization of the United Nations, Rome, Italy, 144 p.

Draper, Norman R., and Smith, Harry, 1998, Applied regression analysis (third edition): New York, John Wiley & Sons, Inc., 706 p.

Duell, Lowell F.W., Jr., 1990, Estimates of evapotranspiration in alkaline scrub and meadow communities of Owens Valley, California, using the Bowen-ration, Eddy-correlation, and Penman-combination methods: U.S. Geological Survey Water-Supply Paper 2370-E, 39 p.

Durbin, T. J., and Berenbrock, C., 1985, Three-dimensional simulation of free-surface aquifers by finite-element method: U. S. Geological Survey Water-Supply Paper 2270.

Durbin, T., J. and Bond, L. D., 1998, *FEMFLOW3D*: A finite-element program for the simulation of three-dimensional aquifers, Version 1.0: U. S. Geological Survey Open-File Report 97-810.

Durbin, T. J., Kapple, G.W., and Freckleton, J.R., 1978, Two-dimensional and three-dimensional digital flow models of the Salinas Valley ground-water basin, California: U.S. Geological Survey Water-Resources Investigations Report 78-113, 134 p.

Durbin, Timothy J., 1983, Application of Gauss algorithm and Monte Carlo simulation to the identification of aquifer parameters: U. S. Geological Survey Open-File Report 81-688, 26 p.

Dverstorp, Bjorn and Andersson, Johan, 1989, Application of the discrete fracture network concept with field data: possibilities of model calibration and validation: Water Resources Research, Vol. 25, No. 3, pp. 540-550.

Eakin, T. E., 1962, Ground-water appraisal of Cave Valley in Lincoln and White Pine Counties, Nevada: Nevada Department of Conservation and Natural Resources Ground-Water Resources Reconnaissance Series Report 13, 19 p.

Eakin, T. E., 1966, A regional interbasin ground-water system in the White River area, southeastern Nevada: U. S. Geological Survey Water Resources Research Vol. 2, No. 2, pp. 251-271.

Eakin, T.E., and others, 1951, Contributions to the hydrology of eastern Nevada: Nevada State Engineer, Water Resources Bulletin 12, 171 p.

Eakin, T. E., Hughes, J. L., and Moore, D. O., 1967, Water-resources appraisal of Steptoe Valley, White Pine and Elko Counties, Nevada: Nevada Department of Conservation and Natural Resources Water Resources-Reconnaissance Series Report 42, 48 p.

Eakin, T. E., Maxey, G. B., Robinson, T. W., Fredericks, J. C., and Loeltz, O. J., 1951, Contributions to the hydrology of eastern Nevada: Nevada State Engineer Water-Resources Bulletin 12, 171 p.

Environmental Modeling Research Laboratory, 2005, Groundwater modeling system tutorials, Volumes I-IV: Brigham Young University, 623 p.

Evenson, R.E., 1959, Geology and ground-water features of the Eureka area, Humboldt County, California: U.S. Geological Survey Water-Supply Paper 1470, 35 p.

Faunt, C. D., 1997, Effect of faulting on ground-water movement in the Death Valley region, Nevada and California: U.S. Geological Survey Water-Resources Investigation 95-4132, 42 p.

Fitts, Charles R., 2002, Groundwater Science: San Diego, California, Academic Press, 450 p.

Freethey, G.W., and Cordy, G.E., 1991, Geohydrology of Mesozoic rocks in the upper Colorado River basin in Arizona, Colorado, New Mexico, Utah, and Wyoming, excluding the San Juan basin: U.S. Geological Survey Professional Paper 1411-C, 118 p., 6 plates.

Freeze, R.A., and Cherry, J.A., 1979, Groundwater: Englewood Cliffs, New Jersey, Prentice-Hall.

Gardner, W.R, 1958, Some steady-state solutions of the unsaturated moisture flow equation with application to evaporation from a water table: Soil Science, Vol. 85, No. 4, pp. 228-232.

Gardner, W.R., and Fireman, Milton, 1958, Laboratory studies of evaporation from soil columns in the presence of a water table: Soil Science, Vol. 85, No. 5, pp. 244-249.

Geldon, A.L., 1989, Hydrologic data for Paleozoic rocks in the Upper Colorado River Basin, Colorado, Utah, Wyoming, and Arizona: U.S. Geological Survey Open-File Report 89-59, 219 p.

Gelhar, Lynn W., 1986, Stochastic Subsurface Hydrology from theory to applications: Water Resources Research, Vol. 22, No. 9, pp. 135S-145S.

Ghilardi, Paolo, Kai, Kai Abdulai, and Menduni, Giovanni, 1993, Self-similar heterogeneity in granular porous media at the representative elementary volume scale: Water Resources Research, Vol. 29, No. 4, pp. 1205-1214.

Greene, Earl A., and Rahn, Perry H., 1995, Localized anisotropic transmissivity in a Karst aquifer: Ground Water, Vol. 33, No. 5, pp. 806-816.

Gupta, H. V., Sorooshian, S., and Yapo, P. O., 1998, Toward improved calibration of hydrologic models, Multiple and non-commensurable measures of information: Water Resources Research, vol. 34, pp. 751-763.

Haan, Charles T., 1977, Statistical methods in hydrology: Ames, Iowa, Iowa State University Press, pp. 135.

Harenberg, W. A., 1980, Using channel geometry to estimate flood flows at ungaged sites in Idaho: U. S. Geological Survey Water-Resources Investigations 80-32, 52 p.

Harrill, J. R., Gates, J. S., and Thomas, J. M., 1988, Major ground-water systems in the Great Basin region of Nevada, Utah, and adjacent states: U. S. Geological Survey Hydrologic Investigations Atlas HA-694-C.

Harrill, James R., 1986, Ground-water storage depletion in Pahrump Valley, Nevada-California, 1962-75: U.S. Geological Survey Water-Supply Paper 2279, 53 p.

Harrill, James R., and Preissler, Alan M., 1994, Ground0watr flow and simulated effects of development in Stagecoach Valley, a small, partly drained basin in Lyon and Storey counties, western Nevada: U.S. Geological Professional Paper 1409-H, 74 p.

Harrill, James R., and Prudic, David E., 1998, Aquifer systems in the Great Basin region of Nevada, Utah, and adjacent states, summary report: U. S. Geological Survey Professional Paper 1409-A, 66 p.

Harrington, R., and Howard, C., 2000, Depth to groundwater beneath vegetation reinventory parcels: Inyo County Water Department, 85 p.

Harrington, R., Steinwand, A., Hubbard, P., and Martin, D., with contributions from Jim Stroh, The Evergreen State College and Dani Or, University of Connecticut, 2004, Evapotranspiration from groundwater dependent plant communities: Comparison of micrometeorological and vegetation-based measurements: Inyo County Water Department and Los Angeles Department of Water and Power, 104 p.

Harrington, Robert, and Steinwand, Aaron, 2003, Development of hydrologic and vadose models to improve groundwater management in the Owens Valley: County of Inyo Water Department, November 10, 2003, 217 p.

Hedman, E. R., 1970, Mean annual runoff as related to channel geometry of selected streams in California: U. S. Geological Survey Water-Supply Paper 1999-E, 17 p.

Hedman, E. R., and Osterkamp, W. R., 1983, Streamflow characteristics related to channel geometry of streams in western United States: U. S. Geological Survey Water-Supply Paper 2193, 17 p.

Hedman, E. Robert, Moore, D. O., and Livingston, R. K., 1972, Selected streamflow characteristics as related to channel geometry of perennial streams in Colorado: U. S. Geological Survey Open-File Report 72-160, 14 p.

Helm, D.C., 1975, One-dimensional simulation of aquifer system compaction near Pixley, California – 1. Constant parameters: Water Resources Research, Vol. 11, No. 3, pp. 465-478.

Helm, D.C., 1976, One-dimensional simulation of aquifer system compaction near Pixley, California – 2. Stress-dependent parameters: Water Resources Research, Vol. 12, No. 3, pp. 375-391.

Helm, D.C., 1977, Estimating parameters of compacting fine-grained interbeds within a confined aquifer system by a one-dimensional simulation of field observations, *in* Land Subsidence Symposium: Proceedings of the second International Symposium on Land Subsidence, held at Anaheim, California, 13-17 December 1976: International Association of Hydrological Sciences, IAHS-AISH Publication Series, No. 121, pp. 145-156.

Helm, D.C., 1978, Field verification of a one-dimensional mathematical model for transient compaction and expansion of a confined aquifer system, *in* Verification of mathematical and physical models in hydraulic engineering: Proceedings, 26th annual Hydraulics Division specialty conference, University of Maryland, College Park, Maryland, August 9-11, 1978: New York, American Society of Civil Engineers, pp. 189-196.

Hester, Kevin and Long, Jane C.S., 1990, Analytical expressions for the permeability of random two-dimensional poisson fracture networks based on regular lattice percolation and equivalent media theories: Journal of Geophysical Research, Vol. 95, No. B13, pp. 21,565-21,581.

Heynekamp, Michiel R., Goodwin, Laurel B., Mozley, Peter S., and Haneberg, William C., 1999, Controls on fault-zone architecture in poorly lithified sediments, Rio Grande Rift, New Mexico: Implications for fault-zone permeability and fluid flow *in* Haneberg W., and others, eds., Faults and subsurface fluid flow in the shallow crust: AGU Geophysical Monograph 113, pp. 27-49.

Hill, M. C., 1998, Methods and guidelines for effective model calibration, With application to UCODE, a computer code for universal inverse modeling, and MODFLOWP, a computer code for inverse modeling with MODFLOW: U. S. Geological Survey Water-Resources Investigation 98-4005.

HIS HydroSystems, 2002, Tule Desert filed activity data report.

Hood, J. W., and Rush, F. E., 1965, Water-resources appraisal of the Snake Valley, Utah and Nevada: Nevada Department of Conservation and Natural Resources Water Resources-Reconnaissance Series Report 34, 43 p.

Hubbell, J.M., Bishop, C.W., Johnson, G.S., and Lucas, J.G., 1997, Numerical ground-water flow modeling of the Snake River Plain aquifer using the superposition technique: Ground Water, Vol. 35, No. 1, pp. 59-66.

Ingebritsen, S.E., and Manning, C.E., 1999, Geological implications of a permeability-depth curve for the Continental Crust: Geology, Vol. 27, No. 12, pp. 1107-1110.

IT Corporation, 1996, Underground test area subproject, phase I: Data analysis task, volume IV: Hydrologic parameter data documentation package, ITLV/10972-181: U. S. Department of Energy.

IT Corporation, 1997a, Underground test area subproject, phase I: Data analysis task, volume VI, Model data documentation package, ITLV/10972-181: U. S. Department of Energy.

IT Corporation, 1997b, Bullion forced-gradient experiment implementation plan, Parts 1 and 2, ITLV/10972-195: U. S. Department of Energy Report DOE/NV-467.

IT Corporation, 2002a, Analysis of well ER-EC-1 testing, Western Pahute Mesa-Oasis Valley FY 2000 testing program, Nevada, Report Revision 0, ITLV/13052-173: U.S. Department of Energy Report DOE/NV/13052-846.

IT Corporation, 2002b, Analysis of well ER-EC-2a testing, Western Pahute Mesa-Oasis Valley FY 2000 testing program, Nevada, Report Revision 0, ITLV/13052-174: U.S. Department of Energy Report DOE/NV/13052-851.

IT Corporation, 2002c, Analysis of well ER-EC-4 testing, Western Pahute Mesa-Oasis Valley FY 2000 testing program, Nevada, Report Revision 0, ITLV/13052-175: U.S. Department of Energy Report DOE/NV/13052-850.

IT Corporation, 2002d, Analysis of well ER-EC-5 testing, Western Pahute Mesa-Oasis Valley FY 2000 testing program, Nevada, Report Revision 0, ITLV/13052-176: U.S. Department of Energy Report DOE/NV/13052-848.

IT Corporation, 2002e, Analysis of well ER-EC-6 testing, Western Pahute Mesa-Oasis Valley FY 2000 testing program, Nevada, Report Revision 0, ITLV/13052-177: U.S. Department of Energy Report DOE/NV/13052-849.

IT Corporation, 2002f, Analysis of well ER-EC-7 testing, Western Pahute Mesa-Oasis Valley FY 2000 testing program, Nevada, Report Revision 0, ITLV/13052-178: U.S. Department of Energy Report DOE/NV/13052-852.

IT Corporation, 2002g, Analysis of well ER-EC-8 testing, Western Pahute Mesa-Oasis Valley FY 2000 testing program, Nevada, Report Revision, ITLV/13052-847: U.S. Department of Energy Report DOE/NV/13052-847.

IT Corporation, 2002h, Analysis of well ER-EC-2 testing, Western Pahute Mesa-Oasis Valley FY 2000 testing program, Nevada, Report Revision 0, ITLV/13052-172: U.S. Department of Energy Report DOE/NV/13052-845.

IT Corporation, 2002i, Summary of well testing and analysis, Western Pahute Mesa-Oasis Valley FY 2000 testing program, Nevada, Report Revision 0, ITLV/13052-180: U.S. Department of Energy Report DOE/NV/13052-853.

Jacob, C. E., 1940, On the flow of water in an elastic artesian aquifer: American Geophysical Union Transactions, Part 2, pp. 574-586.

Jacobson, G., and Jankowski J., 1989, Groundwater-discharge processes at a central Australian playa: Journal of Hydrology Vol. 105, pp. 275-295.

Johnson, A. I., 1967, Specific yield - compilation of specific yield for various materials: U.S. Geological Survey Water-Supply Paper 1662-D, 80 p.

Johnson, A. I., Moston, R. P., and Morris, D. A., 1968, Physical and hydrologic properties of water-bearing deposits in subsiding area in central California: U.S. Geological Survey Professional Paper 497-A, 71 p, 14 plates.

Johnson, Nicolas M., 1995, Characterization of alluvial hydrostratigraphy with indicator semivariograms: Water Resources Research, Vol. 32, No. 12, pp. 3217-3227.

Jorgensen, Donald G., and Petricola, Mario, 1994, Petrophysical analysis of geophysical logs of the National Drilling Company – U.S. Geological Survey Ground-Water Research Project for Abu Dhabi Emirate, United Arab Emirates: U.S. Geological Survey Water-Supply Paper 2417, 35 p.

Kaehler, C. A., and Hsieh, P. A., 1994, Hydraulic properties of a fractured-rock aquifer, Lee Valley, San Diego County, California: U.S. Geological Survey Water-Supply Paper 2394, 64 p.

Kapple, G. W., Mitten, H. T., Durbin, T. J., and Johnson, M. J., 1984, Analysis of the Carmel Valley alluvial groundwater basin, Monterey County, California: U.S. Geological Survey Water-Resources Investigation 83-4280, 45 p.

Kastning, E.H., 1977, Faults as positive and negative influences on ground-water flow and conduit enlargement, *in* Hydrologic problems in karst regions, edited by Dilamarter, R, and Csallany, S: Bowling Green, Kentucky, West Kentucky University, pp. 193-201.

Katzer, Terry, and Donovan, David J., 2003, Surface-water resources and basin water budget for Spring Valley, White Pine and Lincoln counties, Nevada: Las Vegas Valley Water District, Las Vegas, Nevada, 2003, 70 p.

Khadam, I. M., and Kaluarachchi, J. J., 2004, Use of soft information to describe the relative uncertainty of calibration data in hydrologic models: Water Resources Research, vol. 40, W11505, 15 p.

LaBolle, E. M., Ahmed, A. A., and Fogg, G. E., 2003, Review of the Integrated Groundwater and Surface-Water Model (IGSM): Ground Water, Vol. 41, No. 2, pp. 238-246.

LaBolle, E. M., and Fogg, G. E., 2001, A review of California's Integrated Groundwater and Surface-Water Model (IGSM) *in* Geo, H. S., Poeter, E., Zheng, C., and Poeter, O., (eds.) *MODFLOW 2001* and other modeling odysseys, Proceeding Volume J: International Groundwater Modeling Center, Colorado School of Mines, pp. 349-355.

Laczniak, Randell J., DeMeo, Guy A., Reiner, Steven R., Smith, J. LaRue, and Nylund, Walter E., 1999, Estimates of ground-water discharge as determined from measurements of evapotranspiration, Ash Meadows area, Nye County, Nevada: U.S. Geological Survey Water-Resources Investigations Report 99-4079, 77 p., 2 plates.

Laczniak, Randell J., Smith, J. LaRue, Elliott, Peggy E., DeMeo, Guy A., Chatigny, Melissa A., and Roemer, Gaius J., 2001, Ground-water discharge determined from estimates of evapotranspiration, Death Valley regional flow system, Nevada and California: U.S. Geological Survey Water-Resources Investigations Report 01-4195, 51 p.

Lee, Charles H., 1912, An intensive study of the water resources of a part of Owens Valley, California: U.S. Geological Survey Water-Supply Paper 294, 135 p.

Leeds, Hill & Jewell, Inc., 1981a, Groundwater investigation, Phase 1, Technical report for the White Pine Power Project: Los Angeles Department of Water and Power.

Leeds, Hill & Jewell, Inc., 1981b, Groundwater investigation, Phase 2, Technical report for the White Pine Power Project: Los Angeles Department of Water and Power.

Leeds, Hill & Jewell, Inc., 1983, Groundwater investigation, Phase 3, Technical report for the White Pine Power Project: Los Angeles Department of Water and Power.

Lerner, David N., Issar, Arie S., and Simmers, Ian, 1990, Groundwater recharge, a guide to understanding and estimating natural recharge: Hanover, Germany, International Association of Hydrogeologists, Vol. 8, 345 p.

Lohman, S. W., 1972, Ground-water hydraulics: U. S. Geological Survey Professional paper 708, 70 p.

Malek, E., Bingham, G.E., and McCurdy, G.D., 1990, Evapotranspiration from the margin and moist playa of a closed desert valley: Journal of Hydrology, Vol. 120, pp. 15-34.

Manning, Sara J., 2001, The 2000 status of Owens Valley vegetation parcels according to the drought recovery policy: Inyo/Los Angeles Technical Group Report, 115 p.

Margolin, Gennady, Berkowitz, Brian, and Scher, Harvey, 1998, Structure, flow, and generalized conductivity scaling in fracture networks: Water Resources Research, Vol. 34 (9), pp. 2103-2121.

Mason, James L., 1998, Ground-water hydrology and simulated effects of development in the Milford area, an arid basin in southwest Utah: U. S. Geological Survey Professional Paper 1409-G, p. G 1-69.

Maurer, D. K., Lopes, T. J., Medina, R. L., and Smith, L. L., 2004, Hydrogeology and hydrologic landscape regions of Nevada: U. S. Geological Survey Scientific Investigations Report 2004-5431.

Maurer, Douglas K., 2002, Ground-water flow and numerical simulation of recharge from streamflow infiltration near Pine Nut Creek, Douglas County, Nevada: U.S. Geological Survey Water-Resources Investigations Report 02-4145, 37 p.

Maxey, G. B., and Eakin, T. E., 1949, Ground water in White River Valley, White Pine, and Lincoln counties, Nevada: Nevada State Engineer Water Resources Bulletin No. 8, 59 p.

Menking, Kirsten M., Anderson, Roger Y., Brunsell, Nathaniel A., Allen, Bruce D., Ellwein, Amy L., Loveland, Thomas A., and Hostetler, Steven W., 2000, Evaporation from groundwater discharge playas, Estancia Basin, central New Mexico in Yu, Zhongbo, and Barron, Eric J. (editors), Integrated Study of Regional Climate and Hydrology: Global and Planetary Change, Vol. 25, No. 1-2, pp. 133-147.

Moore, D. O., 1968, Estimating mean runoff in ungaged semiarid areas: Nevada Department of Conservation and Natural Resources Water Resources Bulletin No. 36, 11 p.

Morgan, David S., and Dettinger, Michael D., 1996, Ground-water conditions in Las Vegas Valley, Clark County, Nevada, part 2, hydrogeology and simulation of ground-water flow: U.S. Geological Survey Water-Supply Paper 2320-B, 126 p.

Morris, D.A., and Johnson, A.I., 1967, Summary of hydrologic and physical properties of rock and soil materials, as analyzed by the hydrologic laboratory of the U.S. Geological Survey 1948-60: U.S. Geological Survey Water-Supply Paper 1839-D, 42 p.

Murtagh, Bruce A., and Saunders, Michael A., 1987, MINOS 5.1 user's guide: Department of Operations Research, Stanford University, Technical Report SOL 83-20R, 127 p.

Muskat, M., and Wyckoff, R.D., 1946, The flow of homogeneous fluids through porous media: Ann Arbor, Michigan, J.W. Edwards, Inc., 763 p.

Narasimhan, T. N., Kanehiro, B. Y., and Witherspoon, P. A., 1984, Interpretation of earth tide response of three deep, confined aquifers: Journal of Geophysical Research, Vol. 89, No. B3, pp. 1913-1924.

Nichols, W. D., 1993, Estimating discharge of shallow groundwater by transpiration from greasewood in the northern Great Basin: Water Resources Research Vol. 29, No. 8, pp. 2771-2778.

Nichols, W. D., 1993, Ground-water discharge by phreatophyte shrubs in the Great Basin as related to depth to groundwater: Water Resources Research, Vol. 30, No. 12, pp. 3265-3274.

Nichols, W. D., 2000, Regional ground-water evapotranspiration and ground-water budgets, Great Basin, Nevada: U. S. Geological Survey Professional Paper 1628, 57 p.

Nichols, W.D., Laczniak, R.J., DeMeo, G.A., and Rapp, T.R., 1997, Estimated ground-water discharge by evapotranspiration, Ash Meadows area, Nye County, Nevada, 1994: U.S. Geological Survey Water-Resources Investigations Report 97-4025, 18 p.

Nielsen, Martha G., 2002, Estimated quantity of water in fractured bedrock units on Mt. Desert Island, and estimated groundwater use, recharge, and dilution of nitrogen in septic waste in the Bar Harbor area, Maine: U.S. Geological Survey Open-File Report 02-435, 45 p.

Niswonger, Richard G., Prudic, David E., Pohll, Greg, and Constantz, Jim, 2004, Incorporating seepage losses into the unsteady streamflow equations for simulating intermittent flow along mountain front streams: Water Resources Research, Vol. 41, W06006, 16 p.

Nordqvist, A. Wille, Tsang, Y.W., Tsang, C.F, Dverstorp, Bjorn, and Andersson, Johan, 1992, A variable aperture fracture network model for flow and transport in fractured rocks: Water Resources Research, Vol. 28, No. 6, pp. 1703-1713.

Omang, R. J., Parrett, Charles, and Hull, J. A., 1982, Mean annual runoff and peak flow estimates based on channel geometry of streams in southeastern Montana: U.S. Geological Survey Water-Resources Investigations 82-4092, 33 p.

Osterkamp, W. R., 1979, Variation of alluvial-channel width with discharge and character of sediment: U. S. Geological Survey Water-Resources Investigations 79-15, 11 p.

Osterkamp, W. R., and Hedman, E. R., 1982, Perennial-streamflow characteristics related to channel geometry and sediment in Missouri River Basin: U.S. Geological Survey Professional Paper 1242, 37 p.

Painter, Scott, 2001, Flexible scaling model for use in random field simulation of hydraulic conductivity: Water Resources Research, Vol. 37 (5), pp. 1155-1163.

Parrett, Charles, Omang, R. J., and Hull, J. A., 1983, Mean annual runoff and peak flow estimates based on channel geometry of streams in northeastern and western Montana: U.S. Geological Survey Water-Resources Investigations Report 83-4046, 53 p.

Pinder, George F. and Gray, William G., 1977, Finite element simulation in surface and subsurface hydrology: New York, Academic Press, 295 p.

Plume, R. W., 1996, Hydrogeologic framework of the Great Basin region of Nevada, Utah, and adjacent states: U. S. Geological Survey Professional Paper 1409-B, 64 p.

Poeter, Eileen P., and Hill, Mary C., 1998, Documentation of UCODE, a computer code for universal inverse modeling: U. S. Geological Survey Water-Resources Investigations Report 98-4080, 116 p.

Poland, J.F., 1961, The coefficient of storage in a region of major subsidence caused by compaction of an aquifer system, *in* Geological Survey Research 1961: U.S. Geological Survey Professional Paper 424-B, pp. B52-B54.

Poland, J.F., Lofgren, B.E., Ireland, R.L., and Pugh, R.G., 1975, Land subsidence in the San Joaquin Valley, California, as of 1972: U.S. Geological Survey Professional Paper 437-H, 78 p.

Proce, Christopher J., Ritzi, Robert W., Dominic, David F., and Dai, Zhenxue, 2004, Modeling multiscale heterogeneity and aquifer interconnectivity: Ground Water, Vol. 42, No. 5, pp. 658-670.

Rantz, S. E., 1968, A suggested method for estimating evapotranspiration by native phreatophytes in Geological Survey Research 1968, Chapter D: U. S. Geological Survey Professional Paper 600-D, pp. D10-D12.

Reilly, Thomas E., Franke, O. Lehn, and Bennett, Gordon D., 1987, The principle of superposition and its application in ground-water hydraulics: U.S. Geological Survey Techniques of Water-Resources Investigation 03-B6, 28 p.

Reiner, Steven R., Laczniak, Randell J., DeMeo, Guy A., Smith, J. LaRue, Elliott, Peggy E., Nylund, Walter E., and Fridrich, Christopher J., 2002, Groundwater discharge determined from measurements of evapotranspiration, other available hydrologic components, and shallow water-level changes, Oasis Valley, Nye County, Nevada: U. S. Geological Survey Water Resources Investigations Report 01-4239, 65 p.

Renshaw, Carl E., 1998, Sample bias and the scaling of hydraulic conductivity in fractured rock: Geophysical Research Letters, Vol. 25 (1), pp. 121-124.

Ripple, C. D., Rubin, Jacob, and van Hylckama, T. E. A., 1972, Estimating steady-state evaporation rates from bare soils under conditions of high water table: U. S. Geological Survey Water-Supply Paper 2019-A, 39 p.

Ritzi, Robert W. Jr., 2000, Behavior of indicator variograms and transition probabilities in relation to the variance in lengths of hydrofacies: Water Resources Research, Vol. 36, No. 11, pp. 3375-3381.

Robinson, T.W., 1958, Phreatophytes: U.S. Geological Survey Water-Supply Paper 1423, 84 p.

Robinson, T.W., 1970, Evapotranspiration by woody phreatophytes in the Humboldt River Valley near Winnemucca, Nevada: U.S. Geological Survey Professional Paper 491-D, 45 p.

Robson, S. G., and Banta E. R., 1990, Determination of specific storage by measurement of aquifer compression near a pumping well: Ground Water, Vol. 28, No. 6, pp. 868-874.

Robson, S.G., 1993, Techniques for estimating specific yield and specific retention from grain-size data and geophysical logs from clastic bedrock aquifers: U.S. Geological Survey Water-Resources Investigations Report 93-4198, 19 p.

Rovey, Charles W., II, 1998, Digital simulation of the scale effect in hydraulic conductivity: Hydrogeology Journal, Vol. 6, pp. 216-225.

Rush, F. E., and Eakin, T. E., 1963, Ground-water appraisal of Lake Valley in Lincoln and White Pine Counties, Nevada: Nevada Department of Conservation and Natural Resources Ground-Water Resources Reconnaissance Series Report 24, 29 p.

Rush, F. E., and Kazmi, S. A. T., 1965, Water-resources appraisal of Spring Valley, White Pine and Lincoln Counties, Nevada: Nevada Department of Conservation and Natural Resources Water Resources-Reconnaissance Series Report 33, 36 p.

Saar, M.O., and Manga, M., 2004, Depth dependence of permeability in the Oregon Cascades inferred from hydrogeologic, thermal, seismic, and magmatic model constraints: Journal of Geophysical Research, Vol. 109.

Schaefer, Donald H., and Harrill, James R., 1995, Simulated effects of proposed ground-water pumping in 17 basins of east-central and southern Nevada: U. S. Geological Survey Water-Resources Investigations Report 95-4173, 71 p.

Schulze-Makuch, Dirk, and Cherkauer, Douglas S., 1998, Variations in hydraulic conductivity with scale of measurement during aquifer tests in heterogeneous, porous carbonate rocks: Hydrogeology Journal, Vol. 6, No. 2, pp. 204-215.

Shepard, F.P., 1954, Nomenclature based on sand-silt-clay ratios: Journal of Sedimentary Petrology, Vol. 24, No. 3, pp. 151-158.

Sigda, John M., Goodwin, Laurel B., Mozley, Peter S., and Wilson, John L., 1999, Permeability alteration in small-displacement faults in poorly lithified sediments: Rio Grande rift, central New Mexico *in* Haneberg W., and others, eds., Faults and subsurface fluid flow in the shallow crust: AGU Geophysical Monograph 113, pp. 51-68.

Singhal, B.B.S., and Gupta, R.P., 1999, Applied hydrogeology of fractured rocks: The Netherlands, Kluwer Academic Publishers, 400 p.

Sneed, Michelle, 2001, Hydraulic and mechanical properties affecting ground-water flow and aquifer-system compaction, San Joaquin Valley, California: U.S. Geological Survey Open-File Report 01-35, 26 p.

Snow, David T., 1968, Rock fracture spacings, openings, and porosities: Journal of the Soil Mechanics and Foundations Division, Proceedings of the American Society of Civil Engineers, pp. 73-91.

SNWA. See Southern Nevada Water Authority.

Snow, David T., 1969, Anisotropic permeability of fractured media: Water Resources Research, Vol. 5, No. 6, pp. 1273-1289.

Southern Nevada Water Authority, 2006a, Water resources appraisal for Spring Valley, Nevada.

Southern Nevada Water Authority, 2006b, Water resources data for Spring Valley area, Nevada, Volume 1.

Southern Nevada Water Authority, 2006b, Water resources data for Spring Valley area, Nevada, Volume 2.

Southern Nevada Water Authority, 2006b, Water resources data for Spring Valley area, Nevada, Volume 3.

Southern Nevada Water Authority, 2006b, Water resources data for Spring Valley area, Nevada, Volume 4.

Southern Nevada Water Authority, 2006b, Water resources data for Spring Valley area, Nevada, Volume 5.

Southern Nevada Water Authority, 2006b, Water resources data for Spring Valley area, Nevada, Volume 6.

Southern Nevada Water Authority, 2006b, Water resources data for Spring Valley area, Nevada, Volume 7.

Southern Nevada Water Authority, 2006c, Geologic and hydrogeologic framework for the Spring Valley area: 122 p.

Southern Nevada Water Authority, 2006d, *FEMFLOW3D* Version 2.0, a finite-element program for the simulation of three-dimensional groundwater systems: 126 p.

SRK Consultants, 2001, Installation Report, Harvey Well replacement, Well RW-1, prepared for Nevada Power Company, Las Vagas and Reno, Nevada

Stannard, D.I., and Weaver, H.L., 1995, Measurements of evapotranspiration, surface-energy fluxes, weather variables, and water-table depths in the closed basin of San Luis Valley, Alamosa County, Colorado, 1985-1988: U.S. Geological Survey Open-File Report 93-639, 61 p.

Stroller-Navarro Joint Venture, 2004a, Analysis of well ER-7-1 testing, Yucca Flat FY 2003 testing program, Nevada Test Site, Nevada, Revision No. 0, S-N/99205-021: U. S. Department of Energy.

Stroller-Navarro Joint Venture, 2004b, Analysis of well ER-12-2 testing, Yucca Flat FY 2003 testing program, Nevada Test Site, Nevada, Revision No. 0, S-N/99205-015: U. S. Department of Energy.

Stroller-Navarro Joint Venture, 2004c, Hydrologic data for the groundwater flow and contaminant transport model of Corrective Action Units 101 and 102, Central and western Pahute Mesa, Nye County, Nevada, Revision No. 0, S-N/99205-002: U. S. Department of Energy.

Stroller-Navarro Joint Venture, 2004d, Integrated analysis report for single and multiple-well aquifer testing at Frenchman Flat well cluster RNM-2s, Nevada Test Site, Nevada, Revision No. 0, S-N/99205-021: U. S. Department of Energy.

Stroller-Navarro Joint Venture, 2004e, Interpretation of hydraulic test and multiple-well aquifer test at Frenchman Flat well cluster ER-5-3, Revision No. 0, S-N/99205-028: U. S. Department of Energy.

Thomas, James M., Carlton, Stephen M., and Hines, Lawrence B., 1989, Ground-water hydrology and simulated effects of development in Smith Creek Valley, a hydrological closed basin in Lander County, Nevada: U.S. Geological Survey Professional Paper 1409-E, 57 p.

Thomas, James M., Welch, Alan H., and Dettinger, Michael D., 1996, Geochemistry and isotope hydrology of representative aquifers in the Great Basin region of Nevada, Utah, and adjacent states; Regional aquifer-system analysis: U. S. Geological Survey Professional Paper 1409-C, 100 p.

Thorn, Condé R., 1995, Surface-water discharge and evapotranspiration rates for grass and bare soil along a reach of the Rio Grande, Albuquerque, New Mexico, 1989-95: U.S. Geological Survey Open-File Report 95-419, 23 p.

Todd, David Keith, 1959, Groundwater Hydrology: New York, Wiley & Sons, Inc., 539 p.

Tyler, S.W., Kranz, S., Parlange, M.B., Albertson, J., Katul, G.G., Cochran, G.F., Lyles, B.A., and Holder, G., 1997, Estimation of groundwater evaporation and salt flux from Owens Lake, California, USA: Journal of Hydrology, Vol. 200, No 1-4, pp. 110-135.

Van Der Kamp, G., and Gale, J. E., 1983, Theory of earth tide and barometric effects in porous formations with compressible grains: Water Resources Research, Vol. 19, No. 2, pp. 538-544.

Vanmarcke, Erik, 1983, Random fields, analysis and synthesis: Cambridge, Massachusetts, MIT Press, 382 p.

Walton, William C., 1970, Groundwater resource evaluation: New York, McGraw-Hill Book Company, 664 p.

Waterloo Hydrogeologic, Inc., 2002, Visual PEST-ASP User's Manual: Waterloo, Ontario, Canada, Waterloo Hydrogeologic Inc., 305 p.

Weissmann, Gary S., Carle, Steven F., and Fogg, Graham E., 1999, Three-dimensional hydrofacies modeling based on soil surveys and transition probability geostatistics: Water Resources Research, Vol. 35, No. 6, pp. 1761-1770.

Wetherbee, Gregory A., and Van Liew, William P., 1991, Geophysically estimated porosity of selected Paleozoic rocks in the upper Colorado River basin, Colorado, Utah, Wyoming, and Arizona: U. S. Geological Survey Water-Resources Investigation 90-4049, 30 p.

White, W.N., 1932, A method of estimating ground-water supplies based on discharge by plants and evaporation from soil: U.S. Geological Survey Water-Supply Paper 659-A.

Williamson, A.K., Prudic, D.E., and Swain, L.A., 1989, Ground-water flow in the Central Valley, California: U.S. Geological Survey Professional Paper 1401-D, 127 p.

Wilson, David H., Reginato, Robert J., and Hollett, Kenneth J., 1992, Evapotranspiration measurements of native vegetation, Owens Valley, California, June 1986: U. S. Geological Survey Water Resources Investigations Report 91-4159, 83 p.

Wolff, Roger G., 1982, Physical properties of rocks; porosity, permeability, distribution coefficients, and dispersivity: U. S. Geological Survey Open-File Report 82-166, 118 p.

Yapo, P. O., Gupta, H. V., and Sorooshian, S., 1998, Multi-objective global optimization for hydrologic models: Journal of Hydrology, vol. 204, pp. 83-97.

Yates, E. B., 1988, Simulated effects of groundwater management alternatives for the Salinas Valley, California: U. S. Geological Survey Water-Resources Investigation 87-4066, 79.

Yates, E. B., and Van Konyenburg, K. M., 1998, Hydrogeology, water qualities, water budgets, and simulated responses to hydrologic changes in Santa Rosa and San Simeon groundwater basins, San Luis Obispo County, California: U. S. Geological Survey Water-Resources Investigation 98-4061, 103p.

Young, Arthur A., and Blaney, Harry F., 1942, Use of water by native vegetation: State of California, Department of Public Works, Division Of Water Resources, 160 p.